LMSC-P352227
JUNE, 1989

EFFECT OF ALLOYING, RAPID SOLIDIFICATION, AND SURFACE KINETICS ON THE HIGH TEMPERATURE ENVIRONMENTAL RESISTANCE OF NIOBIUM

by

R.A. Perkins and K.T. Chiang
Lockheed Missiles & Space Company, Inc.
Palo Alto, Ca.

and

G.H. Meier and R.A. Miller
University of Pittsburgh
Pittsburgh, Pa.

prepared for

AIR FORCE OFFICE OF SCIENTIFIC RESEARCH
Bolling Air Force Base
Washington, D.C.

CONTRACT F49620-86-C-0018
A.H. Rosenstein, Project Manager

EFFECT OF ALLOYING, RAPID SOLIDIFICATION, AND SURFACE KINETICS ON THE HIGH TEMPERATURE ENVIRONMENTAL RESISTANCE OF NIOBIUM

Lockheed Missiles & Space Company, Inc.
RESEARCH AND DEVELOPMENT • PALO ALTO, CALIFORNIA

UNCL

SECURITY CLASSIFICATION OF THIS PAGE

REPORT DOCUMENTATION PAGE

Form Approved
OMB No. 0704-0188

1a. REPORT SECURITY CLASSIFICATION: UNCL.	1b. RESTRICTIVE MARKINGS: DTIC FILE COPY
2a. SECURITY CLASSIFICATION AUTHORITY	3. DISTRIBUTION/AVAILABILITY OF REPORT: Approved for public release, distribution unlimited
2b. DECLASSIFICATION/DOWNGRADING SCHEDULE	
4. PERFORMING ORGANIZATION REPORT NUMBER(S): LMSC F352227	5. MONITORING ORGANIZATION REPORT NUMBER(S): AFOSR-TR- 89-0909
6a. NAME OF PERFORMING ORGANIZATION: LOCKHEED MISSILES & SPACE CO. / 6b. OFFICE SYMBOL (If applicable): LMSC	7a. NAME OF MONITORING ORGANIZATION: AFOSR/NE
6c. ADDRESS (City, State, and ZIP Code): O/93-10, B/204, 3251 HANOVER ST. PALO ALTO, CA., 94304	7b. ADDRESS (City, State, and ZIP Code): BULIDING 410, BOLLING AIR FORCE BASE WASHINGTON, D.C., 20332-6448
8a. NAME OF FUNDING/SPONSORING ORGANIZATION: AFOSR / 8b. OFFICE SYMBOL (If applicable): AFOSR/NE	9. PROCUREMENT INSTRUMENT IDENTIFICATION NUMBER: F49620-86-C-0018
8c. ADDRESS (City, State, and ZIP Code): Bldg. 410 Bolling AFB, DC, 20332-6448	10. SOURCE OF FUNDING NUMBERS: PROGRAM ELEMENT NO. 61102F / PROJECT NO. 2306 / TASK NO. A1 / WORK UNIT ACCESSION NO.

11. TITLE (Include Security Classification)
EFFECT OF ALLOYING, RAPID SOLIDIFICATION, AND SURFACE KINETICS ON THE HIGH TEMPERATURE ENVIRONMENTAL RESISTANCE OF NIOBIUM (U)

12. PERSONAL AUTHOR(S)
R.A. PERKINS AND G.H. MEIER

13a. TYPE OF REPORT	13b. TIME COVERED	14. DATE OF REPORT (Year, Month, Day)	15. PAGE COUNT
FINAL TECHNICAL	FROM 11/85 TO 1/89	89/6/23	137

16. SUPPLEMENTARY NOTATION

17. COSATI CODES			18. SUBJECT TERMS (Continue on reverse if necessary and identify by block number)
FIELD	GROUP	SUB-GROUP	
21	06		NIOBIUM, OXIDATION, MECHANISMS, NIOBIUM-ALUMINUM ALLOYS, ALUMINA FORMATION, NIOBIUM-TITANIUM-ALUMINUM ALLOYS
21	05, 08		

19. ABSTRACT (Continue on reverse if necessary and identify by block number)

Factors affecting the formation of protective alumina scales on Nb-base alloys by selective oxidation have been investigated. Alumina cannot be formed in air at 1atm. on binary Nb-Al alloys at any N_{Al}. Theoretical knowledge of selective oxidation has been applied to Nb-Al alloys to alter behavior. The effects of Al-content, temperature, atmosphere, third element additions, and microstructure on the transition from internal to external oxidation of aluminum has been evaluated and conditions under which protective alumina scales can form on Nb-Al alloys have been defined. Third element additions are required to form protective alumina. The most effective additions are those which can reduce the solubility and diffusivity of oxygen, enhance diffusion of Al, and limit transient oxidation. Additions of Ti, Cr, V and Si were identified as most promising for providing oxidation resistance in Nb-Al alloys. The feasibility of forming compact, adherent alumina scales on Nb alloys at a minimum N_{Al}=0.32 in air at 1100°-1600°C has been demonstrated. Alumina scale could not be formed below 1100°C. Preoxidation above 1100°C can be used to preform alumina scales that will protect at lower temperatures but is effective only if the alloy is not (contimued)

20. DISTRIBUTION/AVAILABILITY OF ABSTRACT	21. ABSTRACT SECURITY CLASSIFICATION
☒ UNCLASSIFIED/UNLIMITED ☐ SAME AS RPT. ☐ DTIC USERS	UNCL
22a. NAME OF RESPONSIBLE INDIVIDUAL: DR. HIAN KOELSTEIN	22b. TELEPHONE (Include Area Code): (202)767-4939 / 22c. OFFICE SYMBOL: NE

DD Form 1473, JUN 86 — Previous editions are obsolete. — SECURITY CLASSIFICATION OF THIS PAGE: UNCL

cooled to room temperature prior to exposure at lower temperatures. Thermal stresses generated in even one cooldown cycle are sufficient to crack the alumina scale. Rapid solidification processing does not appear to offer any significant benefit. The alumina-forming capability of alloys that are borderline alumina formers is enhanced but there is little effect on alloys that are not alumina formers. Ion implantation of Al or Si had a similar effect and only improved behavior of alloys which are borderline alumina formers. The type of alloying elements and the concentrations necessary to ensure alumina formation resulted in a solidus temperature of 1650°C for oxidation resistant Nb-Al alloys.

EXECUTIVE SUMMARY

The factors affecting the formation of protective alumina scales on Nb-base alloys by selective oxidation have been extensively investigated. Alumina cannot be formed in air at 1atm. on binary Nb-Al solid solutions or any Nb-aluminides including $NbAl_3$. The existing theoretical knowledge of selective oxidation has been applied to oxidation of Nb-Al alloys and aluminides to determine approaches by which this behavior may be altered. The effects of Al-content, temperature, atmosphere, third element additions, and microstructure on the transition from internal to external oxidation of aluminum have been evaluated and the the conditions under which protective alumina scales can be formed on Nb-Al alloys has been defined.

Third element additions are required to form alumina by selective oxidation of Al on Nb-base alloys. The most effective additions are those which can reduce the solubility and diffusivity of oxygen in the alloy, enhance the diffusion of Al in the alloy, and limit transient oxidation. The addition of high e/a elements such as Mn and Ru, which should reduce solubility and diffusivity of oxygen and suppress the internal oxidation of Al, were not effective. These additions produced transient oxides that grew with linear kinetics at very rapid rates. The addition of oxygen active elements such as Zr, Hf, and Be, which should reduce oxygen diffusivity, also was not effective. Ternary alloys with these additions also oxidized with fast linear kinetics. Titanium was added to alter alloy microstructure and was most effective of all third element additions. Large additions of Ti produced a high temperature B2 phase in which diffusivity of Al is rapid and on which protective alumina scales could be formed.

Although alumina scales could be formed on Nb-Ti-Al alloys with 44at.% Al in air at 1400°C, the rates of oxidation were 1-2 orders of magnitude greater than those of other alumina formers such as NiAl. This was the result of a slow growth rate of alumina coupled with a high growth rate of the base alloy transient oxide. It was established that Nb-Ti-Al alloys must be modified with a fourth element in order to form transient oxides which grow with slow linear or parabolic kinetics. Additions of Cr, V, and Si were identified as most promising for reducing transient oxidation and enhancing alumina formation on Nb-Ti-Al alloys.

Additions of Cr and V to Nb-Ti-Al alloys were very effective in promoting formation of alumina at temperatures above 1200°C The appeared to have little effect on transient oxides and are believed to function by reducing solubility and diffusivity of oxygen in the alloy. A synergism was found in which these two elements together were more effective than either one alone. Additions of 3 at.% Cr and 4 at.% V resulted in protective alumina formation at 32 at.% Al in air at 1400°C. Similar results were obtained by additions of Mo in place of V. The alloys did not form alumina at lower temperatures as a result of fast kinetics for transient oxidation. The best balance of composition in at.% is 24Nb, 24Ti, 44Al, 3Cr, 5V for this class of alloys.

The addition of 3-10% Si to Nb-Ti-Al alloys was found to reduce the amount of transient oxidation. This reduced the temperature at which continuous alumina scales could be formed. Best performance was found for a Nb-Ti-Al-Cr-V-Si alloy with 10 at.% Si and 32 at.% Al which formed protective alumina scales in air at 1100°C. Alumina forming behavior was improved by substituting 10% Si for Al in Nb-Ti-Al-Cr-V alloys, however, the rates of oxidation were still 2 orders of magnitude greater than that of NiAl at 1100°C. Nb-Ti-Al alloys modified with Cr+V and Cr+V+Si to form alumina scales without significant transient oxidation oxidized with slow parabolic kinetics at the same rate as NiAl from 1300-1600°C.

The oxidation behavior of Nb-Ti-Al-Cr-V alloys was studied in greater detail to establish the effect of significant composition and microstructural variables on alumina formation. The major effect of Al content of the alloy was found to be on the temperature at which a transition from internal to external oxidation of Al will occur and the amount of transient oxidation that occurred before it was cut off by formation of a continuous alumina scale. The transition temperature and the amount of transient oxidation decreased as Al content increased. There was no effect of Al content on oxidation kinetics of alloys that did not form continuous alumina scales.

The ratio of Nb:Ti in the alloy also was an important variable. The amount of internal oxidation of Al was reduced and the transition from internal to external oxidation of Al occurred at lower Al contents when the Nb:Ti ratio was increased. The best ratio is in the range of 1-1.3. At ratios higher than 1.3, the alloys are not alumina formers. At lower ratios, the alloys are

γ-TiAl modified with Nb. Alloys in the range of 1-1.3 are single phase B2 above 1400°C and have a two phase γ-TiAl + Nb_2Al (sigma) structure at lower temperature

Rapid solidification processing was evaluated as an approach to improving oxidation resistance of Nb-Ti-Al-Cr-V alloys. Best results were obtained by undercooling below 125°C to retain a stable B2 structure in the alloy at room temperature. On heating, however, the alloy rapidly transformed to the basic two phase microstructure. The finer grain size that was produced by RSP enhanced alumina diffusion, resulting in formation of alumina scales at temperatures below 1400°C. However, the effect was minimal with respect to reducing the temperature for alumina formation and RSP was effective only at temperatures close to the transition temperature. It was effective only if the alloy was a borderline alumina former.

Surface enrichment with Al and Si by ion implantation also was investigated as an approach to enhancing alumina formation. Results were similar to those achieved by rapid solidification processing. The transition temperature for alumina formation was reduced slightly but no effect on kinetics below the transition temperature was observed. Ion implantation was effective only under conditions where the alloy was a marginal alumina former.

Preoxidation was evaluated as an approach to improving oxidation resistance at low temperature where alumina scales could not be formed. Alumina scales preformed in air or oxygen at 1500°C remained protective at 1100°C provided that the sample was not cooled to room temperature after preoxidation. The thermal stresses generated in one thermal cycle were sufficient to crack the preformed alumina scales and no protection was provided on re-exposing to the lower temperature range.

Niobium-Al alloys modified to form alumina must contain at least 32 At.% Al and are intermetallic compounds (aluminides). Results of the investigation indicate little possibility to form protective alumina scales on BCC Nb-Al solid solution-type alloys with a lower concentration of Al. The major factor that precludes alumina formation in such alloys is the low solubility of Al in Nb coupled with the high solubility and diffusivity of oxygen in the BCC solid solution. In addition, the base alloy oxides grow with fast linear kinetics

which precludes alumina formation. The only solution to this problem appears to be the addition of large amounts of Ti to stabilize a high temperature B2 phase on which alumina can be formed. The type of alloying elements and the concentrations necessary to ensure alumina formation lowers the alloy solidus temperatures to around 1650°C. Additions of Si further reduced the solidus temperature to below 1600°C.

Publications

1. R.A. Perkins, K.T. Chiang, and G.H. Meier, "Formation of Al on Nb-Al Alloys..", Scripta Met., v22, p419, 1988.
2. R.A. Perkins, K.T. Chiang, G.H. Meier, and R. Miller, "Formation of Alumina on Nb and Ti-Base Alloys", in Oxidation of High Temperature Intermetallics, T. Grobstein and J. Doychak, eds., The Minerals, metals, and Materials Society, Warrendale, Pa., p157, 1989.
3. G.H. Meier, "Fundamentals of the Oxidation of High Temperature Intermetallics", IBIB, p1.
4. R.A. Perkins and G.H. Meier, "Oxidation Resistant Aluminides for Metal Matrix Composites", to appear in Proceedings of Advanced Materials Conference, Denver, CO., March, 1989.
5. R.A. Miller, G.H. Meier, and R.A. Perkins, "A Study of the Effects of Alloying and Rapid Solidification on the Oxidation of Nb-Ti-Al Alloys", manuscript in preparation for submission to Oxidation of Metals.
6. G.H. Meier and R.A. Perkins, "Effect of Ion Implantation on the Selective Oxidation of Aluminum from Nb-Base Alloys", manuscript in preparation for submission to Scripta Met.
7. G.H. Meier, R.A. Miller and R.A. Perkins, "Effect of Preoxidation on the Oxidation Behavior of Nb-Ti-Al-Cr-V Alloys", manuscript in preparation for submission to High Temperature Technology.

Professional Personnel

The following professional personnel have participated in the program:

LMSC

Mr. R.A. Perkins

Dr. K.T. Chiang

Dr. J.S. Lee

UNIVERSITY OF PITTSBURGH

Prof. G.H. Meier

Mr. R.A. Miller (Graduate Research Assistant)

Coupling Activities

(1) The program supported the M.S. thesis research of R.A. Miller at the University of Pittsburgh which was completed successfully in March, 1989. Mr. Miller was awarded an MS degree by the University of Pittsburgh in June, 1989. The title of his thesis is "A Study of the Effect of Alloying and Rapid Solidification on the Oxidation of Nb-Ti-Al Alloys".

(2) A contract from DARPA has been awarded to Pratt and Whitney for "Development of High Temperature Metallics for Structural Aerospace Applications" (N00014-87-C-0862) as a result of the advanced understanding of Nb alloy oxidation that was obtained during the first year of research on this project. The demonstration of technical feasibility for oxidation resistant Nb-based alloys convinced DARPA that the design of effective alloys would be possible. Lockheed is a subcontractor to Pratt and Whitney with prime responsibility for design of the oxidation resistant alloy. Results of this AFOSR program were factored into the P&W program to provide technical guidelines for alloy design as the research progressed. P&W in turn supplied samples of selected alloys for use in the AFOSR program.

(3) A Contract from NRDC has been awarded to the Martin Marietta Research Laboratories for basic research on strengthening of aluminides with XD dispersions. A Nb-Ti-Al alloy has been selected as the model system for this project and the results of the AFOSR program provided the basis for this selection.

(4) The following presentations based on results of this research have been made:

(a) Invited presentation to NMAB committee on Advanced High Temperature Composites- "Oxidation of Refractory Metals", R.A. Perkins, Feb. 1987.

(b) Invited presentation at Gordon Research Conference on Corrosion,

Panel on Oxidation Resistance of Reactive Materials, R.A. Perkins, July 1987.

(c) Presentation to J. Stevens and Structural Materials Group at NASA-LRC, R.A. Perkins, Aug. 1987.

(d) Presentation to F.H. Froes, NASP Materials Committee, Sept. 1987.

(e) Invited review of Nb oxidation behavior to DARPA/URI Research Groups, Santa Barbara, CA, G.H. Meier, Jan. 1988.

(f) Invited presentation on oxidation of Nb alloys to NASA-LRC Symposium on Oxidation of Intermetallics, Cleveland OH, R.A. Perkins, Sept. 1988.

(g) Invited presentation on Fundamentals of the Oxidation of High Temperature Intermetallics to NASA-LRC Symposium on Oxidation of Intermetallics, Cleveland, OH, G.H. Meier, Sept.1988.

(h) Invited lecture on "Oxidation of Refractory Metals", Spring '88 Meeting of the Materials Research Society, Reno, NV, R.A.Perkins, April 1988.

(i) Invited research seminar presentation on "Oxidation of Refractory Metals", Rensselaer Polytechnic Institute, Troy, NY, R.A. Perkins, March 1988.

(j) Paper entitled "Oxidation Resistant Aluminides for Metal Matrix Composites" presented to Industry-University Advanced Materials Conference, Denver. CO, R.A. Perkins, March 1989

(k) Invited paper entitled "Oxidation Behavior of Nb and Ti Aluminides presented to ASM WESTEC, R.A. Perkins, March, 1989.

(l) Invited presentation entitled "Oxidation Resistant Intermetallics" to General Electric Co., Engine Div., Cincinnati, OH, G.H. Meier, Jan. 1989.

FOREWORD

This report covers research performed under contract F49620-86-C-0018 for the period 1 January, 1987 to 31 December, 1988. The project was administered by the Air Force Office of Scientific Research with Dr. A.H. Rosenstein as project manager. The report was prepared by Mr. R.A. Perkins of Lockheed Missiles & Space Co., Palo Alto, Ca. and Prof. G.H. Meier of the University of Pittsburgh, Pittsburgh, Pa.

The program was conducted as a joint research investigation by the Research and Development Division of the Lockheed Missiles & Space Co. (LMSC) and the Materials Science and Engineering Department of the University of Pittsburgh with LMSC as the prime contractor. Mr. R.A.Perkins of Lockheed and Prof. G.H.Meier of the University of Pittsburgh were co-principal investigators. The following personnel assisted in conducting the experimental work:

LMSC-

Dr. K.T. Chiang
Dr. J.S. Lee
Mr. L.R. Iosty
Mr. R.N. Hall
Mr. A.H. Heynen

University of Pittsburgh-

Mr. R.A. Miller
Mr. K.F. Andrew
Mr. E. Hewitt

CONTENTS

	PAGE
REPORT DOCUMENTATION PAGE	i
EXECUTIVE SUMMARY	ii
FOREWORD	ix
CONTENTS	xi
INTRODUCTION	1
TECHNICAL BACKGROUND	3
OXIDATION RESISTANT NIOBIUM ALLOYS	3
Oxidation of Unalloyed Nb	3
Oxidation of Niobium Alloys	3
BASIS FOR OXIDATION RESISTANT ALLOYS	6
FORMATION OF ALUMINA ON Nb-BASE ALLOYS	8
Case 1- Alumina Fortmation in Absence of Transient Oxides	8
(A)- Effect of Third Element Additions	11
(B)- Effect of Microstructure	19
(C)- Effect of Oxidation Temperature	20
Case 2- Alumina Formation in Presence of Transient Oxides	20
PREOXIDATION	21
EXPERIMENTAl	22
PREPARATION OF ALLOYS	22
RAPID SOLIDIFICATION PROCESSING	23
ION IMPLANTATION	23
OXIDATION EXPERIMENTS	24
Screening Studies	24
Oxidation Kinetics	25
MATERIALS ANALYSIS	26
Optical Metallography	26
Scanning Electron Microscopy	26
X-Ray Diffraction Analysis	26
Melting Point	27
RESULTS AND DISCUSSION	28
OXIDATION BEHAVIOR OF $NbAl_3$	28
OXIDATION BEHAVIOR OF Nb-Al-X ALLOYS	28
Alloying to Decrease D_O	30
Alloying to Decrease N_O	37
Alloying to Increase D_{Al}	43
OXIDATION BEHAVIOR OF Nb-Ti-Al-X ALLOYS	48
Effect of Cr, V, Mo	48
Effect of Si, Pt	58
OXIDATION BEHAVIOR OF Nb-Ti-Al-Cr-V ALLOYS	60
Effect of Al	64
Effect of Nb:Ti Ratio	71
Effect of Temperature	75
Effect of Environment (Air vs O_2)	86
Effect of Preoxidation	90
Effect of Rapid Solidification Processing	100
Effect of Ion Implantation	112

MELTING POINT OF ALLOYS 119

SUMMARY AND CONCLUSIONS 121

REFERENCES 124

APPENDIX 126
A-1 ALLOY COMPOSITIONS 126
A-2 RESULTS OF OXIDATION SCREENING TESTS 129
A-3 OXIDATION RATE LAW EXPONENTS 131
A-4 LINEAR AND PARABOLIC RATE LAW CONSTANTS 132

INTRODUCTION

Alloys of Niobium are among the most logical materials in terms of mechanical properties, producibility, cost, and availability for use in aerospace propulsion and thermal protection systems at temperatures of 800-1500°C. The major deterrent to effective use of these materials in advanced gas turbines, rocket engines, and thermal protection systems is the lack of adequate resistance to oxidation. Commercially available alloys have high rates of oxidation above 650°C and are embrittled by dissolution of oxygen, carbon, and nitrogen.

Niobium alloys can be coated with oxidation resistant intermetallic compounds of Nb with Si and, as such, find limited use in rocket and propulsion applications. Most notable among these are thrust deflectors for aircraft gas turbines and the combustion chambers and exit cones for liquid propellant rocket engines. Useful life is limited, particularly under cyclic use conditions, and random coating failures can lead to rapid attack of the alloy. Coating performance and reliability are not adequate for extended use in advanced gas turbines, ramjet engines, and hot structures for hypersonic vehicles. Niobium alloys with improved resistance to oxidation are needed for use as high temperature structural alloys and composites.

A review of the current status of technology for oxidation resistant alloys indicates that major advances in the oxidation behavior of Nb-base alloys may now be possible. Advanced metal processing, such as rapid solidification, offers the ability to produce compositions and structures that have not been attainable by conventional processing. New technology and fundamental knowledge of the formation of protective oxide scales on complex alloys in mixed oxidants coupled with a wide range of new and sophisticated surface analysis techniques can provide a better insight into how to control the oxidation behavior of niobium. The feasibility of providing a technical basis for the design of improved alloys by basic research on the mechanisms by which protective oxide scales can be formed on niobium is considered to be good.

A fundamental study has been initiated under this contract to provide such a technical basis. The research is directed to develop an understanding of the mechanisms by which protective alumina scales can be formed on niobium by the

selective oxidation of aluminum. The specific goals of the study are to

1- derive a model for the selective oxidation of aluminum from niobium to form protective alumina scales
2- define the factors in composition and structure that govern the selective oxidation of aluminum from niobium alloys
3- establish the feasibility of alloying niobium to produce compact, adherent alumina scales
4- determine the limiting kinetics of oxidation of alumina-forming Nb-base alloys as a function of temperature and atmosphere composition.

The research was conducted over a three year period starting in January, 1986, and results are presented in this report.

TECHNICAL BACKGROUND

OXIDATION RESISTANT NIOBIUM ALLOYS

The oxidation behavior of Nb-alloys was the subject of considerable research in the period 1955 to 1970. The impetus to most of this research was provided by the desire to utilize the high melting point of Nb and the significant high temperature strength obtainable in Nb-base alloys. The research conducted prior to 1975 has been reviewed extensively by Stringer(1). The purpose of this review is to briefly assess the results of research conducted since 1975 and to discuss the current understanding of the factors which control the oxidation behavior of Nb-base alloys with particular emphasis on the selective oxidation of Al. The results of work prior to 1975 will not be reviewed except in cases where it illustrates particular fundamental aspects of Nb-alloy oxidation. The interested reader is referred to the review by Stringer(1) and the original papers cited therein.

Oxidation of Unalloyed Niobium

Three oxides of Nb have been identified - NbO, NbO_2, and Nb_2O_5 (α or γ). The oxidation of Nb at oxygen partial pressures high enough to form Nb_2O_5 exhibits paralinear kinetics, i.e., for short times the rate is nearly parabolic and becomes linear with longer exposure times. The transition to linear kinetics occurs because the Nb_2O_5 scale begins to crack under the influence of large compressive growth stresses(2,3). The rapid linear oxidation of Nb has been the major limitation to its extensive use at high temperatures. Oxidation of Nb at low oxygen pressures which can form NbO_2, but not Nb_2O_5, follows a slow parabolic rate with no indication of scale cracking(3). Oxidation of Nb is accompanied by significant dissolution of O and N in the metal substrate which has an embrittling effect.

Oxidation of Niobium Alloys

A large number of alloy compositions have been studied under various exposure conditions(1). Nearly all of the early work prior to 1975 was conducted under the constraint of striving for a balance between oxidation resistance and mechanical behavior. Few definitive or basic studies of the oxidation

behavior of niobium alloys were conducted. Most of the work was of an alloy development character and largely was conducted in an empirical manner. A significant effort was directed to the addition of elements that would dope the major oxide of niobium (Nb_2O_5) or would alter its fracture behavior. The efforts were not successful in improving the oxidation resistance of Nb-base alloys and it was recognized by a number of investigators that alloying to produce a surface oxide other than Nb_2O_5 was required.

Svedberg conducted an extensive investigation of alloying to produce oxidation-resistant Nb-base alloys from 1975-1976(4). This was done without any constraints imposed by mechanical behavior and hence provides a broader basis for developing an understanding of oxidation behavior. The alloys and parabolic rate constants for the most resistant alloys from this study for air oxidation at 1200°C are listed in Table 1.

TABLE 1

Parabolic Oxidation Rate Constants

Compositions	Parabolic Rate Constant
	$(mg/cm^2)^2/min$
$NbAl_3$	0.018
$NbCr_2$	0.176
$NbFe_2$	0.310
$NbCo_2$	25.000*
Nb-19Cr-10Al-15Co	0.45 - 0.037**
Nb-10Cr-10Al-15Ni	0.115 - 0.543
Nb-9Cr-10Al-25Ni	0.300 - 1.200
Nb-10Fe-19Al	0.323 - 1.320
Nb-30Fe-10Al	0.042
Nb-15Fe-12Al	0.170
Nb-16Fe-10Al	0.240
Nb-15Al-15Co	0.150
Nb-14Al-6Co	0.260
Nb-10Al-11Co	0.470
Nb-7Al-8Co-5Cr	0.300
Nb-15Ti-10W-10Ta-2Hf-3Al (B-1)	3.106

* Apparent melting during oxidation
** Two distinct slopes measured (Initial/Final)

The slowest oxidation rate of all the alloys was observed for $NbAl_3$ which was reported to form a continuous Al_2O_3 protective layer. Binary Nb-Al alloys

with lower Al contents (<75a/o) are not able to form Al_2O_3 scales in air at 1200°C. Svedberg(4) found that Nb_2Al and Nb_3Al oxidized with a rapid, linear rate. The factors which control the selective oxidation of Al from Nb-base alloys are not clearly defined.

Other Nb-base alloys which have proven to exhibit the slowest oxidation rates are those which form complex or mixed oxides with niobium, particularly those based on rutile-type structures. The most effective additions for this purpose were found to be Fe, Cr, and Al. These alloys may be put into two groups based on the type of protective scale identified by x-ray diffraction and metallography. One group, which includes $NbFe_2$ (and perhaps $NbCo_2$ at lower temperatures), involves the interesting phenomenon of the formation of a compound oxide which grows much more slowly than the binary oxides which would form on either pure component. For $NbFe_2$, this phase is apparently $NbFeO_4$, a rutile structure compound. Protective Nb-Fe oxides ($FeO-Nb_2O_5$) were reported previously to form on Nb-25 wt % Fe(5). The second group includes the remaining alloys in Table 1 and involves the formation of protective rutile structure ternary oxides, particularly $AlNbO_4$ and $CrNbO_4$.

Wukusick (6) studied the oxidation behavior of intermetallic alloys in the Nb-Al-Ti system. He found that by adding large amounts of titanium to binary Nb-Al alloys, the "pest" phenomenon usually encountered in binary Nb-Al alloys between 593-982°C was suppressed by the formation of a titanium oxide scale. However, the scale was not protective and the rate of oxidation by surface recession was high. In the higher temperature range from 1004-1298°C a duplex oxide, $TiO_2 + Al_2O_3$ (with TiO_2 as the matrix), formed but the oxidation rate was still high. At still higher temperatures, selective oxidation of aluminum resulted in formation of a protective, continuous Al_2O_3 scale.

The addition of chromium to ternary Nb-Al-Ti alloys was found to improve the intermediate temperature oxidation behavior by reducing the amount of oxide spallation and increasing the tendency for Al_2O_3 film formation at lower temperatures. However, the oxidation behavior of Cr-containing alloys was very dependent upon the aluminum content. When chromium was substituted for titanium in the alloy, the oxidation resistance was improved but when chromium was substituted for aluminum, resistance decreased as a result of oxide spall. Wukusick also reported that although the addition of chromium improved the

oxidation behavior of Nb-Al-Ti-Cr alloys, the presence of the second phase, $NbCr_2$, increased the brittleness of the alloy and lowered the melting point. In addition, changes in microstructure were observed between 1260-1427°C. Wukusick concluded that although the addition of chromium improved the oxidation resistance, the detrimental effects such as a lower melting point, structural instability and increased brittleness, made it unlikely that a useful oxidation resistant alloy could be developed.

BASIS FOR OXIDATION RESISTANT ALLOYS

The principle underlying the high temperature oxidation resistance of alloys is the addition of an element which can form an external layer of oxide to separate the alloy from the corrosive environment (selective oxidation). The formation of such a layer generally requires that the oxide of the added element be the most stable oxide of any of the major components in the alloy. For this reason, Al, because of the high stability of Al_2O_3 and slow diffusion rates through Al_2O_3 films, is often the preferred elemental addition for oxidation resistance. The only other element and oxide that satisfiy this criterion with respect to selective oxidation from Nb alloys are Si and silica.

Among the single oxides, minimum diffusion rates are found for alumina. The melting point of alumina is 2050°C and the oxide has only small deviations from stoichiometry and low point defect concentrations. Silica has a melting range of 1405 to 1700°C, depending on structure, and is more permeable to oxygen and nitrogen than alumina at high temperature. However, the activation energy for diffusion in silica is low. The activation energy for diffusion in alumina is high such that alumina becomes less effective than silica as a barrier for oxidation as temperature is increased. This is illustrated by the effect of temperature on the parabolic rate constant for the growth of alumina on NiAl and silica on silicon as shown in Fig. 1 (7).

The maximum temperature of useful resistance to oxidation with different oxide barriers can be estimated from the parabolic rate constants as plotted in Fig. 1. A useful limit for materials in thin sections is a k_p of 10^{-10} $g^2cm^{-4}s^{-1}$ which results in a weight gain of 19 $mgcm^{-2}$ in 1000 hr. At this limit, alloys that form chromia as a scale would be useful to 1100°C which is close to the

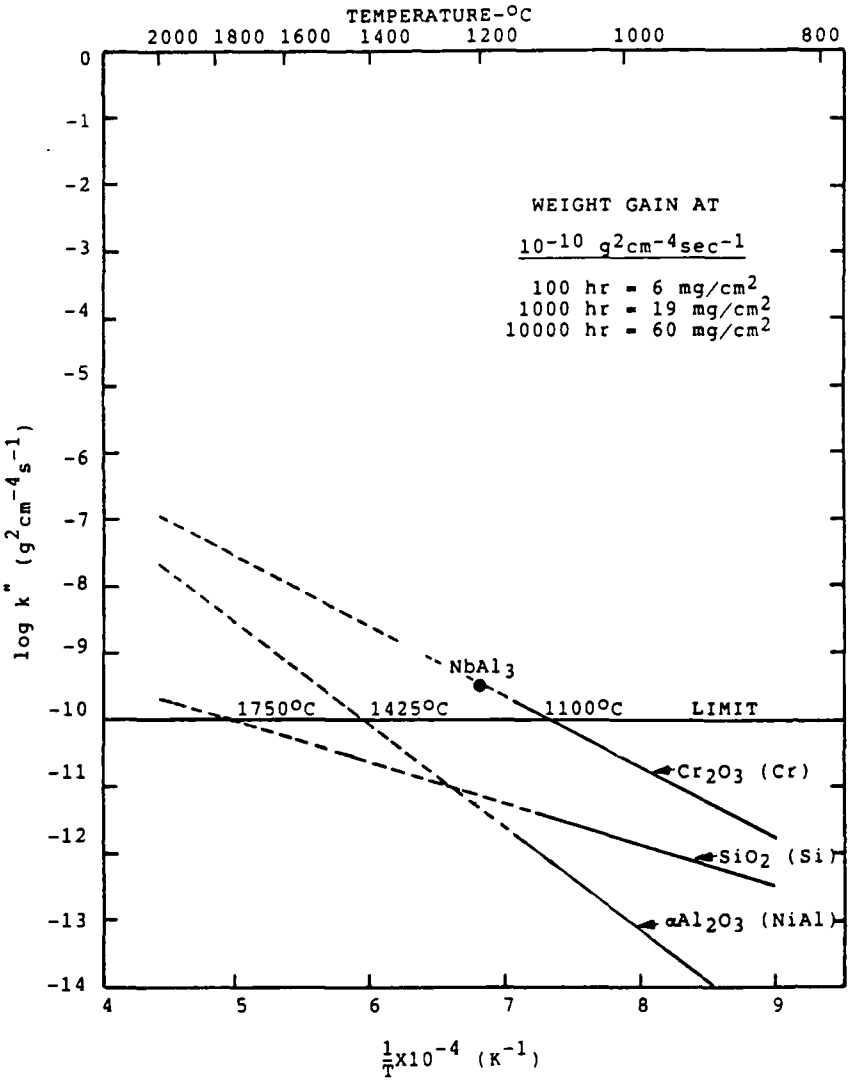

Figure 1: Parabolic rate constant vs temperature for chromia, silica, and alumina scale forming alloys.

upper limit for chromium base alloys and high-Cr nickel or cobalt base alloys. Alumina formers would be useful to 1425°C while silica formers would be good to 1750°C. The maximum useful temperature for niobium alloys is 1500°C based on the melting point of Nb_2O_5. Alumina lowers this temperature to 1400°C by forming a eutectic between mixed oxides of Al and Nb. Above 1400°C, niobium-aluminum alloys may be susceptible to catastrophic rates of oxidation if mixed oxides are formed. Alumina scales offer the potential to protect niobium from oxidation for long times at temperatures to 1400°C where niobium can be used safely without concern for oxide melting and catastrophic oxidation if

breakaway occurs.

FORMATION OF ALUMINA ON NIOBIUM-BASE ALLOYS

Once the proper thermodynamic conditions for selective oxidation of Al have been established, the critical consideration is whether this oxidation will result in a continuous surface film (and slow oxidation rates) or the formation of internal oxide precipitates (and continued rapid oxidation) as summarized in Fig. 2. One complication in this process is the presence of transient oxides which can affect the transition from internal to external oxidation. Two different cases will be considered.

Case 1- Alumina Formation in the Absence of Transient Oxides

In this case, the oxidation of Al from alloys must occur at an oxygen pressure below that required for the oxidation of base metal. The transition from internal to external oxidation for this case has been treated by Wagner(8). Consider the concentration profiles in Fig. 2. The penetration of the zone of internal oxidation may be expressed

$$X = 2\gamma(D_o t)^{1/2} \qquad (1)$$

Fick's second law for the diffusion of oxygen through the internally oxidized zone is

$$\frac{\partial N_O}{\partial t} = D_O \frac{\partial^2 N_O}{\partial x^2} \qquad (2)$$

with the initial conditions

$$t = 0 , \quad N_O = N_O^{(s)} \quad \text{for} \quad x \leq 0$$

$$N_O = 0 \quad \text{for} \quad x > 0$$

and the boundary condition

$$t > 0 , \quad N_O = N_O^{(s)} \quad \text{for} \quad x = 0$$

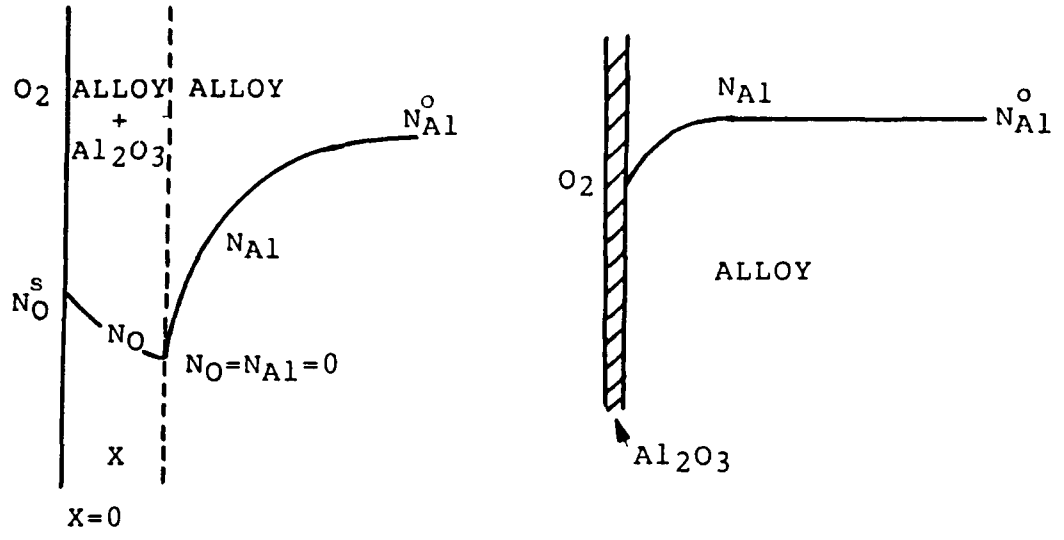

A- *INTERNAL OXIDATION OF ALUMINUM*

$(N_{Al} < N_{Al}^{crit})$

B- *EXTERNAL ALUMINA SCALE FORMATION*

$(N_{Al} > N_{Al}^{crit})$

$$N_{Al}^{crit} = \frac{\pi g^*}{3} N_O^{(s)} \frac{D_O V_M}{D_{Al} V_{ox}}^{1/2}$$

Figure 2: Wagner model for transition from internal to external oxidation.

The solution to equation (2) is

$$N_O(x,t) = N_O^{(s)} \left[\frac{1 - \text{erf}\left(\frac{x}{2(D_O t)^{1/2}} \right)}{\text{erf}\ \gamma} \right] \qquad (3)$$

Similarly, Fick's second law for the counter-diffusion of Al is

$$\frac{\partial N_{Al}}{\partial t} = D_{Al} \frac{\partial^2 N_{Al}}{\partial x^2} \qquad (4)$$

with initial conditions

$$t = 0, \quad N_{Al} = 0 \quad \text{for} \quad x < 0$$

$$N_{Al} = N_{Al}^{(o)} \quad \text{for} \quad x > 0$$

The solution to equation 4, therefore, becomes

$$N_{Al}(x,t) = N_{Al}^{(o)} \left[1 - \frac{\operatorname{erfc}\left(\frac{x}{2(D_{Al}t)^{1/2}}\right)}{\operatorname{erfc}\left(\theta^{1/2}\gamma\right)} \right] \qquad (5)$$

where $\theta = D_o/D_{Al}$.

If $\underline{f}$ represents the mole fraction of Al_2O_3 in the internal oxidation zone and V_m the molar volume of the alloy, then f/V_m will be the concentration in moles/volume and the number of moles in a volume element, AdX, will be $f/V_m dX$, where A is the cross-sectional area for diffusion. This quantity must be equal to the number of moles of Al arriving at x = X in the time dt as a result of diffusion from within the sample, i.e., for x > X. Therefore,

$$\frac{fAdx}{\bar{V}_m} = \lim_{\varepsilon \to 0} \left[\frac{AD_{Al}}{\bar{V}_m} \frac{\partial N_{Al}}{\partial x} \right]_{x=x+\varepsilon} dt \qquad (6)$$

Substitution of equations, (1) and (5) yields an enrichment factor, α, where

$$\alpha = \frac{f}{N_{Al}^{(o)}} = \frac{1}{\gamma\pi^{1/2}} \left(\frac{D_{Al}}{D_o} \right)^{1/2} \frac{\exp(-\gamma^2\theta)}{\operatorname{erfc}(\gamma\theta^{1/2})} \qquad (7)$$

For the case of interest here, $D_o N_o^{(s)} << D_{Al} N_{Al}$, i.e., the oxygen permeation is significantly less than that of Al, the product $\gamma\theta^{1/2} << 1$. Therefore

$$\alpha \sim \frac{3}{\pi} \left(\frac{N_{Al}^{o} D_{Al}}{N_{Al}^{(s)} D_o} \right) \qquad (8)$$

When α is large, one expects the accumulation and lateral growth of the internal oxides to form a continuous layer, i.e., the transition to external oxidation. Wagner states that when the volume fraction of oxide, $g = f(V_{ox}/V_m)$, reaches a critical value, g*, the transition from internal to external scale formation should occur. Rearrangement of equation (8) then gives the criterion for external oxidation as

$$N_{Al}^{(o)} > \left[\frac{\pi g^*}{3} N_o^{(s)} \frac{D_o V_m}{D_{Al} \bar{V}_{ox}} \right]^{1/2} \qquad (9)$$

Consideration of equation (9) allows estimation of how the critical concentration for external Al_2O_3 formation (or formation of an Al-rich oxide such as $NbAlO_4$) in Nb-Al alloys will be affected by (A) third element additions, (B) fabrication and (C) oxidation temperature. Clearly, the three parameters which can be significantly affected are $N_O^{(s)}$, D_O, and D_{Al} with decreases in the first two and increases in the third favoring external scale formation at lower $N_{Al}^{(o)}$.

(A)-Effect of Third Element Additions

Third element additions can affect any or all of the three important parameters: N_O, D_O, and D_{Al}.

(1) Oxygen Solubility- The solubility of oxygen in Nb , i.e., at the Nb/NbO equilibrium(9), may be represented as

$$N_O^{(s)} = 0.4657 \exp\left[\frac{-3864}{T}\right] \qquad (10)$$

The oxygen solubility may be decreased through a gettering effect of the third element addition similar to that which is well known for the addition of Cr to Ni-Al alloys. Unfortunately, since ideally the oxide of the third element should be intermediate in stability between that of Al and the lowest oxide of Nb, there are a limited number of elements which can perform this function. Principal among these are V, Si, and Ti.

The oxygen solubility may also be influenced by some elements in a direct manner. Additions of Mo, Re, and Ru have been found to decrease the oxygen solubility in Nb with the effectiveness of the additions corresponding to the amount by which they increase the electron/atom ratio (e/a) in the alloy(10), as shown in Fig. 3. These same additions have been found to increase the heat of solution of nitrogen in Nb with a corresponding decrease in solubility (11,12). The initial rate of nitrogen absorption was also found to decrease markedly as the heat of solution was increased by alloying additions. The only detailed study of the effect of alloying on the thermodynamics of the Nb-O system, of which the authors are aware, is that by Albert et al(13) on the effect of Mo and V additions. Additions of Mo were found to increase the activity coefficient of O in Nb at 1000°C which is consistent with decreased

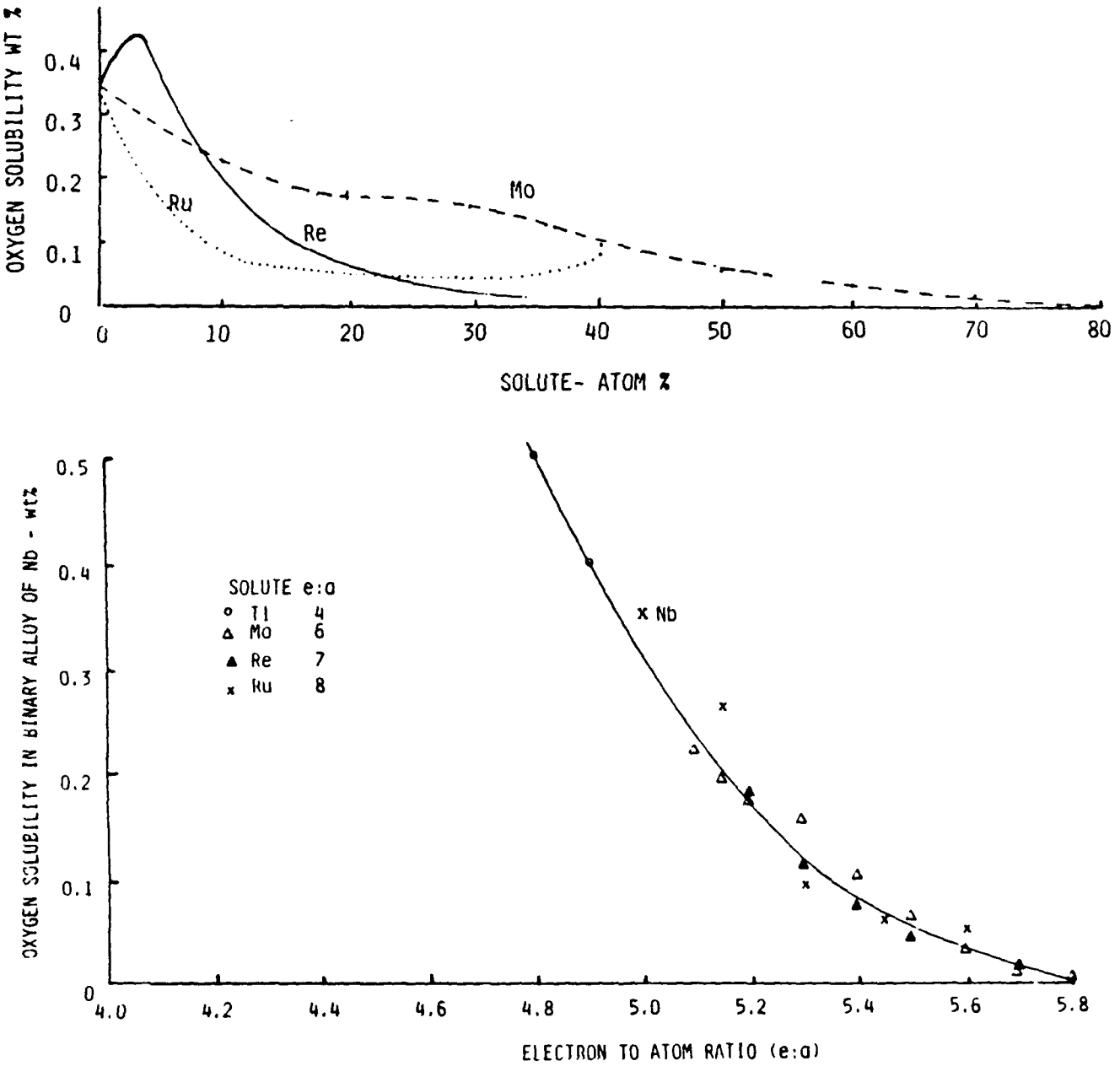

Figure 3: Effect of electron to atom ratio on solubility of oxygen in Nb base alloys (after Ref.10).

oxygen solubility. The effect was concluded to result from alterations of the electronic structure of Nb, presumably, increasing e/a. However, V additions, which should have no effect based on e/a considerations, resulted in a significant decrease in activity coefficient. This was explained on the basis of an unspecified attractive interaction between V and O. The origin of the

interaction is not clear since there is only a small difference in the free energies of formation of VO and NbO.

Nevertheless, there appear to be significant effects of elemental additions which increase the electron concentration in Nb on increasing the activity and, hence, decreasing the solubility of oxygen and nitrogen with the effectiveness of an element correlating with the amount by which it increases e/a. (Parallel effects have been observed for additions to Ta(11-13). On this basis, the effect of an alloying addition of fixed atomic percent will be determined by its Group in the Periodic Table, e.g., Ru > Re > (Cr, Mo, or W).

Those elements which decrease e/a (Ti, Zr, Hf) would be expected to increase the solubility of O and N. This has been observed for Ti additions(10), as shown in Fig. 3. This effect may be masked, however, by the opposing influence that Ti can have on oxygen solubility in Nb as a result of the high stability of TiO relative to that of NbO. Titanium also will reduce oxygen diffusivity in Nb. The e:a effects for Zr and Hf also may be masked because of the high stability of ZrO_2 which results in oxide precipitation at very low concentrations of dissolved oxygen.

(2) Oxygen Diffusivity- The data for oxygen diffusivity in Nb from a large number of sources have been analyzed by Lauf and Alstetter(14) who propose the equation

$$D_0 = 6.95 \times 10^{-3} \exp\left[\frac{-110{,}000 \text{ J. mol}^{-1}}{RT}\right] \qquad (11)$$

(in cm^2/sec)

for the temperature range 25 to 1900°C. The data were not considered precise enough to substantiate the curvature in the Arrhenius plot proposed by Farraro and McClellan(15).

A number of substitutional solutes have been observed to decrease the oxygen diffusivity in Nb. These include Mo(13), Ta(14), V(13,14,16), Ti(14), and Zr(15,17). The solutes have negligible effect on the activation energy but decrease the preexponential term by processes generally described as trapping(13,14,16,17). The trapping energy is proposed to consist of a

chemical and an elastic interaction(14).

$$\Delta E_x = f(A) + g(\varepsilon) \qquad (12)$$

where

$$A = \Delta H^{o}_{NbO} - \Delta H^{o}_{MO}$$

$$\varepsilon = \frac{\gamma_{Nb} - \gamma_{M}}{\varepsilon_{Nb}}$$

"A" is a measure of the relative affinity for oxygen between Nb and the solute, as measured by the enthalpy of formation of their oxides and "ε" is a measure of the size mismatch of the solute in the Nb lattice. Thus solutes with more negative enthalpies of formation of their oxides and/or smaller atomic radii, as compared with Nb, are expected to provide attractive traps and decrease D_o. These parameters are compared in Table 2. The solutes for which trapping energies are available fit the model reasonably well. Thus V, with a value of A only slightly larger than Ta, is a considerably more effective trap than Ta because the V atom is considerably smaller. Similarly Ti is as effective as Zr as a trap even though the A parameter is somewhat more favorable for Zr. Additions of Mo to Nb have produced small decreases in D_o(13), even though the A parameter for Mo is quite unfavorable, presumably because of the negative value of ε. Data for Re additions to Nb are not available but Re additions to Ta(13) were observed to slightly increase D_o at high temperatures which is consistent with a large negative value for A. Based on the above considerations, two elements which should provide effective oxygen traps in Nb are Hf based on its large positive value of A, coupled with a slightly smaller radius than Zr and Cr, based on its large negative value of ε.

(3) Aluminum Diffusivity- Unfortunately, extensive diffusivity data for Al in Nb are not available. The only data available were obtained by back-calculating diffusivity from the evaporation rates of Al from dilute Nb-Al alloys (18). These data may be summarized as

$$D_{Al} = 450 \exp\left[\frac{-429{,}820 \text{J/mol}^{-1}}{RT}\right] (m^2/sec) \qquad (13)$$

TABLE 2

Parameters Affecting Substitutional
Oxygen Interactions in Niobium

Element M	ΔE_{M-O} (kJ/mole)	Chemical Affinity A, kJ/mole O	Size Mismatch $\varepsilon^{(o)}$
Re		-203.4	-4.2
Mo		-125.8	-4.7
Cr		-43.1	-12.6
Ta	29*	-10.5	0
V	53	+12.1	-7.9
Ti	67*	+123.0	0
Zr	67*	+130.7	+11.2
Hf		+136.8	+10.5

*- MEASURED IN REF. 17

Combination of this diffusivity with the solubility and diffusivity of oxygen in Nb allow $N_{Al}^{(o)}$ to be calculated from Equation (9) assuming a reasonable value of $g^* \sim 0.3$. These values are tabulated as a function of temperature in Table 3. It is seen that the amount of Al required decreases markedly with increasing temperature but never decreases below unit mole fraction. These impossible values indicate the conditions used in deriving eq.9 are not valid for the binay Nb-Al system. The calculation, of course, is based on parameters for the b.c.c. β phase. It has been observed that Al_2O_3 can form on the intermetallic compound $NbAl_3$ ($N_{Al}^{(o)} = 0.75$). However, a rutile-type oxide of Nb and Al ($NbAlO_4$) also is formed. Furthermore, the diffusivity data for D_{Al} are somewhat questionable and pertain to extremely dilute Al concentrations. In b.c.c. Ti-Al alloys, the interdiffusion coefficient has been found to markedly increase with Al content(19) so that the value of D_{Al} used here is probably an underestimate. Nevertheless, these calculations indicate that it is difficult or impossible to form Al_2O_3 scales on binary Nb-Al alloys at low enough Al contents to consider them "Nb-base."

The use of other alloying elements to accelerate the diffusion of Al would enhance the ability of a Nb-alloy to form a protective Al_2O_3 surface layer. Morral et al(20) have provided a formalism for describing the effects of ternary (and higher order) alloying additions on the flux of Al to the surface of an alloy undergoing oxidation. Unfortunately, no data are available for evaluation of the formalism. Indeed, Table 3 indicates that at 1100°C a

decrease of about three orders of magnitude in $N_{Al}^{(o)}$ is required for a viable alloy. As a result of the square-root form of Eq. 9, this would require an

TABLE 3

Estimated Values of $N_{Al}^{(o)}$ for External Al_2O_3 Formation on Nb-Base Alloys

T °C	$N_{Al}^{(o)}$ (Binary)	$N_{Al}^{(o)}$ (Nb-10Cr-20Ti)
1100	445.0	2.65
1400	46.5	0.465
1700	9.7	0.14
2000	3.0	0.06

increase of D_{Al} of about six orders of magnitude which is unlikely to be accomplished. An increase of 2-3 orders of magnitude might be possible if the solubility of Al in Nb could be increased such that a high Al content b.c.c. solid solution existed. The D_o in b.c.c. solid solutions and compounds is highest for all crystal structures. As shown in Fig.4, the maximum solid solubility of Al in Nb is about 10 at.% at 1100°C and only 15 at.% at 1600°C. It is deemed unlikely that alumina could be formed on alloys with less than 15 at.% Al based on the behavior of other known alumina formers based on Fe, Ni, or Co. An alternate approach would be to use a Nb-Al compound with a b.c.c. structure as the base. Even with this, however, it seems likely that alloying additions to Nb-Al alloys must be directed at both maximizing D_{Al} and minimizing D_o and $N_o^{(s)}$.

(4) Summary of Third Element Effects- The addition of third elements to Nb-Al alloys to promote external Al_2O_3 scales must be directed at (1) decreasing $N_o^{(s)}$, (2) decreasing D_o, and (3) increasing D_{Al}. The elements which should be most effective in (1) are Ru, Re, Mn, Cr, Mo, and W. Those which should be most effective in (2) are Hf, Zr, Ti, V, and probably Cr and Mn. Sufficient data are not available to determine which elements are effective in (3) but increased Al concentration probably results in an increased value of D_{Al}. An additional consideration is the effect of the third element in maintaining the phase with the largest values of D_{Al}. As

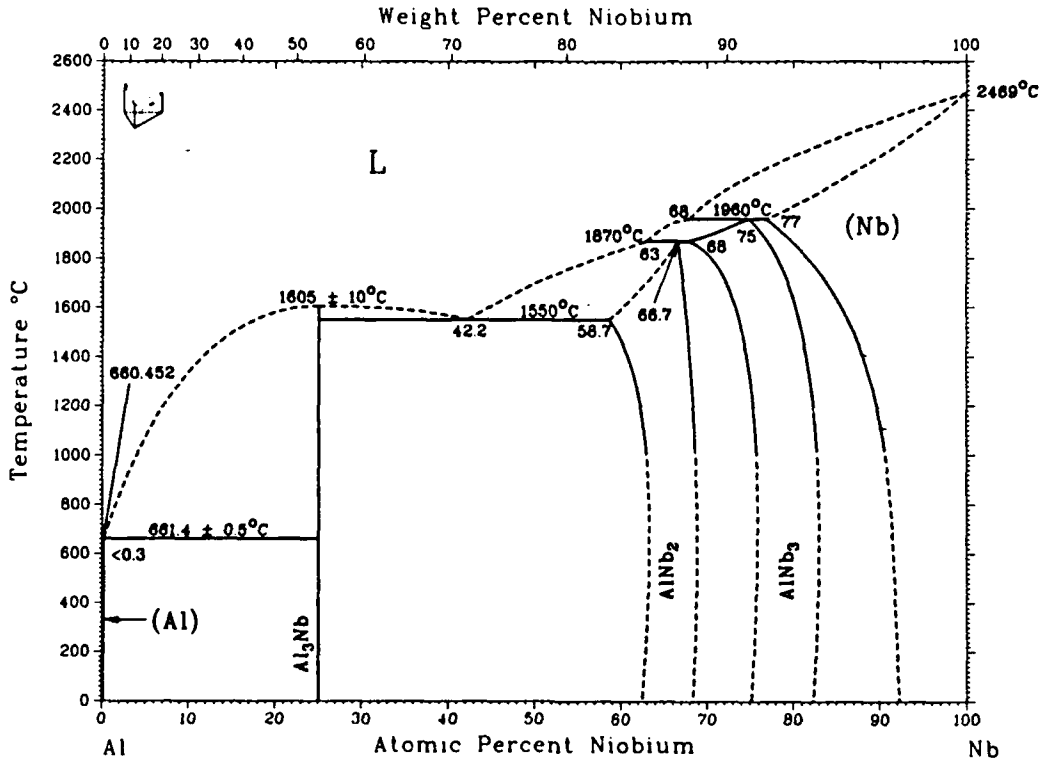

Figure 4: Nb-Al Phase Diagram (Ref.21)

noted above, this phase should be either an extended b.c.c. solid solution or a b.c.c. ordered compound. The only cubic phase in the Nb-Al system other than the terminal solid solution is Nb_3Al which is very brittle and does not form an alumina scale(4). As indicated in Fig.4, the cubic Nb_3Al phase has a narrow range of stoichiometry that decreases to less than 5 at.% with increasing temperature. This phase has a maximum solubility of only 20 at.% Al at 1600°C. Increasing the solubility of Al in the b.c.c. solid solution to levels above 20 at.% may be feasible whereas a significant increase in Al solubility in Nb_3Al may be quite difficult to achieve. Therefore, those elements which increase the solubility of Al in b.c.c Nb will be of most interest. Additions of Ti, Fe, Cr, and V should be most beneficial. Iron and Cr will reduce the melting point of Nb significantly at large addition levels. This, in effect, may help to increase D_{Al} since the homologous temperature (T/T_m) will be increased.

Based on their appearance in several of the above categories, Ti, Cr, and V would appear to be the most effective alloying additions for increasing D_{Al} and decreasing N_o and/or D_o. Based on e/a considerations(10) 10 at % Cr should give a factor of 0.5 decrease in $N_o^{(s)}$ with an additional effect in

decreasing D_o approximated as 0.1 based on atomic size. Also, using the trapping model described by Lauf and Altstetter(14), one would predict that 20 at % Ti would decrease D_o by a factor of 0.007 at 1100°C and 0.02 at 1400°C. As shown in Fig. 5, 50 at.% Ti should nearly double the solubility of Al in Nb at 1100°C.

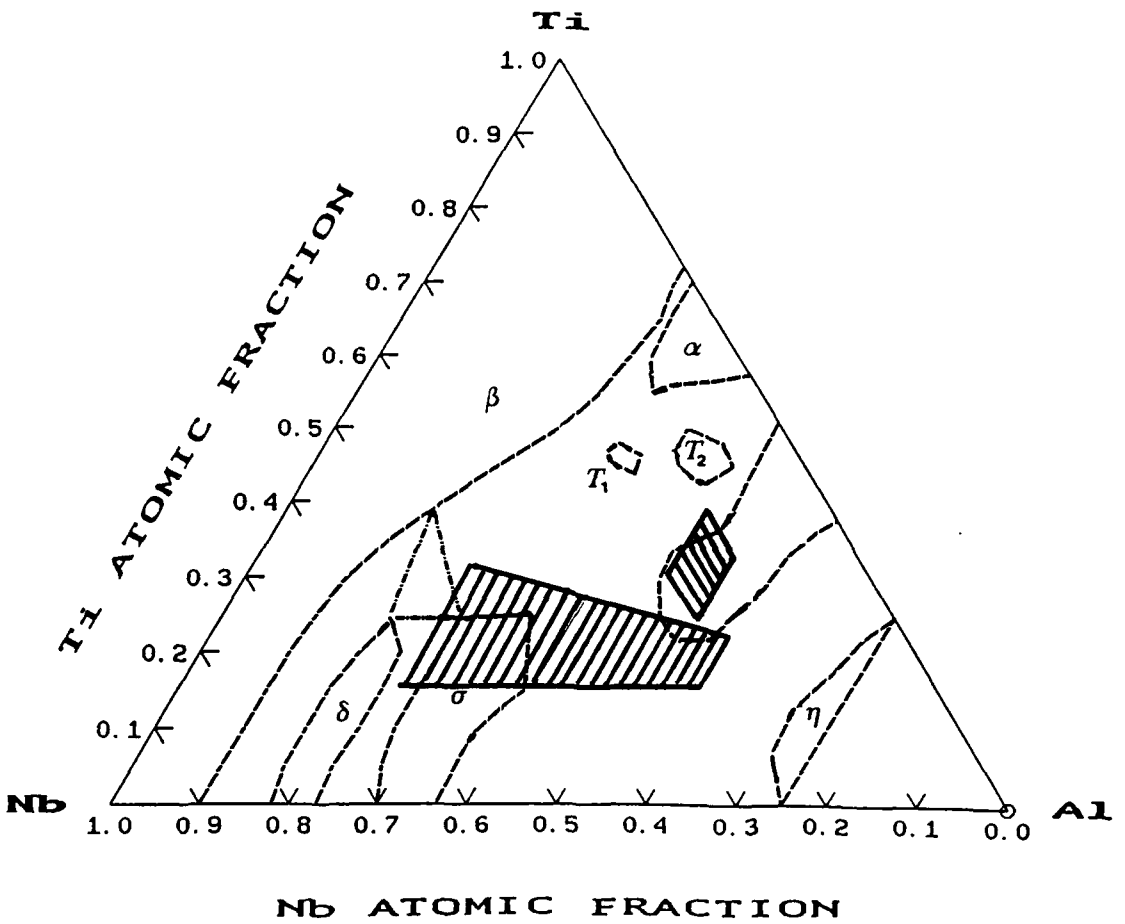

Figure 5: Phase equilibria in the Nb-Ti-Al system(22).

It is estimated the the solubility of Al at 1400°C will be doubled by the addition of as little as 20 at.% Ti. A similar effect should be observed with additions of vanadium. These elements form a continuous b.c.c. solid solution with Nb and can dissolve 42-48 at % Al in a b.c.c solid solution as binary systems. Based on these considerations and assuming that the Al additions produce an increase in D_{Al} by a factor of 10, the critical value of $N_{Al}^{(o)}$ has been calculated for an Nb-10 at % Cr-20 at % Ti based alloy and results are

included in Table 3. At 1400°C, $N_{Al}^{(o)}$ is calculated to be 0.465 for this base.

(B)-Effect of Microstructure

There are few data on the effects of microstructure on the oxidation behavior of Nb-based alloys. Nevertheless, experience from other alloy systems suggests that uniformity of composition is an important factor in obtaining a protective oxide film on an alloy surface. In this regard, alloy preparation by consolidation of fine powder or by rapid solidification should provide superior oxidation resistance over conventionally cast materials with their propensity for macrosegregation of the component elements. Also, previous experience with Ni-base alloys has shown that a fine alloy grain size is advantageous in providing a larger effective diffusion coefficient for the element to be selectively oxidized, e.g., Al. In some systems, oxide dispersions have aided the formation of protective oxide films by providing preferential nucleation sites. Therefore, there are likely significant effects of microstructure on the oxidation behavior, as well as other properties of Nb-base alloys.

The use of ion implantation to alter composition and microstructure of surfaces also may be an effective approach. This technique has been used effectively in semiconductor technology and has proven to be useful in altering the low temperature, aqueous corrosion resistance of metals and alloys. Recent work, reviewed by Bennett and Tuson(23), has, however, shown that ion implantation may also allow significant alterations in high temperature corrosion to be accomplished. Bernabai et al(24) found that implantation of Al to a dose of 10^{17} ions/cm^2 into an Fe-24Cr-1.5Al-0.085Y alloy decreased the parabolic oxidation rate constant in air at 1100°C by two orders of magnitude. The reason for this difference was that the Al content of the unimplanted alloy was too low to allow formation of a continuous Al_2O_3 film so the scale was composed primarily of rapidly-growing Fe-containing oxides while an Al_2O_3 film developed rapidly on the implanted alloy. This effect may result from the increased Al concentration in the implanted region and/or enhanced Al diffusion caused by the implantation damage. Nevertheless, the existence of such implantation effects on the formation of Al_2O_3 scales on Nb alloys is worthy of study.

(C) Effect of Oxidation Temperature

The calculations leading to Table 3 indicate that Nb-alloys require significantly lower Al contents to form external Al_2O_3 films as the oxidation temperature is increased. This is the result of the fact that the activation energy for Al-diffusion is considerably greater than that for the oxygen permeability ($N_O^{(s)}D_O$). This has been experimentally observed in the work of Svedberg(4) which showed that the oxidation rate of a Nb-5.6Co-13.9Al alloy in air decreased at successively higher oxidation temperatures between 1000 and 1275°C. The solubility of Al in a BCC Nb or Nb-Ti (V) base also will increase with increasing temperature, permitting a higher concentration gradient for diffusion of Al. The analysis indicates that alumina may be formed more readily at high temperatures and that the ability to form alumina may decrease as temperature is reduced. A strong temperature dependency for alumina formation is likely to exist.

Case 2- Alumina Formation in the Presence of Transient Oxidation

The transition from internal to external oxidation of Al can no longer be determined directly from Eq. 9 when the oxygen pressure is high enough to oxidize other elements in the alloy, particularly Nb. The formation of these "transient oxides" will increase the amount of Al in the alloy required for continuous Al_2O_3 film formation. In fact, if a linearly growing transient oxide forms, the enrichment factor will be unity, i.e., there will be no enrichment of Al at the alloy surface since the Al_2O_3 nuclei formed will be continually removed into the growing transient oxide. Therefore, the transient oxides, such as Nb_2O_5, which grow with a linear rate, must be completely suppressed in order for an Al_2O_3 film to possibly form. An alloy base (Nb plus additional elements) which oxidizes parabolically (i.e., by diffusion control) in the absence of Al is required as the starting point to which Al additions may result in external Al_2O_3 formation. Moreover, the rate at which the transient oxides grow will determine how much Al, over and above that predicted by Eq. 9, is required for external Al_2O_3 formation. This problem has been recently analyzed by Gesmundo and Viani(25). These calculations show that for conditions that yield values for the initial mole fraction of solute on the order of 0.04 with no transient oxidation the critical concentration can be approximately doubled in the presence of a

rapidly growing transient oxide. Therefore, not only is a parabolically oxidizing alloy base required for Al additions to form an external film, but the oxidation rate of the alloy base is an important factor with the slowest oxidation rate being the most favorable. In this regard, the wealth of existing empirical rate data for the oxidation of various Nb base alloys provides valuable guidelines for the most favorable alloy base compositions in which to attempt to form protective Al_2O_3.

PREOXIDATION

High temperature pre-oxidation may provide an auxiliary technique for developing protective Al_2O_3 films on Nb-base alloys. Pettit (26) found that alumina scales could be formed on Ni-11.8%Al alloys at low oxygen pressures but not in oxygen at 1 atm. Scales preformed at low pressure initially were protective but eventually gave way to accelerated kinetics that were comparable to those for the alloy without preoxidation when the oxygen pressure was increased. Preoxidation also has been effective in reducing transport of second oxidants through chromia scales. Oxides formed on pure Cr in oxygen are barriers to transport of nitrogen whereas oxides formed in air are not (27). Chromia formed on stainless steels is a barrier to the transport of sulfur if the scale is preformed in the absence of sulfur(28). The protection, however, could not be sustained at 982°C and the scales broke down after 100-500h exposure to sulfidizing gases. A similar behavior was found for the formation of alumina scales on FeCrAl alloys. In general, preformed oxide scales are susceptible to failure by cracking as a result of thermal cycling or by a change in growth mechanisms when the atmosphere is changed. If the preformed scale is damaged, it most likely cannot be reformed in the more aggressive atmosphere. Most results indicate a low potential for long term protection by preoxidation. The technique, however, does provide an additional means for defining more clearly the factors that govern the formation, growth, and breakdown of protective oxide scales.

EXPERIMENTAL

PREPARATION OF ALLOYS

Most experimental alloys were prepared by low pressure argon arc- melting and drop casting at LMSC. A 20-30 gm charge of high purity elemental alloy additions was premelted on a water-cooled copper hearth with a non-consumable tungsten electrode. The furnace was evacuated to 10^{-5} torr and back filled with high purity argon to 1/2 atm. for melting. The button ingots were melted four times and were turned over after each melt. The flat hearth was then replaced with a water cooled copper drop cast hearth. The casting cavity was 14mm x 14mm deep. The button ingot was placed over the cavity and melted with the arc until the metal dropped into the mold.

Good quality castings of most of the Nb-base alloys were produced by this technique. However, problems with thermal stress cracking were encountered in melting alloys containing large additions of Re, Mo, and Fe. Drop cast buttons cracked on cooling and often shattered on arc heating to remelt an ingot. This problem was solved by going to a micro-arc melting process in which a small 1-5 gm button ingot was produced without severe cracking. A small mass of the alloys could be cooled rapidly without cracking.

In addition to the drop cast ingots and micro-melted buttons, several larger buttons of selected alloys were prepared by arc melting at Teledyne Wah Chang, Albany, Or (TWCA). These ingots, weighing about 150g each, were melted in argon on a water cooled copper hearth using a non-consumable tungsten electrode. Ingots were melted four times and were turned over after each melt.

The composition of all alloys prepared during the three years of research is presented in Table A1, Appendix. Alloy compositions are reported as atom %, nominal, and are based on the charged weight used in melting buttons unless otherwise stated. Negligible weight loss on melting was found in all cases. At LMSC, for example, the weight loss for a 3g micro-melted button ranged from 0.006 to 0.03 g (0.2-1.0 wt.%) with loss directly proportional to the total aluminum content of the alloy. The two alloys melted by TWCA were analyzed for composition and results are given in Table 4:

TABLE 4

Chemical Analysis of arc-cast alloys

	wt.%					ppm by wt.		
	Nb	Ti	Al	Cr	V	O	H	N
70-1 Nominal	45	22	24	4	5			
Obtained	45.3	22.6	24.3	4	5	470	6	26
70-3 Nominal	41.6	19.5	24.2	8.5	6.2			
Obtained	41.7	20.0	24.1	8.2	6.1	460	<5	31

The actual compositions are very close to the nominal (% added). Interstitial content is low, indicating good materials and process controls on melting.

RAPID SOLIDIFICATION PROCESSING

Four Nb-Ti-Al-Cr-V alloys (70-1, 70-3, L4001, L4002) were first consolidated in the form of small buttons or ingots by vacuum arc melting. Small pieces of each alloy were sent to the University of Florida where they were remelted and rapidly solidified as splats by the Solidification Processing group of the Department of Materials Science and Engineering. Pea sized samples were levitation induction melted in a vacuum drop tower with a variety of superheat or undercool conditions. The samples were dropped by cutting the induction power and splats were formed by impacting the molten drop between cooled anvils. Stops were used to regulate splat thickness to between 1000 and 2000μm. While thinner splats would be more desirable with respect to beneficial effects of rapid solidification, they could not be evaluated for oxidation behavior. A thickness of 1000μm was considered to be a minimum thickness for oxidation testing considering the amount of material consumed by scaling, alloy depletion, and interstitial penetration in tests at 1100-1300°C.

ION IMPLANTATION

Specimens of alloys 70-1 and 70-3 were polished through 600 grit SiC and implanted with Si^+ or Al^+ ions. The implantation was performed in the Surface Modification and Characterization Collaborative Research Center of Oak Ridge National Laboratory. In all cases the acceleration potential was 150keV and the dose was 10^{17} ions/cm^2. Computer simulation of the implantation process

resulted in predicted maximum concentrations at depths of 1700Å for Al^+ and 1500Å Si^+ ions, respectively. One specimen of 70-1 which was Al-implanted on one side was examined by Auger electron spectroscopy during sputtering. The sputter profiles indicated a 100A thick layer on the implanted surface which contained Al and O and was, presumably, alumina. The total specimen depth sampled in the sputter profiles was approximately 500Å so it was not possible to evaluate the accuracy of the computer-calculated profiles.

Samples of Nb-Ti-Al-Cr-V also were implanted with Al and Y ions at a facility in the Lawerence Berkeley Laboratories, Berkeley, Ca. The 10x15x1mm samples polished through 600 grit were implanted on one side with an accelerating voltage of 100 kev. The dosage was $1x10^{17}$ ions/cm^2 nominal. The effect of implantation was evaluated by a comparison of the oxide scales formed on the implanted and unimplanted sides after exposure to air for 2h at 1100°C.

OXIDATION EXPERIMENTS

Oxidation reactions and kinetics were studied under isothermal conditions in oxygen at 800 to 1300°C and air at 800 to 1600°C. Oxidation coupons were cut from the as-cast ingots using a diamond wafering blade. The coupons were polished through 600 grit SiC paper and cleaned in acetone and methanol immediately prior to oxidation.

Screening Tests

Short term isothermal screening tests were performed in air using a $MoSi_2$ element box furnace for a preliminary examination of the oxidation and microstructural behavior of experimental alloys. Samples were weighed to an accuracy of 0.01 mg and measured for calculation of surface area. The samples were placed in high purity, dense alumina boats and the sample + boat combination was weighed a second time. The boat was used to collect oxide flakes that may spall from the surface on cooling of the samples and provided a more accurate measurement of weight gain on oxidation. The sample + boat assemblies were loaded into a pre-heated furnace and held in static air at 1100 to 1600°C for 1-2h. Samples reached the test temperature in less than five minutes. The boats were removed from the furnace on completion of the test, air-cooled to room temperature, and re-weighed. The net gain in weight

for the sample + boat was used to calculate the gain per unit area ($mgcm^{-2}$). Each sample was examined visually for the color and adherence of the oxide scale. Selected samples were cross sectioned and polished for metallographic examination of the oxide scale and alloy interface. Qualitative SEM analyses were made in some cases to identify the elements present in the oxide scales.

Oxidation Kinetics

Reaction kinetics in oxygen (1 atm.) at 800 to 1300°C were studied at the University of Pittsburgh using a Cahn 2000 microbalance. The specimens were suspended on silica or alumina hooks in slowly flowing O_2 at room temperature and the reaction was initiated either by raising a preheated furnace around the reaction tube or lowering the sample into a heated furnace. The specimens reached the reaction temperature within 5 minutes. Oxidation runs were terminated by lowering the furnace. Holes for supporting the specimen in the weighing mechanism were drilled using an electric discharge machine.

Oxidation kinetics in air at 800-1500°C were studied at LMSC using two Cahn 1000 microbalances. A specimen was placed in an alumina boat suspended from a Pt or Rh hangdown wire. The oxidation test was started by raising a preheated furnace around the specimen. All tests were conducted with the sample and boat suspended in an open furnace (no reaction tube). A Kanthal wound tube furnace was used for tests at 2200°F (1204°C) or below while a $MoSi_2$ element box furnace was used for tests at higher temperatures to 2800°F (1538°C). The oxidation test temperature was attained in less than five minutes. Testing times ranged from 10 to 100 hours. The balance scale factor was 10mg full scale with sensitivity of 0.001mg.

A log-log plot of the weight gain per unit area vs time was made for all runs to determine the order of reaction kinetics. If the slope was close to 0.5 (parabolic kinetics) or 1.0 (linear kinetics), the data were replotted on rectangular coordinate paper with weight gain vs square root of time (parabolic) or vs time (linear) to obtain the rate constants. The parabolic rate constant was expressed in $g^2cm^{-4}s^{-1}$ while the linear rate was in $gcm^{-2}s^{-1}$.

MATERIALS ANALYSIS

Optical Metallography

Specimens were not cut for mounting in order to preserve the oxide scales. The samples were placed on edge and mounted in a special blend of wet-ground bakelite (Klarmont) specifically designed to aid in edge retention during polishing. The mount was ground by hand on 120 grit SiC paper to reveal the desired cross section of the sample for examination. About 0.125 to 0.25 in. of material was removed. The ground samples were then rough polished with 1μm diamond paste on an automatic polisher with a 300 gm load. The final polish was done on an automatic well-type polisher with a hard surface cotton cloth over a micro cloth. Samples were polished for about 30 min. with a CeO_2-Al_2O_3 abrasive using a 240 gm. weight. This technique provided excellent edge retention and permitted metallographic study of the oxide scale and metal interface at magnifications up to 3000X. Samples were etched by immersion in a solution of 2 parts HF and 100 parts methonal for 16m when it was desired to delineate the alloy structure. In most cases, however, samples were examined only in the as-polished condition.

Scanning Electron Microscopy

Selected specimens were examined using a JEOL-JSM35CF scanning electron microscope with energy dispersive x-ray analysis. Observations included the scale/gas interface and, in some cases, the cross section of the specimen and scale. All analyses were qualitative in nature and were designed to indicate significant but not absolute elemental makeup or changes in composition of the oxide scales and underlying alloy.

X-Ray Diffraction Analysis

XRD analysis of external scales was performed with a General Electric XRD-5 diffractometer. A computer program was developed to aid in the evaluation of the complex patterns obtained from most samples. Considerable difficulty was encountered as a result of numerous superimposed peaks generated by the complex oxide scales. Patterns were obtained from the top (gas exposed) surface of samples with adherent oxides and from both sides of scales that spalled from the surface. Simple scales such as alumina, titania, or aluminum

niobate were readily identified as were some scales in which these were major phases. In most cases, however, the scales were too complex with many unidentified peaks and conclusive results could not be obtained.

Melting Point

A vacuum chamber equipped with a pyrex sight glass and a calibrated disappearing filament optical pyrometer was used to determine the melting point of selected alloys. The sample is heated in a black body cavity and true temperature is measured directly without the need for an emittance correction. A small (0.125-in. dia) fractured piece of the alloy with sharp edges was placed on a zirconia rod in the center of a tubular heater made from tantalum foil. The foil was heated by direct resistance and the temperature of the sample was increased rapidly while sighting on the surface with the pyrometer. The melting range was reached in 30-45 sec. after power was applied to the heater. Rapid heating was necessary to minimize loss of Al and Ti by vaporization which would change the alloy melting point during the test. The temperature at which the sharp edges began to round and curl was taken as the solidus temperature of the sample. Heating was continued until the sample became a fully molten spherical ball. This temperature was taken to be the liquidus. The apparatus was qualified by checking the melting points of pure Pt and V. The melting point of both metals was checked within +/-5°C. The reproducibility of test data for the Nb-base alloys was +/-10°C at temperatures of 1500-1800°C.

RESULTS AND DISCUSSION

OXIDATION BEHAVIOR OF $NbAl_3$

Stoichiometric $NbAl_3$ was prepared by pack aluminizing high purity Nb sheet samples using high purity aluminum as the source material and NH_4Cl as an activator. Coatings of single phase $NbAl_3$ 50-75μm thick were deposited on the surface in 20h at 1093°C. The coated samples were exposed to air at 1350°C for 1h to form a stable oxide scale. The scale was very thick and tended to spall on cooling as shown in Fig. 6. The scale had a layered structure consisting of alternating bands of discontinuous alumina and $NbAlO_4$. The alloy beneath the scale had been depleted in Al, forming a thin layer of Nb_2Al at the scale/metal interface.

The experiment indicates that alumina can be formed in air on $NbAl_3$ at 1350°C but that the growth of a protective alumina scale cannot be sustained. Since $NbAl_3$ is a line compound (Fig.4), the next compound in equilibrium with this phase is formed as Al is removed to form the oxide. This is Nb_2Al, which, as shown in Fig.4, is an open compound with a reasonably wide range of stoichiometry. Apparently, Al diffusivity through this phase is not sufficient to maintain the flux required to form alumina as the layer thickness of the phase increases and the phase itself does not contain sufficient Al to form an alumina scale as indicated by the Wagner model (Table 3) and the experimental results of Svedberg (4). The result is a breakaway effect in which both Nb and Al are oxidized, forming $NbAlO_4$ under the original alumina scale with accelerated kinetics. This will continue until the thin Nb_2Al layer has been consumed at which time the cycle will repeat and a new alumina layer will be formed, cutting off growth of the $NbAlO_4$ scale and reforming the Nb_2Al phase at the interface.

OXIDATION BEHAVIOR OF Nb-Al-X ALLOYS

As indicated by the theoretical model, a third element must be added to reduce the N_{Al} required to form alumina. Niobium-Al alloys containing 17-40 at.% Al were used as a base for a study of third element effects. The lower Al alloys would have single or two phase structures in which both phases have a b.c.c.

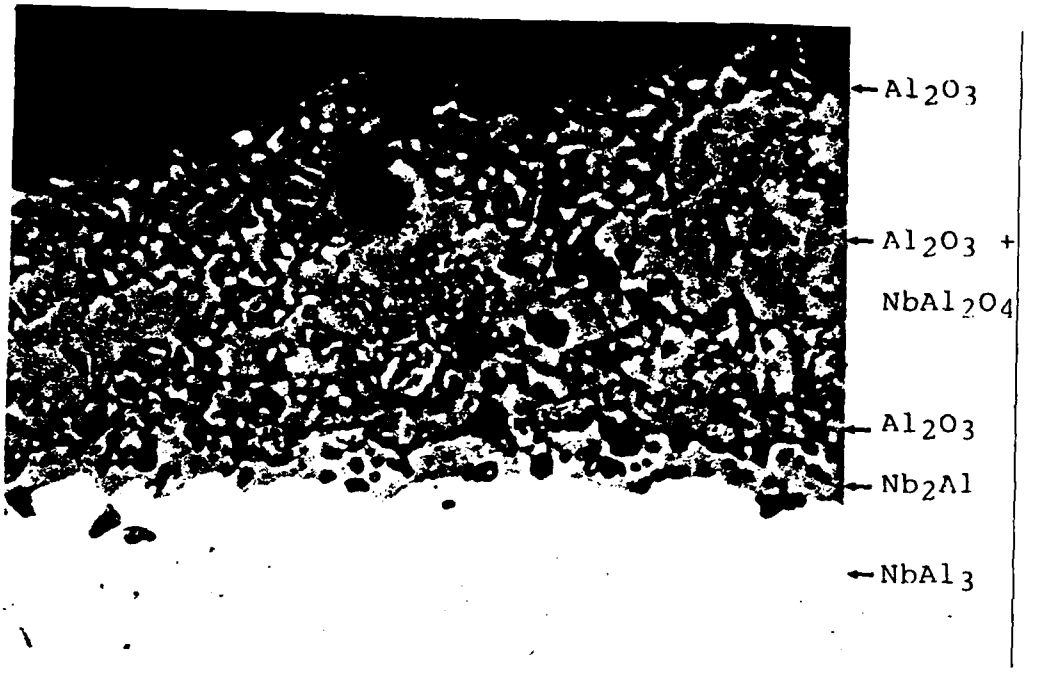

A- $NbAl_3$, 1h-1350oC, Air

13µm

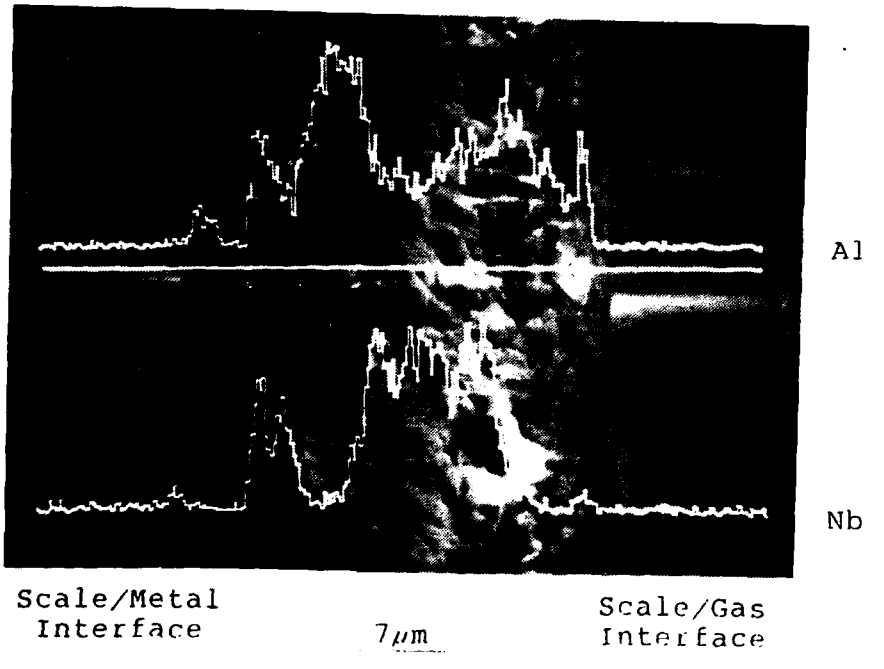

Scale/Metal Interface

7µm

Scale/Gas Interface

B- Al and Nb Profiles of Oxide Scale

Figure 6: Oxide scale formed on $NbAl_3$ in air at 1350°C.

structure (Nb-Al solid solution, Nb_3Al) while the higher Al alloys would have single or two phase structures with b.c.c Nb_3Al as the matrix and Nb_2Al as a second phase. Alloys with more than 30% Al would be single or two phase with a sigma phase (Nb_2Al) as the matrix and $NbAl_3$ as a second phase (Fig.4). Third elements selected on the basis of their potential for reducing D_o or N_o or increasing D_{Al} were added as replacements for part of the Nb. The results of experiments are summarized in the following sections on the basis of the class of element added.

Alloying to Decrease D_o

Hafnium and Zr were selected as elements to add to Nb-Al alloys to decrease oxygen diffusivity. Alloys containing 20-29 at.% Al and 1-4 at.% Zr or Hf were prepared and tested for resistance to oxidation by oxygen at 1100°C. Alloy compositions are presented in Table A1 (alloys 1a,4b,7c,39-4,39-5,39-6, and 39-7). The results of oxidation tests are summarized in Fig.7. Oxidation behavior of the alloys was similar to that of pure Nb. Plots of the data on a log-log basis indicated an essentially linear rate of oxidation. The linear rate constant was decreased slightly with additions of Zr and Hf as indicated below:

Table 5

Effect of Zr and Hf on Oxidation Behavior of Nb-Al Alloys

	Slope "n"	Log k_1 ($gcm^{-2}s^{-1}$
Pure Nb	1.0	-4.73
21Al-1.7Zr	0.79	-5.29
28Al-1.6Zr	0.86	-5.33
28Al-3.3Zr	0.72	-5.11
29Al-3.9Hf	0.88	-4.93

Hafnium appeared to be less effective than Zr but neither addition had any appreciable effect on oxidation behavior.

The analysis of XRD patterns from the scales and visual appearance of the scale indicate the formation of Nb_2O_5 as a principal scale component. The growth mode of this oxide results in continuous scale cracking which,

apparently, incorporates any alumina that is formed into the outer scale before it can become continuous. While these additions may have decreased the

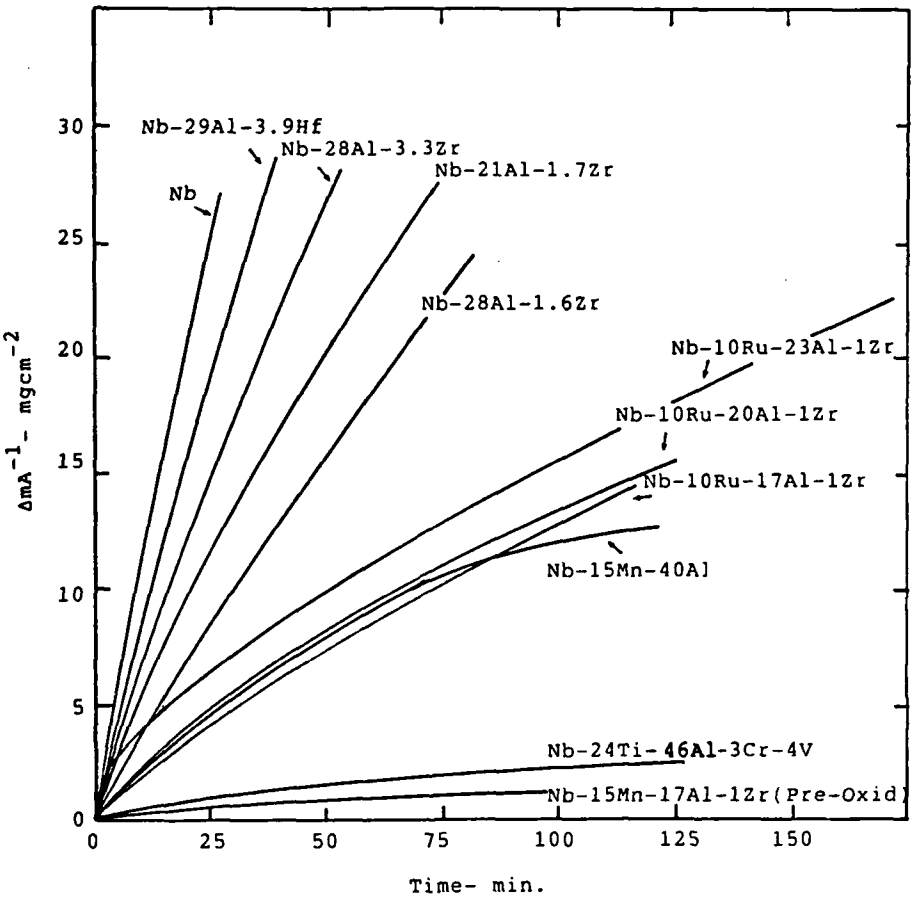

Figure 7: Oxidation rate curves for Nb-Al alloys modified to reduce D_o and N_o.

diffusivity of oxygen in the alloy, they did not alter the basic oxidation process and did not suppress the formation of a rapidly growing transient oxide. As indicated by the analysis of the theoretical model (Case 2), a slow growing (parabolic rate) transient oxide must be formed to permit surface enrichment of Al. Transient oxides that grow at a linear rate must be suppressed completely in order for an alumina film to form.

A second series of experiments was conducted in which Ti, V, and Cr were added as substitutional solutes in place of Nb as an approach to reducing D_o and altering the basic transient oxidation products as well. These elements would be expected to act as oxygen traps in the alloy and with sufficiently large additions, should produce complex oxides with Nb or Al to replace Nb_2O_5 as the

transient oxide. Wukusick(6) found that oxidation resistance was improved and that complex niobate and alumina scales could be formed on Nb-Al alloys modified with Ti and Cr. However, as shown by shaded area #1 in Fig.5, the alloys that he found to be improved are, in effect, gamma TiAl modified with Nb. The alloys were reported to have a gamma TiAl structure as determined by XRD analysis. The current study by LMSC covered a wider range of alloys with lower Ti and higher Nb contents as indicated by shaded area #2 in Fig.5.

Screening studies of Nb-Ti-Al alloys with a 1:1 Nb:Ti ratio and 33 to 50 at.% Al revealed that a dramatic change in oxidation behavior occurred when the Al content was increased to 44 at.% as shown below:

Table 6

Effect of Ti on Oxidation Behavior of Nb-Al Alloys

	1h-1400°C-Air $\Delta m/a$ - $mgcm^{-2}$
33Nb-33Ti-33Al	14.1
33Nb-32Ti-35Al	10.2
28Nb-28Ti-44Al	2.94
25Nb-25Ti-50Al	2.92

As shown in Fig.8, the alloy with 33% Al formed a mixed oxide scale with internal oxidation of Al at 1100-1400°C while the alloy with 50% Al formed an external mixed oxide scale with a continuous inner scale of alpha alumina and no internal oxidation. The external scale is a transient oxide that is a mixture of Al and Ti niobates whose growth at 1400°C was cut off by a slower growing inner scale of pure alumina. At 1100°C, the alumina scale was not continuous and growth of the niobate external scale was not cut off in the 2h exposure.

Oxidation rate curves for the alloys in air and oxygen at 800-1300°C are shown in Figs. 9-10. The curves at 800 and 1100°C are curved upward and have rate law exponents of 1 or greater than 1 (Table A-3). Although a complex niobate scale was formed in the place of Nb_2O_5 as the principal oxide, a linear rate law still prevailed in this temperature range. The log of the linear rate constants at 1100°C were -5.46, -6.36, and -6.57 for the alloys with 33, 45, and 50 at.% Al respectively. These are significantly lower than the value of

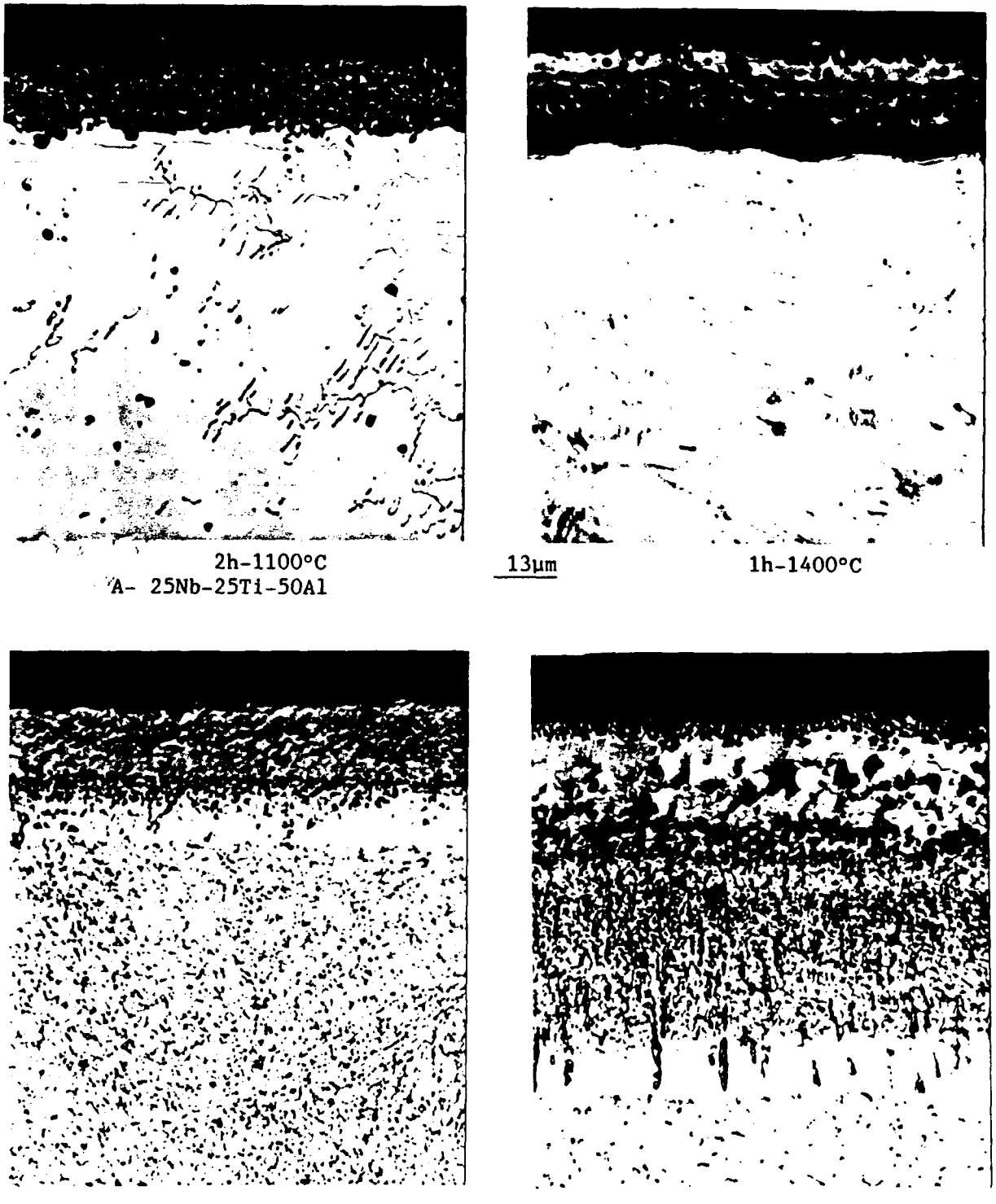

Figure 8: Oxide scales formed on Nb-Ti-Al alloys in air at 1100-1400°C.

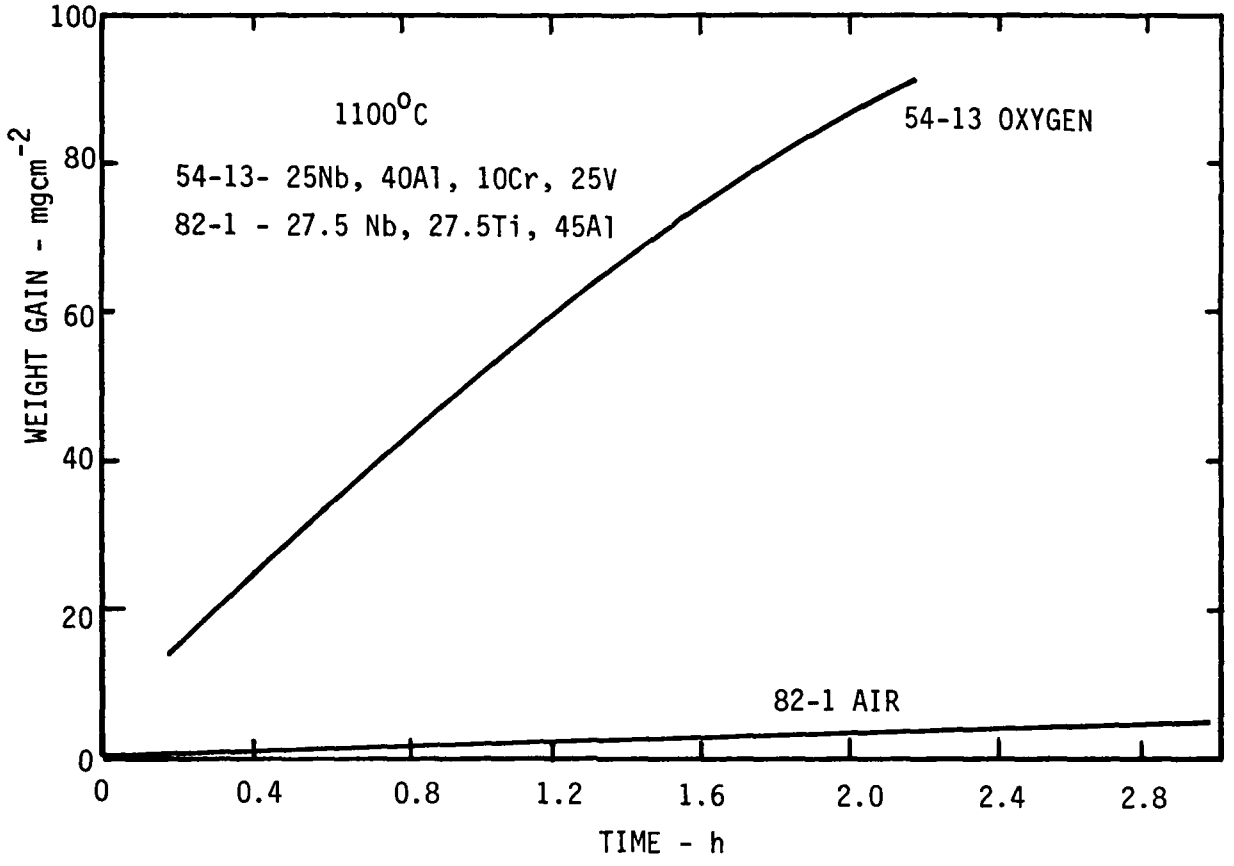

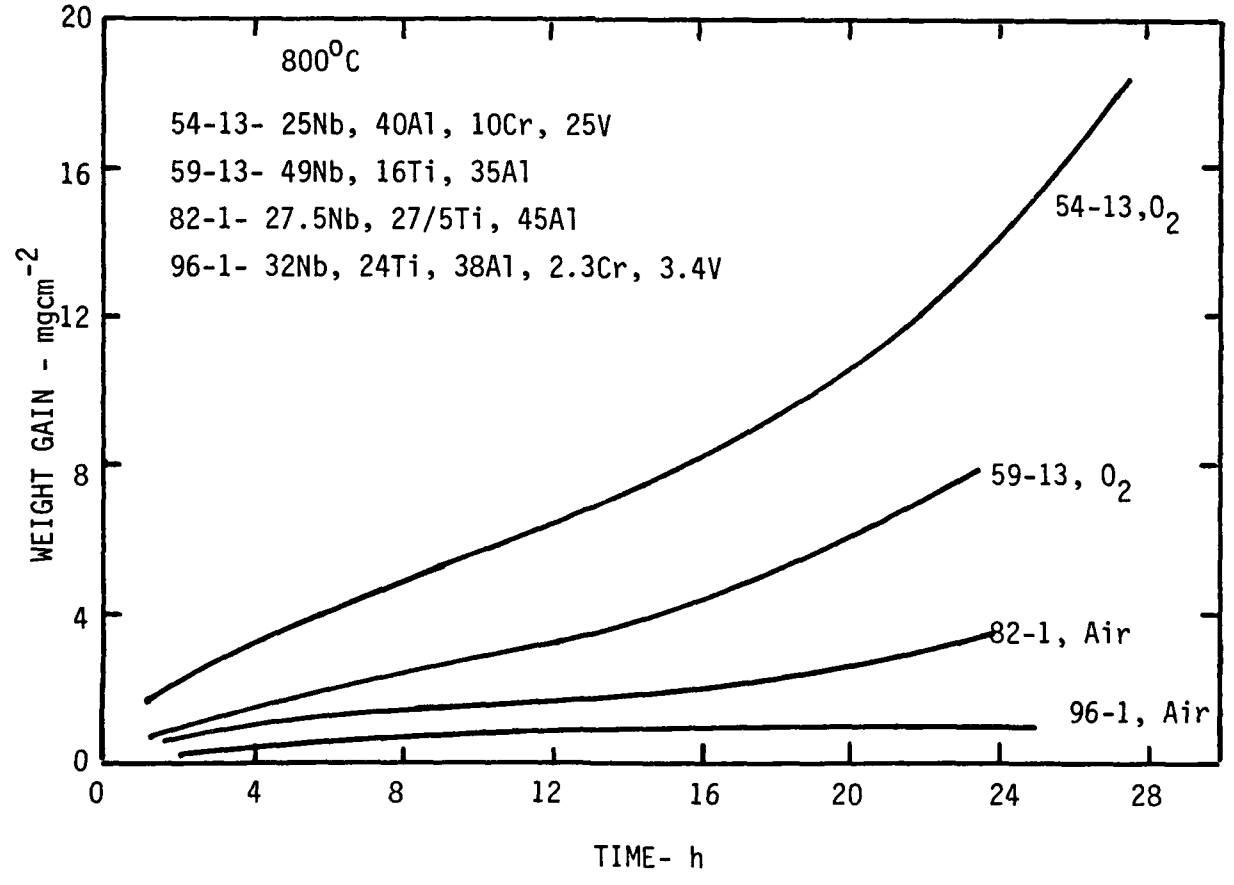

Figure 9: Oxidation rate curves for Nb-Ti-Al alloys at 800-1100°C

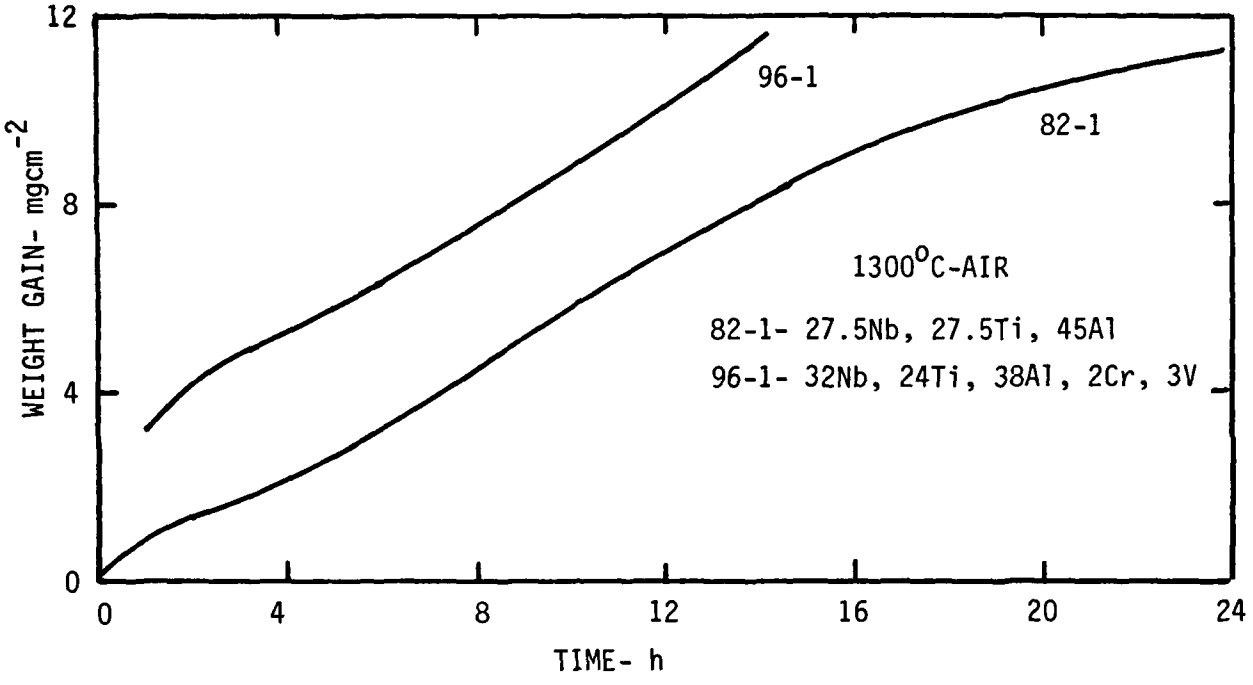

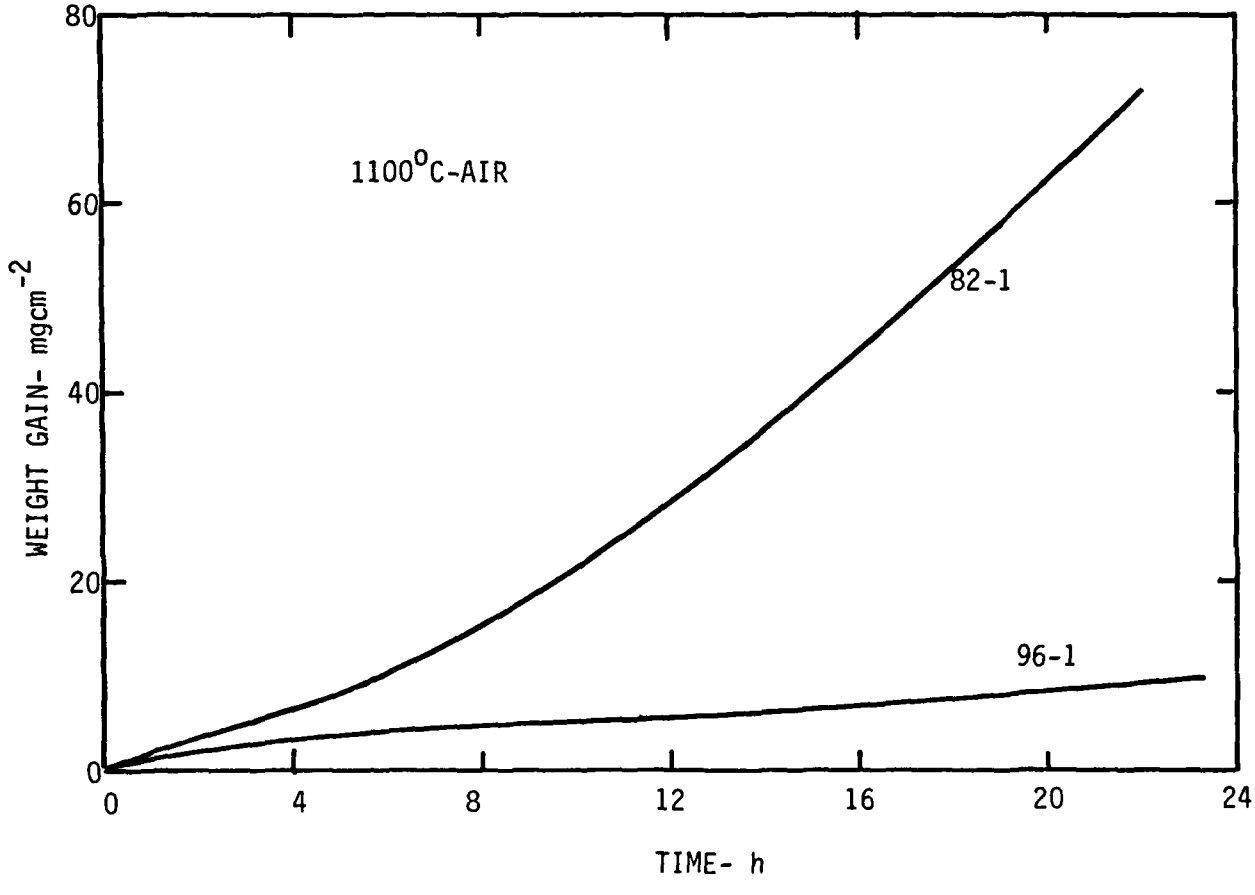

Figure 10: Oxidation rate curves for Nb-Ti-Al alloys at 1100-1300°C.

-4.73 for unalloyed Nb. The addition of Ti reduced the rate of transient oxidation significantly but not to the point where the slower growing alumina phase could be formed below 1300°C. Since alumina forms with a very high activation energy, the growth rate accelerates greatly as temperature is increased and a continuous alumina scale can be formed above 1300°C. The results indicate that the key factor may be the relative growth rates of the two scales.

A similar effect was achieved by the addition of V and Cr to a Nb-Al alloy containing 40 at.% Al. As shown in Fig.11, a continuous alumina scale formed on an alloy of 25Nb-25V-10Cr-40Al in air at 1400°C. A V-rich transient oxide that was molten at this temperature formed initially but was cut off by the growth of the alumina scale in just a few minutes. The oxidation rate

Nb-25V-10Cr-40Al (54-13)

Figure 11: Oxide scale formed on 25Nb-25V-10Cr-40Al alloy in air, 1h 1400°C.

curves for this alloy (Fig.9) had rate law exponents of of 0.77 and 0.72 at 800 and 1100°C respectively in oxygen. The log of the linear growth rate constant was -4.89, the same as that of Nb, during the first hour of exposure at 1100°C. The growth rate is far too rapid for alumina to be formed at this temperature. However, at 1400°C, the growth of alumina was sufficiently fast

to cut off the rapidly growing liquid transient oxide. It is possible that the high vapor pressure of vanadium oxide at this temperature enriched the oxide and underlying metal in Ti, Al, and Nb, slowing down the rate at which a condensed oxide scale formed on the surface. This would permit surface enrichment of aluminum as needed to form an alumina scale.

It may not be necessary to form a transient oxide that grows with parabolic kinetics as first believed provided that the growth rate is very slow in the low temperature range where alumina grows at a very slow rate. It is considered unlikely, however, that scales formed at a linear rate will grow sufficiently slow at temperatures below 1300°C compared with the rate of alumina growth for the latter to be formed as a continuous scale. Therefore, it may be concluded that elements whose sole effect is the reduction of D_o will not be effective in enhancing protective Al_2O_3 formation. The additions must alter the transient oxidation products, shifting kinetics toward parabolic, as well as reducing oxygen diffusivity in the alloy in order to be effective.

Alloying to Decrease N_o

Rhenium, Mo, Cr, Ru, and Mn were selected as the elements to add to Nb-Al alloys to decrease the solubility of oxygen based on increasing the electron to atom ratio of the alloys. These elements were substituted for Nb in alloys containing 17-40 at.% Al and were screened for resistance to oxidation by heating in air for 1h at 1400°C. The addition of large amounts of Re appeared to reduce significantly the oxidation rate of alloys containing 20-40% Al as indicated by the weight gain data in Table 7. Gains of 1-3 $mgcm^{-2}$ in 1h at 1400°C in air are representative of oxidation resistant alloys forming alumina with a small amount of transient oxide. The weight gain for the Nb-Ti-Al alloy is typical of alloys that form non-protective scales and oxidize with close to linear kinetics. The Re addition was selected to produce a Nb-Re base with an e/a of 5.8, the value at which oxygen solubility was reported by Bryant (10) to be negligible (Fig.3). The results would indicate a very significant effect of oxygen solubility on oxidation behavior.

Examination of metallographic cross sections of the Re-modified alloys, however, revealed that very thick non-protective oxides had formed on these

Table 7

Effect of Re on Oxidation Behavior
of Nb-Al Alloys

	1h-1400°C-Air $\Delta m/a\text{-}mgcm^{-2}$
40Nb-27Ti-33Al	17.9
48Nb-32Re-20Al	1.81
42Nb-28Re-30Al	2.86
36Nb-24Re-40Al	0.72

materials (Fig.12). The low weight gains were not consistent with the observed thickness of oxide scales which indicates a behavior similar to the Nb-Ti-Al alloys with <44% Al. A linear oxidation behavior similar to that of unalloyed Nb is indicated by the alloy cross sections. Rhenium forms a very volatile oxide and it is concluded that a large amount of Re was lost by evaporation as an oxide during the test. Extensive porosity is evident in the oxide scale formed on the alloy with the highest Re content (Fig.12).

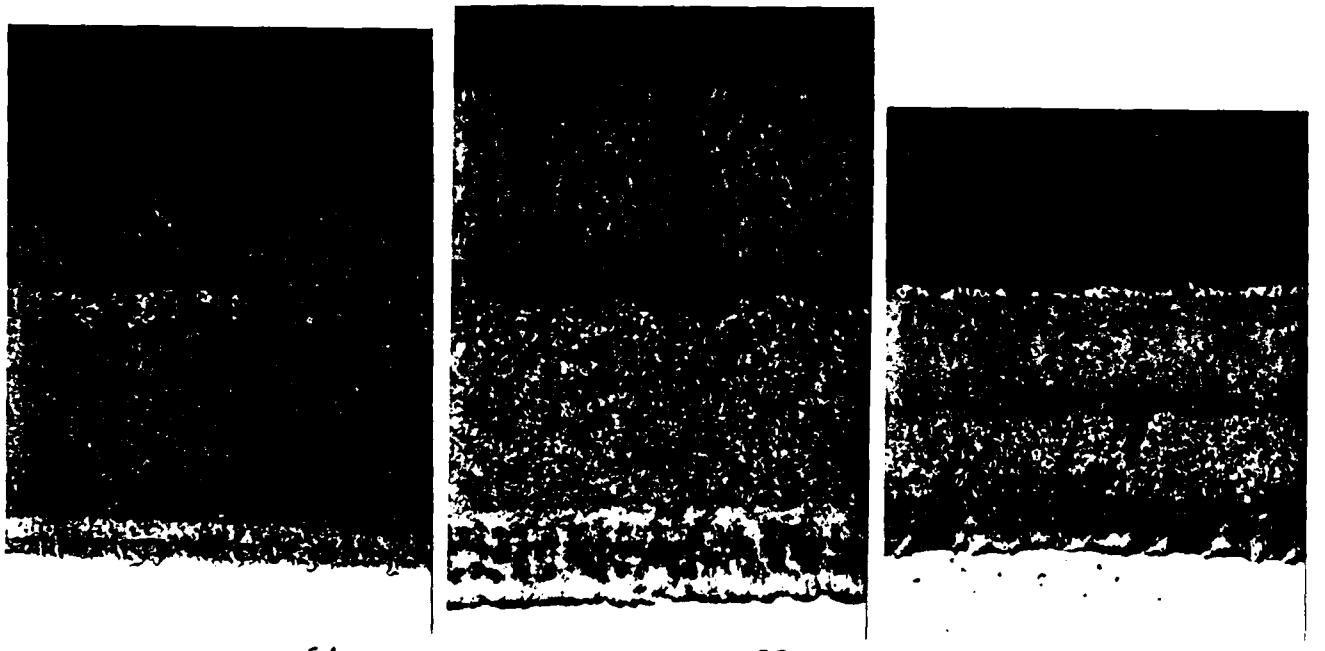

64 μm
A - 32Re-20Al
(54-14)

32 μm
B - 28Re-30Al
(54-15)

32 μm
C - 24Re-40Al
(54-16)

Figure 12: Oxide scales formed on Nb-Re-Al Alloys in air, 1h-1400°C.

Rhenium is a heavy metal and the weight gain data have been offset as a result of Re loss. In some tests, samples were found to lose instead of gain weight even though adherent, thick oxide scales were formed. The addition of Re to increase e/a and to reduce N_o was not effective as a result of the unique behavior of the oxide of this element.

A similar behavior was observed with alloys that were modified by additions of Ti, Ru, Mo, and Cr in addition to Re. Fifteen-25 at.% Ti was added and the Re content was reduced to 10 at.% in a Nb-40Al base in an attempt to form a complex oxide scale that would be stable on the surface. Molybdenum, Ru, and Cr were added at a level of 10 at.% to increase the electron to atom ratio. Weight gains were in the range of 3-10 $mgcm^{-2}$ for an exposure of 1h at 1400°C (Table A2, Appendix), slightly higher than that of the Nb-Re-Al alloy with 24-32% Re. As shown in Fig.13, thick, non-protective oxide scales were formed on all alloys. Porosity was still evident in the surface of some oxide scales and the scales tended to spall on cooling. Regions of significant internal oxidation were observed on all samples, indicating that oxygen permeability remained high. Adding 1 at.% Zr to simultaneously decrease D_o had no significant effect. It was concluded that elements which form volatile oxides such as Re, and Mo cannot be used effectively to increase the electron to atom ratio in Nb-Al alloys.

Manganese and Ru were evaluated as high e/a additions. Unlike Re and Mo, these elements do not form liquid or gaseous oxides at 1100°C. However, the oxides, like that of Cr, have high vapor pressures and some loss by volatilization may occur. The alloys also were modified with 1% Zr in attempt to reduce overall permeability of oxygen. These alloys had significantly lower rates of oxidation in oxygen at 1100°C than unalloyed Nb or Nb-Al-Zr alloys (Fig. 7). Samples gained 10-15 $mgcm^{-2}$ in 2h at 1100°C compared with <35 $mgcm^{-2}$ for the best Nb-Al-Zr alloy. Weight gain was greater than that of Nb-Ti-Al alloys (2-5$mgcm^{-2}$). However, the latter contained more Al. The Nb Ru-Al alloys contained only 17-23 at.% Al compared with 28% Al for Nb-Al-Zr and 38-45% for Nb-Ti-Al alloys. The 10% Ru + 1% Zr addition appeared to be very effective in promoting oxidation resistance at low Al concentrations. As shown in Fig.7, the rate curves for a Nb-10Ru-17Al-1Zr alloy and a Nb-15Mn-40 Al alloy were about the same.

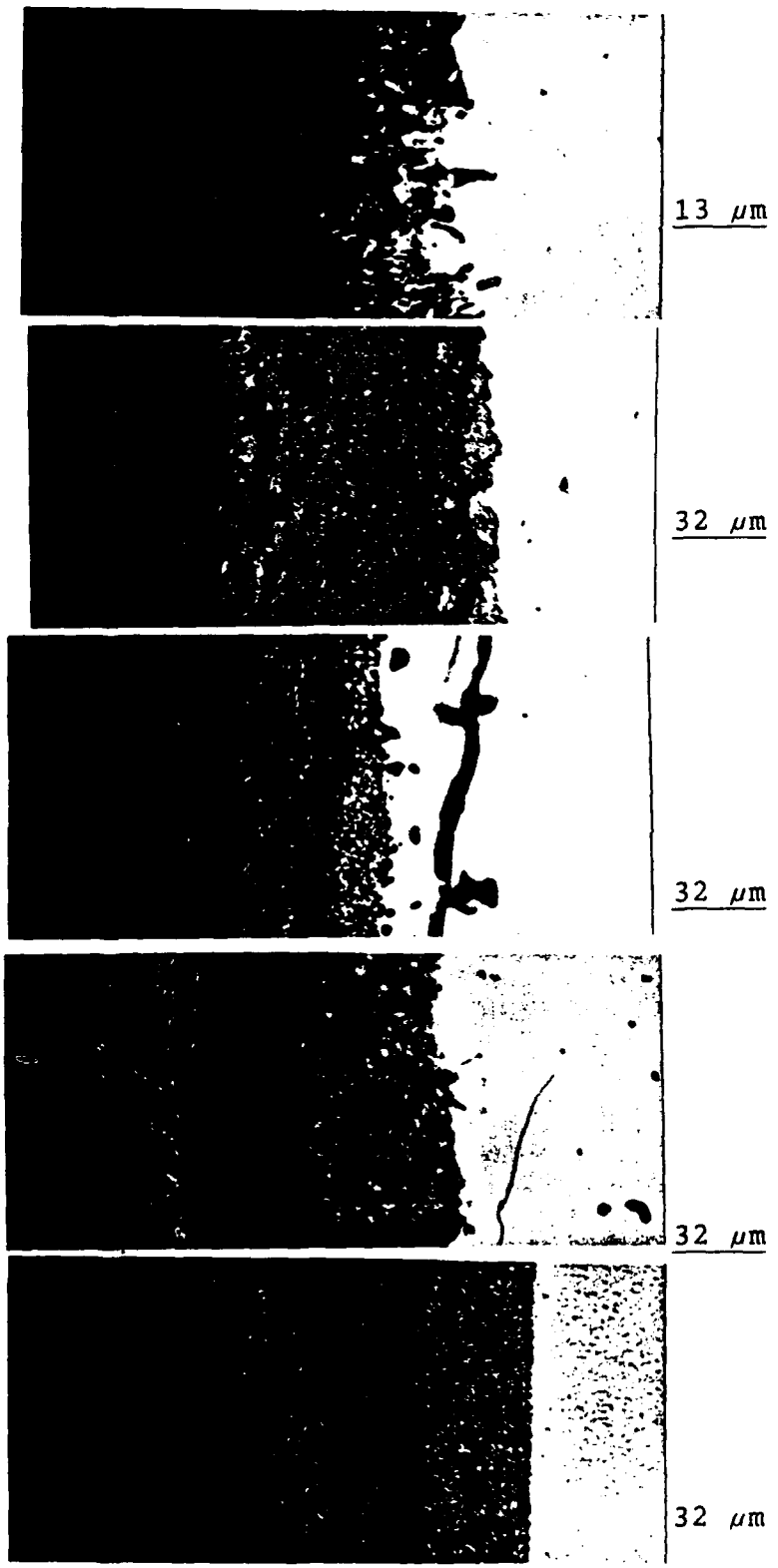

	at.%		
Al	Ti	Re	Other
40	25	10	(54-6)
40	15	10	10 Cr (54-9)
40	15	10	10V (54-10)
40	15	10	10Mo (54-8)
40	15	10	10Ru (54-7)

Figure 13: Effect of elements with a high e/a ratio on oxide scales.

The rate law exponents for alloys modified with Ru or Mn were 0.84-0.86 during the first 1-2 hr but then decreased to values of 0.4-0.7. Oxidation started with linear kinetics but shifted toward a parabolic rate law on continuing exposure (Table A2, Appendix). Behavior indicated that a protective scale may have been formed under a rapidly growing transient oxide. Figure 14 shows cross-sections of several of these alloys. The scales on the Ru-containing alloys consisted of a thick, porous outer layer containing Nb, Ru, and Al and a thin inner layer that is an oxygen contaminated diffusion zone. There is no evidence of an Al_2O_3 layer in the scale. A similar structure was found for the Nb-Mn-Al alloys in which a scale rich in Nb, Mn, and Al was formed over an internally hardened oxygen enriched diffusion zone. The Ru and Mn additions did not suppress the formation of linearly growing Nb-containing oxide so that enrichment of Al_2O_3 to form a continuous scale was impossible. The decrease in rate law exponent with time may be the result of loss of Ru or Mo by evaporation of their oxides from the scale.

A Nb-15Mn-17Al-1Zr alloy was preoxidized in argon with a p_{O2} of 10^{-4} atm. at 1100°C to determine if an alumina scale could be formed by reducing the amount of transient oxidation. The rate of scaling on subsequent exposure to oxygen at 1 atm was reduced significantly as shown in Fig. 7 and the alloy oxidized with parabolic kinetics for a 2h exposure. However, the alloy was oxidized internally to a great depth in the 18 hr preoxidation exposure at 1100°C. Preoxidation in a low p_{O2} atmosphere did not result in the formation of a protective alumina scale and the addition of Mn and Zr did not appear to reduce the permeability of oxygen in the alloy.

In general, the addition of high e/a elements as an approach to reduce N_o was not effective and in most cases, the oxides of these elements had a deleterious effect on oxidation behavior. Volatilization of the oxides of these elements produced anomalous results with low weight gains and rate constants that did not reflect actual behavior. Severe internal oxidation and heavy scaling of all samples was observed.

A final series of tests was conducted using additions of Fe as a high e/a addition. The position of Fe in the periodic table is such that it could act to increase e/a and Svedberg found a low rate of oxidation for an alloy of Nb-34.5%Fe-23.9%Al (4). The oxides of Fe have low vapor pressure and were found

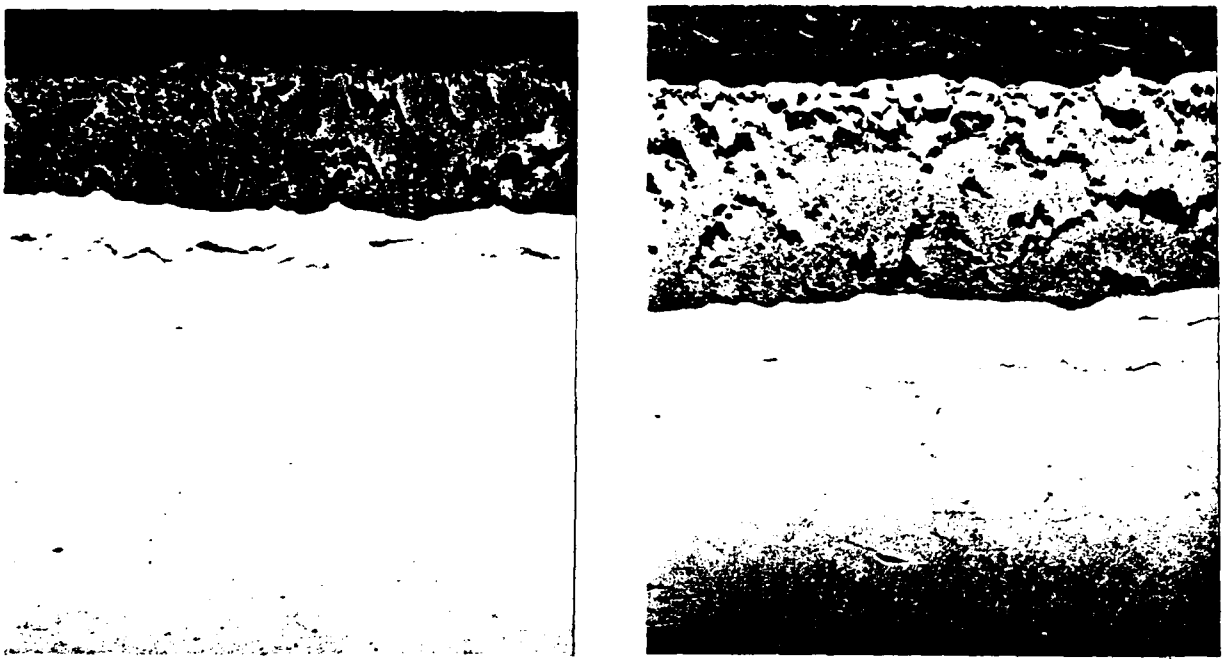

A- Nb-10Ru-17Al-1Zr
40-15, 120 min., +15mgcm^{-2}

B- Nb-10Ru-23Al-1Zr
40-17, 180 min., +23mgcm^{-2}

64μm

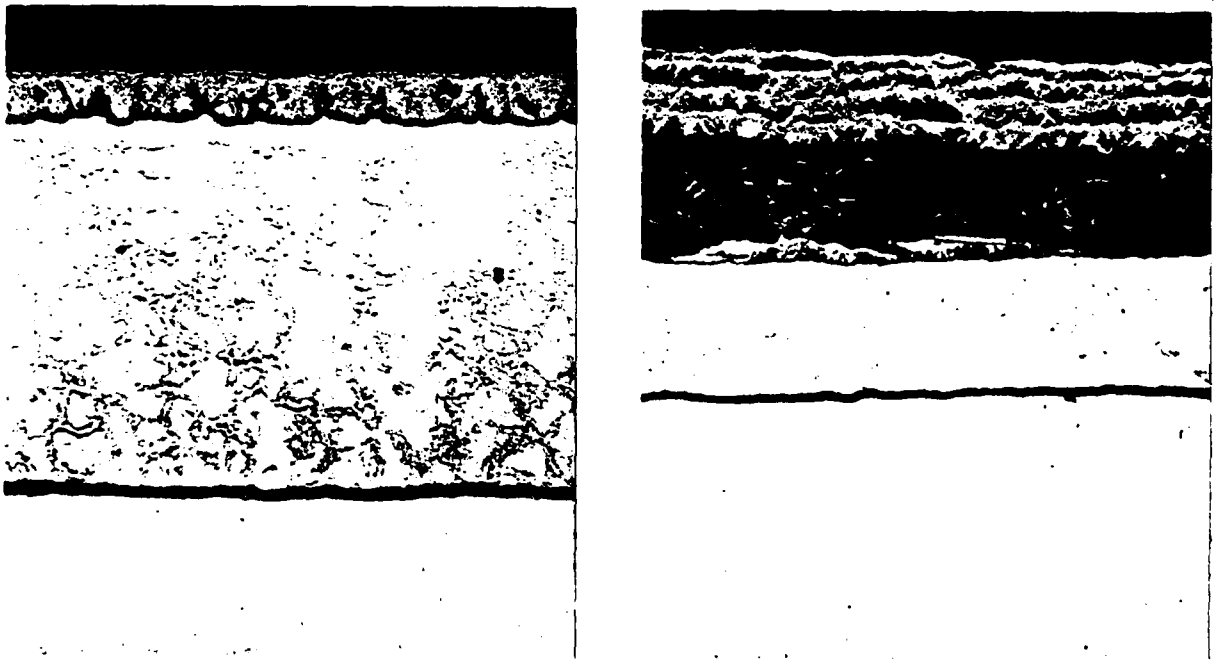

C- Nb-15Mn-17Al-1Zr
40-9, 120 min., +5.2mgcm^{-2}
(Pre-Oxidized 18hr, Argon,
log p_{O2}=-4)

D- Nb-15Mn-20Al-1Zr
40-10, 120 min., +28mgcm^{-2}
(No Pre-Oxidation)

127μm

Figure 14: Cross section of Nb-Ru-Al-Zr and Nb-Mn-Al-Zr alloys exposed to oxygen at 1100°C

to modify the oxide scales on Nb-Fe alloys, forming $NbFeO_4$ which has a rutile structure and is a good barrier to oxygen transport. Perkins (29) found that additions of Fe to Nb up to an e/a of 6.0 reduced permeability of both oxygen and nitrogen based on hardness depth profiles.

Nb-Fe-Al alloys were prepared with an e/a of 4.6 and 5.8 (based on Nb+Fe normalized without Al) at Al contents of 25, 30, and 35 at.% (Table A1, Appendix). All the alloys were extremely sensitive to thermal shock and disintegrated on repeated arc melting as normal buttons. Small micromelted samples were arc melted successfully but were very brittle and disintegrated on diamond saw cutting to produce test samples. No useful materials were produced and no oxidation tests were conducted.

Alloying to Increase D_{Al}

Titanium was selected as the element to add to Nb-Al alloys to increase the diffusivity of aluminum in Nb-Al alloys. The effect of Ti in this case is an indirect one in that Ti per se may have little effect on D_{Al}. Instead, as shown in Fig. 5, Ti increases the solubility of Al in b.c.c Nb. By adding Ti in a 1:1 ratio with Nb, a b.c.c. structure can be maintained at Al contents to 20 at.% at 1100°C. The diffusivity of Al in this structure should be several orders of magnitude greater than that in alloys or compounds which are predominantly non-cubic structures. The solubility of Al should increase with temperature and may extend to 40 at.% above 1400°C. The maximum solubility of Al in beta Ti-Al alloys is increased to 45 at.% at 1400°C.

Four alloys with a Nb:Ti ratio of 1:1 and Al contents of 33 to 50 at.% were prepared and evaluated for oxidation resistance in air at 1400°C. These alloys were used to evaluate two possible effects of Ti additions: 1- reduction of D_O and 2- increase of D_{Al}. Alloy compositions and the oxidation results are shown in Table 6 and results were summarized in the section on Alloying to Decrease D_O (p.32). A clear transition from internal oxidation of Al to external alumina scale formation occurred with increasing Al. The $N_{Al}^{(o)}$ for alumina formation on the Nb-Ti base alloy was between 35 and 44 at.%. This is a significant reduction from the 75 at. % Al in $NbAl_3$ which is the only Nb base material on which formation of a continuous alumina film has been found.

It was concluded in the section on Alloying to Decrease D_o that the beneficial effect of Ti most likely was not the result of its effect on reducing D_o. Elements whose sole effect is to reduce D_o did not appear to be effective in enhancing alumina formation. Nb-Ti-Al alloys with less than 44% Al that did not form alumina were oxidized internally to a great depth as shown in Fig. 8. Permeability of oxygen was high in spite of the large addition of Ti. One observed effect of Ti was an alteration of the transient oxide that was formed. Although the oxide formed with linear-type kinetics, it grew at a much slower rate that Nb_2O_5 (Figs. 9-10). However, the rate with up to 35% Al was not sufficiently slow for alumina to form as a continuous scale. Alumina was still taken up into the growing oxide, precluding the surface enrichment of Al required to form continuous alumina.

With an Al content of >35 at.%, the Nb-Ti-Al alloys formed a two layer scale with an outer layer of a mixed oxide containing Nb, Al, and Ti and an inner layer of alpha alumina. This structure is shown in Figs. 15 and 16 for an alloy with 38 at.% Al modified with a small amount of Cr and V to reduce D_o. The external scale (transient oxide) is a mixture of Al and Ti niobates containing dispersed particles of alumina (Fig.15). After a 24h exposure, the alumina particles in the outer scale have agglomerated into larger particles near the surface (Fig.16). The transient oxide is very much like the oxide formed on an alloy with 33% Al which did not form alumina at 1400°C (Fig.8B). The transition from internal to external oxidation of Al that occurred between 35 and 44% Al does not appear to be the result of any significant change in the transient oxidation process.

It is postulated that the formation of a continuous alumina scale in this case is the result of more rapid transport of Al to the scale metal interface to offset the depletion created by formation of the rapidly growing transient oxide. As shown in Fig.15, the alloy has a uniform concentration of Al beneath the oxide scale with no indication of Al depletion near the scale/metal interface. The alloy has a single phase structure which transforms on cooling to an acicular structure as shown in Figs.15 and 16. Rapidly cooled (as-chill cast) alloys appear to be single phase. XRD analysis of as-cast alloys produced patterns of a primitive cubic cell with a B2 superlattice.

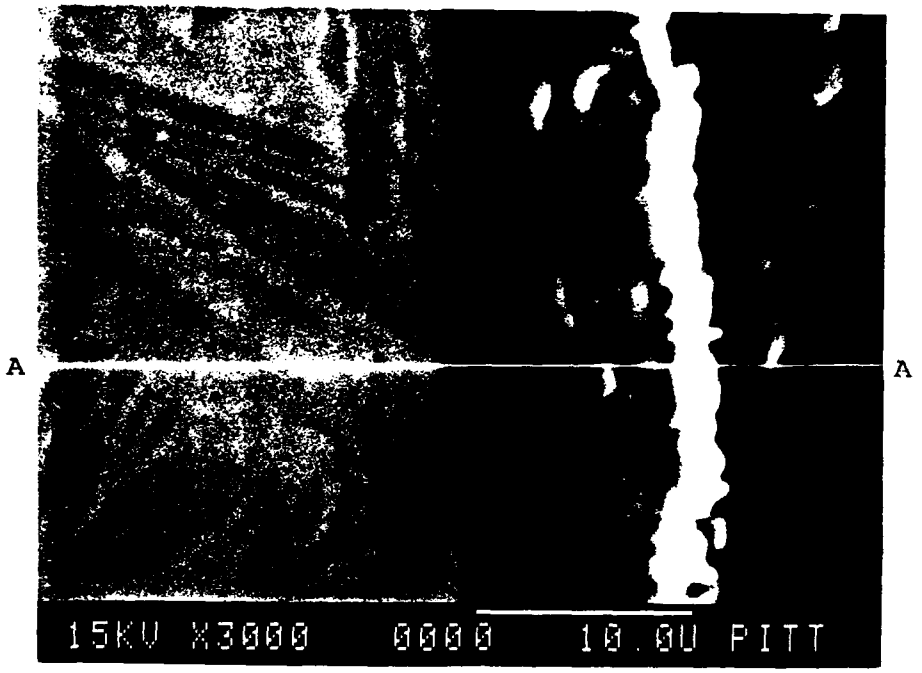

A- SEM of Alloy/Scale Cross Section

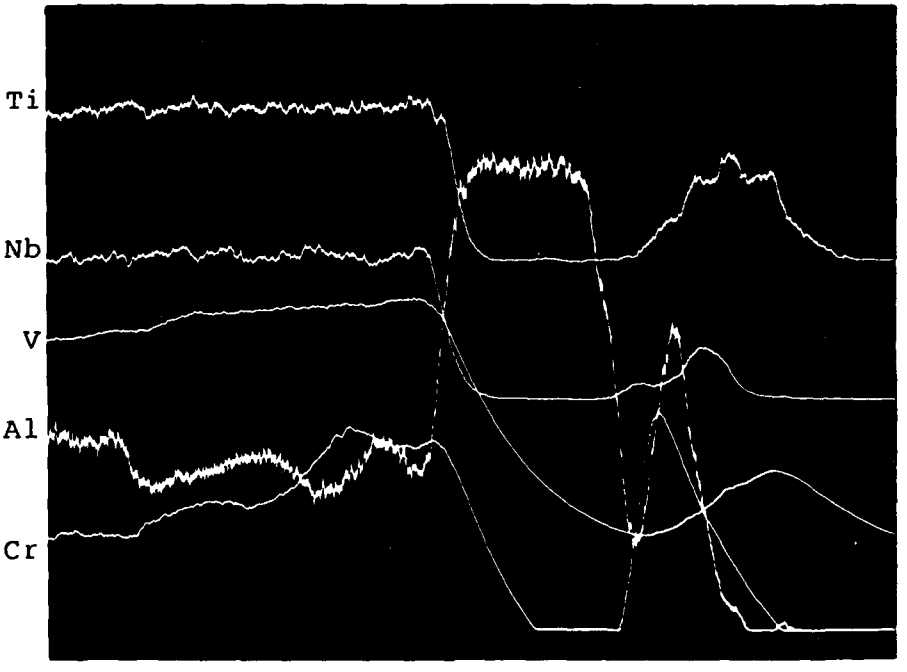

B- Concentration Profiles at Section A-A
(18-17) Nb-24Ti-37Al-3Cr-4V, 1hr-1400°C-Air

Figure 15: Distribution of elements in alloy and oxide scale formed on Nb-Ti-Al-Cr-V alloy in air, 1h-1400°C.

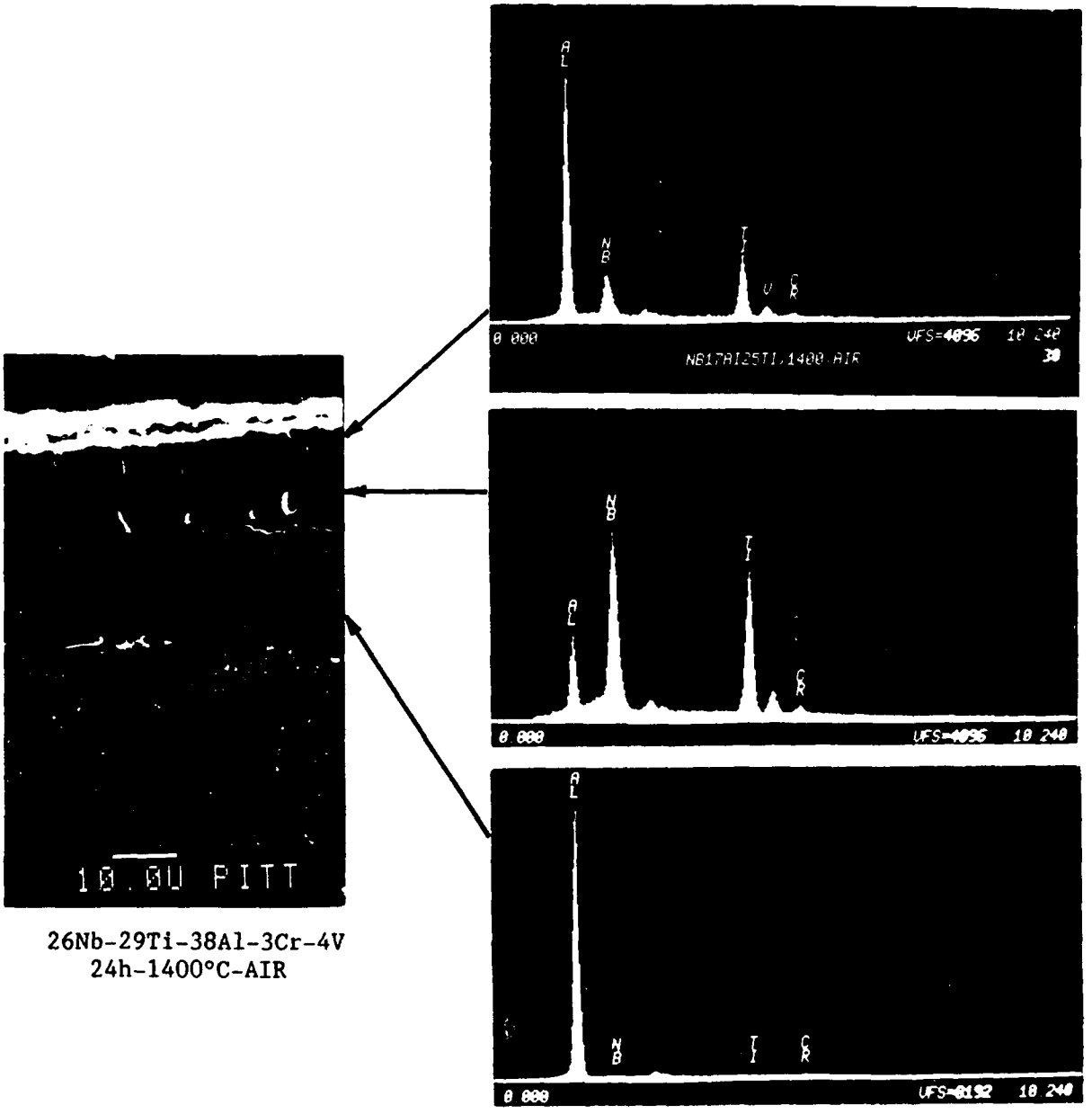

26Nb-29Ti-38Al-3Cr-4V
24h-1400°C-AIR

Figure 16: Oxide scale formed on Nb-Ti-Al-Cr-V alloy in air, 24h-1400°C.

The high temperature b.c.c. phase transforms to a fine two phase structure on heating at 800-1100°C as shown in Fig. 17. A standardless analysis of phases by EDAX revealed one phase to be a Nb-modified gamma TiAl and the other phase to be Ti-modified $NbAl_2$ as indicated below:

Light Phase (Fig.17)- 33.6Nb, 21.6Ti,35.1Al, 3.6Cr, 6.2V (Sigma)
Dark Phase (Fig.17) - 21.8Nb, 26.9Ti, 46.5Al, 2.1Cr, 2.7V

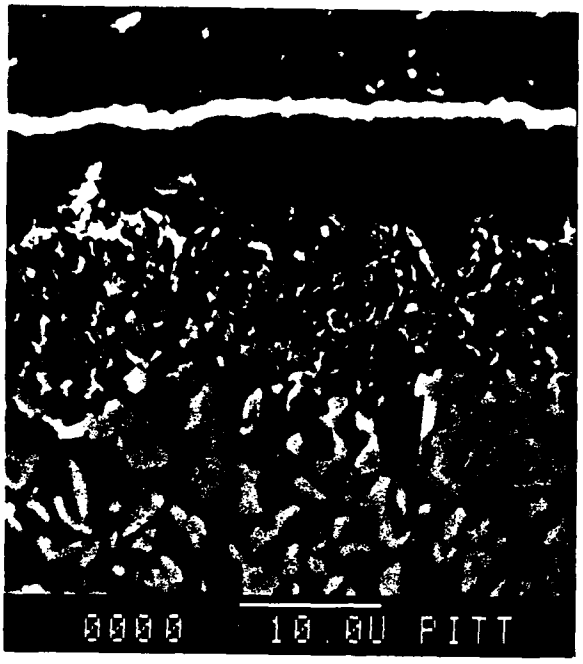

2hr-1100°C, Oxygen

32Nb, 24Ti, 37Al, 3Cr, 4V

Nb:Ti=1.36

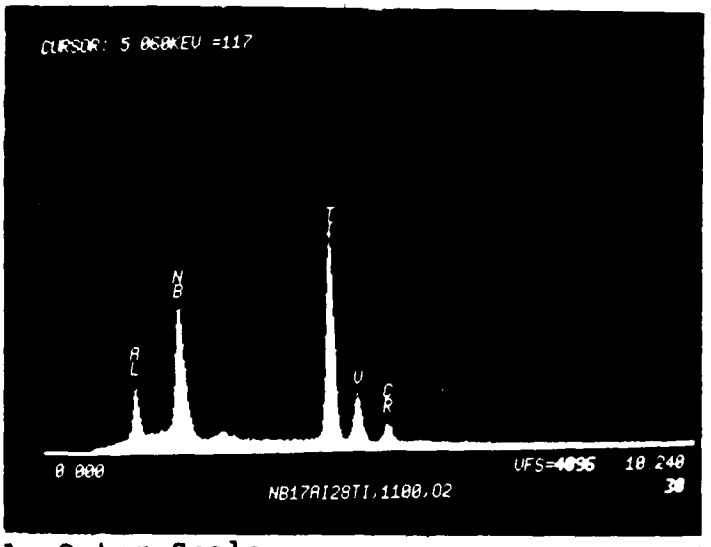

A- Outer Scale

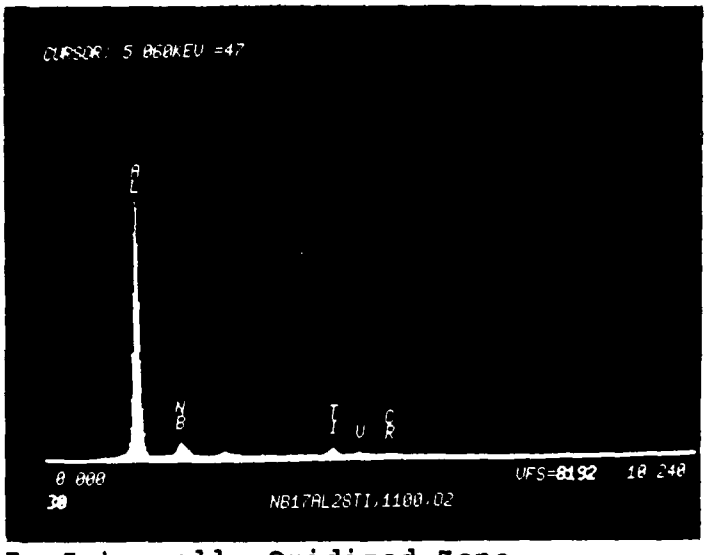

B- Internally Oxidized Zone

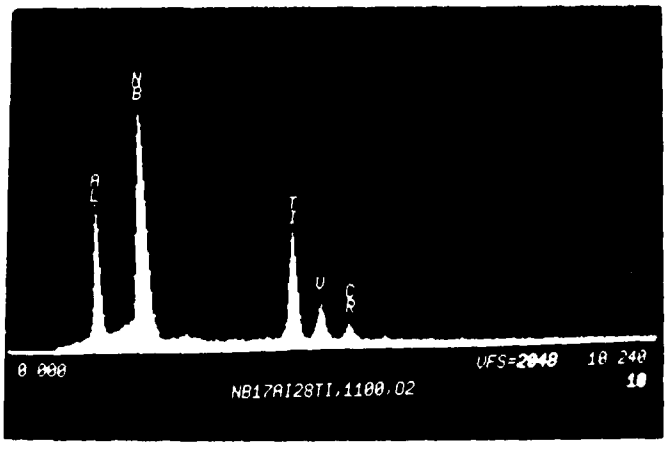

C- Alloy, Light Phase

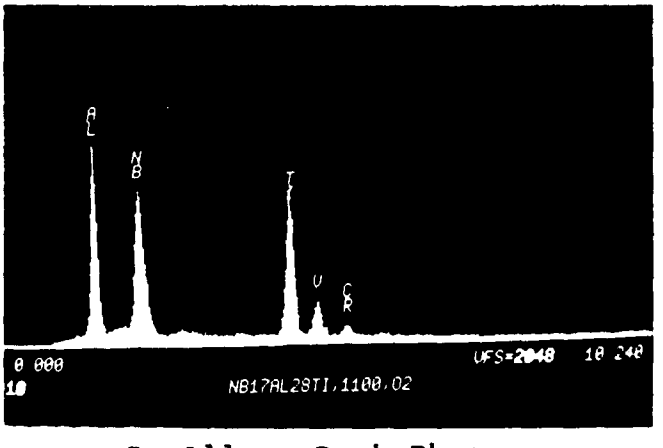

D- Alloy, Dark Phase

Figure 17: External scale and internal oxidation zone formed on a Nb-Ti-Al-Cr-V alloy in oxygen, 2h-1100°C.

These data are in good agreement with the ternary diagram (Fig.5) and the phases are on a tie line with the base alloy assuming that Cr and V substitute for Nb in the base alloy and in the sigma phase and for Ti in the Gamma phase. The Al rich gamma phase is oxidized internally at 1100°C.

The results clearly show the importance of alloy structure with regard to alumina formation and support the hypothesis that the role of Ti is to enhance the diffusivity of Al by stabilizing a b.c.c. phase in which the diffusivity of Al is high. Unfortunately, in this alloy system, the phase is stable only above 1300°C such that alumina is not formed readily in the mid to low temperature range. It is concluded that a large increase in D_{Al} is required to form alumina on Nb-base alloys and that stabilization of a b.c.c. structure by the addition of Ti is an effective approach.

Results of experiments with the Nb-Ti-Al alloys clearly indicate that increasing D_{Al} by stabilizing a b.c.c. phase will reduce significantly the critical N_{Al} for external alumina formation but does not result in the formation of a single layer, highly protective alumina scale. A weight gain of 4.7 $mgcm^{-2}$ in 1 hr at 1400°C gives an estimated parabolic rate constant of $6.14x10^{-9}$ $g^2cm^{-4}s^{-1}$. This is two orders of magnitude greater than the extrapolated rate of oxidation of NiAl which forms a single layer protective alumina scale at 900-1100 °C (Fig.1.) It is concluded that increasing D_{Al} alone will not be sufficient and that simultaneous decreases in $N_O^{(s)}$ and D_O and/or the formation of a transient oxide that grows with very slow (parabolic) kinetics will be required to achieve the formation of protective alumina at lower values of N_{Al}. A fourth element must be added to produce these needed improvements.

OXIDATION BEHAVIOR OF Nb-Ti-Al-X ALLOYS

Effect of Cr,V, and Mo

Chromium, V, and Mo were added to Nb-Ti-Al alloys with 34-44 at.% Al as fourth elements to reduce the solubility and diffusivity of oxygen in the base alloy. Results were evaluated by oxidation screening at 1100 and 1400° and optical metallography of polished cross sections after exposure. Results are summarized in Table 8. The rate of oxidation of alloys with 34-38% Al which

TABLE 8

Effect of Cr, V, and Mo on Oxidation Behavior of Nb-Ti-Al alloys

Composition- at.%						Weight Gain- $mgcm^{-2}$	
Nb	Ti	Al	Cr	V	Mo	2h-1100°C	1h-1400°C
33	33	33				3.39	14.1
33	32	35					10.2
31	32	34	3				3.6
29	32	34	5				1.5
26	31	33	10				6.7
30	32	34		4			4.3
28	31	34	3	4			0.4
30	30	40					4.7
24	29	38	5				2.0
24	29	39	10			3.54	1.3
26	29	38	3	4		1.78	2.2
20	20	37	8		5	1.33	
28	28	44				1.98	2.94
23	29	44	3	3		0.75	
24	23	44	4	5		2.54	1.71
22	24	44	8	6		2.93	1.51
23	28	44	3		1	1.23	
17	27	43	8		5	0.93	

do not form alumina at 1400°C decreased with increasing Cr to 10%. A weight gain of <2 $mgcm^{-2}$ in 1h at 1400°C is representative of an alumina former. Alloys with 34-38% Al and 5-10% Cr appear to form alumina at 1400°C An Al content of >40% is needed to form alumina without Cr at this temperature.

Metallographic cross sections of the alloys (Fig.18) shows that the oxide scale thickness and depth of internal oxidation are decreased with increasing Cr additions. The alloy with 10%Cr and 34%Al has formed a discontinuous alumina scale (Fig.18C). With 38-40% Al in the alloy, continuous alumina scales are formed by the addition of as little as 5% Cr as shown in Fig. 19. The Nb-Ti-Al alloys at this level of Al are marginal alumina formers at 1400°C as shown in Fig.19A. A small amount of Cr is sufficient to promote formation of a continuous alumina scale. Increasing additions have little effect as indicated by the weight gains (Table 8) and oxide scale morphology (Fig.19). With 44% Al in the alloy, alumina scales are formed without Cr on heating in air at 1400°C. As indicated by the weight gain data (Table 8), adding Cr to this alloy cut the weight gain in half. Metallographic observations indicated that the amount of transient oxidation that occurred before a continuous

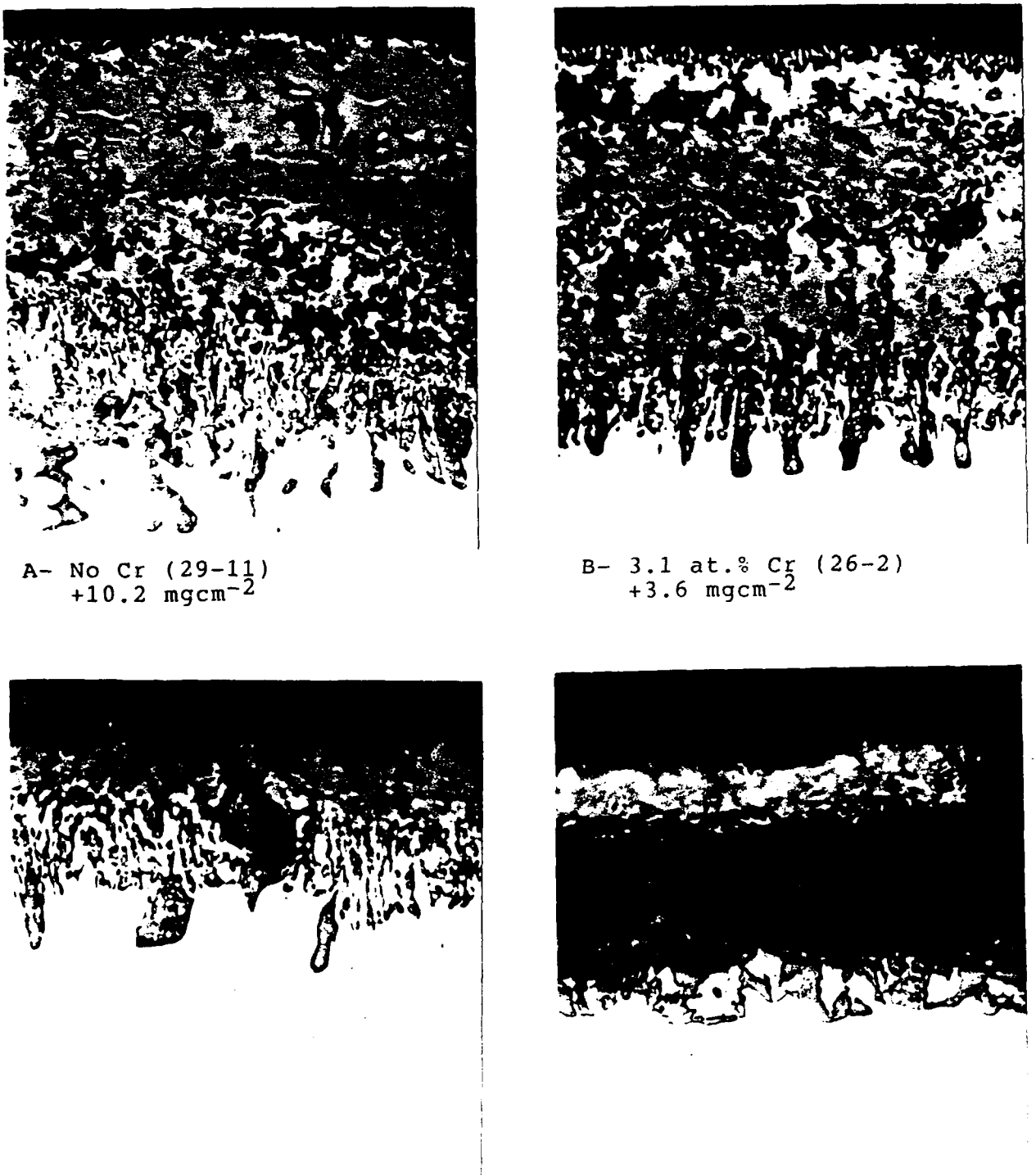

Figure 18: Effect of Cr on oxide scales formed on Nb-32Ti-34Al alloys in air, 1h-1400°C.

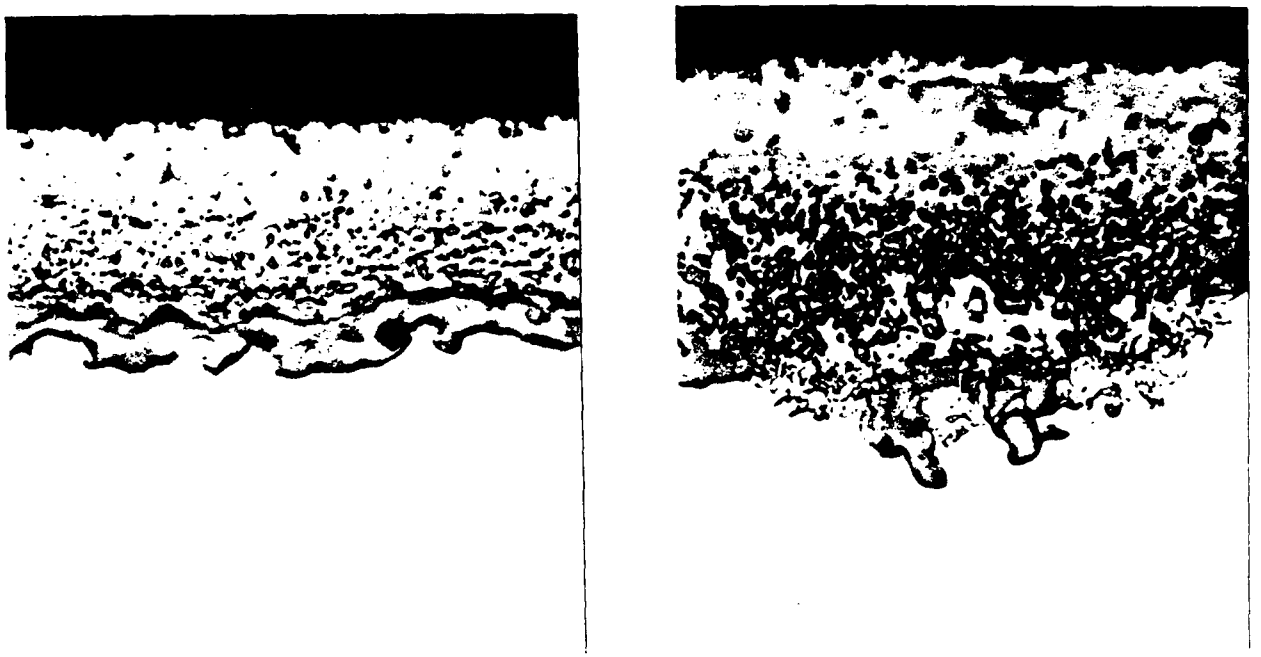

Typical Scale

Random Breakdown

A- No Cr (29-14), +4.7 $mgcm^{-2}$

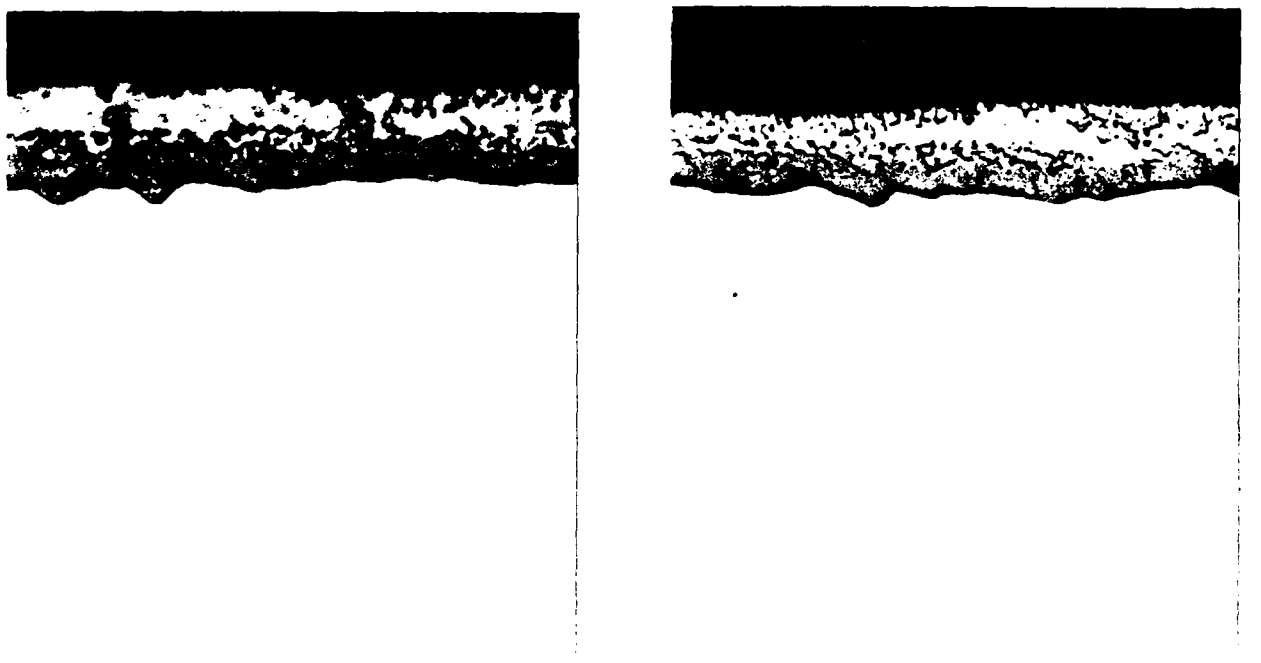

B- 5.0 at.% Cr (29-15)
+2.0 $mgcm^{-2}$

C- 9.8 at.% Cr (29-16)
+1.3 $mgcm^{-2}$

13μm

Figure 19: Effect of Cr on oxide scales formed on Nb-29Ti-39Al alloys in air, 1h-1400°C.

alumina scale formed was reduced by increasing Cr. The addition of Cr appears to have either slowed the rate of transient oxidation or increased the rate of alumina formation, resulting in formation of an alumina scale with reduced transient oxidation.

Vanadium was evaluated as a substitute for Cr in alloys with 34-44% Al. It was more effective in promoting alumina formation on an at.% basis but had the undesirable effect of increasing the amount of transient oxidation and overall weight gain. As shown in Fig.20B, alumina was formed on a 34% Al alloy by the addition of 4% V. Alumina was not formed on alloys with this Al level by the addition of up to 10% Cr (Figs 14C, 20A). A very thick transient oxide containing dispersed particles of alumina was formed on the V-modified alloy. The problem with respect to transient oxidation was solved by adding Cr and V together. Alumina formation was enhanced by the vanadium addition while transient oxidation was slowed by the Cr addition. Only a thin layer of transient oxide was formed on an alloy with 3Cr + 4V (Fig.20C). Oxide scale morphology was similar to that formed on alloys with 5-10Cr but with 39% Al (Fig. 19B,C). It was only through the addition of Cr and V together that alumina was formed on alloys with 34%Al. This is the lowest N_{Al} at which alumina was formed on Nb-Ti-Al alloys in air at 1400°C. Similar results were achieved by adding Mo instead of V to Nb-Ti-Al-Cr alloys.

The effect of Cr and V additions on oxidation behavior at 1400°C is summarized in Fig.21. The weight gain of Nb-Ti-Al alloys in 1h at 1400°C decreases with increasing Al content. reaching a minimum at 44 at.% when a continuous alumina scale is formed. The overall weight gain is high as a result of a large amount of transient oxidation before the continuous alumina scale is formed. When 3-10% Cr or Cr + V were added, the amount of transient oxidation was reduced significantly and a continuous alumina scale was formed with as little as 34-35 at.% Al. Weight gain continued to decrease with increasing Al as a result of decreased transient oxidation.

Additions of Cr and V to alloys with 34-44% Al had little effect on oxidation behavior at 800-1100°C. Alloys at all Al contents, with or without Cr and V, formed thick oxide scales with a layered structure that spalled on cooling (Fig.22,23). Major oxides identified in the scales were TiO_2 (Rutile) and $AlNbO_4$. No alumina was detected in the scales. The dark bands in the

A- 5.2 at.% Cr (29-12)
+1.9 $mgcm^{-2}$

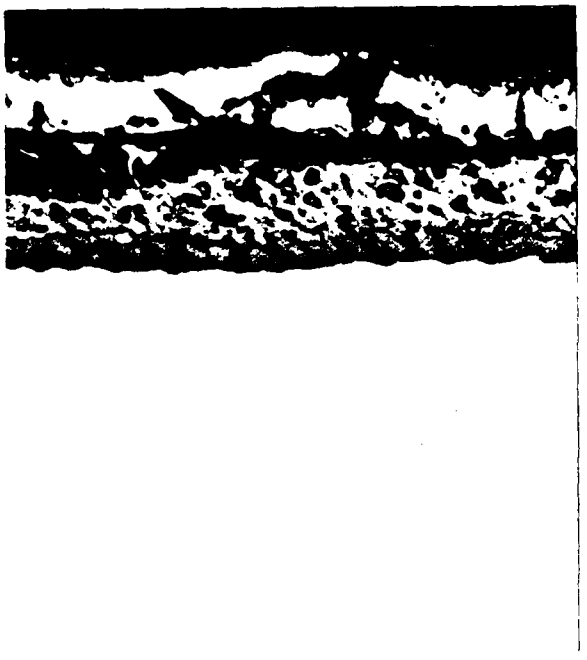

B- 4.3 at.% V (26-3)
+4.3 $mgcm^{-2}$

C- 3.1 at.% Cr + 4.2 at.% V (26-4), +0.4 $mgcm^{-2}$

13μm

Figure 20: Effect of V and Cr + V on oxide scales formed on Nb-32Ti-34Al alloys in air, 1h-1400°C.

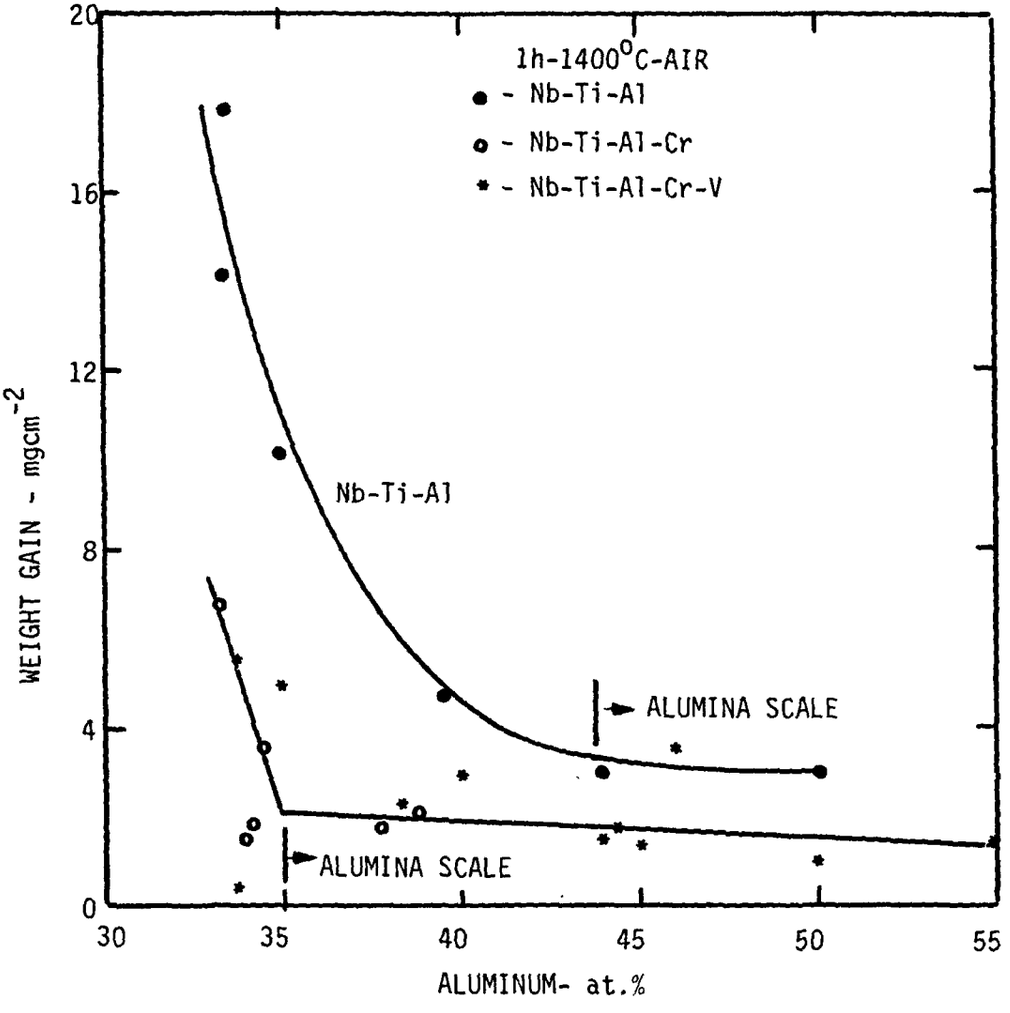

Figure 21: Effect of Cr and V on weight gain in 1h at 1400°C as a function of Al content

laminated scale are rich in Al and probably are the Al-niobate. Aluminum was oxidized internally to a depth of over 150μm on exposure for 24h at 1100°C. Internal oxidation also occurred at 800°C but was unlike that observed at 1100°C. At 1100°C, one phase in the alloy (gamma) is oxidized selectively to form discrete particles of alumina. At 800°C, the internal oxidation appeared more like a diffusion hardened zone with oxygen in solution. No oxide particles were detected at magnifications to 3000X. The zone appears as a darkened layer beneath the oxide in Fig.23B. The depth of penetration was 43μm in 164h. The deep internal oxidation of these alloys at 800-1100°C is

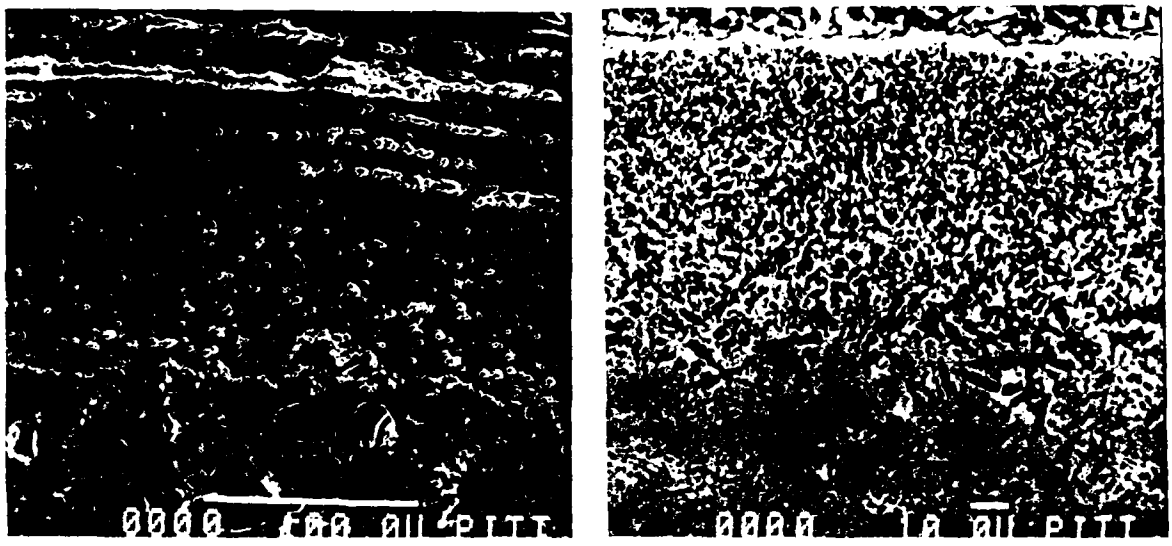

Spalled Oxide Scale
A- 26Nb-29Ti-38Al-3Cr-4V, 24h-1100°C

Internally Oxidized Alloy

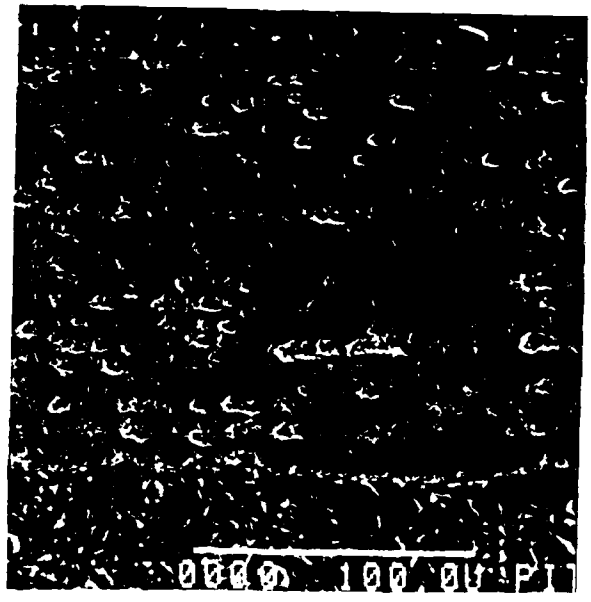

B- 24Nb-29Ti-38Al-10Cr, 73h-1100°C

Figure 22: Oxide scales and internal oxidation zone formed on Nb-Ti-Al-Cr-V alloys in oxygen at 1100°C.

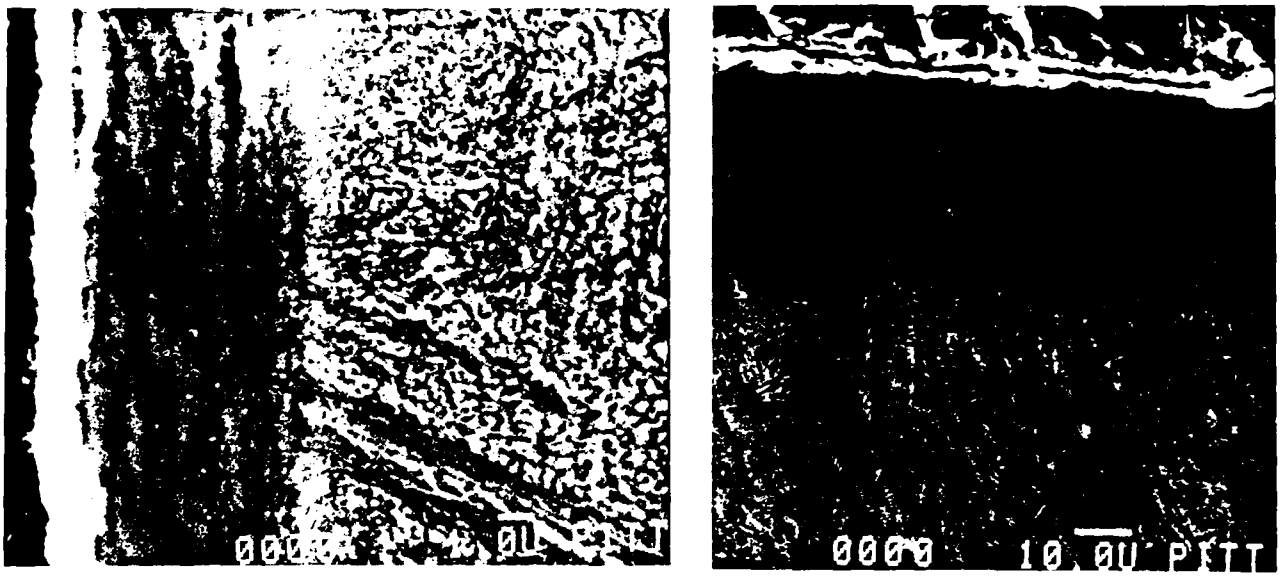

2.5µm 18µm

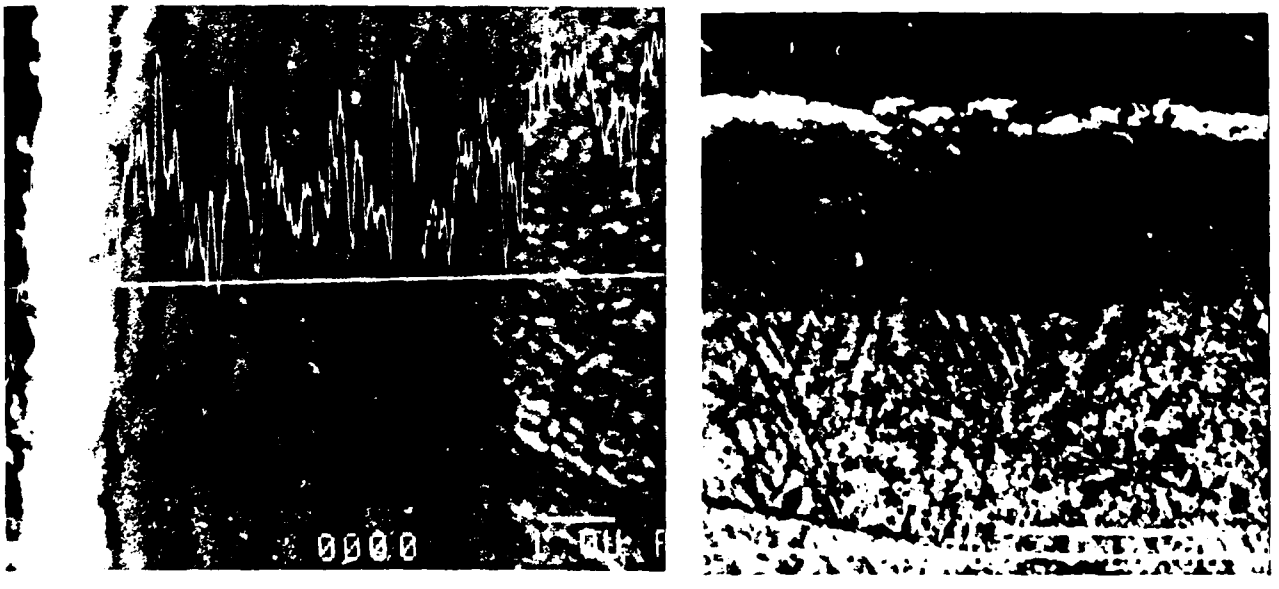

A- Nb-29Ti-38Al-3Cr-4V 1.3µm B- Nb-26Ti-40Al-3Cr-4V 4.1µm

Figure 23: Oxide scales formed on Nb-Ti-Al-Cr-V alloys in oxygen, 160h-800°C.

the result of a high permeability for oxygen and indicates that the small additions of Cr + V have not been effective in reducing either N_o or D_o.

Parabolic rate plots at 1100°C for alloys with 38% Al curved upward initially but tended to straighten out after a few hours as shown in Fig.24. The alloy with 3% Cr + 4% V oxidized a slightly faster rate than the alloy with 10% Cr. The log of the parabolic rate constants is -7.93 and -8.19, respectively (Table A4). It is concluded that the major role of Cr and V is to decrease the rate of transient oxidation. As shown in Figs. 15 and 16, both Cr and V are found in the transient oxide formed at 1400°C. Although the oxide grows with parabolic kinetics, the rate is too fast and precludes the enrichment of Al required for a continuous alumina scale to be formed. It should be noted for comparison that the log of the parabolic rate constant for alumina formation on NiAl at 1100°C is -12.2, a rate that is 4 orders of magnitude slower. The parabolic rate constants at 800°C were 5 orders of magnitude faster than those of an alumina former. The effect of Cr and V on oxygen permeability appears to be negligible based on the behavior at 800-1100°C.

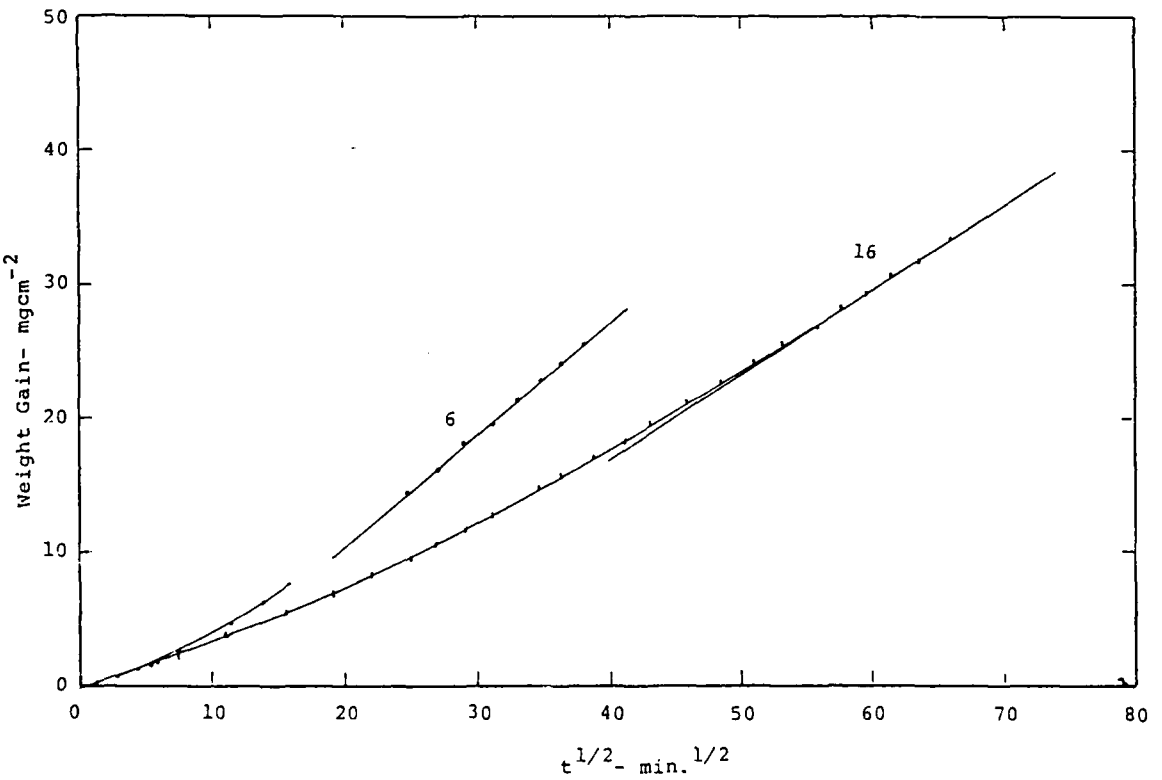

Figure 24: Parabolic rate plots for Nb-29Ti-38Al-Cr-V alloys in oxygen at 1100°C.

Effect of Si and Pt

Small amounts of Si and Pt were added to Nb-Ti-Al and Nb-Ti-Al-Cr-V alloys in an attempt to modify further the base metal oxide and reduce the rate of transient oxidation. Silicon has a tendency in stainless steels and superalloys to form thin silicate films beneath the bulk oxide scales and in alloy grain boundaries. The films are excellent barriers to diffusion of O, N, and C. Platinum has been found to enhance the formation of alumina on nickel aluminide coatings formed on superalloys. Although the mechanism is not clear, rejection of Pt near the scale/metal interface is considered to be a major factor in providing improved behavior.

The addition of 5% Pt to a Nb-20%Al alloy cut the weight gain in half on a 2h exposure at 1100°C. A Nb-20Al-5Pt alloy gained 17.1 $mgcm^{-2}$ compared with 34 $mgcm^{-2}$ for a Nb-21Al-1.7Zr alloy. Oxidation behavior was similar to that of a Nb-20Al-10Ru-1Zr alloy (Fig.7). The weight gain in 1h at 1400°C was 12.4 $mgcm^{-2}$, comparable to that of a Nb-Ti-Al alloy with 33-35% Al. The Pt addition was effective in reducing the rate of transient oxidation at very low Al concentrations. It did not, however, promote the formation of continuous alumina scales. Platinum also was added to a Nb-Ti-Al-Cr-V alloy but had no significant effect. The addition of 5% Pt to an alloy with 46% Al, 4% Cr, and 5% V did not change the oxidation behavior at either 1100 or 1400°C based on short time screening tests.

The addition of Si to Nb-Ti-Al and Nb-Ti-Al-Cr-V alloys had a very marked effect on oxidation behavior at 1100-1300°C. Nb-Ti-Al alloys with 30-40% Al and 5-10% Si oxidized with parabolic kinetics at both 1100 and 1300°C (Tables A3 and A4, Appendix. The log of the parabolic rate constant at 1100°C was between -9.6 and -9.9 for most alloys. This is 2 orders of magnitude lower than that of Nb-Ti-Al-Cr-V alloys containing over 35% Al. The rate constant is only 2 orders of magnitude greater than that for an alumina former such as NiAl, which is a significant improvement. Alloy cross sections (Fig.25) show that alumina has been formed on a Nb-Ti-Al-Si alloy with 40Al and 10 Si at 1100°C. Continuous alumina was not formed at lower Al or Si concentrations. However, a protective oxide scale which grows with slow parabolic kinetics was formed and the the internal oxidation of Al was reduced significantly.

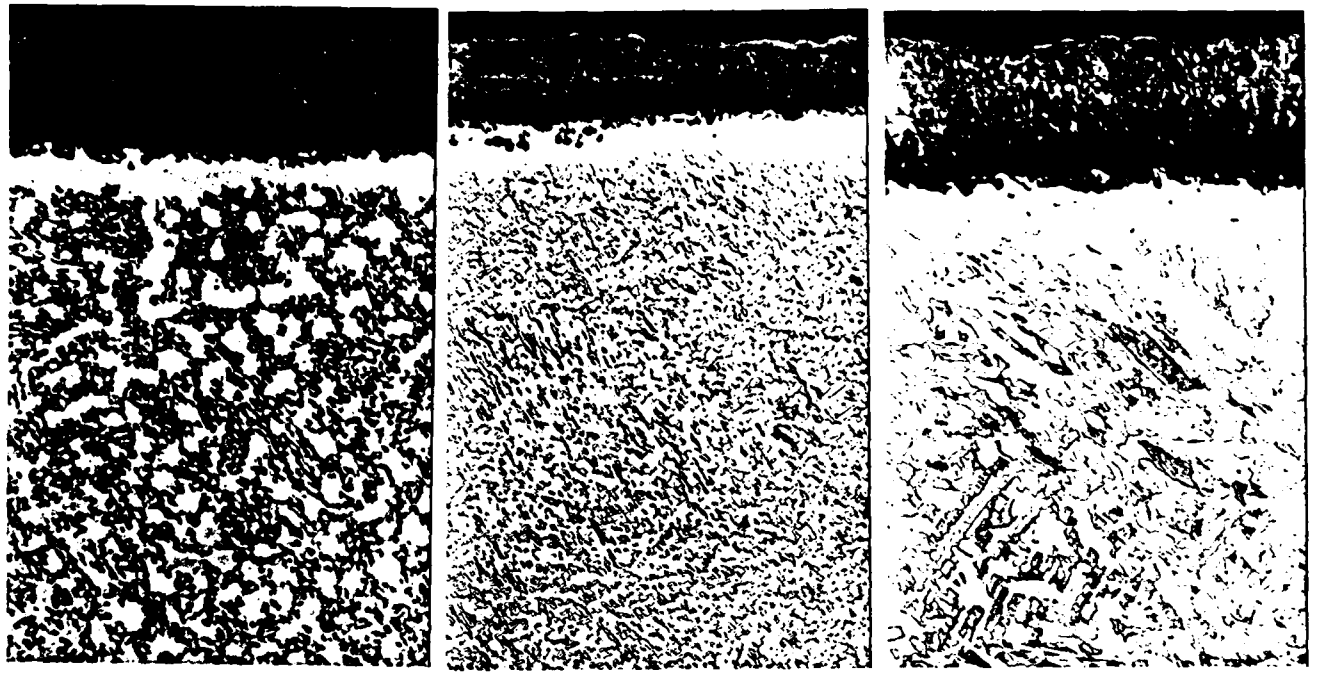

A- 30Al-5Si B- 35Al-5Si C- 40Al-5Si 25μm

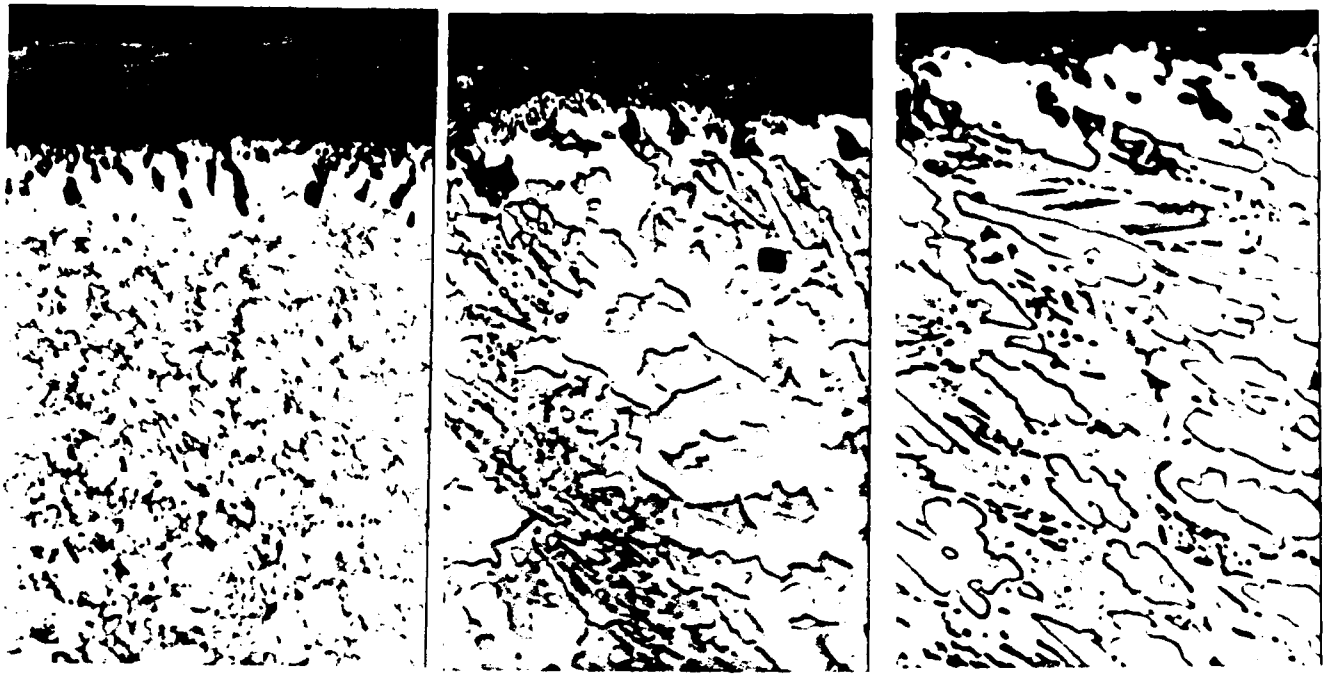

D- 30Al-10Si 25μm E- 35Al-10Si 13μm F- 40Al-10Si 13μm

Air, 19-22h-1100°C

Figure 25: Effect of Al and Si on oxidation of Nb-Ti-Al alloys in air at 1100°C.

When the Al content of the alloy was increased to 45 at.%, continuous alumina scales with no transient oxide were formed at 1100°C as shown in Fig. 26. Weight gains were <1 $mgcm^{-2}$ in 2h at 1100°C. Parabolic rate constants, however, were still 2 orders of magnitude greater than that of NiAl. In addition, the rate tended to increase with time after 10-12h of exposure with the plot curving up and approaching linear kinetics (Table A3 and A4, Appendix). Figure 27 illustrates this effect for tests in air at 1300°C. This was found to be the result of breakaway oxidation at sharp edges and corners of the test samples which spread as time progressed. No alloy depletion layer was evident but selective oxidation of one phase in the alloy was observed (Fig.26). The high Si alloys were very brittle and tended to fracture at edges and corners as oxidation progressed.

Better results were obtained by the addition of 5-10% Si to a Nb-Ti-Al-Cr-V alloy with 32-37 at.% Al. In this case, Si was substituted for Al in the alloy, leaving the Nb and Ti constant at about 25% each. As shown in Fig.28, and alumina scale was formed in air at 1100°C by the addition of 10% Si. Alloys oxidized with parabolic kinetics to about 80h at which point breakaway to an increasing rate occurred. The log of the parabolic rate constants for the first 80h was -10.48 and -10.18 for the alloys with 5 and 10% Si respectively. This is slightly better than that of the alloys without Cr and V but is still about 2 orders of magnitude greater than that for alumina on NiAl.

OXIDATION BEHAVIOR OF Nb-Ti-Al-Cr-V ALLOYS

Analysis of the experiments designed to explore the influence of factors in the Wagner equation for transition to external alumina scale formation indicates that a Nb-Ti-Al-Cr-V alloy would be a good baseline material for use in evaluating the effects of other significant variables. The baseline selected was a Nb-24Ti-44Al-3Cr-4V alloy. The evaluation first addressed the the effect of Al content and the Nb:Ti ratio on oxidation behavior. This was followed by an evaluation of the effects of temperature, environment, preoxidation, rapid solidification processing, and ion implantation on oxidation behavior of the baseline alloy.

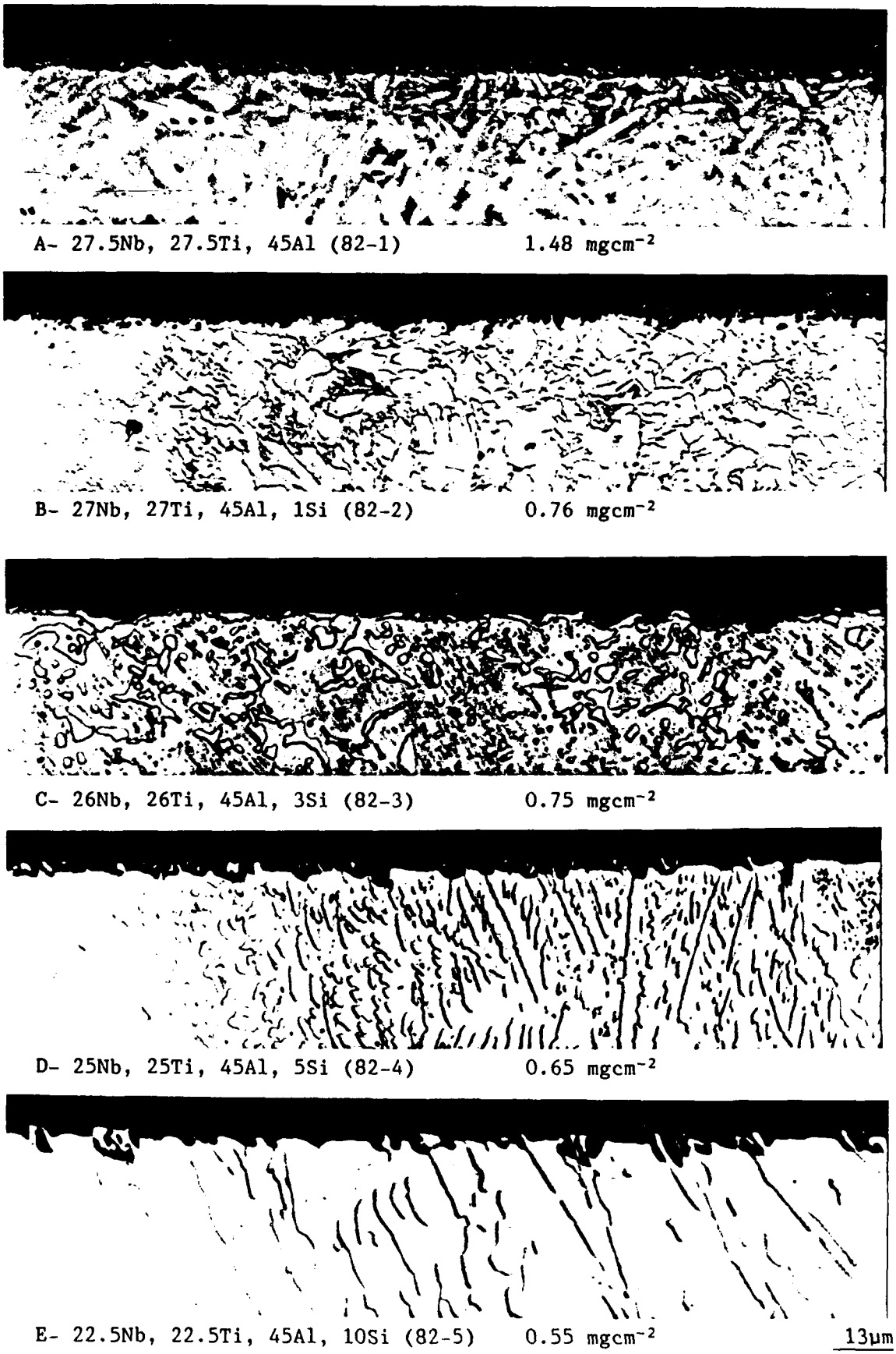

Figure 26: Effect of Si on oxide scales formed on Nb-Ti-45%Al alloys in air at 1100°C

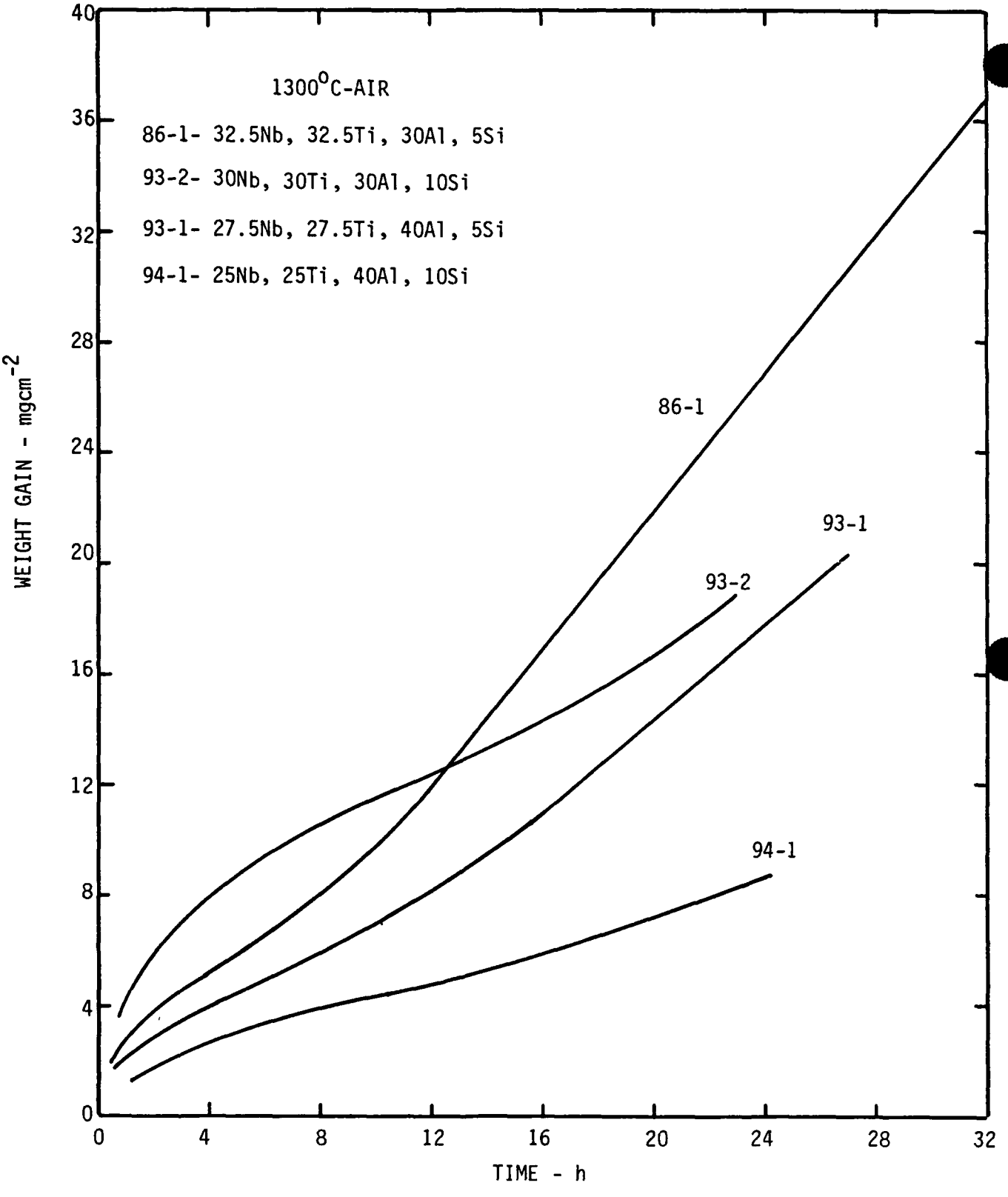

Figure 27: Paralinear oxidation rate curves for Nb-Ti-Al-Si alloys in air at 1300°C.

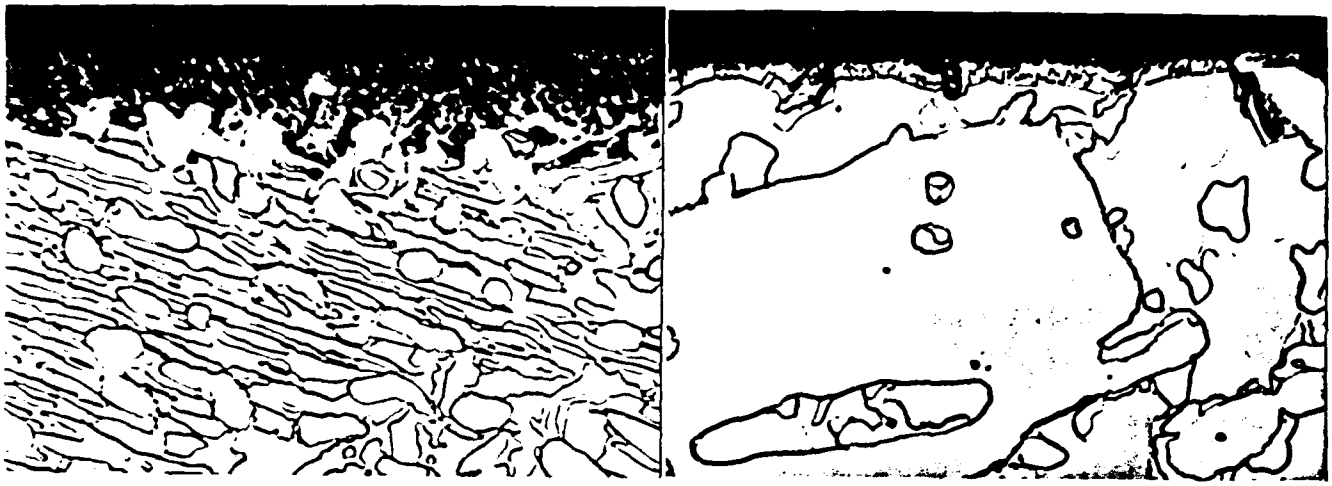

A- P098, 37Al-5Si 13μm B- P099, 32Al-10Si

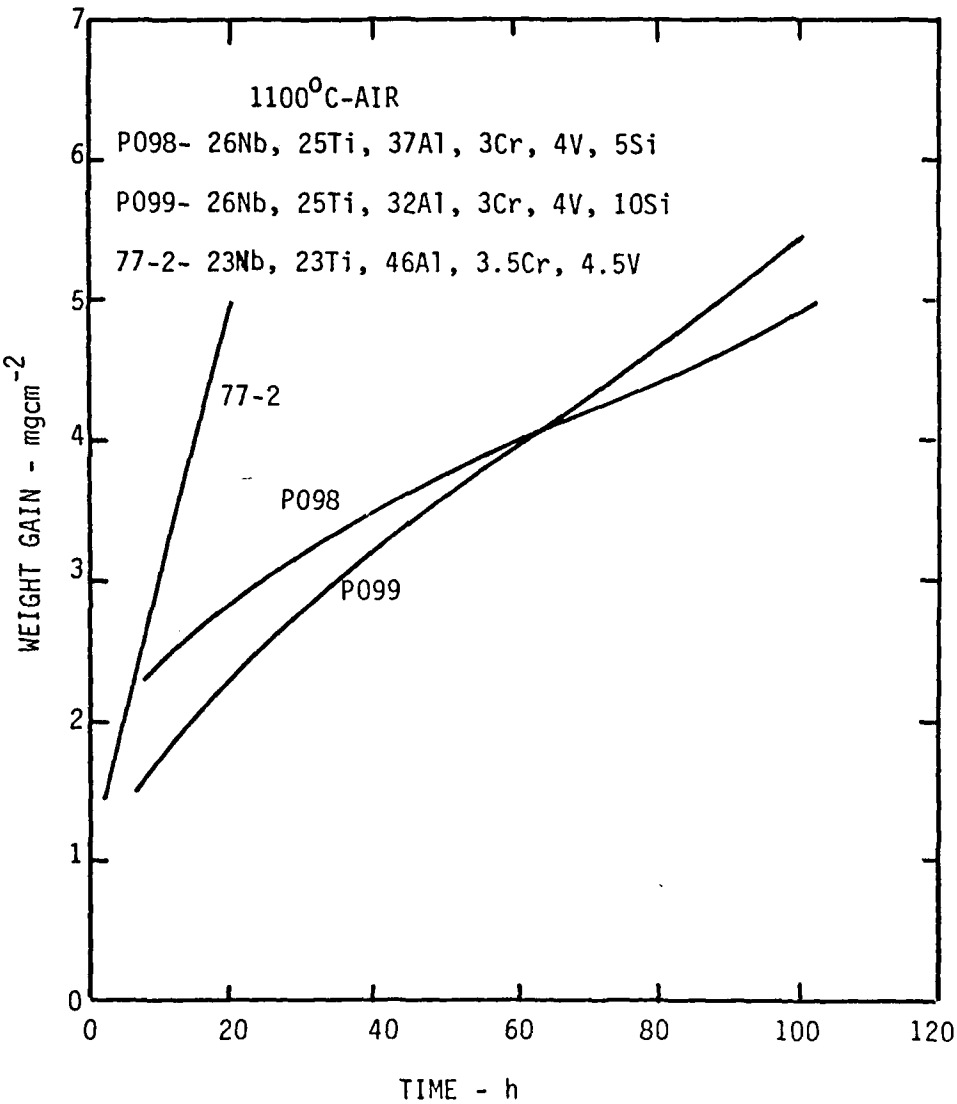

Figure 28: Effect of Si on oxidation behavior of Nb-Ti-Al-Cr-V alloys in air at 1100°C.

Effect of Al

A transition of oxide scale morphology from transient oxide + internal oxidation to transient oxide + continuous alumina to continuous alumina was observed with increased Al content on heating in air at 1400°C. Figure 29 shows that aluminum in the alloy was oxidized internally at a level of 35 at% while a continuous external alumina scale was formed beneath a layer of transient oxide at a level of 40 at% aluminum. Weight gain data (Fig.21) indicate that the transition from internal to external oxidation of Al occurs at about 35 at.%. Alloys with 34-35% Al modified with Cr or Cr+V were marginal alumina formers where alloys with 37-38% Al formed continuous alumina scales in all tests. The amount of transient oxide decreased with increasing Al content to a level of 58 at% Al at which point a single layer of alpha alumina was formed. Similarly, at 1100°C, also shown in Fig.29, the thickness of transient oxide and the depth of internal oxidation decreased steadily with increasing Al content in the alloy from 35 to 58 at% but a continuous alumina scale was not formed. The alloy with 58 at% Al was very close to forming a continuous alumina scale. A much higher aluminum content appears to be needed to form a continuous alumina scale in air at 1100°C.

Behavior at 1300°C was similar to that at 1100°C except that less internal oxidation occurred. As shown in Fig. 30, the alloy is a marginal alumina former at 1300°C. With 48% Al in the alloy, a discontinuous alumina scale is formed under a thick transient oxide. The growth of the transient is not cut off, however, and the rate of oxidation remains high as indicated in Fig. 31. The alloys oxidize with linear kinetics at 1100 and 1300°C at all Al contents from 38 to 58 at.%. There appears to be a slight trend to an increasing rate constant with increasing Al content. The linear rate constants are similar at both temperatures, indicating that the alloy is close to forming a protective alumina scale. Considerably less internal oxidation occurs at 1300°C (Fig.30) compared with that at 1100°C (Fig.29). At 1400°C, a continuous alumina scale is formed and a low parabolic rate with no internal oxidation is attained (Fig.29).

The Nb-Ti-Al-Cr-V alloys did not form alumina at any Al concentrations in air or oxygen at 800°C. However, the alloys did oxidize with parabolic kinetics in this temperature range as shown in Fig. 31. The parabolic rate constant

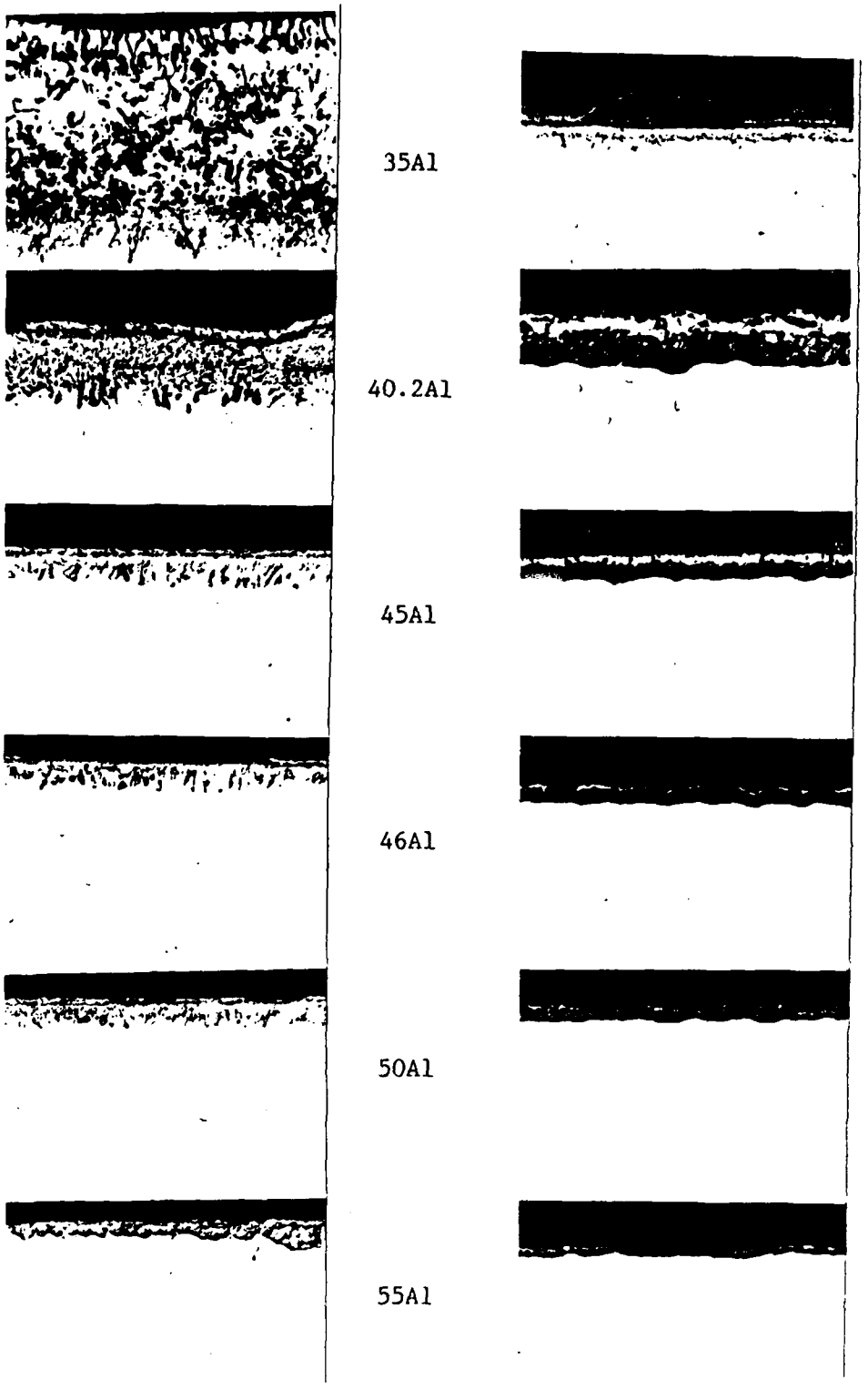

Figure 29: Effect of Al on oxide scales formed on Nb-Ti-Al-Cr-V alloys in air at 1100 and 1400°C.

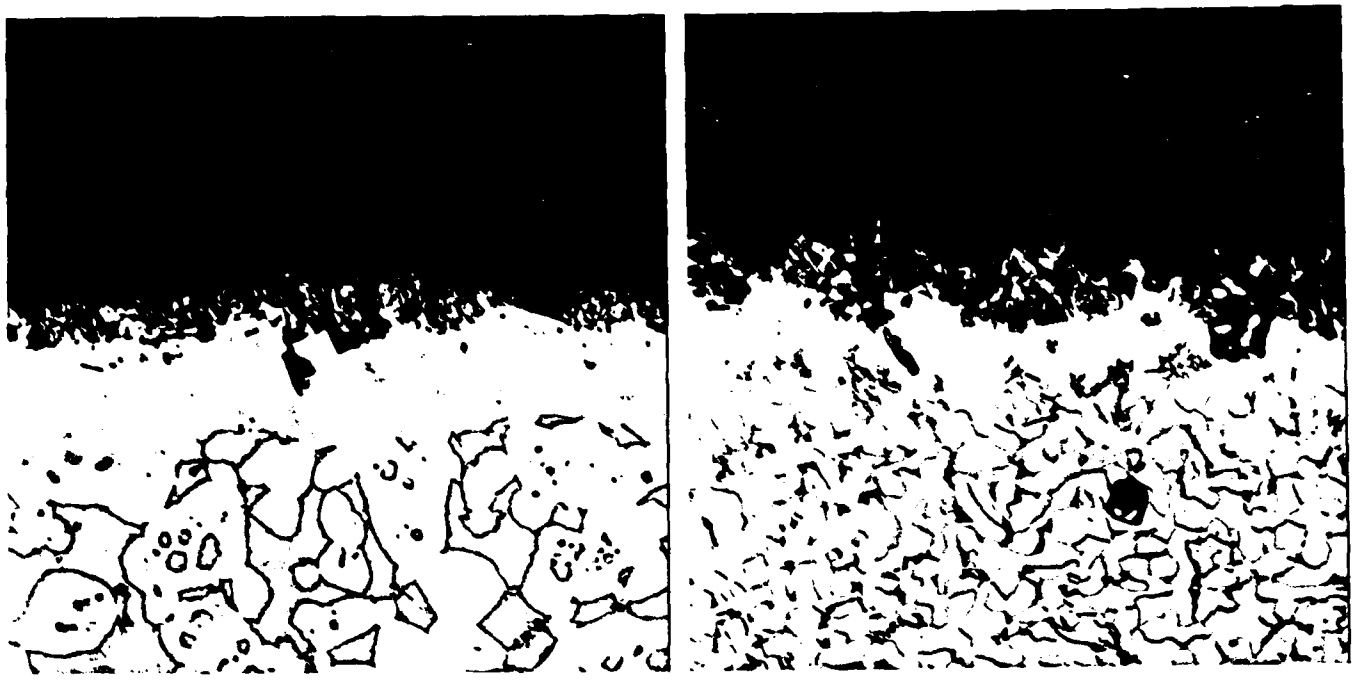

A- 38Al (96-1)

B- 44Al (96-2)

25μm

C- 48Al (96-3)

Nb:Ti=1.33, 3Cr, 4V
20h-1300°C-Air

Figure 30: Effect of Al on oxide scales formed on Nb-Ti-Al-Cr-V alloys in air at 1300°C.

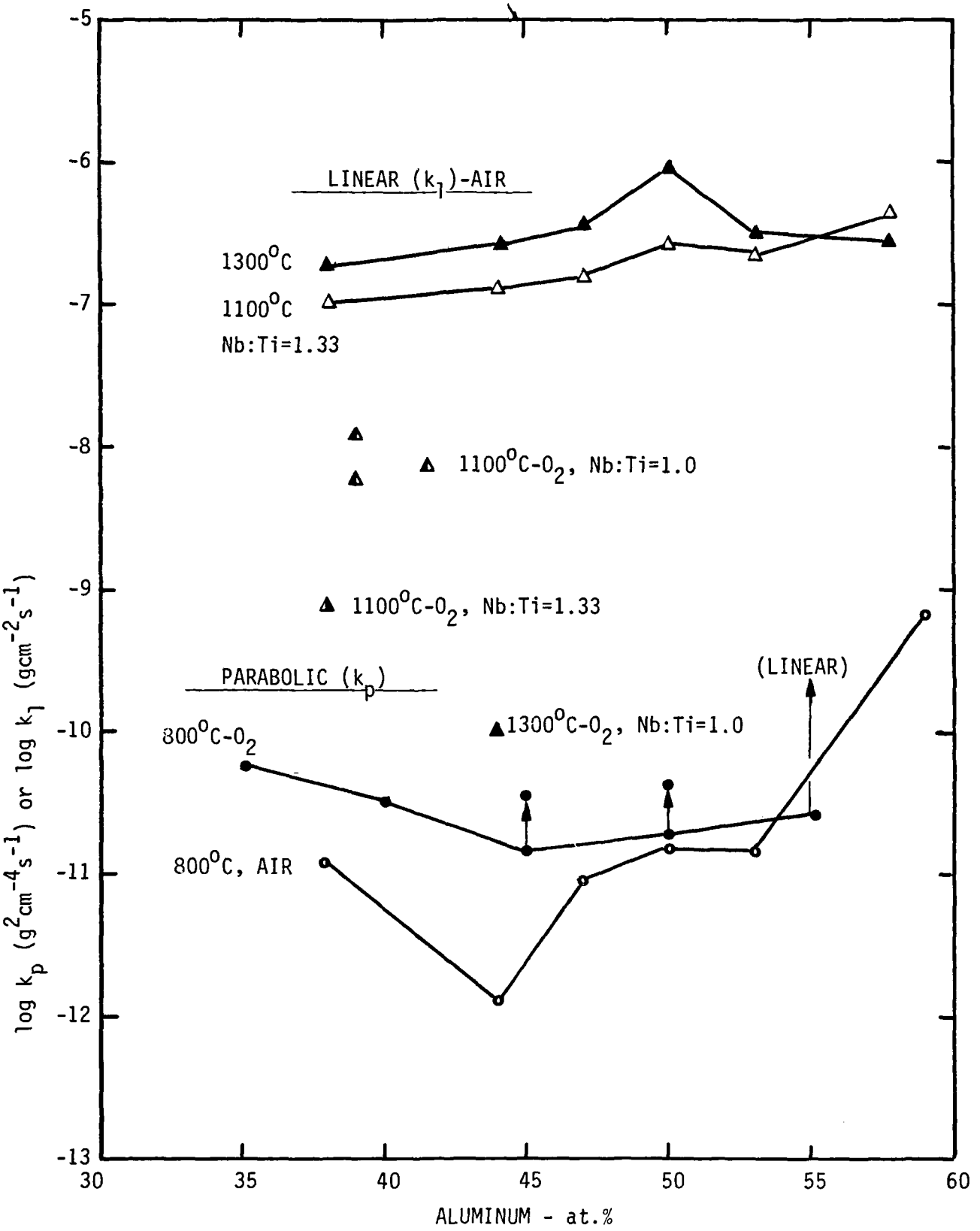

Figure 31: Effect of Al on oxidation rate constants for Nb-Ti-Al-Cr-V alloys at 800-1300°C in air and oxygen.

was largely independent of Al content from 35-58% Typical rate plots are shown in Figs. 32 and 33. All curves essentially are the same regardless of Al content considering the variability in kinetic data obtained by microbalance tests. As shown in Fig. 33, plots of weight gain vs square root

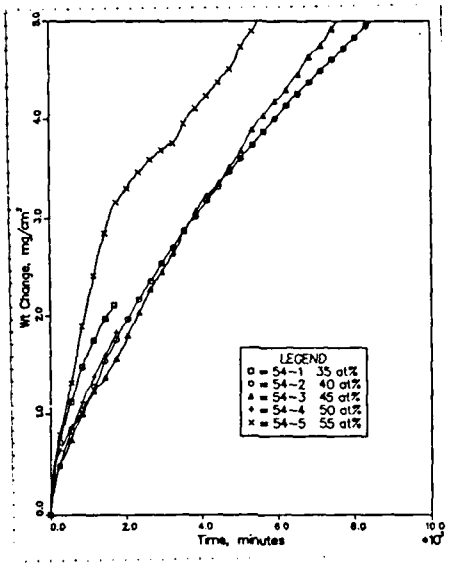

Figure 32: Effect of Al content on oxidation rate curves at 800°C in oxygen.

of time tend to curve upward. The plots should be linear for a true parabolic behavior. Each plot appears to have linear segments but the rate for each segment increases with time. These curves were analyzed to determine the rate law exponent as a function of time and the results are plotted in Fig. 34. No consistent trends are indicated and the instantaneous rate constant is close to parabolic at all times, except for alloy 54-5 with 55% Al. The rate constant for this alloy increased with time and became linear at 6600m (110h). A breakaway oxidation behavior is indicated at the highest Al content.

It is concluded that the major effect of Al is on the transition from internal to external oxidation and the amount of transient oxidation that occurs before growth is cut off by a continuous alumina scale. In compositions that do not form continuous alumina, the rate of oxidation is relatively independent of Al content at all temperatures. There is a slight trend to increased rate of oxidation with increased Al, particularly at 1100-1300°C but the effect is minor. Large variations in Al content appear to have little effect on the rate of base alloy oxidation unless the alloy is close to forming a continuous alumina scale.

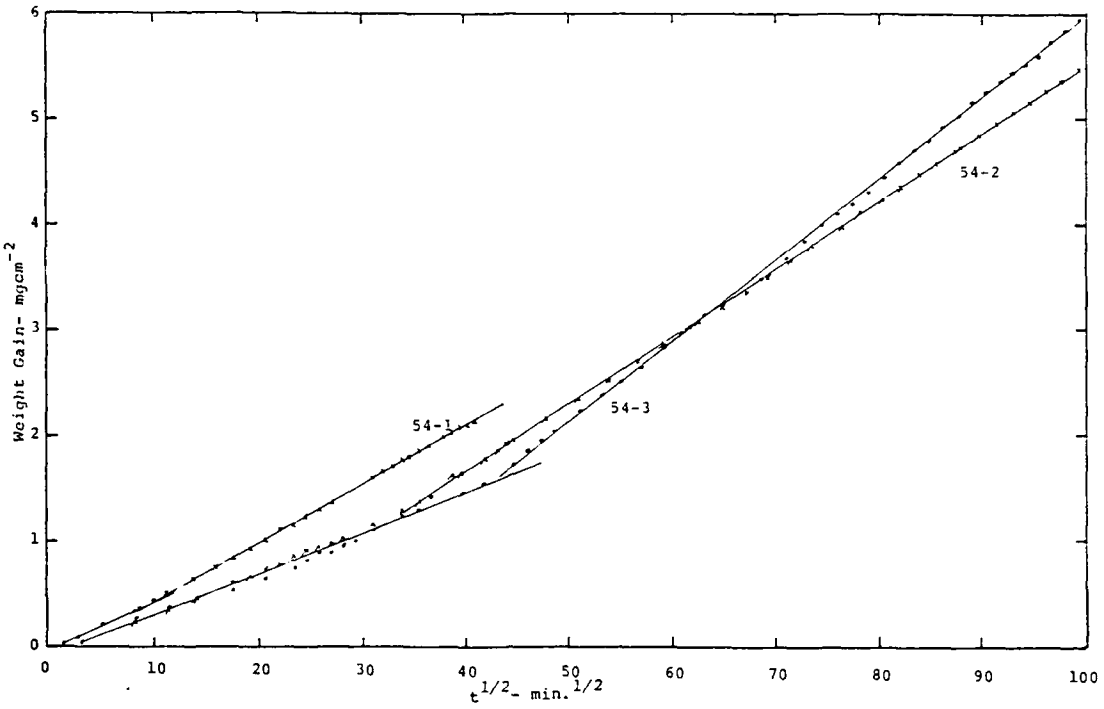

A- Alloys with 35-45% Al.

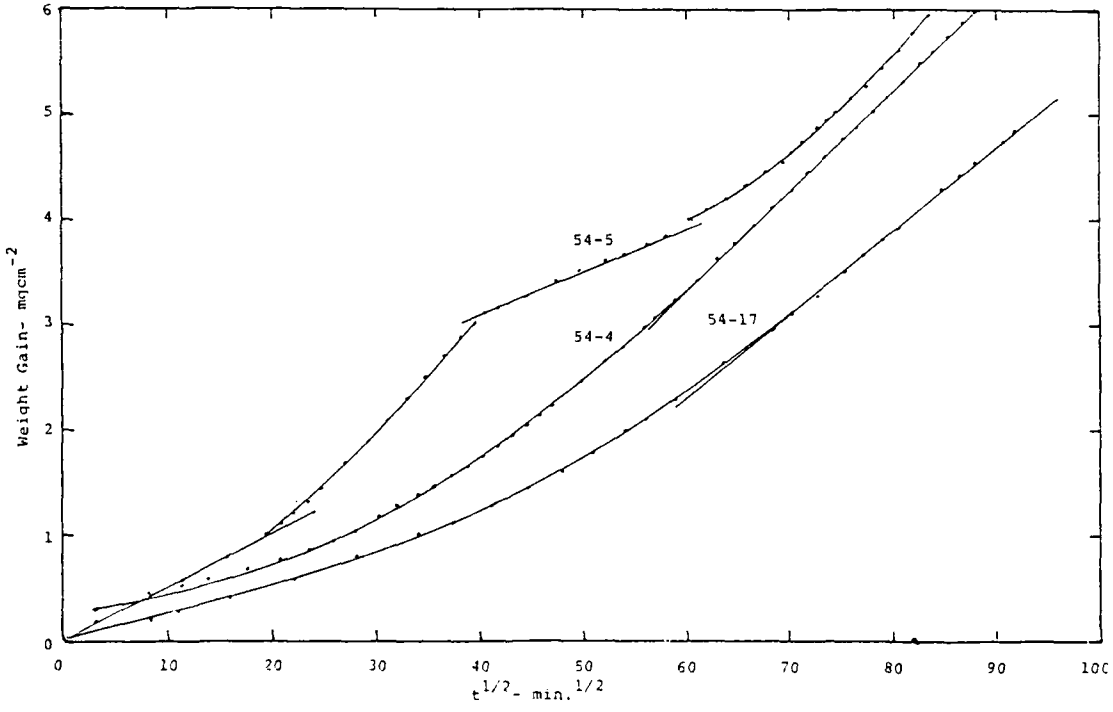

B- Alloys with 46-55% Al

Figure 33: Parabolic plots of rate curves at 800°C for alloys with 35-55% Al.

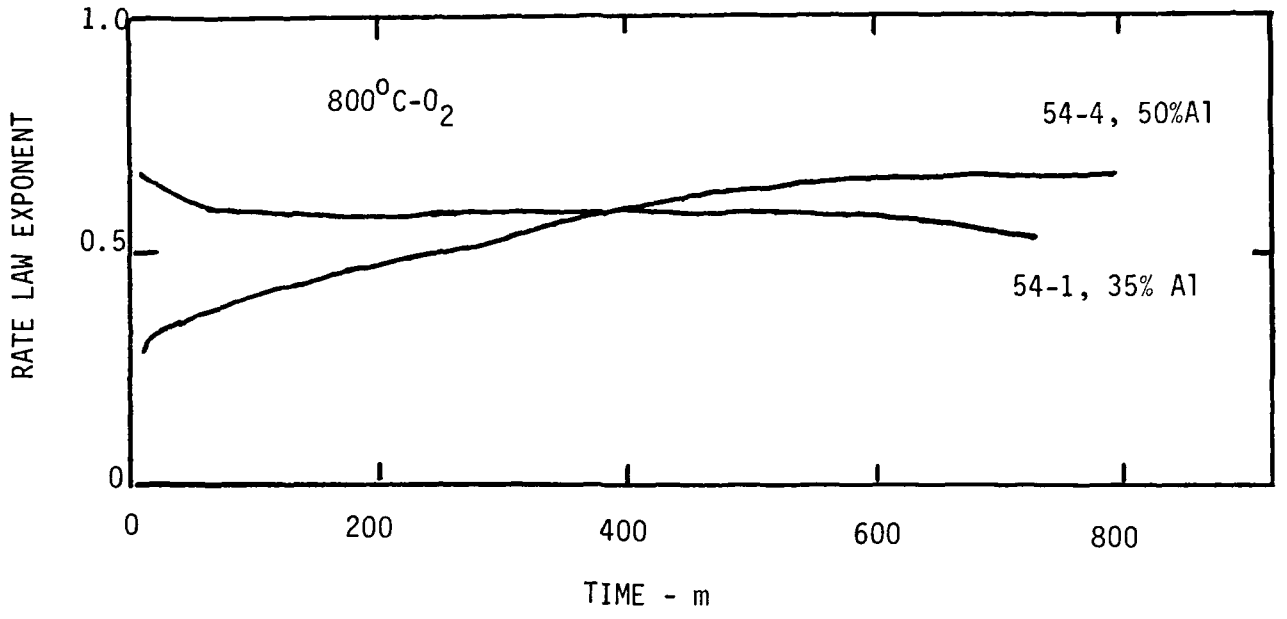

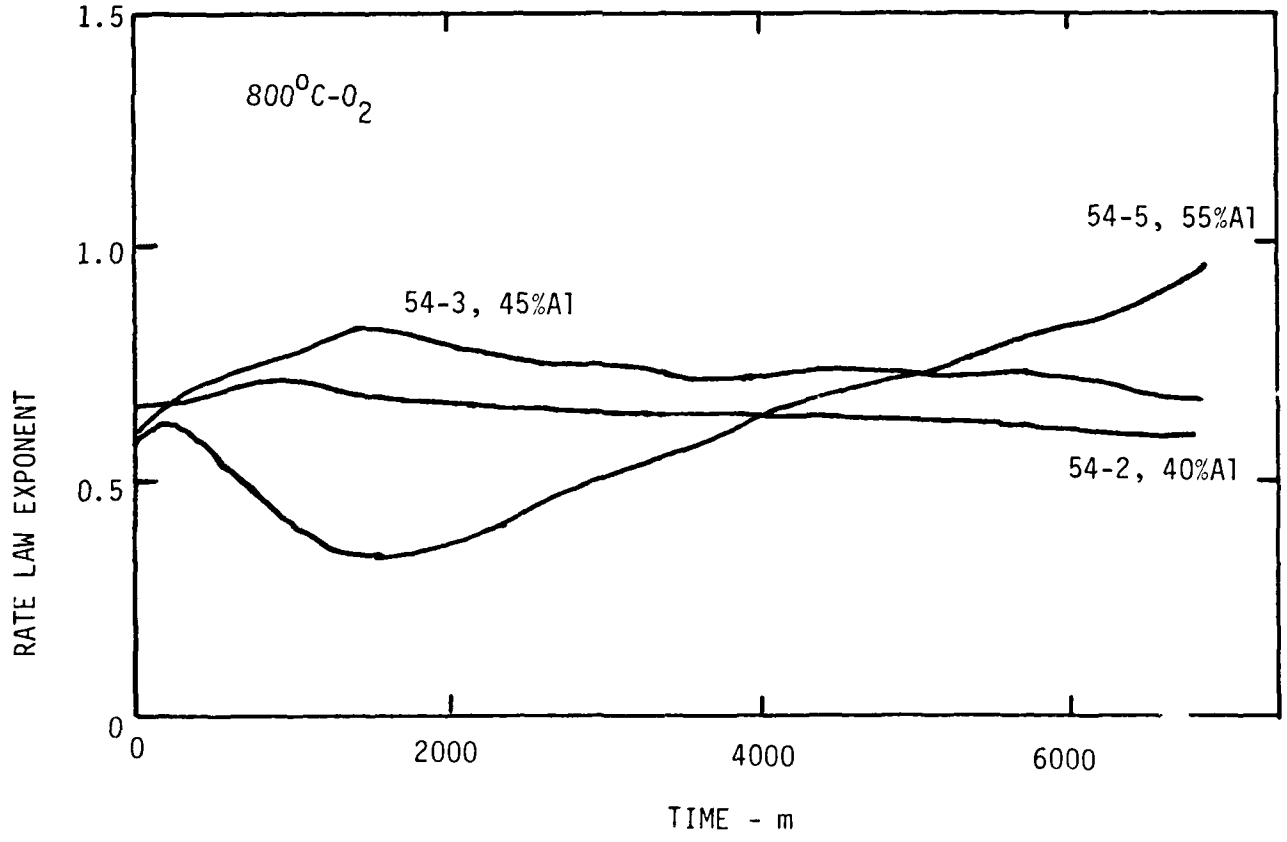

Figure 34: Variation of rate law exponent with time in oxygen at 800°C.

Effect of Nb:Ti Ratio

Two classes of Nb-Ti-Al alloys were prepared for evaluation: 1- those with a low ratio of Nb:Ti (0.8-1.0) and 2- those with a high ratio of Nb-Ti (1.1-1.4). The Nb:Ti ratio had a significant effect on the $N_{Al}^{crit.}$ for the transition from internal to external oxidation of Al. As shown in Fig. 35, continuous alumina scales were formed on alloys with 34-35% Al at the low Nb:Ti ratio and at 27-32% Al on alloys at the high Nb:Ti ratio.

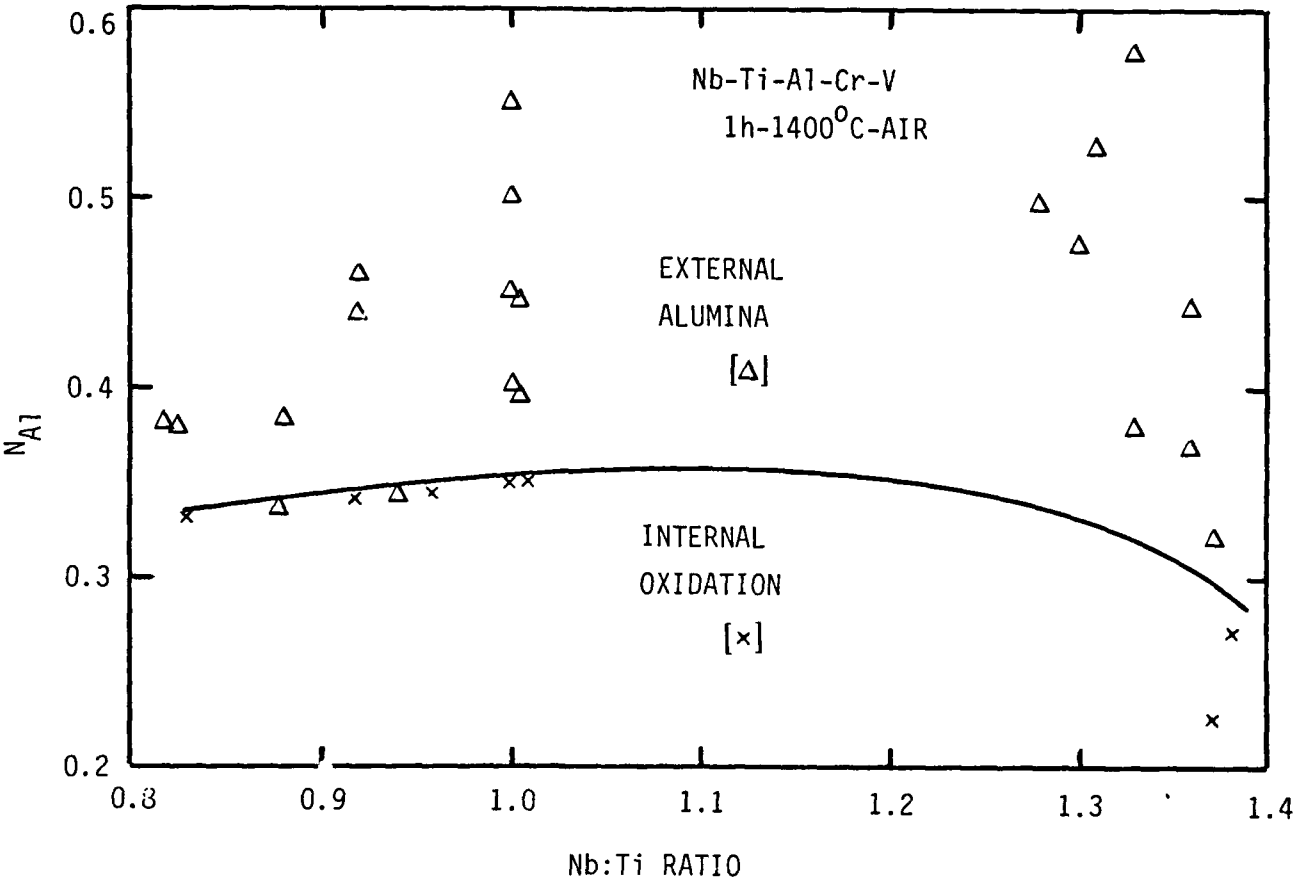

Figure 35: Effect of Nb:Ti ratio on $N_{Al}^{crit.}$ for external alumina scale formation.

The effect of the Nb:Ti ratio appears to be related to a decrease in kinetics for transient oxidation with increasing Nb:Ti ratio. As shown in Fig. 31, the parabolic rate constant for base metal oxidation at 800°C, where a continuous alumina scale does not form, is one-half to one order of magnitude lower for alloys with a high Nb:Ti ratio and >47% Al compared with alloys having a low Nb:Ti ratio. At higher Al contents, the rate constants are similar for both classes of alloys. However, when the total weight gain is considered instead

of the rate constant, the effect of Nb:Ti ratio is observed at all Al contents as shown in Fig 36. The total weight gain reflects the differences in the amount of oxidation that occurs before a steady parabolic rate is established. It is concluded that the major effect of the Nb:Ti ratio is to alter the transient oxidation kinetics.

The effect of Nb:Ti ratio most likely is the result of a change in microstructure of the alloys. As shown in Fig.5, alloys with a high Nb:Ti ratio lie within the shaded area and have a two phase structure ($\sigma+\gamma$) at 1100°C. The balance of the two in the structure changes as both the Al content and the Nb:Ti ratio are varied within the shaded area (Fig.5). However, when the Nb:Ti ratio is decreased to 1:1 or less, a three phase field is entered in which α-Ti_3Al (modified with Nb) can exist as a stable phase. This phase has poor resistance to oxidation at all temperatures by virtue of the low Al content and is believed to be the source of increased rates of transient oxidation. A high ratio of Nb:Ti (>1) is needed to stay in the two phase field where overall oxidation rates will be lower. A ration of 1.3:1 is preferred.

Alloys with a high Nb:Ti ratio have a minimum amount of oxidation when the Al content is in the range of 45-47% as shown in Fig. 36. The rate of oxidation increases rapidly, however, when the Al content is increased beyond 50%. This effect again appears to be the result of a change in microstructure of the alloys. The amount of γ-TiAl phase in the structure increases as the Al content is increased (Fig.5). As shown in Fig.37, the amount of γ-TiAl in the structure increases rapidly beyond 47% Al. At 58% Al, the alloy is nearly all γ-TiAl and the rate of oxidation is very rapid. This phase can be an alumina former above 1200°C but does not form alumina at lower temperatures and oxidizes with rapid kinetics. Alloy oxidation appears to be increased when this phase becomes the continuous or matrix phase in the alloy. The reason for this behavior is not clear but may be related to changes in diffusivity of Al in the matrix. The gamma phase has a primitive tetragonal ($L1_o$) structure similar to AuCu with four atoms in a small unit cell whereas the Nb_2Al sigma phase has a tetragonal ($D8_b$) structure similar to that of the FeCr sigma phase with 30 atoms in a very large unit cell. The latter is a very densely packed structure and it is unlikely that Al would have a higher diffusivity in this phase compared with γ-TiAl. Grain size rather than crystal structure of

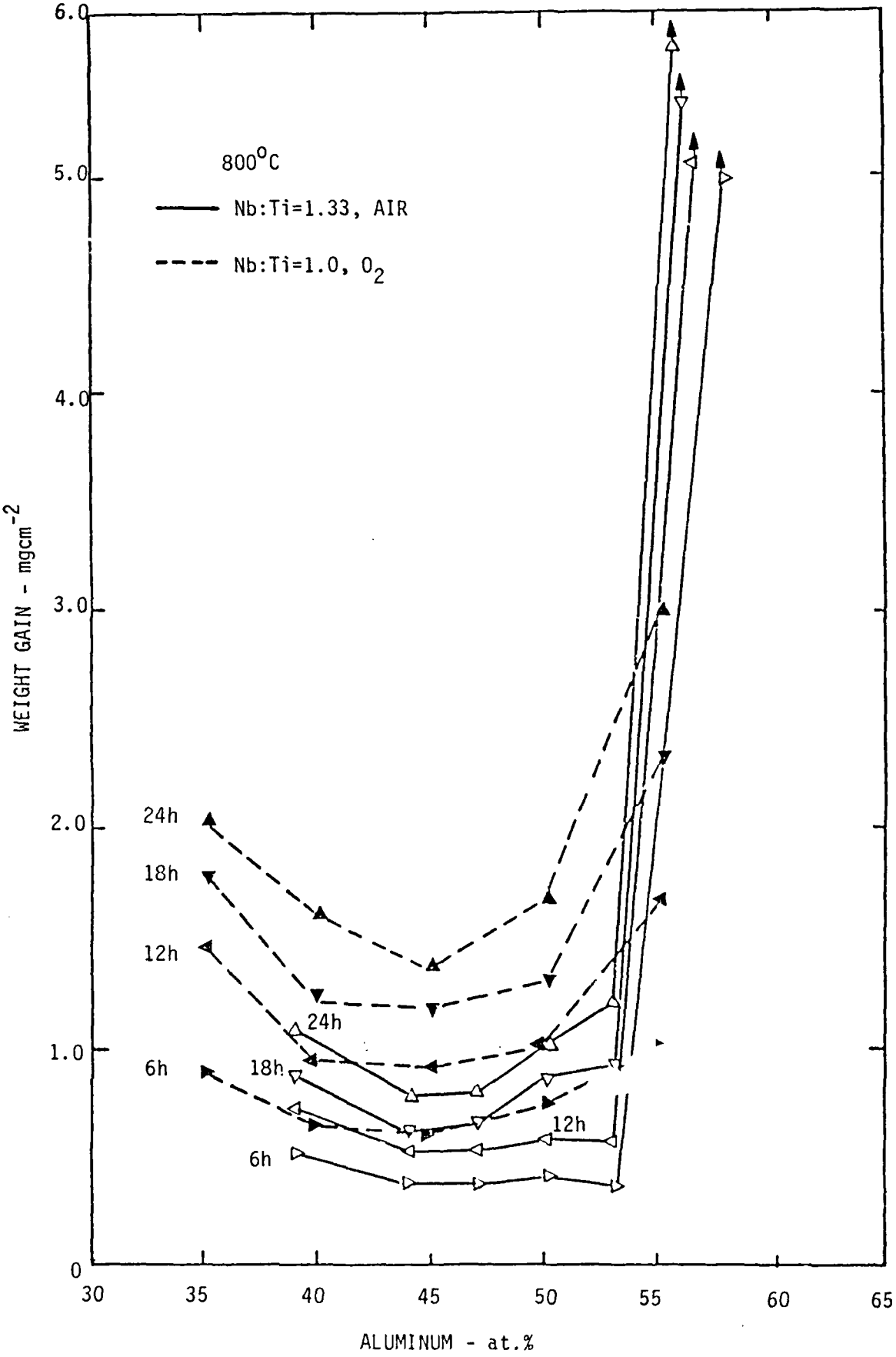

Figure 36: Effect of Al content and Nb:Ti ratio on weight gain at 800°C.

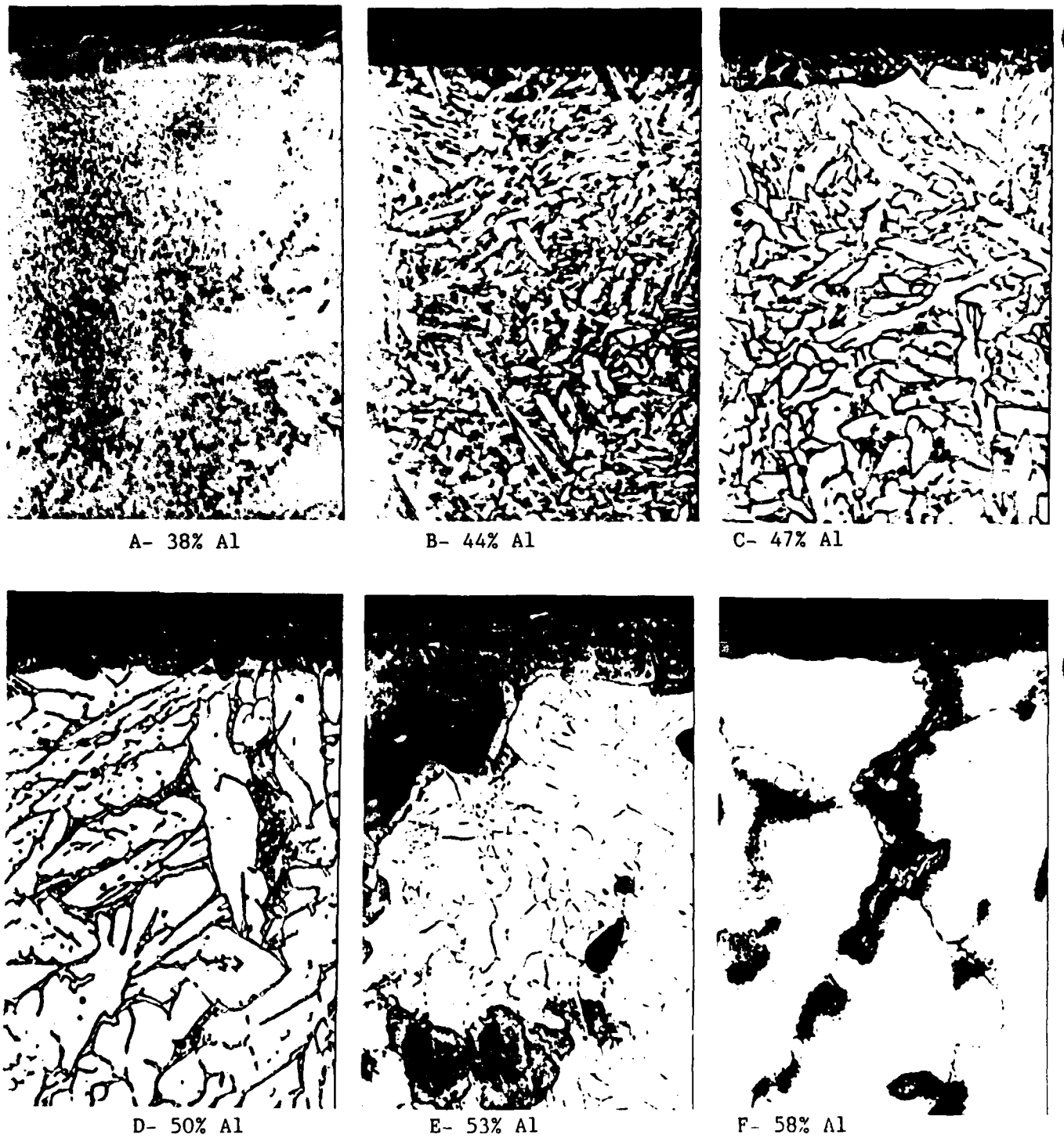

Figure 37: Effect of Al content on alloy microstructure of Nb-Ti-Al-Cr-V alloys at 800°C.

the matrix is more likely to be the controlling factor in this case. As shown in Fig. 37, an alloy with 44% Al has a very fine grained two phase structure with a very large interfacial area between two phases with widely different unit cells. The interface boundaries are likely to have a high concentration of defects and may provide paths for rapid diffusion. As the Al content is increased, the grain size of the two phases is increased and the amount of rapid diffusion paths is decreased. Finally, at 58% Al, the structure becomes single phase with a very coarse grain size and few, if any, high defect interfaces for diffusion (Fig. 37F).

The ratio of Nb:Ti also affects the amount of internal oxidation that occurs in alloys under conditions where continuous alumina scales are not formed. Alloys with a low Nb:Ti ratio tend to oxidize internally at 1100°C as shown in Fig.38B. The Al-rich γ-TiAl phase is attacked selectively. When the Nb-Ti ratio is increased, however, the amount of internal oxidation is reduced significantly from 49 μm penetration at a ratio of 0.88 to 19 μm penetration at a ratio of 1.33 in 2h at 1100°C (Fig.38A). As the Al content of alloys with a high Nb:Ti ratio is increased, an Al depleted layer, which is single phase sigma is formed under a rapidly growing oxide scale. This phase does not tend to be oxidized internally as shown in Figs. 30 and 39. Alloys with a 1:1 Nb:Ti ratio oxidize internally at all Al contents as shown in Fig. 29. A high rate of scale formation at 1100°C in alloys with a high Nb:Ti ratio is offset by reduced internal oxidation, resulting in an overall reduced oxygen pickup and weight gain. Increasing the Nb:Ti ratio appears to enhance formation of sigma phase by alloy depletion at the scale/metal interface.

Effect of Temperature

Temperature of exposure has the greatest effect on oxidation behavior compared with composition variables. As shown in Fig. 40, the rate of oxidation increases dramatically with increasing temperature in the range of 1100-1200°C where continuous alumina scales are not formed. Alloys which oxidize with linear kinetics in oxygen in this temperature range approach parabolic behavior at 1300°C when alumina scales begin to form and the rate of oxidation drops precipitously. As the transition to continuous alumina formation is approached, the rate of oxidation first increases and then decreases rapidly. The result is a peak in the curve of oxidation weight gain

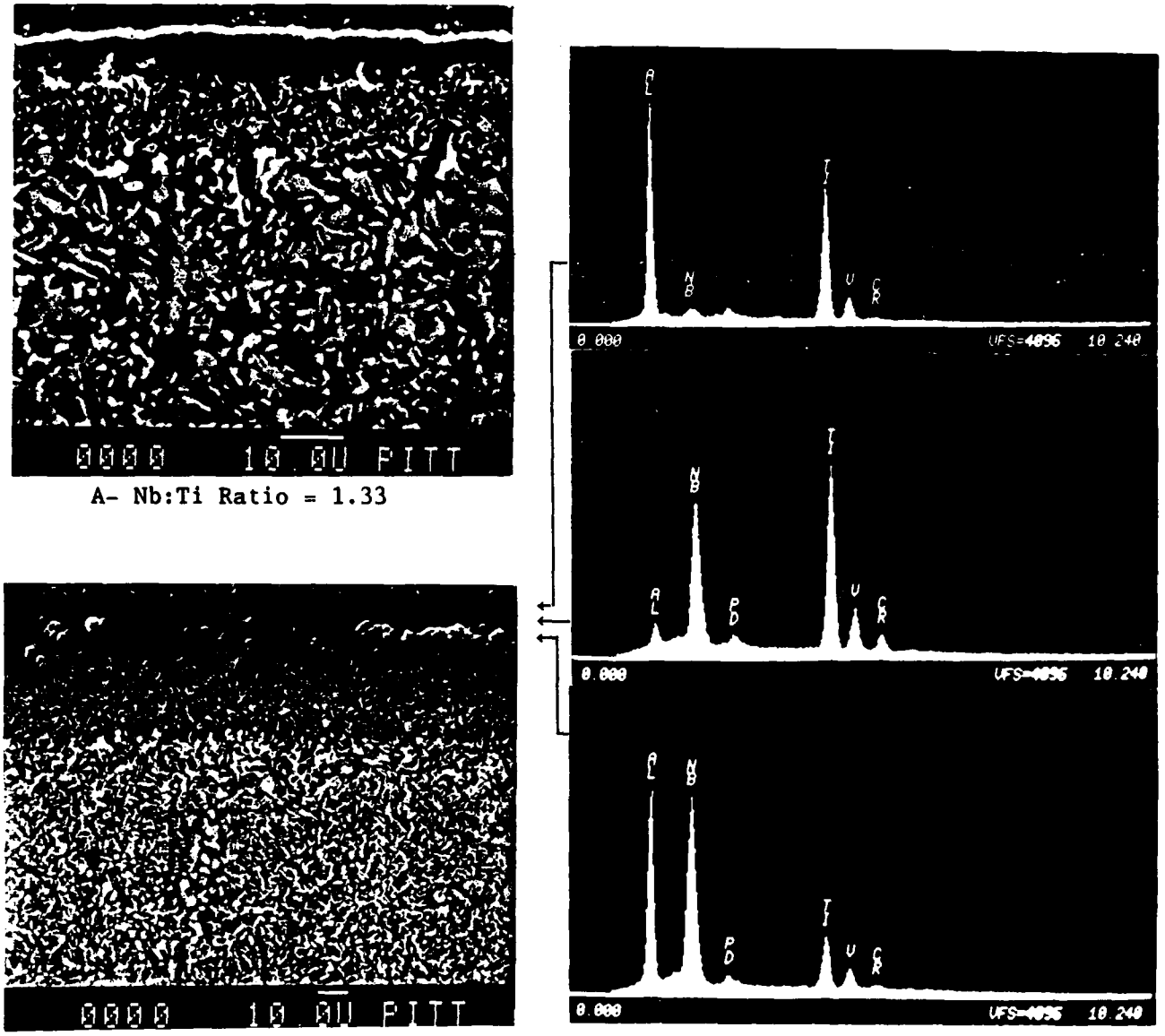

A- Nb:Ti Ratio = 1.33

B- Nb:Ti Ratio = 0.88

Nb-Ti-38Al-3Cr-4V
2h-1100°C

Figure 38: Effect of Nb:Ti ratio on internal oxidation at 1100°C.

for a fixed time of exposure vs temperature as shown in Fig. 41. The total weight gain is a maximum at 1200°C for a baseline alloy with a Nb:Ti ratio of 1.04. The alloy is oxidized internally and forms a thick external scale at 1100-1200°C while a thin, continuous alumina scale is formed at 1300°C. The change in internal oxidation and scale morphology with increasing temperature is shown more clearly in Figs. 42-43. It is significant to note in Fig. 42

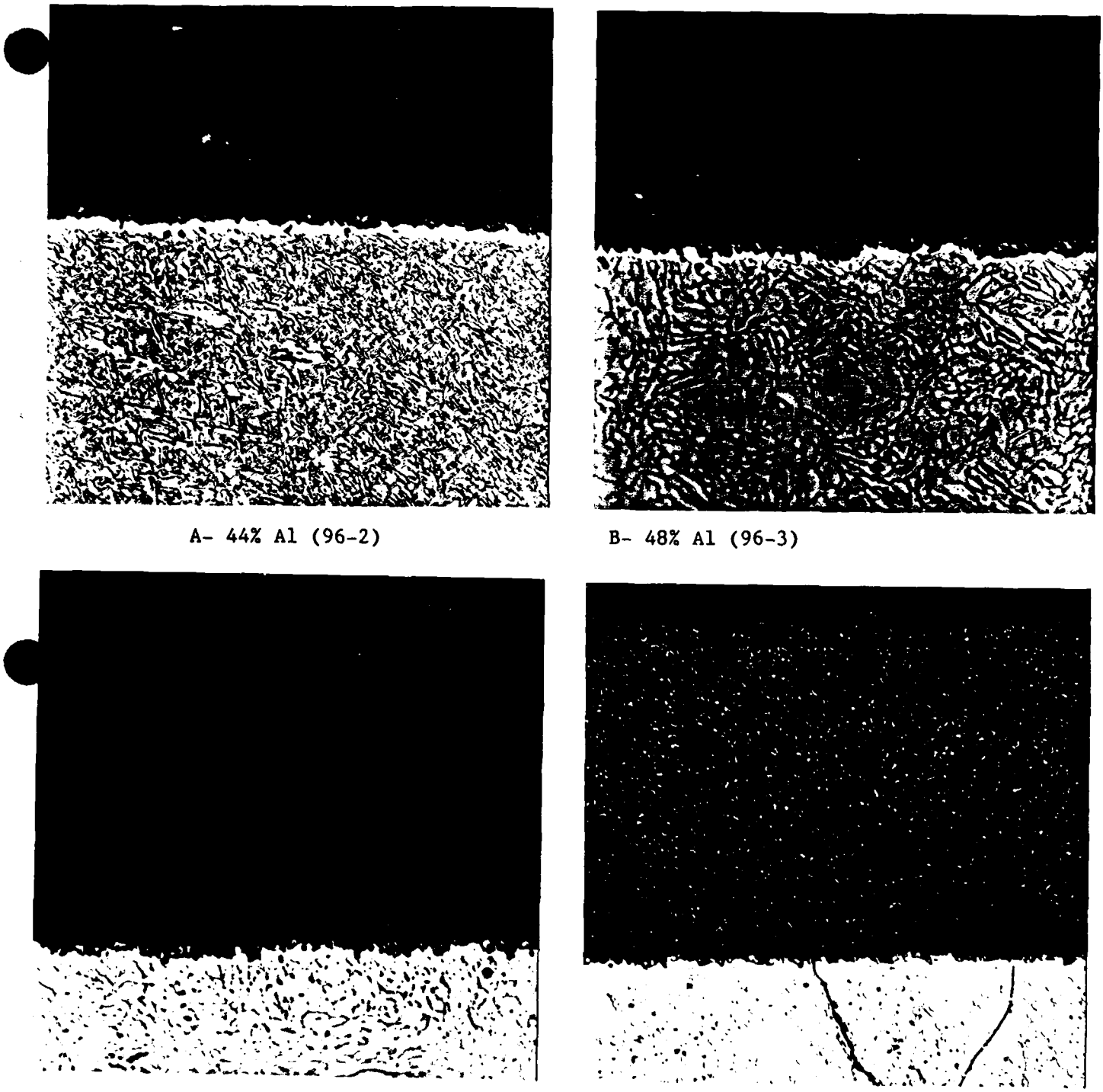

Figure 39: Effect of Al on oxide scales formed at 1100°C.

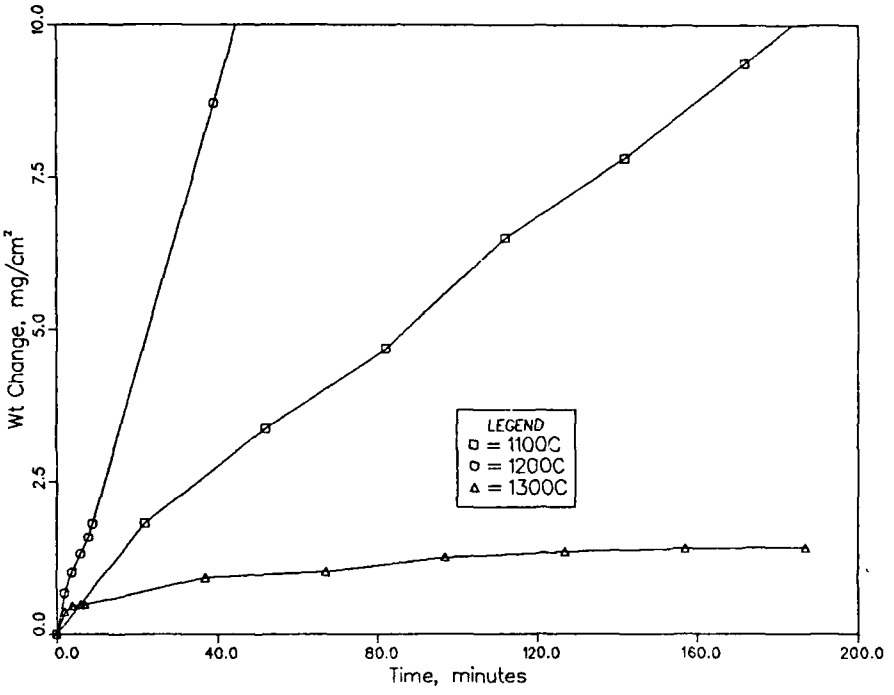

A- 24Nb-23Ti-44Al-4Cr-5V (70-1)

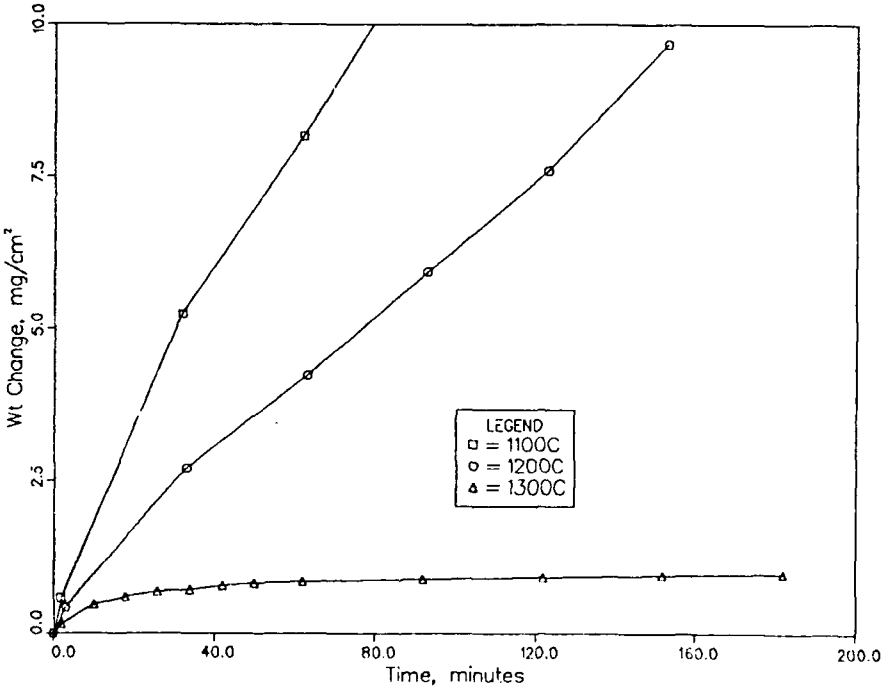

B- 22Nb-24Ti-44Al-8Cr-6V (70-3)

Figure 40: Variation of oxidation kinetics with temperature for Nb-Ti-Al-Cr-V alloys in oxygen.

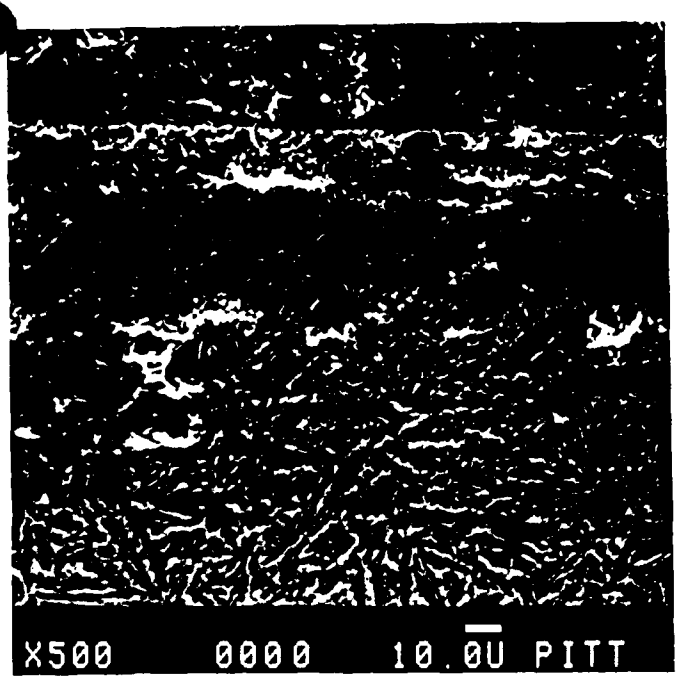

A- 3h-1100°C

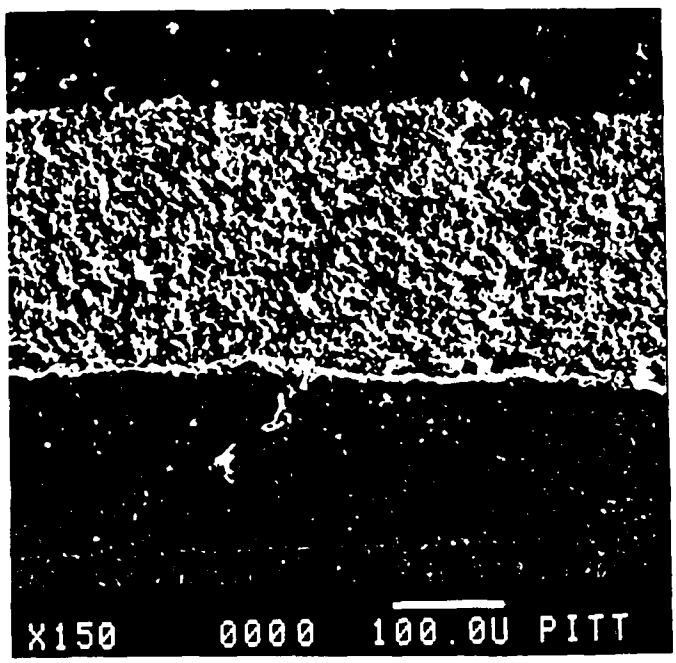

B- 3h-1200°C

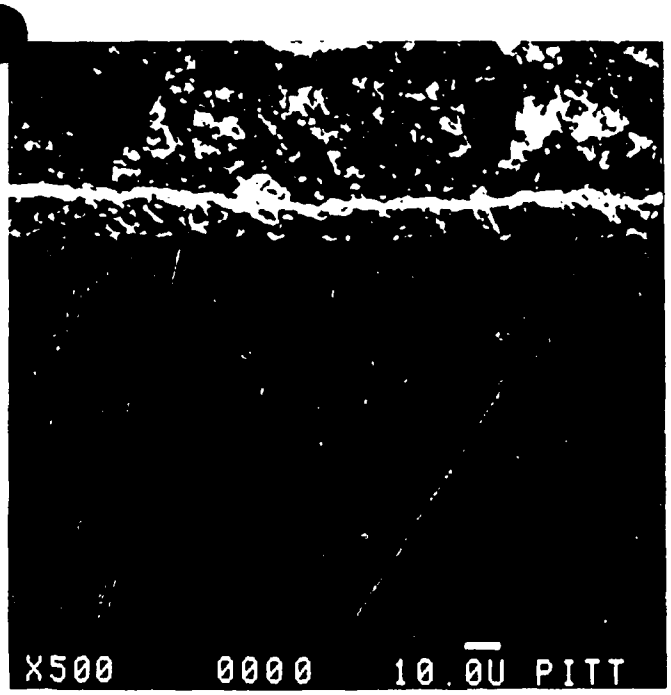

C- 3h-1300°C

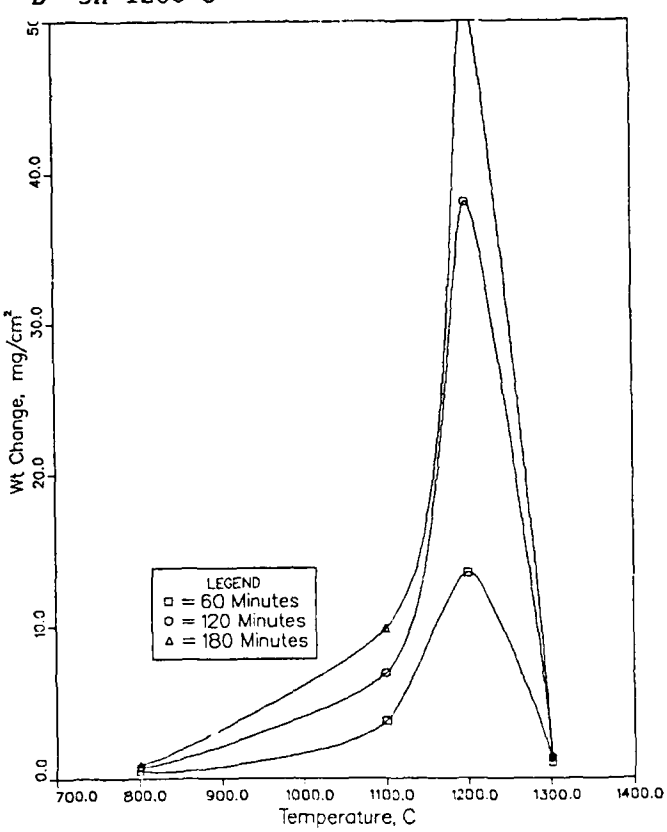

24Nb-23Ti-44Al-4Cr-5V (70-1)

Figure 41: Variation of weight gain with temperature for a Nb-Ti-Al-Cr-V alloy with 4Cr and 5V.

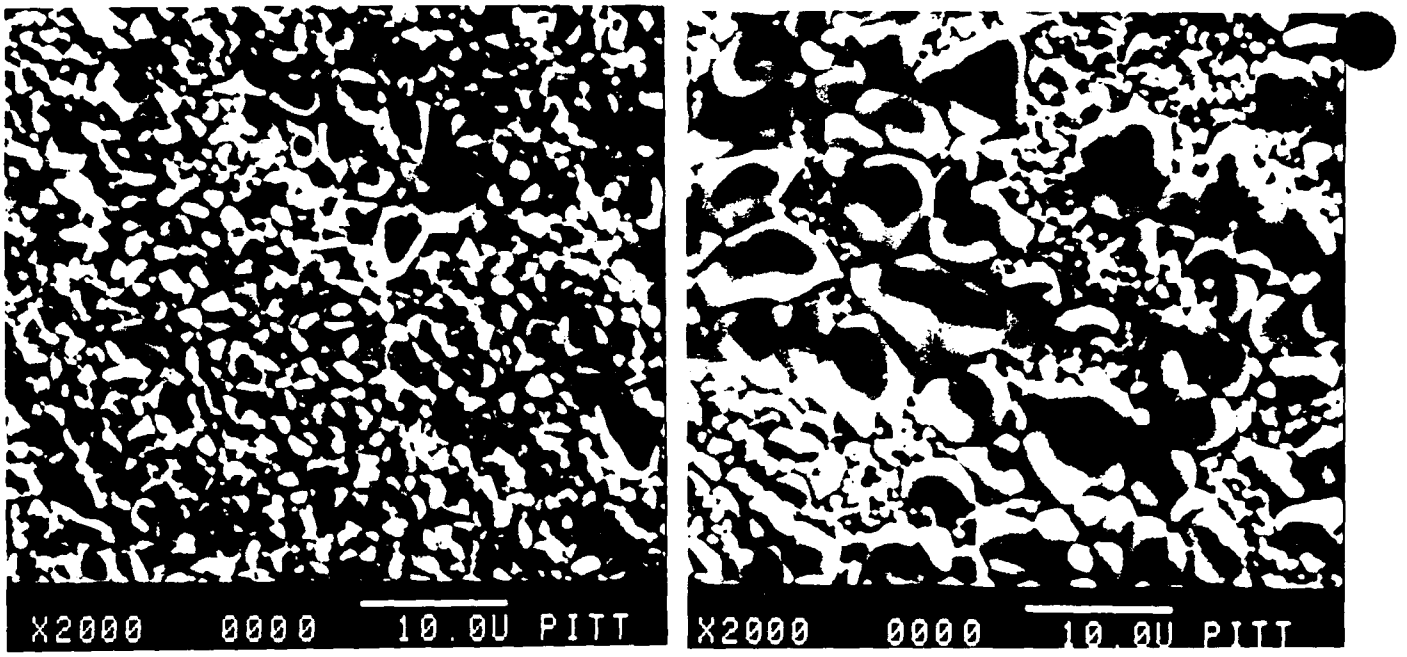

Oxide Surface

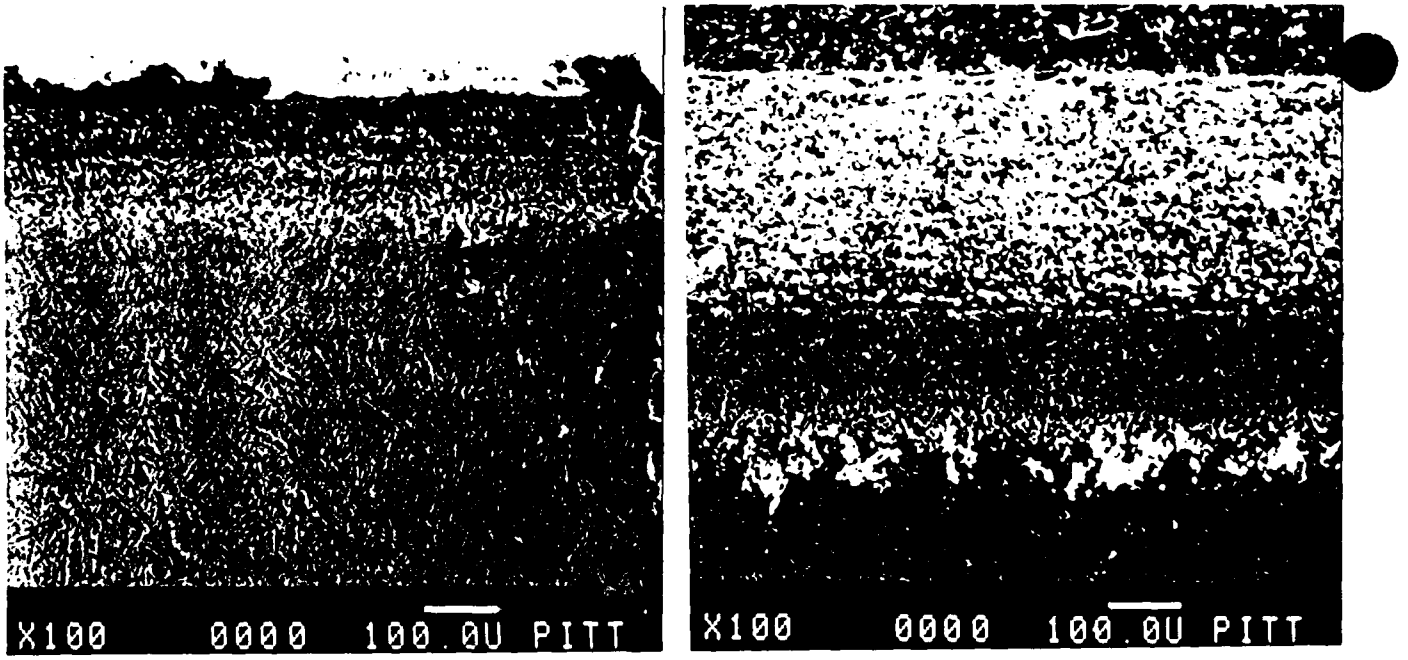

Cross Section

24h 168h

1100°C-Oxygen
24Nb-23Ti-44Al-4Cr-5V (70-1)

Figure 42: Oxide scales formed on Nb-Ti-Al-Cr-V alloys having a low Cr and V content.

A- 27h-800°C 13µm

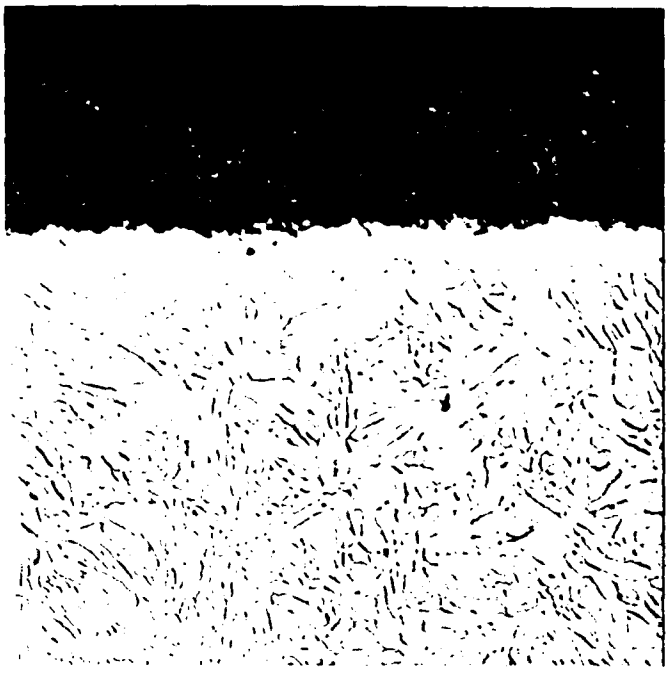

B- 22h-1100°C 25µm

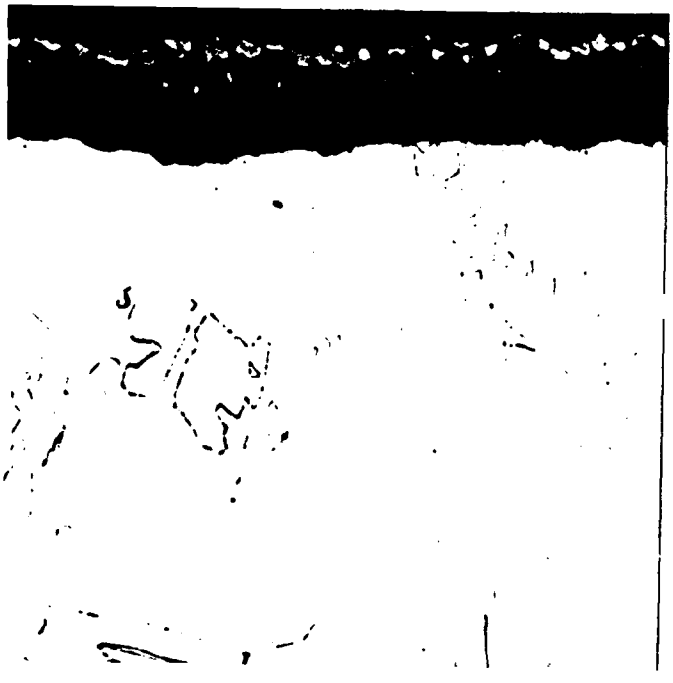

C- 19h-1300°C 13µm

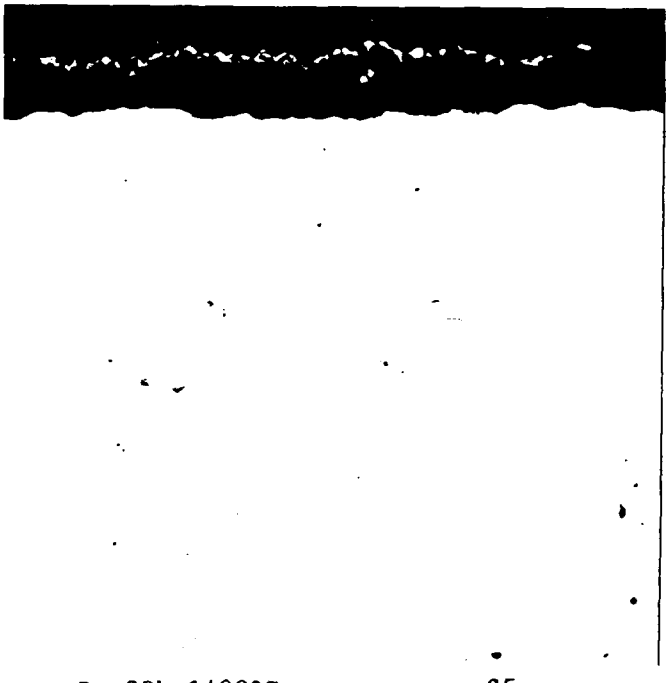

D- 20h-1400°C 25µm

24Nb-23Ti-44Al-4Cr-5V (70-1)

Figure 43: Effect of temperature on oxides scales and microstructure of a Nb-Ti-Al-Cr-V alloy having a low Cr and V content.

that the depth of internal oxidation does not increase significantly with increased time of exposure beyond 24h, only the thickness of the external scale appears to increase with time beyond this point. At 1300°C, the continuous external scale of alumina is protective and no internal oxidation occurs. A significant change in microstructure also is observed at his point. The fine grained two phase structure is replaced by a coarse grained acicular structure (Fig.43D). The alloy appears to be single phase at temperature and transforms on cooling. As noted earlier, these alloys become single phase ordered B2 at high temperature and transform to $\sigma+\gamma$ on cooling. A continuous alumina scale is formed more readily on the B2 phase. The coarse grain size does not appear to be a factor in this case.

The sharp transition from internal to external oxidation of Al with increasing temperature is believed to be the result of a change in the diffusivity of Al in the alloys as controlled by microstructure. At temperatures below 1300°C, the alloys have a two phase structure in which diffusivity of Al is not sufficient to nucleate and grow a continuous alumina scale. Above 1300°C, the alloys have a single phase BCC structure in which the diffusivity of Al should be much higher. The effect of composition on alloy behavior appears to be related primarily to changes in the microstructure of the alloy. The B2 phase can be stabilized to lower temperatures by increasing the amount of Ti in the alloy as discussed on pp.46-48. It also can be stabilized by increasing the Cr and V content as shown in Fig. 44. The peak in rate of oxidation vs temperature is reduced by 100°C when the Cr and V are increased to 8 and 6% respectively. A discontinuous alumina scale is formed at 1200°C and the rate of oxidation is reduced significantly. The alloy microstructure is largely transformed B2 with small islands of sigma phase, similar to that of the alloy with lower Cr and V contents at 1300°C. As shown in Fig. 45C, the alloy with high Cr and V contents is 100% transformed B2 on cooling from 1300°C. At temperatures of 800 and 1100°C, both alloys have a stable fine grained two phase structure and do not form protective alumina scales. Aluminum is oxidized internally and a thick complex scale of Ti and Al niobates is formed. The behavior of the high Cr and V content alloy at 1100°C (Fig. 46) is similar to that of the low Cr and V content alloy (Fig. 42). The internal oxidation zone reaches a limiting depth after a few hours and only the external scale thickness increases on continued exposure to 168h.

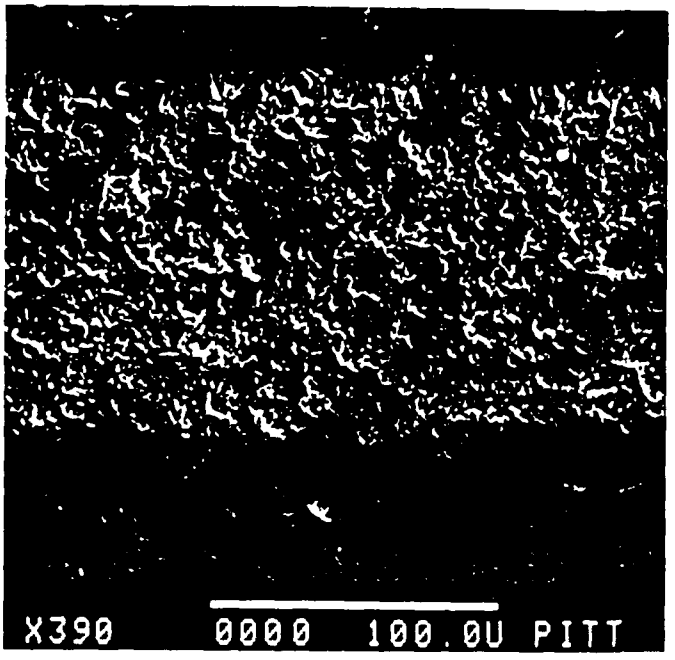

A- 3h-1100°C

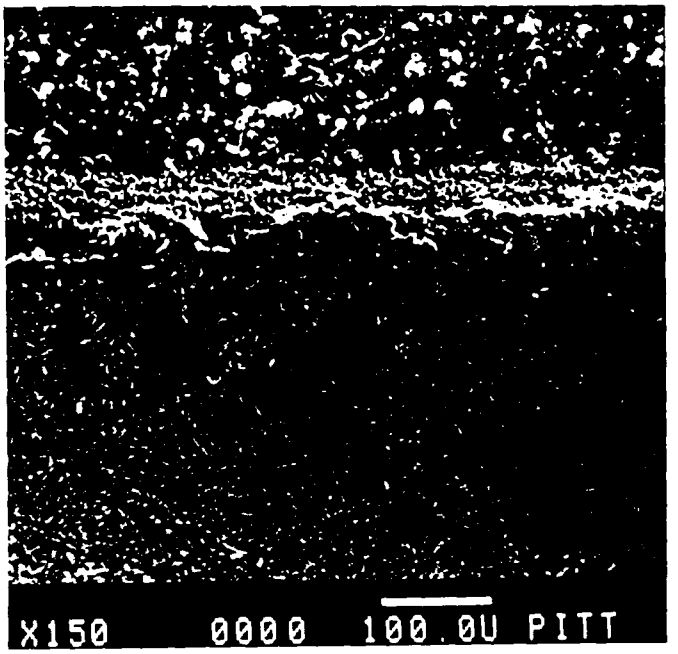

B- 3h-1200°C

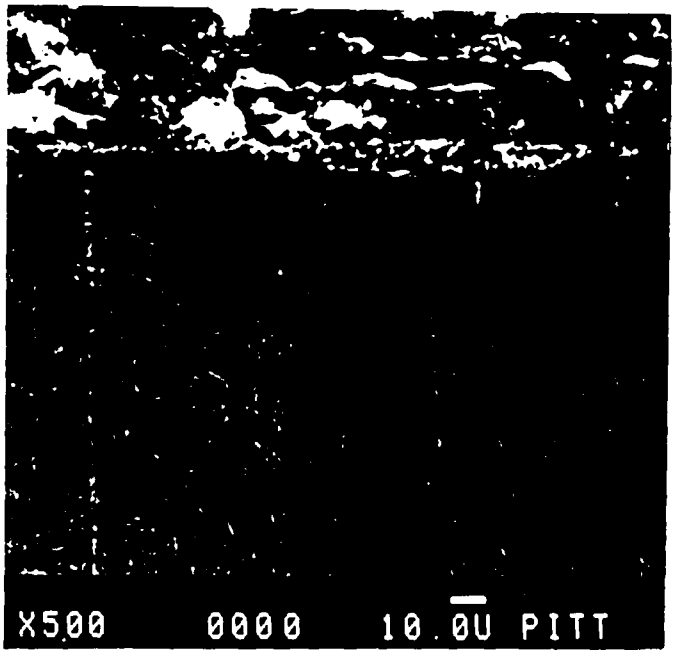

C- 3h-1300°C

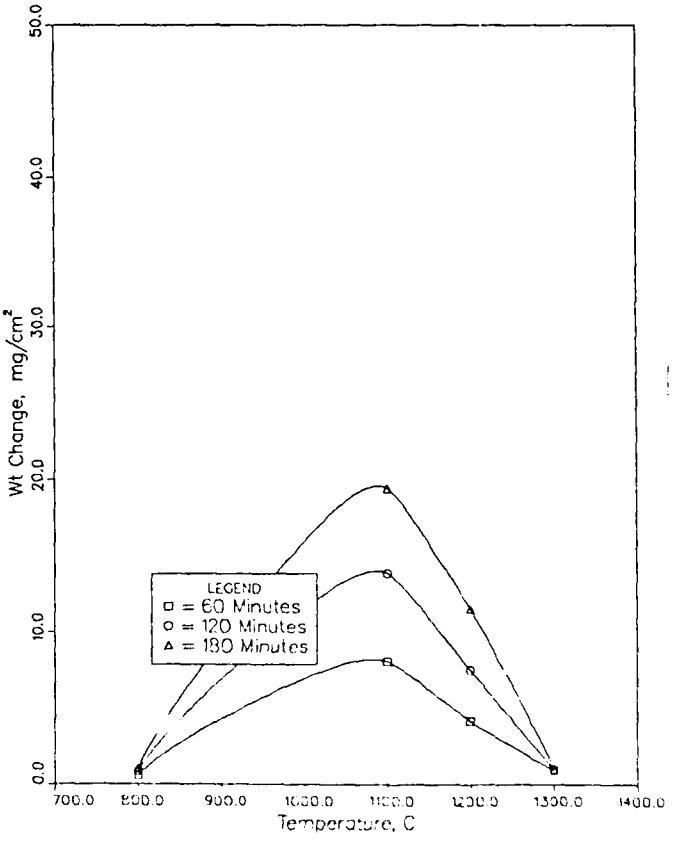

22Nb-24Ti-44Al-8Cr-6V (70-3)

Figure 44: Variation of weight gain with temperature for a Nb-Ti-Al-Cr-V alloy having a high Cr and V content.

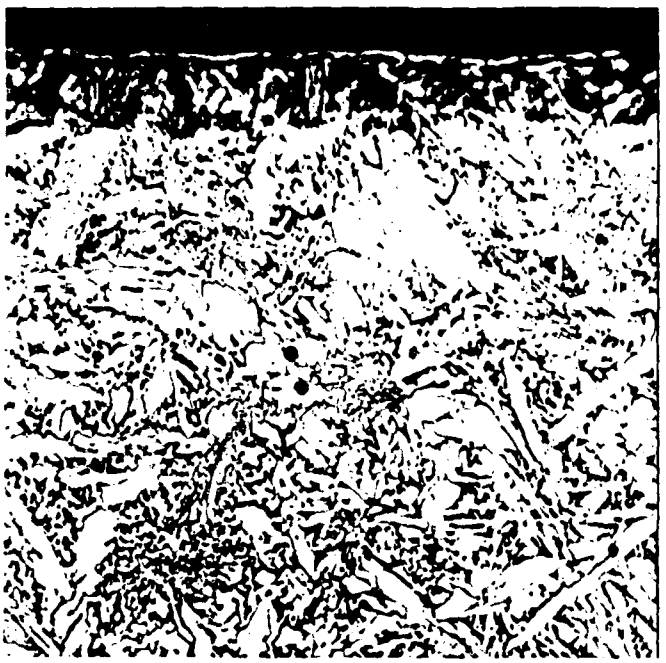

A- 21h-800°C 13μm

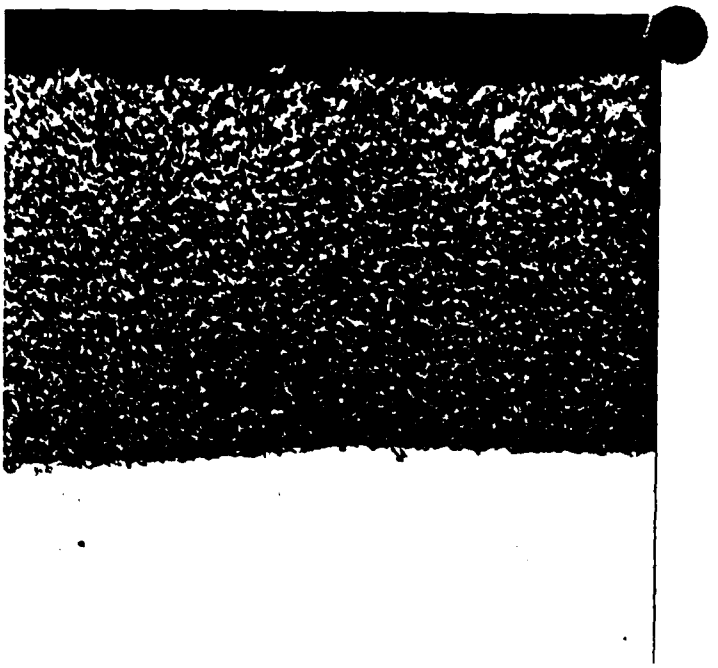

B- 25h-1100°C 32μm

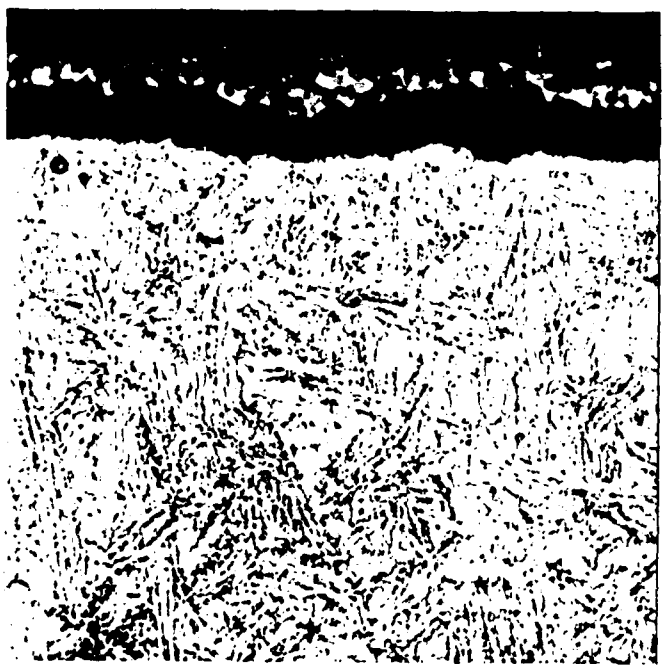

C- 23h-1300°C 13μm

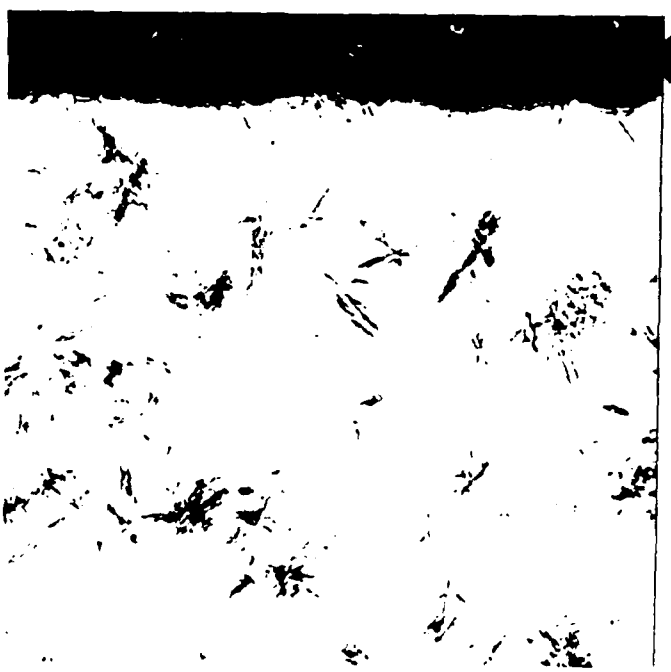

D- 23h-1400°C 25μm

22Nb-24Ti-44Al-8Cr-6V (70-3)

Figure 45: Effect of temperature on oxide scales and microstructure of Nb-Ti-Al-Cr-V alloys having a high Cr and V content.

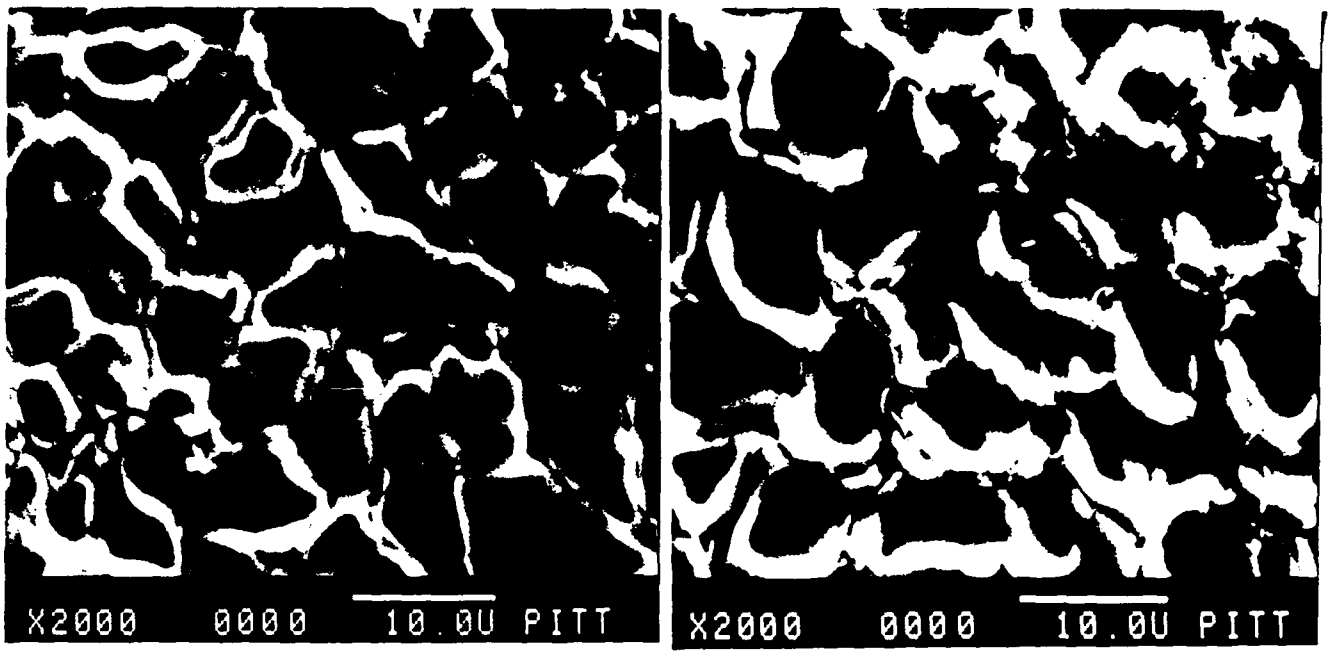

Oxide Surface

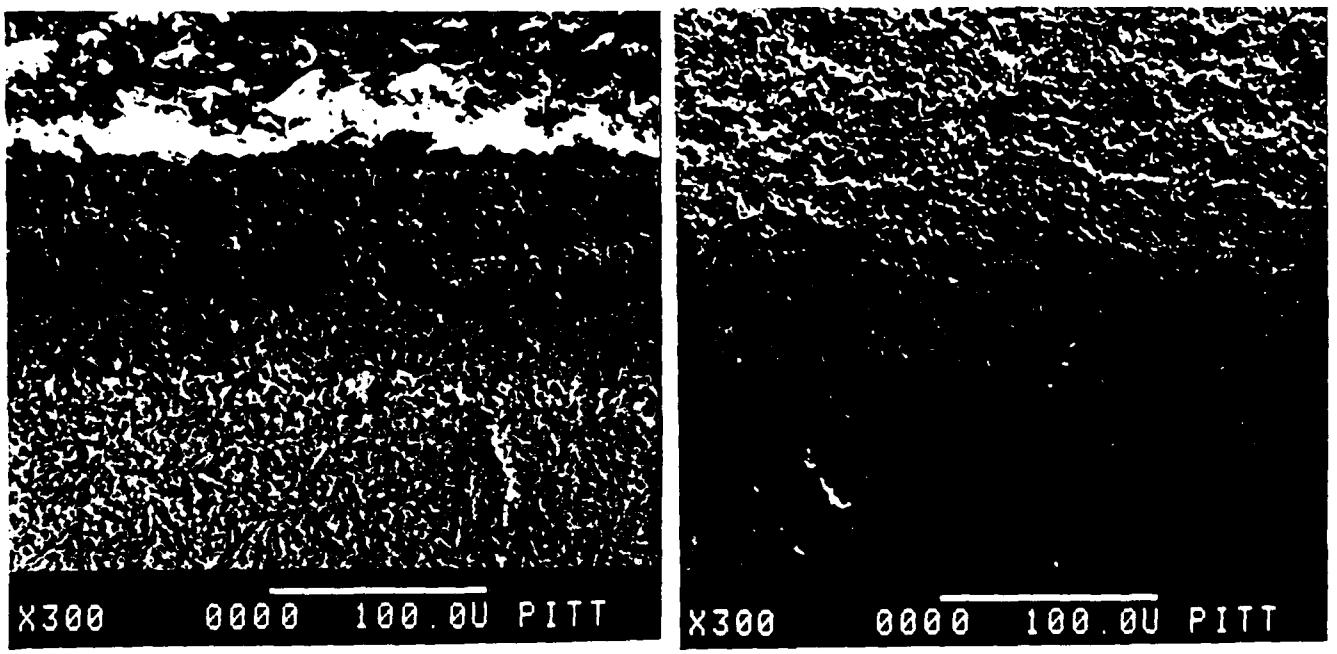

Cross Section

24h 168h

22Nb-24Ti-44Al-8Cr-6V (70-3)
1100°C-Oxygen

Figure 46: Oxide scales formed on Nb-Ti-Al-Cr-V alloys having a high Cr and V content.

Large variations in composition appear to have comparatively little effect on oxidation behavior when data are compared for only one test temperature. Figures 47 and 48 are compilations of oxidation rate curves for a wide range of alloy compositions at 800 and 1100°C respectively. With a few exceptions, the alloys have close to parabolic behavior with a breakaway toward linear on longer time exposure. The total gains in weight for any given time of exposure are almost within a scatter band for reproducibility for testing of any one alloy. The major effect of composition is on the temperature at which an external alumina scale can be formed. This temperature is controlled by composition and microstructure and is the primary basis on which alloy behavior should be judged. Oxidation behavior above or below this transition temperature was found to be similar for wide ranges of alloy compositions.

The variation of the parabolic rate constant with temperature for the best Nb-Ti-Al-Cr-V alloys is shown in Figure 49. These alloys have a Nb:Ti ratio of 1 to 1.3 and contain 38-53% Al, 2-8% Cr, and 3-6%V. At temperatures above 1250°C, they form continuous alumina scales and oxidize with kinetics the same as those of NiAl. Below 1250°C, the alloys form mixed Al-Ti niobate scales and oxidize with parabolic kinetics faster than those of NiAl. The slope of the curves indicates a lower activation energy for the growth of these scales compared with alumina scales. This was the lowest transition temperature found for Nb-base alloys in this range of Al contents. Adding Si to Nb-Ti-Al-Cr-V alloys reduced the rate of transient oxidation but did not result in formation of alumina at temperatures below 1250°. Parabolic rate constants (Table A4) for the best Si-modified alloys at 1100°C were one half to one order of magnitude lower than those of the best Nb-Ti-Al-Cr-V alloys (Fig.49), but neither class of materials formed continuous alumina at this temperature.

Effect of Environment (Air vs Oxygen)

Oxidation tests to evaluate alloy behavior were conducted both in air and oxygen on the assumption that behavior would not be sensitive to the small difference in oxygen pressure. However, it is possible that nitrogen as a major component in air might have an effect. Niobium, Ti, and Al are strong nitride formers and might be susceptible to selective nitridation, even in the presence of oxygen. A few tests were conducted with the same alloys in both

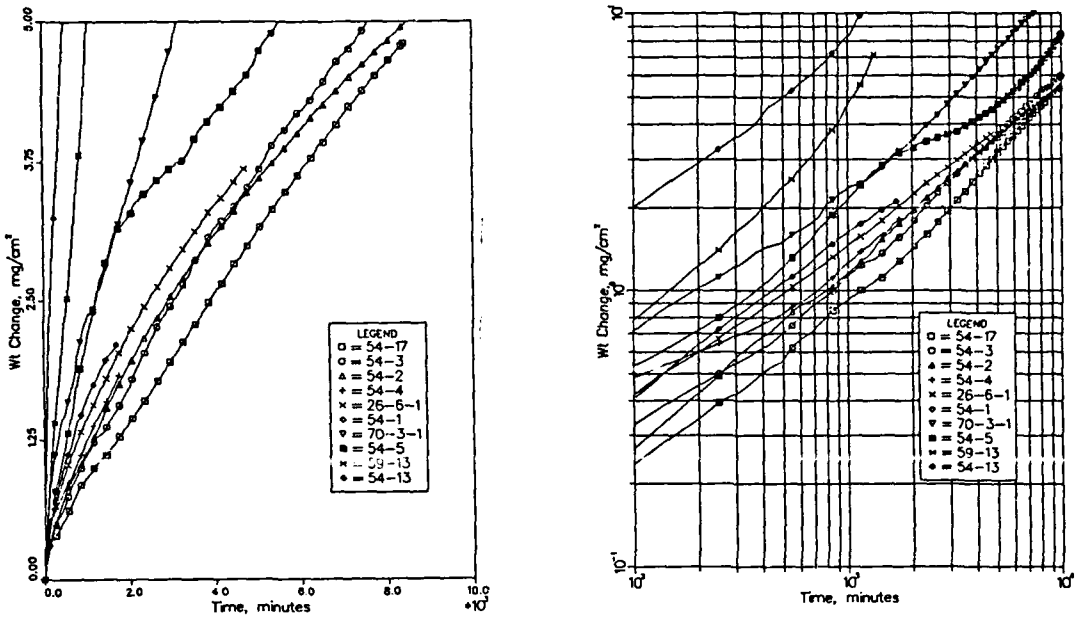

Linear Plot log-log Plot

Figure 47: Oxidation rate curves for Nb-Ti-Al-Cr-V Alloys in oxygen at 800°C.

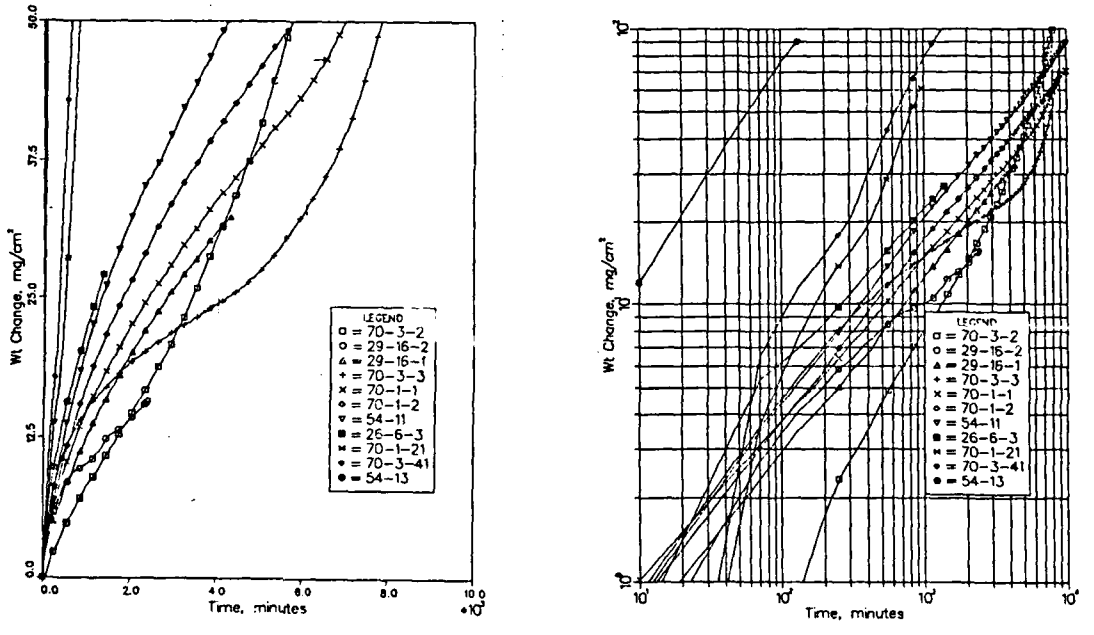

Linear Plot log-log Plot

Figure 48: Oxidation rate curves for Nb-Ti-Al-Cr-V alloys in oxygen at 1100°C.

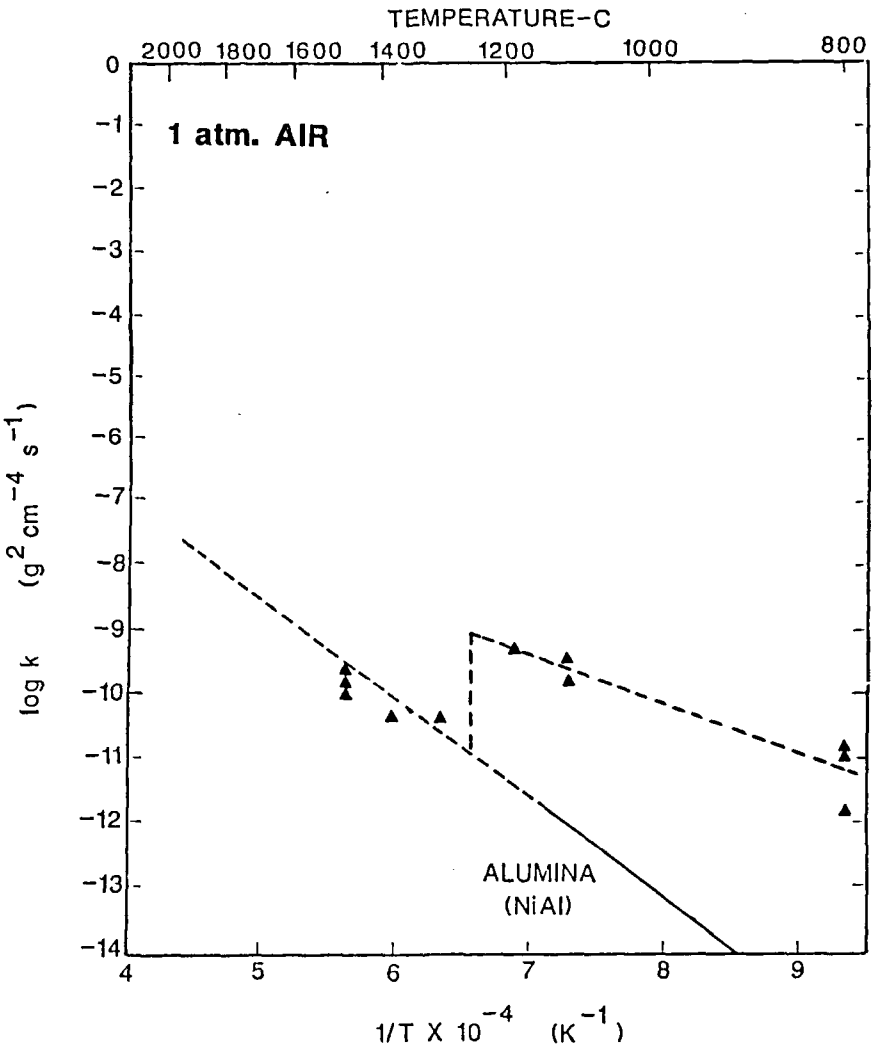

Figure 49: Parabolic rate constants as a function of temperature for Nb-Ti-Al-Cr-V alloys.

air and oxygen to determine whether or not atmosphere composition has a significant effect. As show in Fig. 50, a Nb-Ti-Al-Cr-V alloy with low Cr and V oxidizes more rapidly in oxygen than in air at 1100°C while a similar alloy with higher Cr and V behaves just the opposite. However, at 800 and 1300°C, the alloy with low Cr and V contents oxidizes at the same rate in both air and oxygen (Fig.51). An examination of all other test data (Tables A3 and A4) indicates no clear trends and reaction rates appear to be the same in both atmospheres. The differences which do exist most likely are random variations which are within the scatter band of, experimental results for kinetic microbalance tests. They are not considered to be significant.

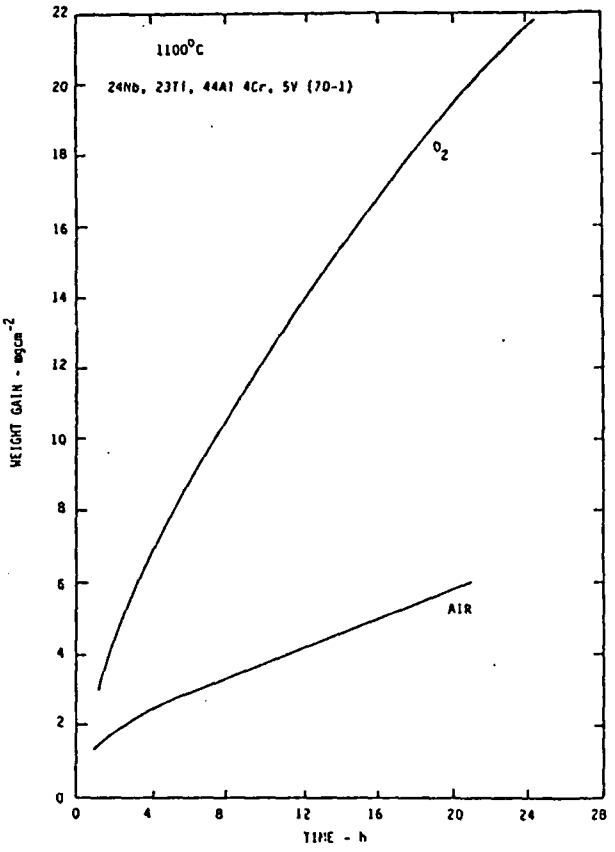

A- 24Nb-23Ti-44Al-4Cr-5V (70-1)

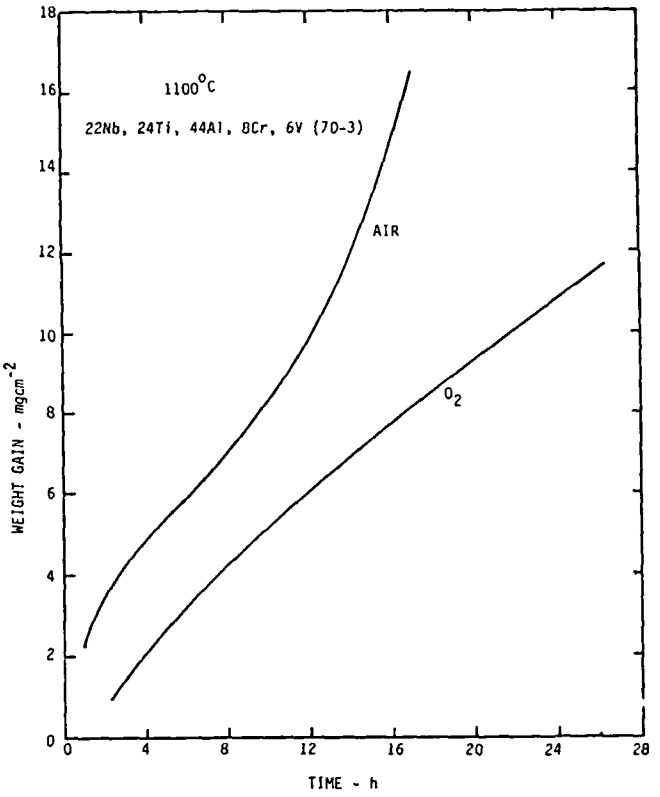

B- 22Nb-24Ti-44Al-8Cr-6V (70-3)

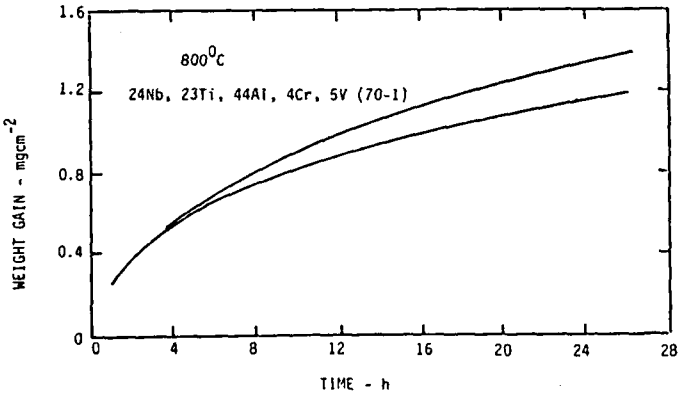

C- 24Nb-23Ti-44Al-4Cr-5V, 800°C

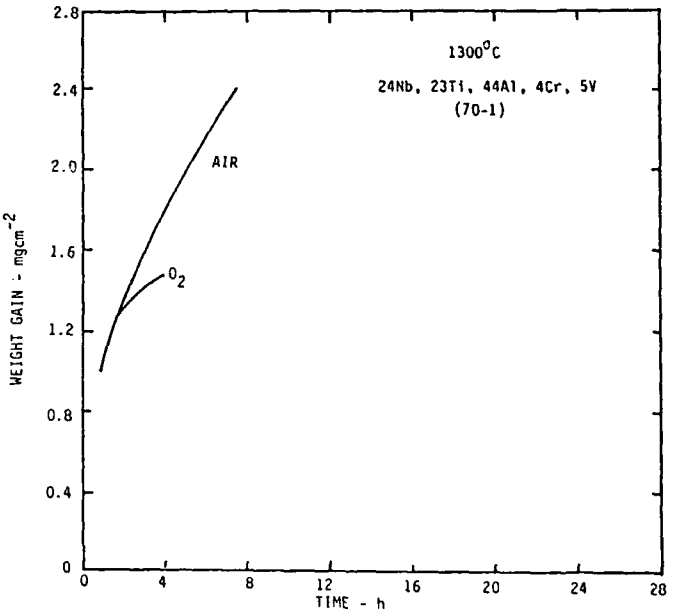

D- 24Nb-23Ti-44Al-4Cr-5V, 1300°C

Figure 50: Effect of environment on oxidation kinetics.

Effect of Preoxidation

An alloy with 38% Al and 10% Cr was preoxidized for 20h in impure argon (log P_{O2} = -4.0) in an attempt to reduce the amount of transient and internal oxidation and to preform an alumina scale. As shown in Fig.51, the alloy formed a thick external scale and was heavily oxidized internally on subsequent exposure in O_2 for 55h at 1100°C. Oxidation rate plots (Fig.51) were similar for both the as cast and the preoxidized samples. Both plots initially curved upward, ending in short parabolic segments after about 45h.

Figure 52 indicates the effect of preoxidation on the oxidation behavior of alloys 70-1 and 70-3 in one atmosphere oxygen at 1100°C. The curves labelled "oxygen" indicate the rate for direct exposure of the alloy to oxygen, those labelled "air" indicate the effect of an alumina scale preformed in air for 60 minutes at 1500°C, and those labelled "hydrogen" indicate the effect of a scale preformed in a hydrogen/steam mixture(p_{O2} = 10^{-15} atm.) at 1100°C for 4 hours. The preoxidized specimens were cooled to room temperature prior to insertion into the oxygen. The hydrogen/ steam preoxidation is seen to have a minimal effect on the subsequent oxidation kinetics in oxygen. In fact, the preoxidation actually increased the rate slightly for alloy 70-3. The high-temperature air preoxidation resulted in a marked acceleration in the oxidation of both alloys during subsequent oxidation in oxygen. The microstructures of the preoxidized specimens, both before and after exposure to oxygen, are illustrated in Figure 53. The 1500°C, air preoxidation produced a continuous alumina film (Fig.53A) but this film was broken down and a thick mixed oxide scale was formed during subsequent exposure at lower temperature (Fig. 53B). The hydrogen/steam preoxidation produced a discontinuous alumina film (Fig. 53C) which continued to oxidize in a similar manner to alloys without preoxidation (Fig.53D). The inability of the alloys to form continuous alumina films in the low oxygen pressure hydrogen atmosphere is not totally understood but is believed to be associated with the nature of the transient oxides which form on these alloys. The existing literature indicates that most of the oxides of Nb and Ti are n-type semiconductors. The growth rates of n-type oxides are relatively insensitive to the oxygen partial pressure in the oxidizing gas and, therefore, are not slowed by the reduced p_{O2}.

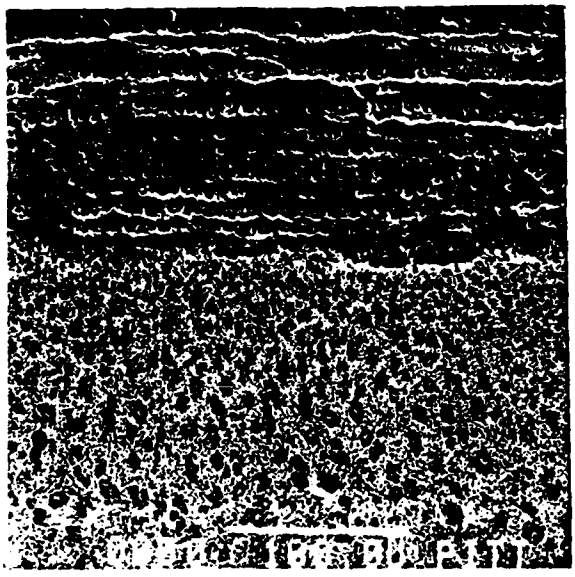

Preoxidized 19.8h-1100°C-Argon
Followed by 55.8h-1100°C-Oxygen

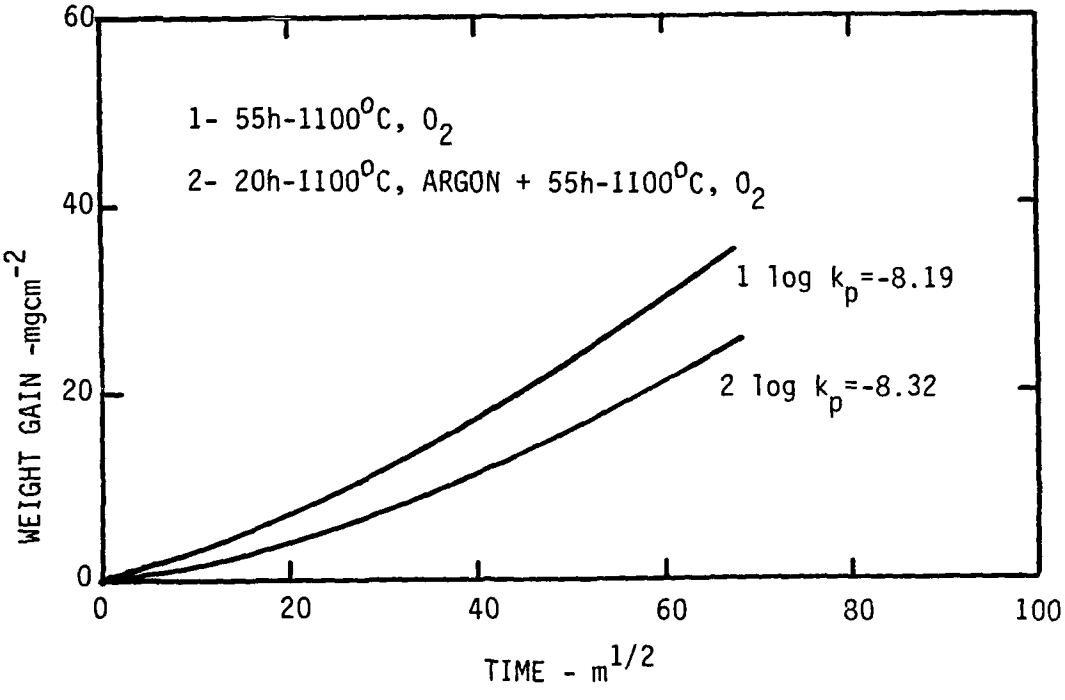

Figure 51: Effect of preoxidation in argon at 1100°C on oxidation behavior in oxygen at 1100°C.

It was suspected that scale damage during cooling after the preoxidation was responsible for the detrimental effects, particularly for the high-temperature, air preoxidation. Therefore, an experiment was conducted in which an alumina scale was grown on alloy 70-1 at 1300°C in oxygen following

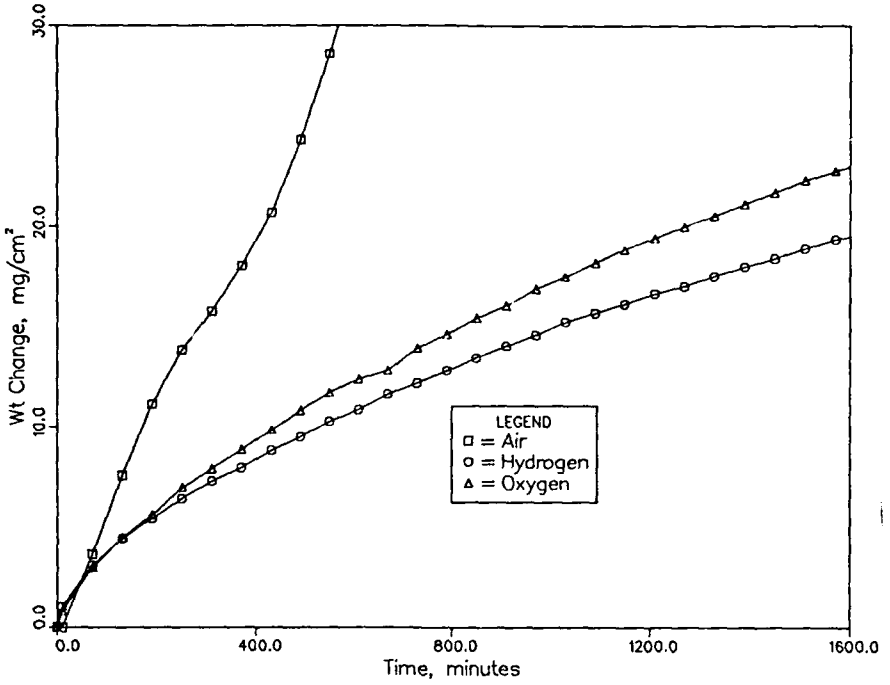

A- 24Nb-23Ti-44Al-4Cr-5V (70-1)

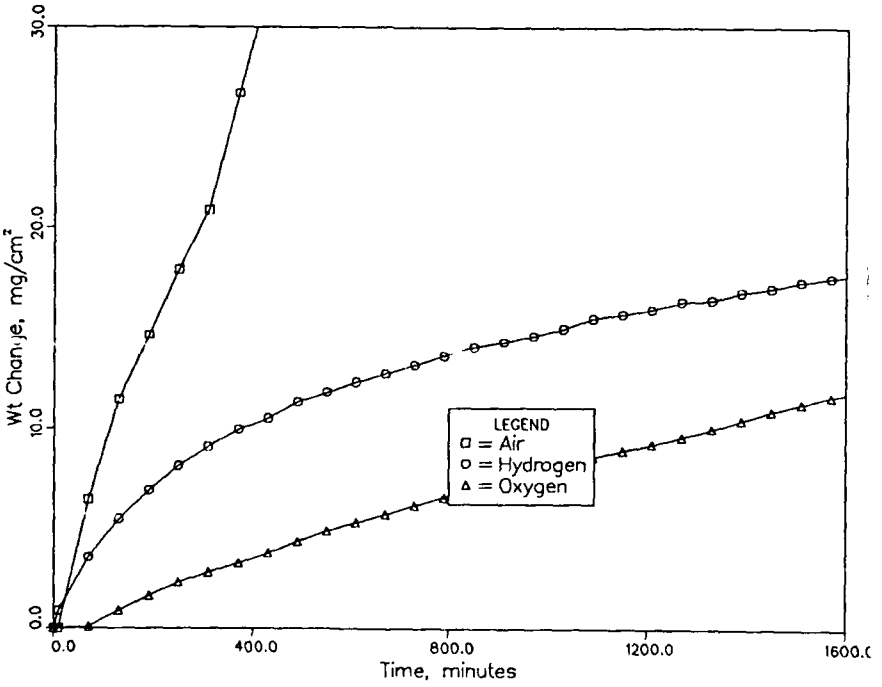

B- 22Nb-24Ti-44Al-8Cr-6V (70-3)

Figure 52: Effect of preoxidation in different atmospheres on oxidation in air at 1100°C.

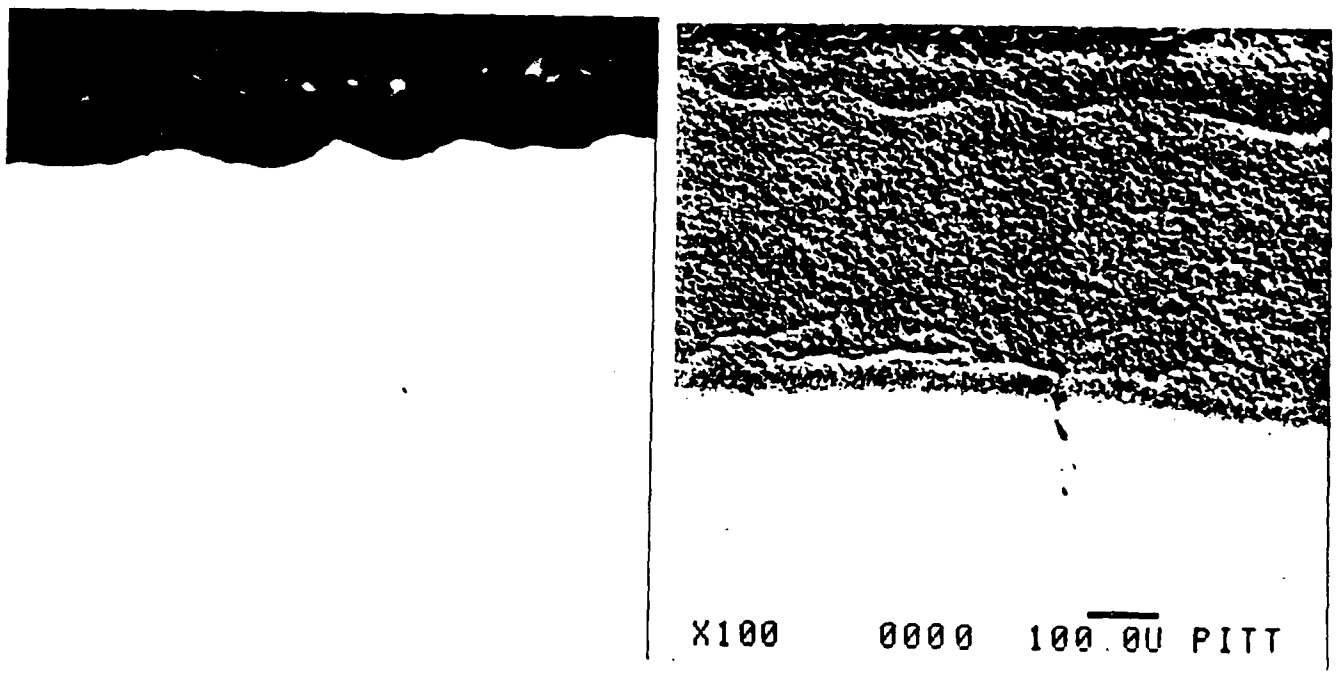

A- 60m-1500°C-Air 13µm B 60m-1500°C-Air + 168h-1100°C-O_2

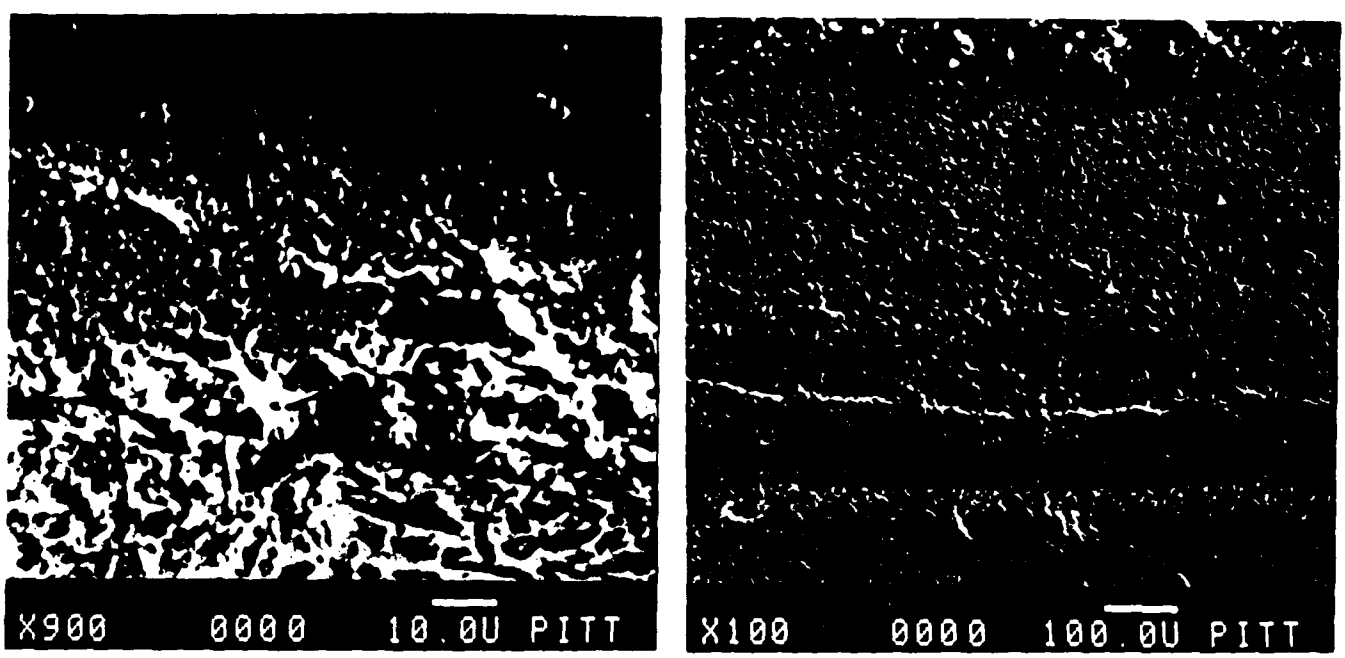

C- 4h-1100°C-H_2 (Moist) D- 4h-1100°C-H_2 + 168h-1100°C-O_2

24Nb-23Ti-44Al-4Cr-5V (70-1)

Figure 53: Oxidation behavior of preoxidized Nb-Ti-Al-Cr-V alloys.

which the temperature was lowered to 1100°C without an intermediate cooldown. The results (Figure 54A) show that the thick, preformed alumina remained protective and thickened at a rate at 1100°C that was within the sensitivity of the microbalance. The rate at 1100°C was negligible compared with that of a sample which had not been preoxidized (Fig.54B). Similar effects were obtained for air exposures, as indicated in Figure 55. Specimens of alloys 70-1 and 70-3 were preoxidized in air at 1500°C in the microbalance and then cooled to 1100°C where they continued to be exposed to air. The rates for both alloys became unmeasureably slow at 1100°C. However, an intermediate cooldown to room temperature of alloy 70-1 after 26 hours exposure resulted in a catastrophic oxidation rate when the specimen was reheated to 1100°C (Fig.55). The same behavior was observed for a sample preoxidized 4h-1500°C, cooled to room temperature, and reheated to 1100°C (Fig.54B). The 1100°C rate of oxidation of the preoxidized sample with the a cooldown was considerably greater than that of a sample that had not been preoxidized.

These results clearly indicate that the scale damage during cooling is responsible for the ineffectiveness of high-temperature preoxidation. The scale damage associated with cooling to room temperature was found to involve cracking which occurred primarily at corners and edges of the oxidation coupons as illustrated in Figures 56-57. The oxide and pieces of the underlying metal spalled from sharp edges and corners on cooling (Fig. 56). Cracks formed both in the alumina scale and the alloy at corners on cooling from the preoxidation temperature and rapid oxidation was initiated at these sites on subsequent exposure to lower temperatures (Fig.57). Cracking of the preformed alumina scale on flat surfaces on cooling from high temperature also was observed (Fig.58), but this did not result in accelerated oxidation at these sites.

Accelerated oxidation at sites where the oxide was cracked on cooling is related to the formation of Al-depleted regions. Depletion was observed first at sharp corners (Fig.57B) where a three directional growth of the alumina scale resulted in greater loss of Al. A brittle sigma phase layer often was developed in these regions. In fact, the depletion of Al from the underlying alloy during growth of the scale at high temperature makes the alloy even less oxidation resistant than an alloy which has received no preoxidation (Fig.54B). It is concluded that preoxidation does not provide a practical

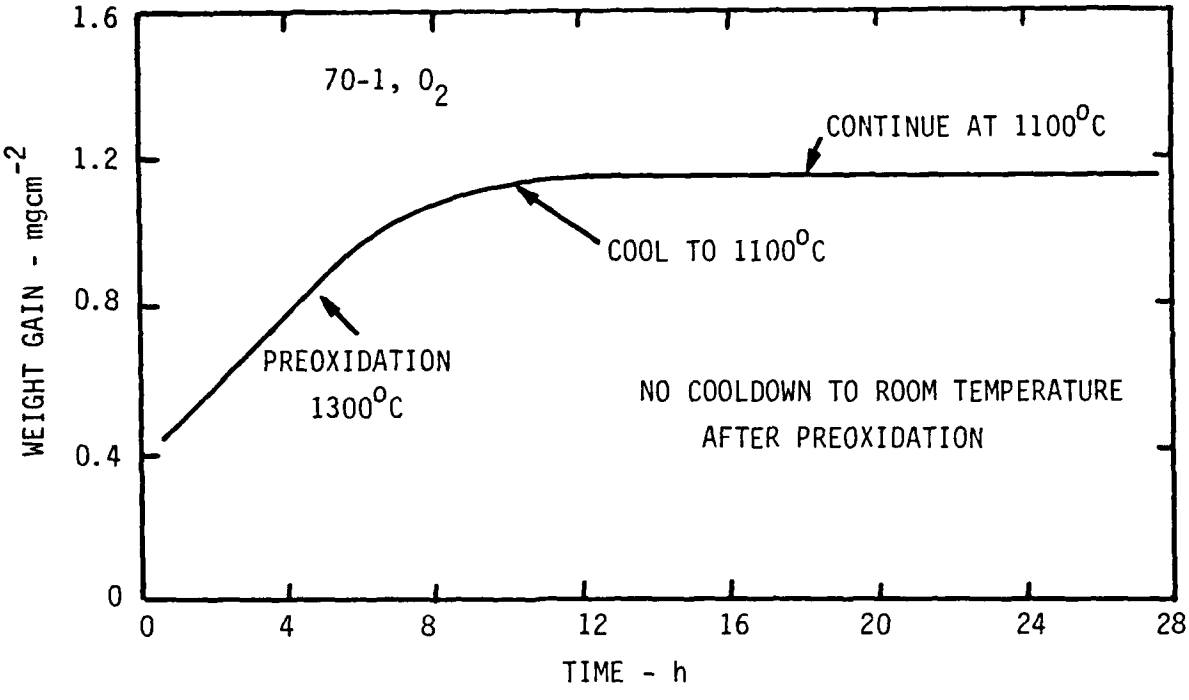

A- Preoxidation Without Cooldown.

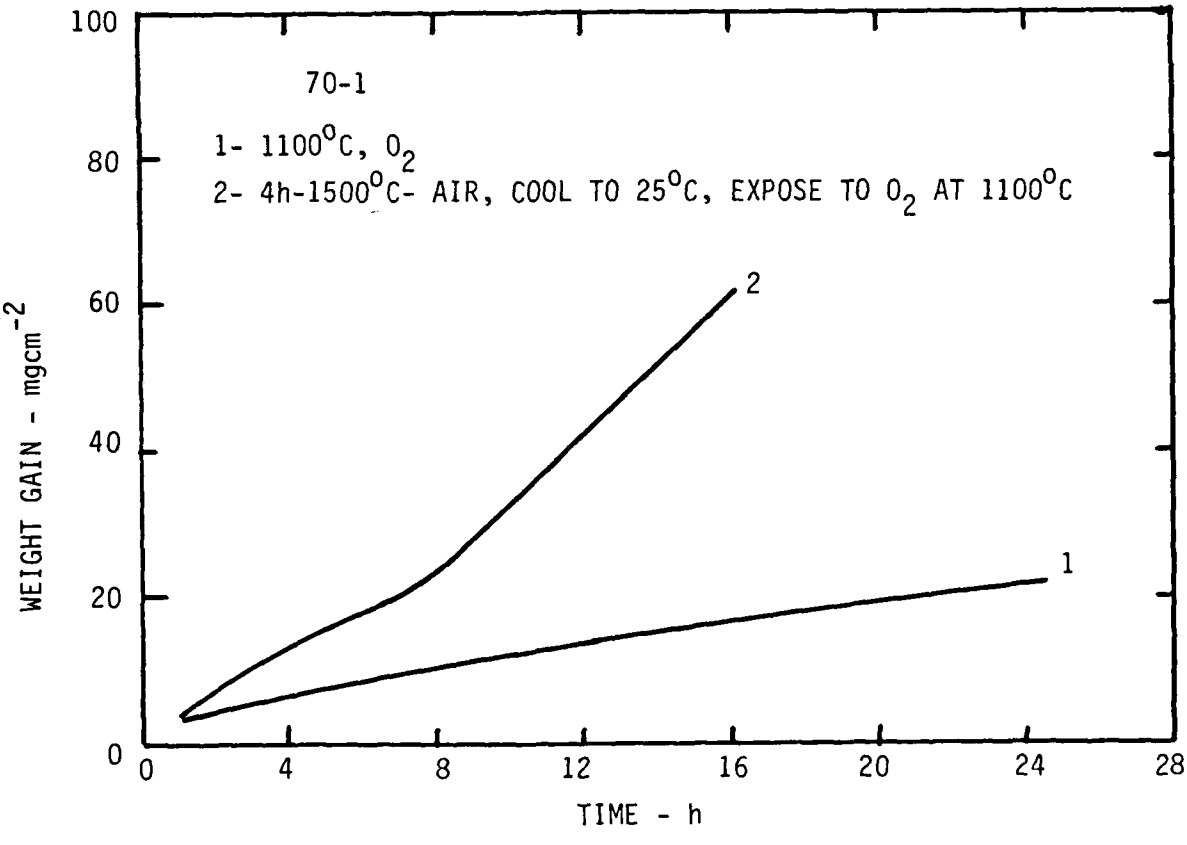

B- Preoxidation With Cooldown to Room Temperature.

Figure 54: Oxidation rate curves for preoxidized samples.

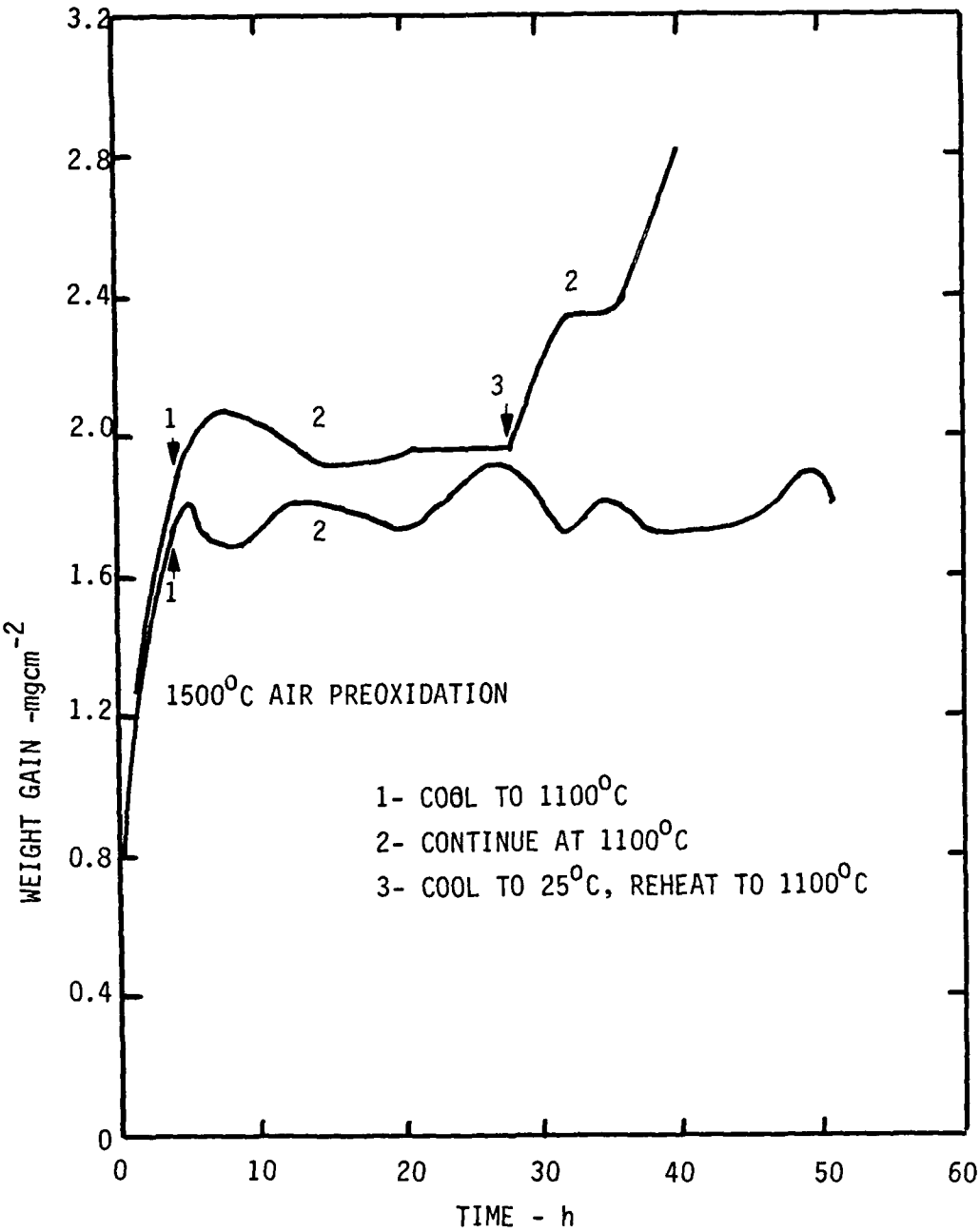

Figure 55: Effect of an intermediate cooldown on oxidation behavior of preoxidized samples.

approach to improving oxidation behavior in the low temperature regions where alumina scales are not formed on direct exposure to air. Preoxidation is effective only if the alloy is not cooled to room temperature before it is exposed to the lower temperature environment. One cooldown cycle is sufficient to destroy the preformed, protective alumina scale. Results of this study indicate that the alloys will be degraded by cyclic oxidation.

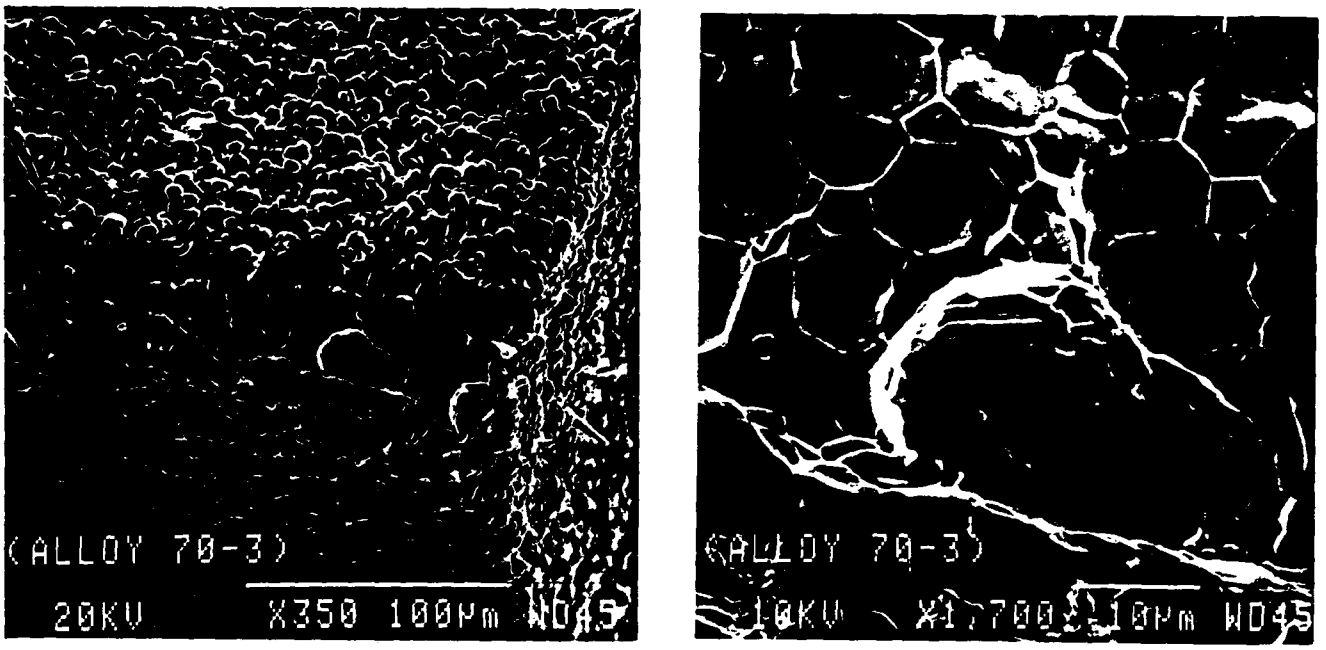

A- Corner Spall

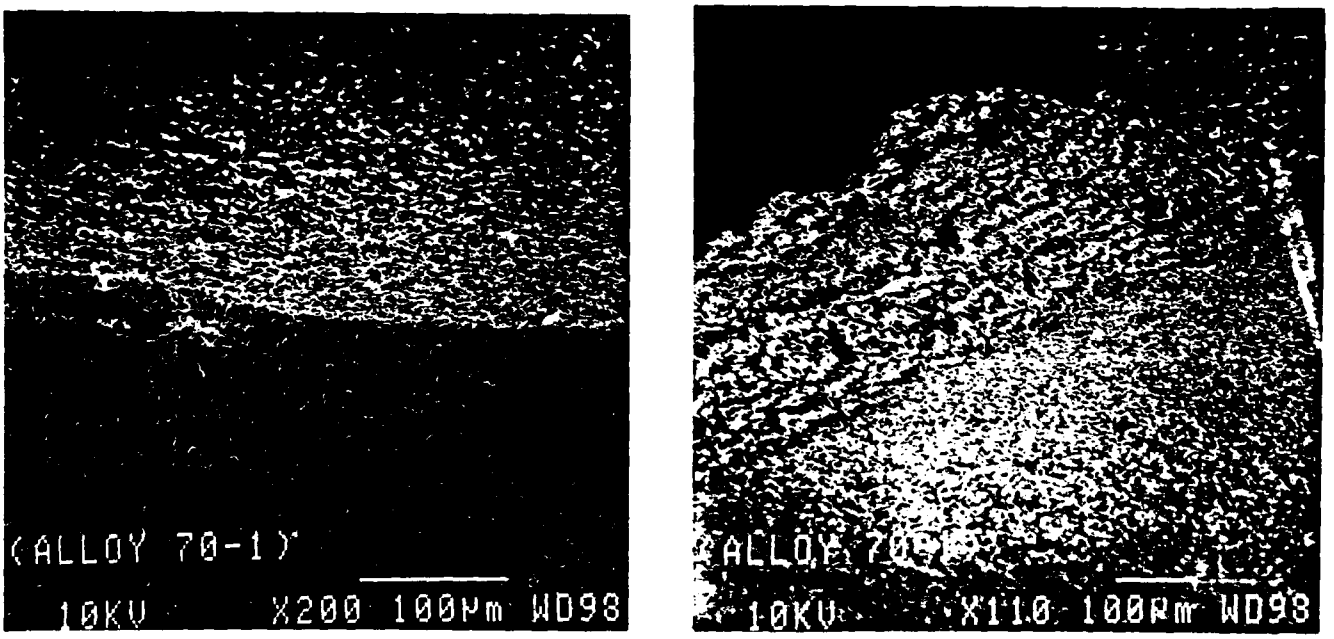

B- Edge Spall and Accelerated Oxidation

4h-1500°C + 24h-1100°C, Cool to R.T., 20h-1100°C

Figure 56: Corner and edge failures on thermal cycling Nb-Ti-Al-Cr-V alloy.

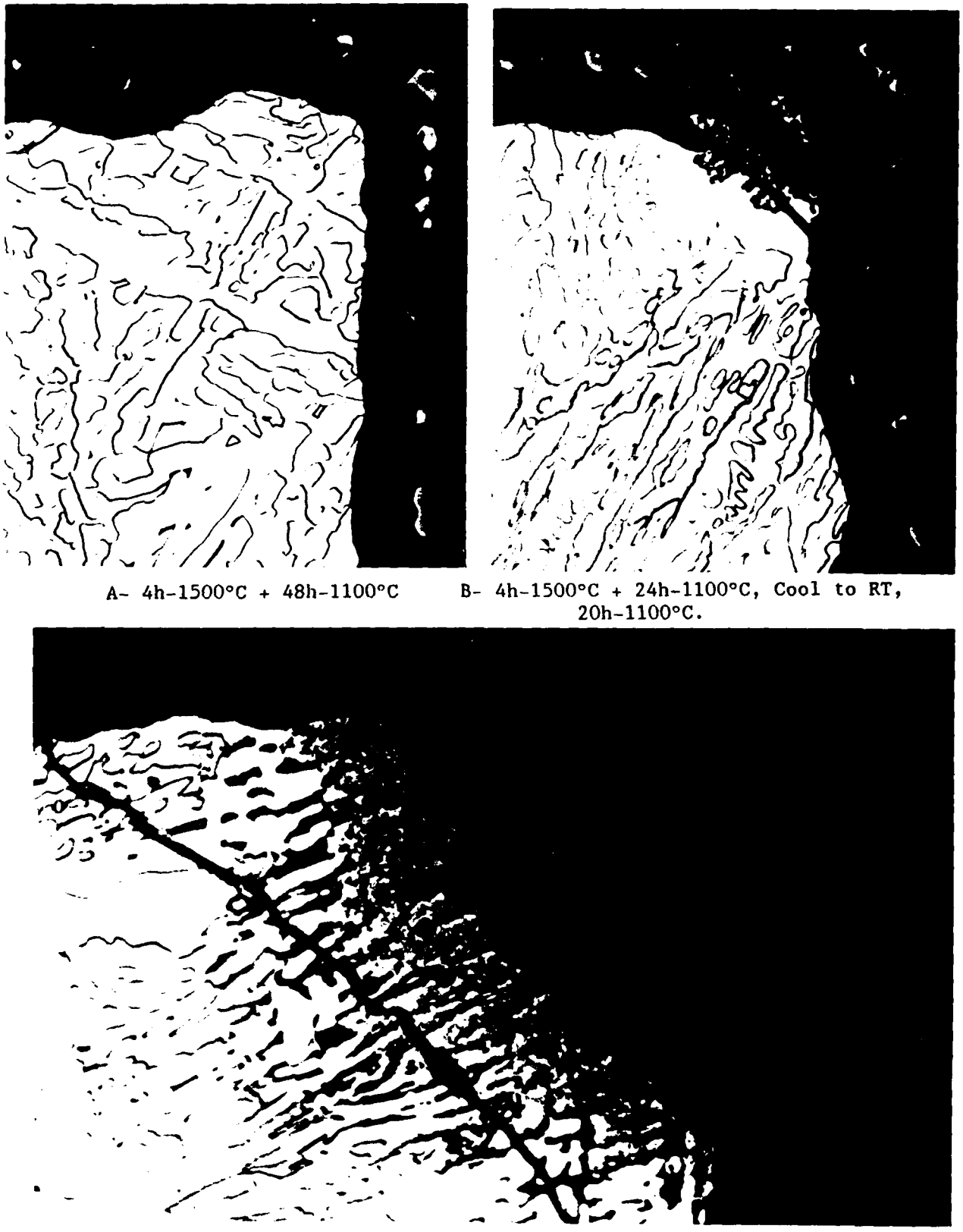

A- 4h-1500°C + 48h-1100°C

B- 4h-1500°C + 24h-1100°C, Cool to RT, 20h-1100°C.

C- 4h-1500°C + 24h-1100°C, Cool to RT, 20h-1100°C

13µm

Figure 57: Breakdown of preformed alumina scale at edges after 1 thermal cycle.

A- 4h-1500°C + 48h-1100°C (No Cooldown). 13μm

B- 4h-1500°C + 24h-1100°C, Cool to RT, 20h-1100°C 13μm

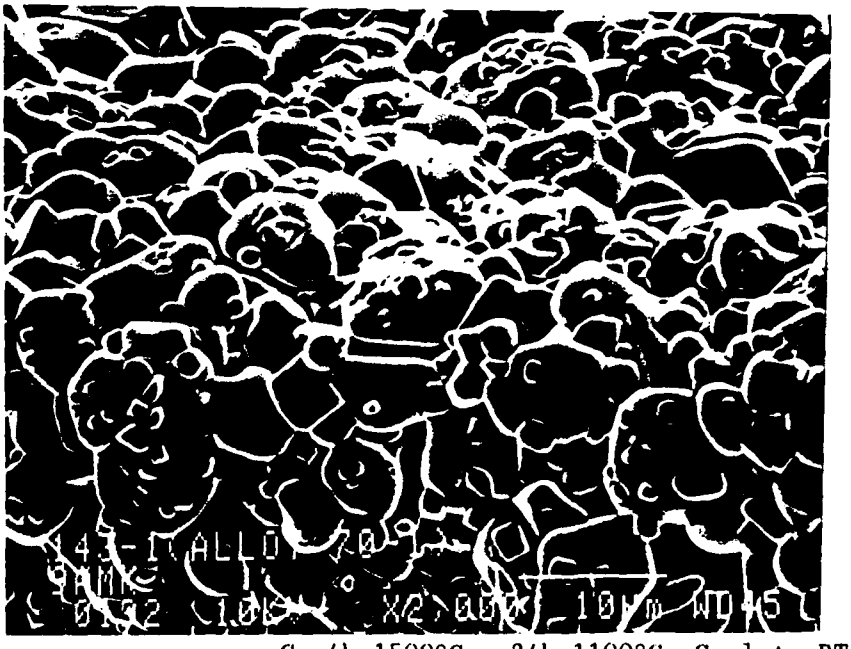

Surface

Edge (Cracked)

C- 4h-1500°C + 24h-1100°C, Cool to RT

Figure 58: Cracking of alumina scale on one thermal cycle.

Effect of Rapid Solidification Processing

The effects of rapid solidification on the air oxidation behavior of a 38 at.% Al alloy at 800 and 1100°C are presented in Figure 59. The RS alloy oxidized at a slightly slower rate than an arc melted specimen at 800°C but oxidized at a substantially faster rate at 1100°C. Similar data for a 44 at.% Al alloy are shown for 800 and 1300°C in Figure 60 and for 1100°C in Figure 61. The RS alloy is again observed to oxidize at a slightly slower rate at 800°C but oxidized in a catastrophic manner at 1300°C. The RS alloy oxidized much slower than the arc melted alloy at 1100°C but still at a rate which is more rapid than would be expected for an alumina-forming alloy. All samples were supercooled in the range of 90-170°C during RS processing. The amount of supercool in this range appeared to have little effect on oxidation behavior.

The starting microstructure of the supercooled RS splats with 44 at.% Al and cross-sections after oxidation at 800 and 1100°C is shown in Figure 62. The starting microstructure of the RS alloy is different from that of arc melted alloys of the same composition (Fig.62A,B). The splat solidified as single phase (B2) with a small amount of transformation on cooling to form a fine acicular two phase structure along grain boundaries and at random sites within the grains. The arc-melted alloys also solidify as a single phase beta but transforms fully to complex 3 phase structure. RS processing tends to quench in the high temperature B2 phase and produces a much finer matrix grain size. In spite of the major change in microstructure, the oxidation morphology of the splats at 800°C is essentially the same as that for the arc melted alloys which is consistent with the kinetic data. There is, however, a substantial difference in alloy microstructure and oxidation morphology at 1100°C. The RS alloy does not exhibit the internal oxidation typical of arc melted alloys of this composition. Rather it has formed a multiphase scale with several bands of nearly-continuous alumina running through it and an aluminum-depleted band below the scale. This morphology is typical of an alloy which is borderline with respect to continuous alumina formation. This splat oxidized at significantly lower rate compared with as cast samples (Fig.61).

The effects of rapid solidification on the oxidation kinetics of alloys 70-1 and 70-3 in 1 atm. oxygen at 800 and 1100°C are presented in Figures 63 and

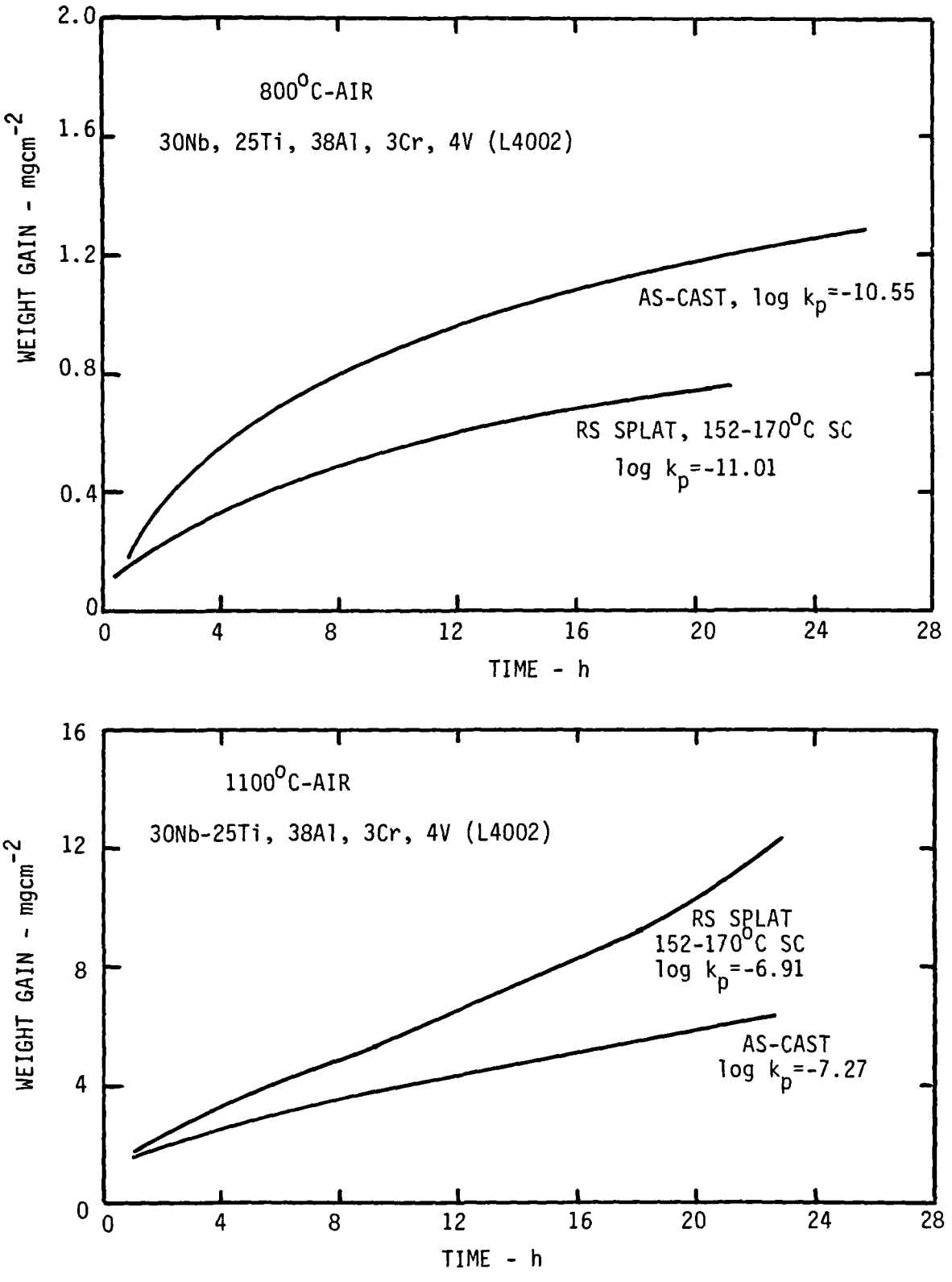

Figure 59: Oxidation kinetics of RS Nb-Ti-Al-Cr-V alloy with 38% Al in air at 800 and 1100°C.

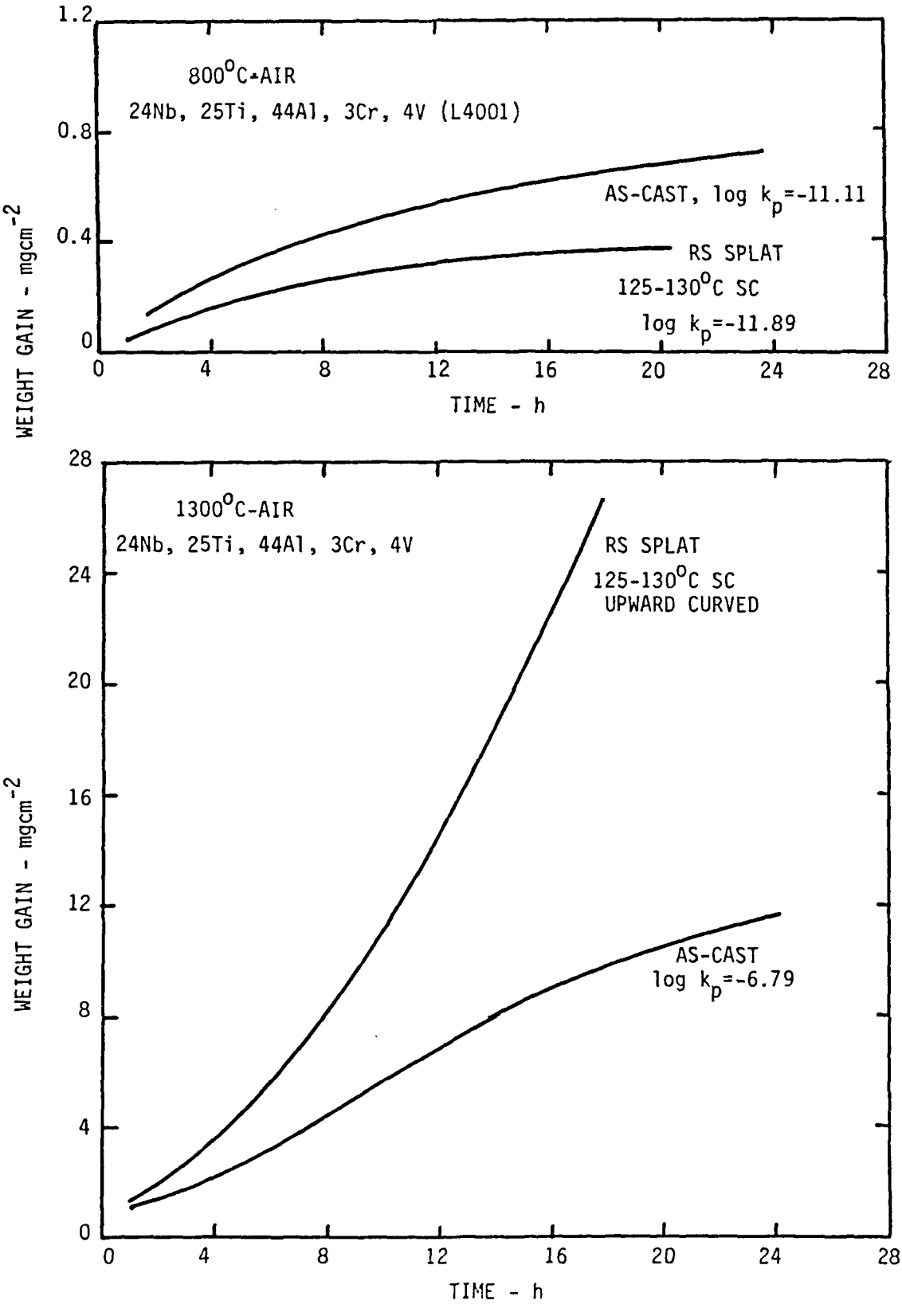

Figure 60: Oxidation kinetics of RS Nb-Ti-Al-Cr-V alloy with 44% Al in air at 800 and 1300°C

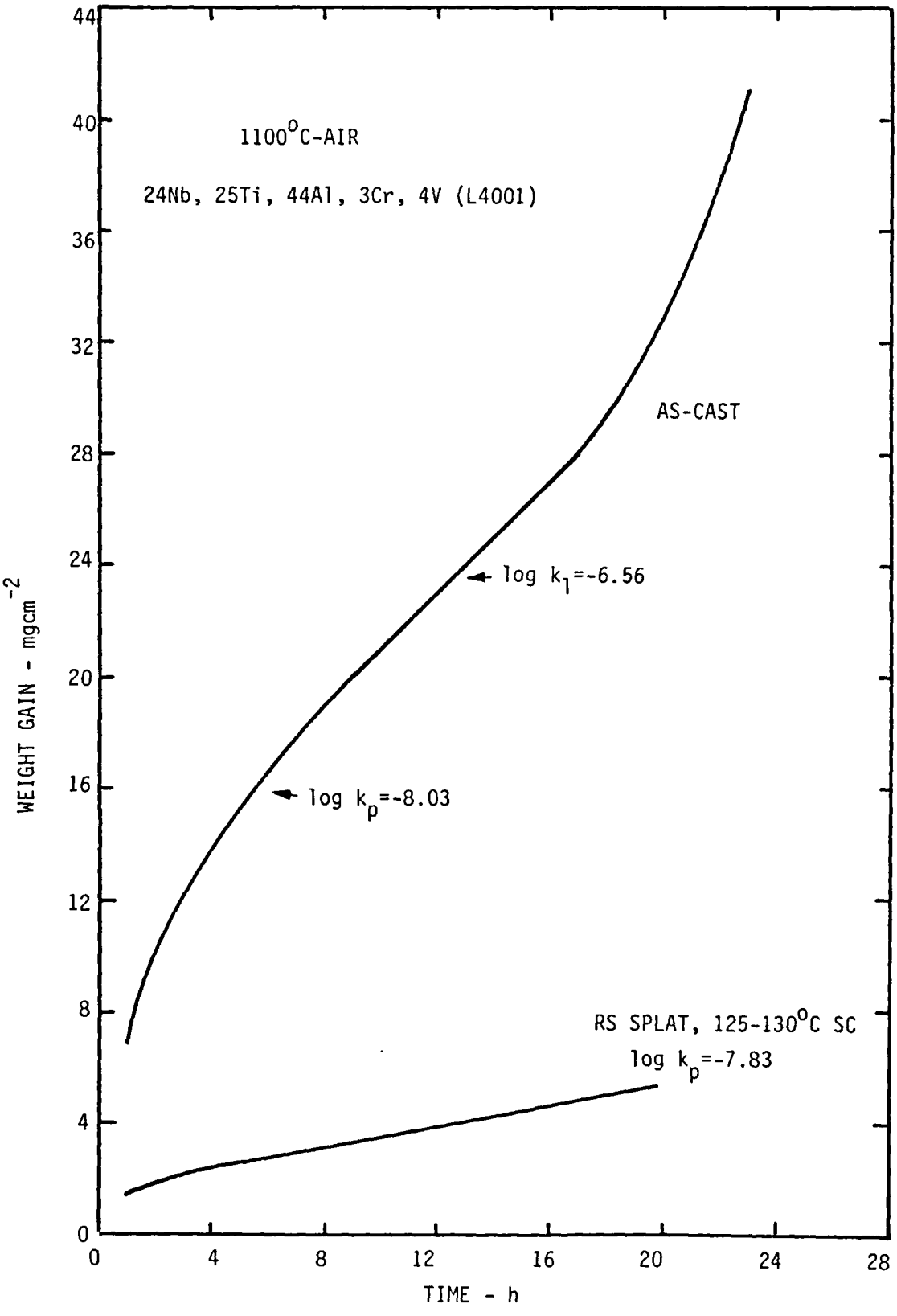

Figure 61: Oxidation kinetics for RS Nb-Ti-Al-Cr-V alloy with 44% Al in air at 1100°C.

A- Arc-Melted (Etched) 4μm B- RS Splat, 95°C Supercool

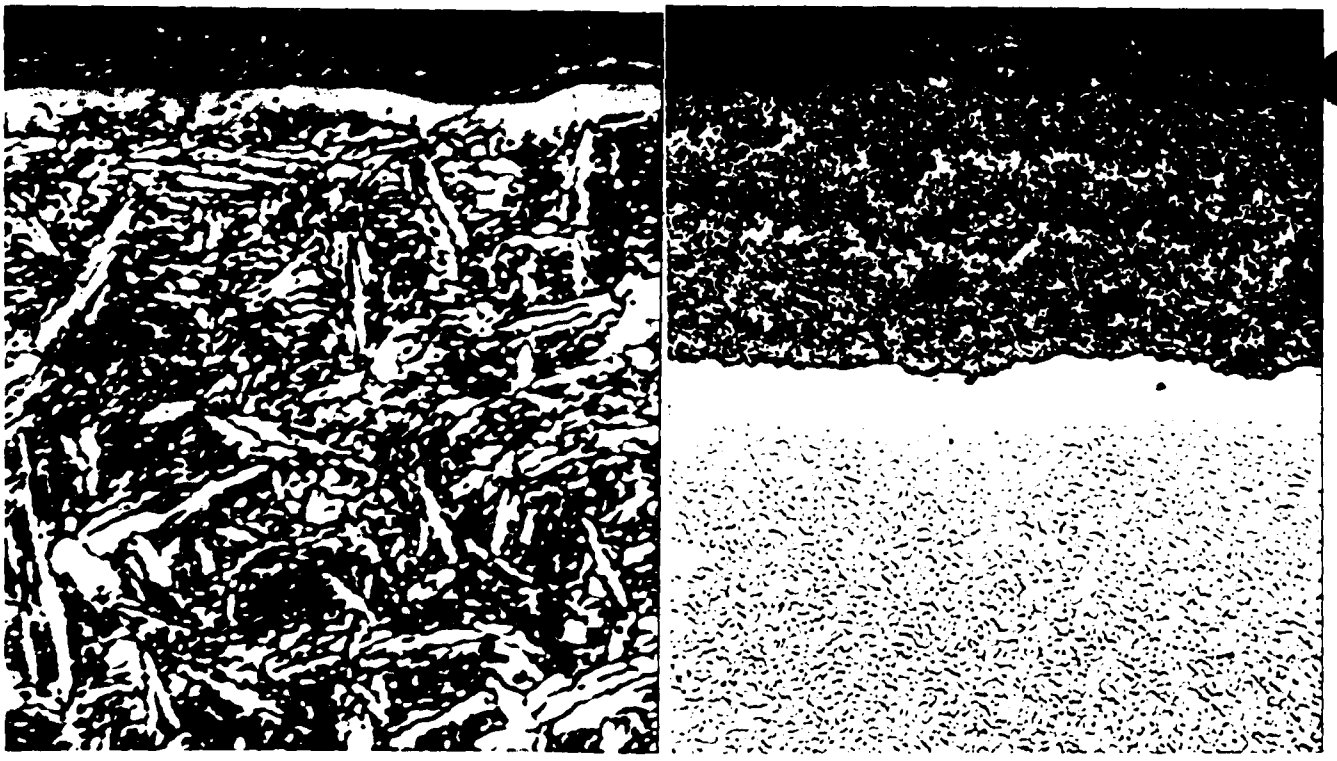

C- 20h-800°C 6μm D- 20h-1100°C 25μm

RS Splat, 125-130°C Supercool

Figure 62: Structure of cast and oxidized splats from Nb-Ti-Al-Cr-V alloy with 4Cr and 5V (70-1).

64. The oxidation rates for both alloys are essentially the same for splats and cast material at 800°C (Fig. 63). As shown in Fig 64, the rates of RS and arc melted alloys are indistinguishable from each other at 1100°C. This behavior is quite different from that observed in air but this is not the result of a change in test environment. Instead, it appears to be the result of a change in RS processing of the splats used for tests in oxygen. These splats either were superheated (40-105°C) or supercooled (90-93°C) before solidification as indicated in Fig.64. All tests in air were conducted with splats that had been supercooled 125-170°C before solidification. The lower degree of supercooling for splats tested in oxygen appears to have reduced the amount of B2 phase retained on solidification. As shown in Figure 65, the splats with a lower degree of supercool or with superheat had more transformation on cooling. Microstructures of the splats tested in oxygen are all similar and approach those of the arc-melted alloys which is in agreement with the kinetic data that indicates no significant effect of RS processing on behavior. Alloy grain size of the splats also is larger than that of splats prepared for tests in air. The oxidation morphologies (Figs.66, 67) are similar for arc-melted, superheated, and supercooled samples.

Figure 68 presents the effects of rapid solidification on the oxidation rates and morphologies of alloy splats (70-1 and 70-3) in oxygen at 1200°C. Rapid solidification is seen to produce a modest decrease in the rate for alloy 70-1 which is consistent with the increased alumina coverage observed at the scale base compared with the oxidation morphology for the arc melted alloy (Fig.68 vs Fig.41B). As shown in Fig.41, this alloy has a peak in oxidation rate at 1200°C. Rapid solidification reduced the height of the peak, resulting in a weight gain of 26 $mgcm^{-2}$ in 38h compared with >50 $mgcm^{-2}$ in 3h for an arc-melted sample. Rapid solidification had a much greater effect on the oxidation rate of alloy 70-3 at 1200°C. A continuous alumina film was formed on the RS splat (Fig. 68) compared with a discontinuous film for the arc melted sample (Fig.44B). As shown in Fig 44, this alloy has a peak in oxidation rate at 1100°C and is a marginal alumina former with increased resistance to oxidation at 1200C. RS processing resulted in this alloy becoming an alumina former at 1200°C with a major reduction in rate of oxidation. It is believed that more rapid aluminum diffusion in the initially finer-grained RS alloy is sufficient to seal the surface with a continuous alumina film. It is concluded that RS processing may be effective in

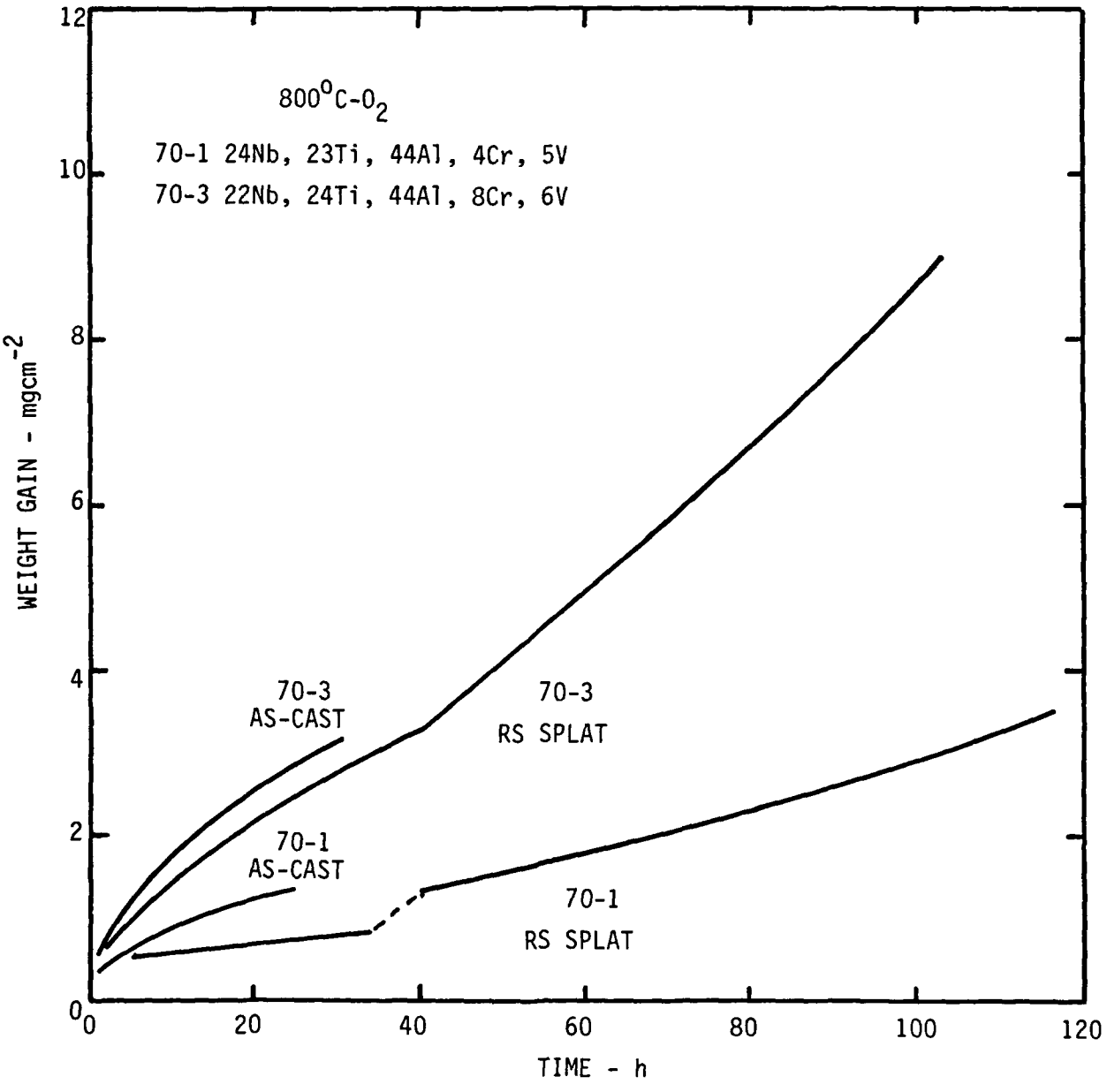

Figure 63: Oxidation kinetics Nb-Ti-Al-Cr-V alloy splats in oxygen at 800°C.

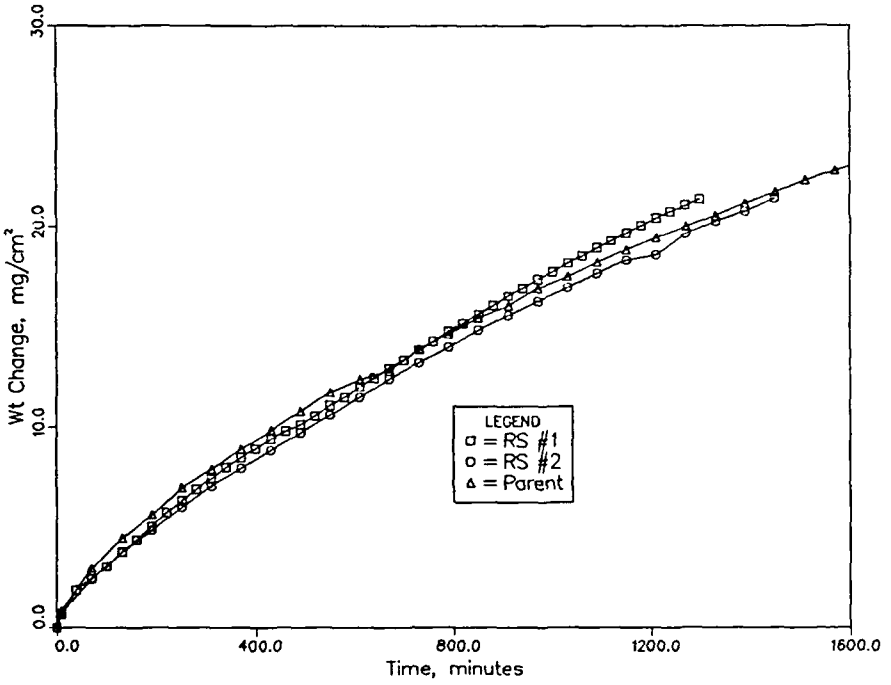

A- 24Nb-23Ti-44Al-4Cr-5V (70-1)

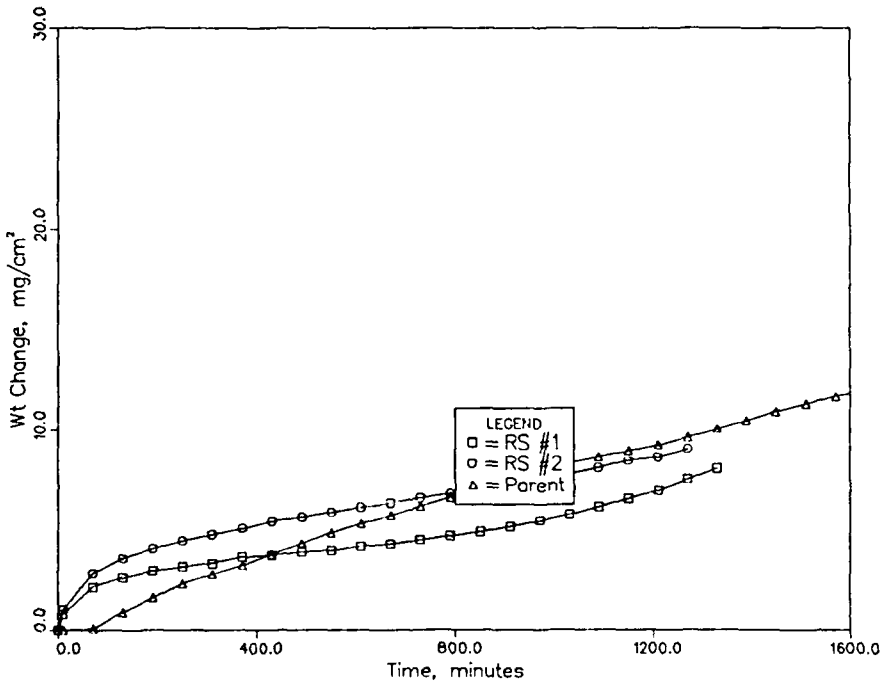

B- 22Nb-24Ti-44Al-8Cr-6V (70-3)

1100°C-Oxygen

Figure 64: Oxidation kinetics for Nb-Ti-Al-Cr-V alloy splats in oxygen at 1100°C.

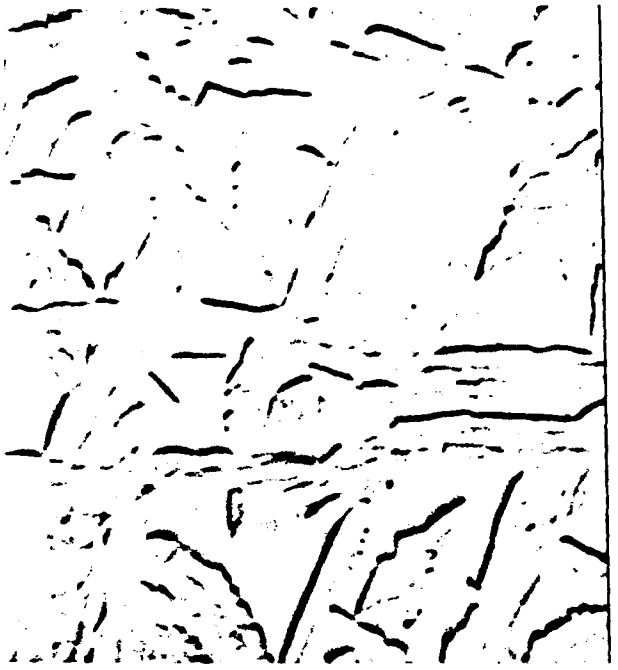

90°C Supercool, 850μm Thick

105°C Superheat, 1550μm Thick

A- 24Nb-25Ti-44Al-4Cr-5V (70-1)

93°C Supercool, 950μm Thick

40°C Superheat, 1400μm Thick

B-22Nb-24Ti-44Al-8Cr-6V (70-3)

Figure 65: Effect of superheat and supercool on the microstructure of RS Splats.

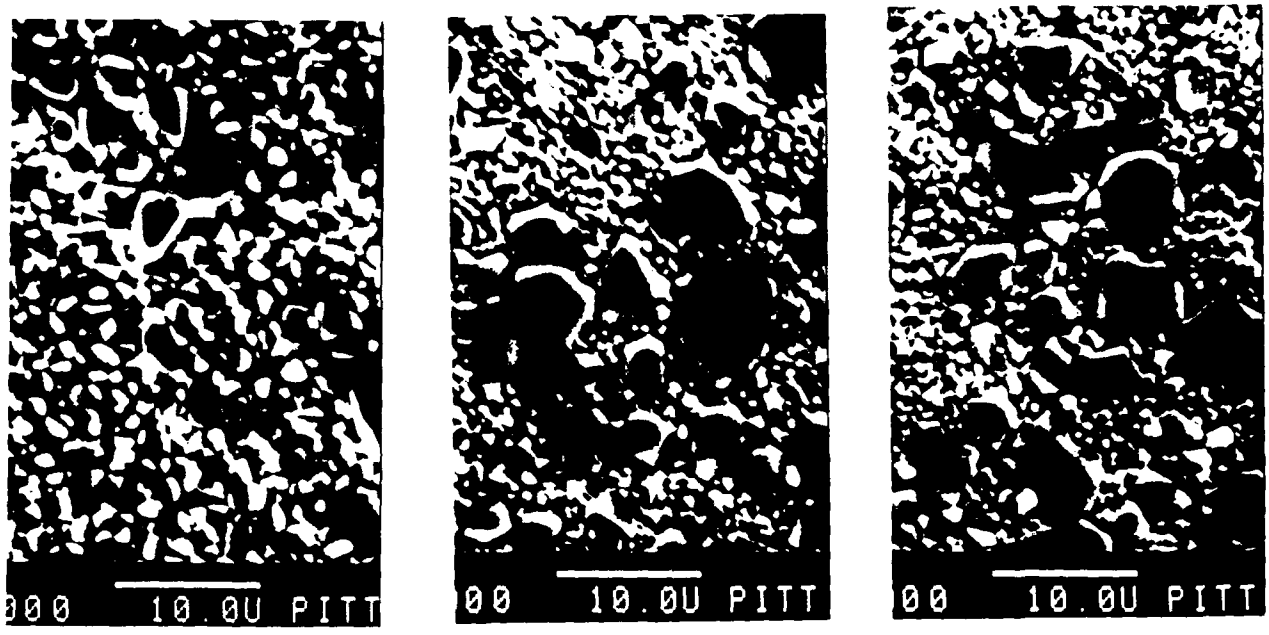

A- Surface

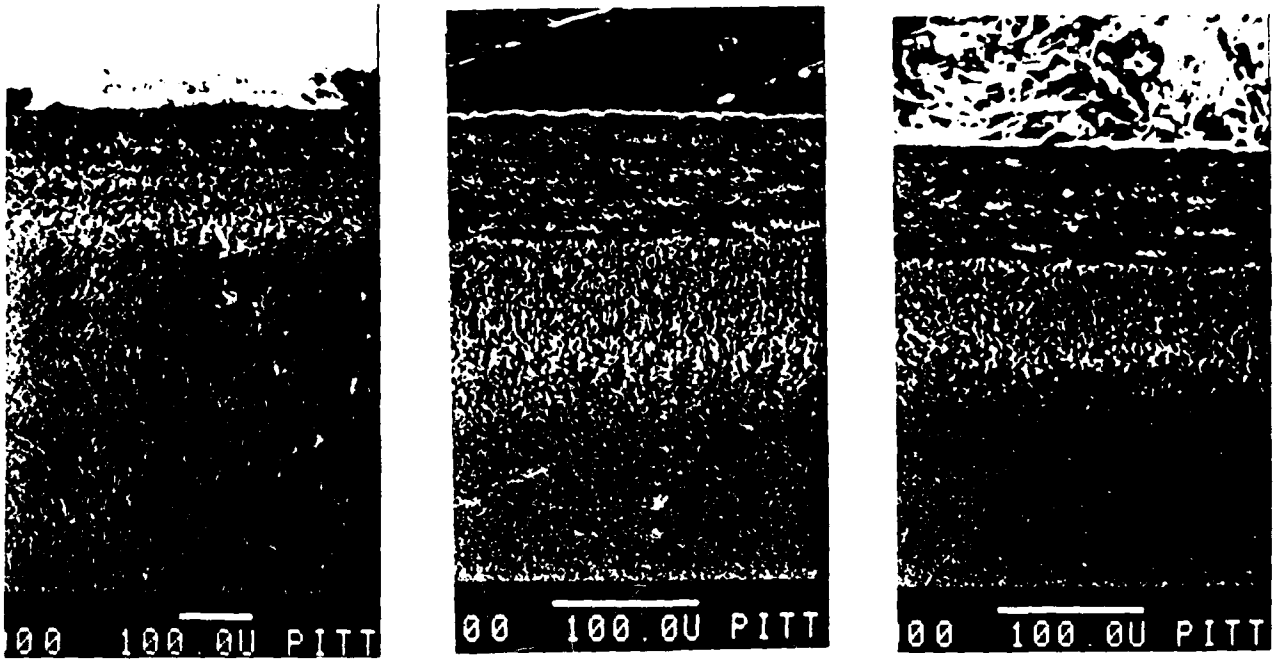

B- Cross Section

Arc-Melted

Rapidly Solidified Splats

105°C Superheat

90°CSupercool

Figure 66: Microstructure of arc-melted and RS splats of alloy 70-1 oxidized in oxygen at 1100°C.

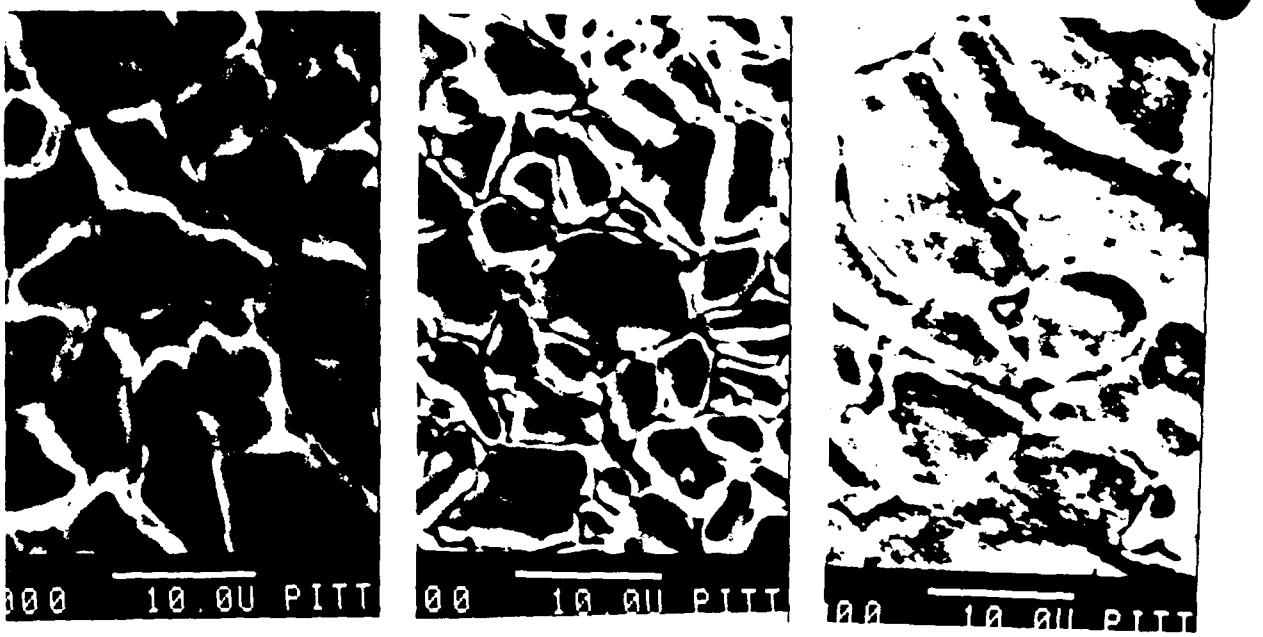

A- Surface

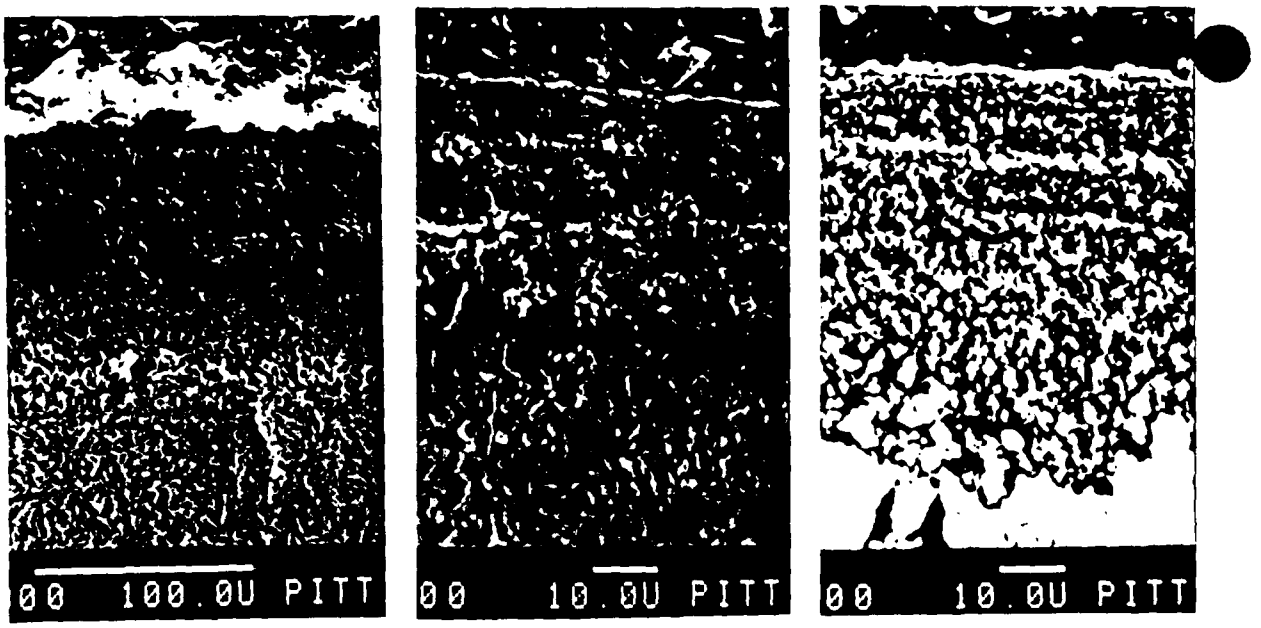

B- Cross Section

Arc-Melted

Rapidly Solidified Splats

40°C Superheat

93°CSupercool

Figure 67: Microstructure of arc-melted and RS splats of alloy 70-3 oxidized in oxygen at 1100°C.

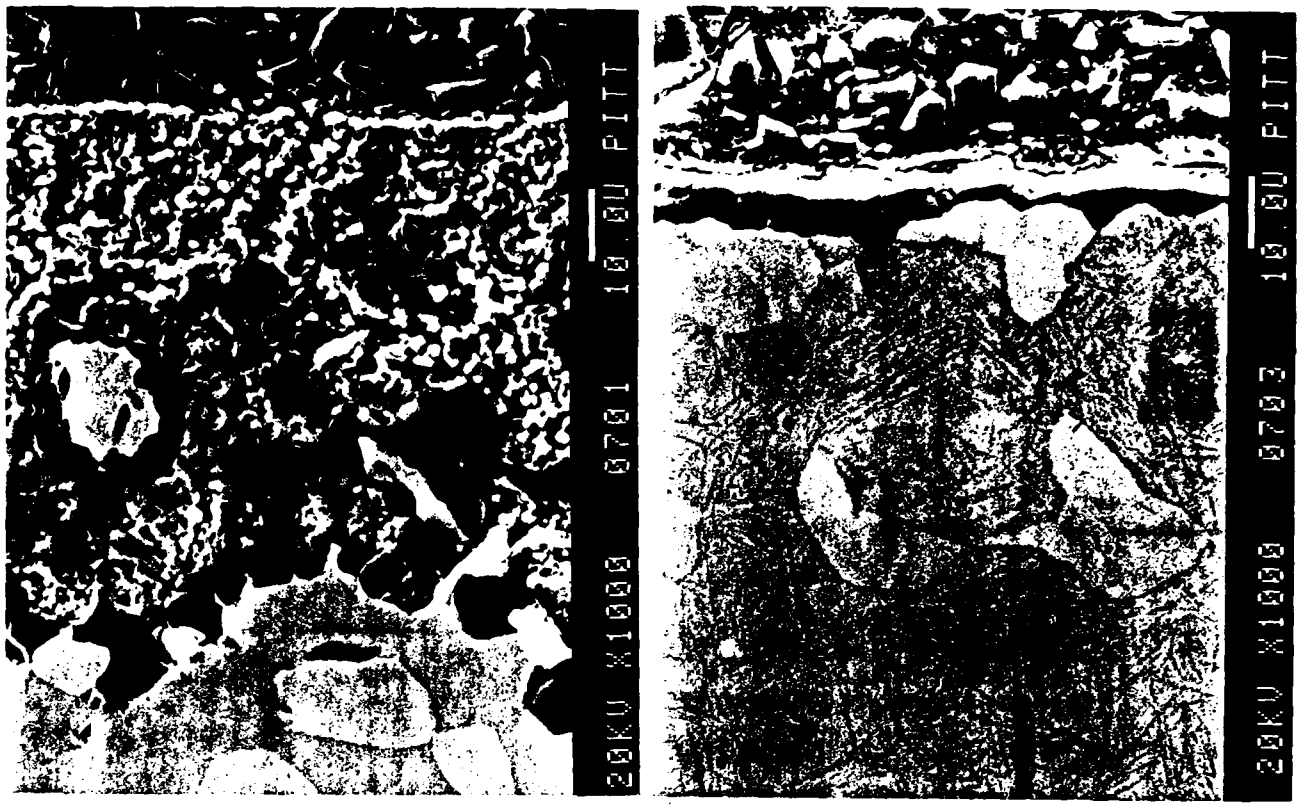

24Nb-23Ti-44Al-4Cr-5V (70-1)

22Nb-24Ti-44Al-8Cr-6V (70-3)

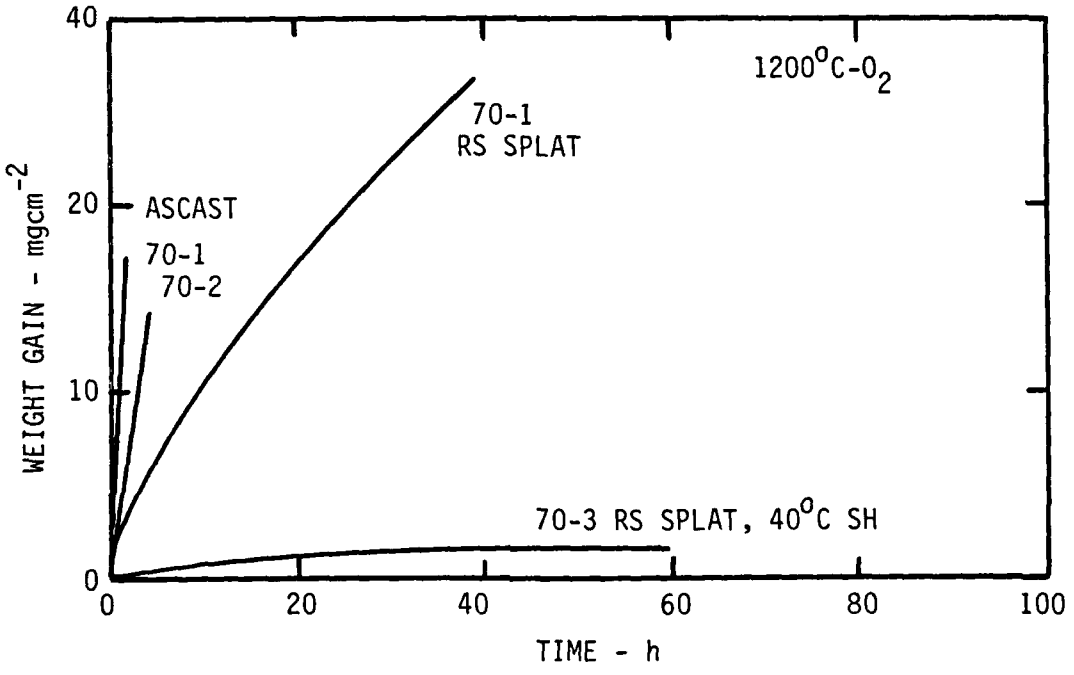

Figure 68: Oxidation kinetics of Nb-Ti-Al-Cr-V alloy splats in oxygen at 1200°C.

improving the alumina-forming capability of alloys that are borderline alumina formers. The effect on alloys which are not marginal in respect to alumina formation, however, appears to be negligible except for samples solidified with a high degree of supercooling (>100°C).

Effect of Ion Implantation

The effects of ion implanted Si and Al on the isothermal oxidation kinetics of alloy 70-1 in oxygen at 1100°C are presented in Figure 69. There is no observable effect of Al while Si produces a small decrease in rate at times longer than 10 hours. This difference in rate did not correspond to a change in oxidation mechanism and the oxidation morphologies of both Si- and Al-implanted alloys was similar to that described previously for unimplanted alloy 70-1 oxidized at this temperature. The morphology for the Al-implanted alloy is illustrated in Figures 70 and 71. The upper left micrograph of Figure 70 shows the overall morphology which consists of an outer scale of mixed oxides and an inner zone of internal oxidation. The outer scale consists of a more Al-rich phase in which the Nb/Ti ratio is greater than unity and one in which it is less than unity. Phase analysis by x-ray diffraction has indicated the presence of structures consistent with $NbAlO_4$ and TiO_2. Therefore, it is concluded that the more Al-rich phase is $NbAlO_4$ with a substantial amount of Ti in solution and the Al-lean phase is TiO_2 with Nb in solution. The morphology of the internal oxidation zone is shown in more detail in Figure 71. This zone consists of three phases: a black phase which was indicated by EDS analysis to be pure alumina, a grey phase(spectrum A) indicated to contain mainly Ti which is presumably TiO_2, and a white phase(spectrum B) which is indicated to be unreacted sigma phase. Therefore, there does not appear to be a significant effect of ion implantation at 1100°C.

The effects of Al- and Si-implantation on the oxidation kinetics of alloy 70-3 at 1200°C in oxygen are presented in Figure 72. The implantation of both elements is seen to produce a reduction in oxidation rate and a different oxidation morphology, which is illustrated in Figures 73 and 74. Continuous alumina scales are formed on both implanted alloys but unimplanted 70-3 was unable to develop such a scale (fig. 44B). The reason for the implantation

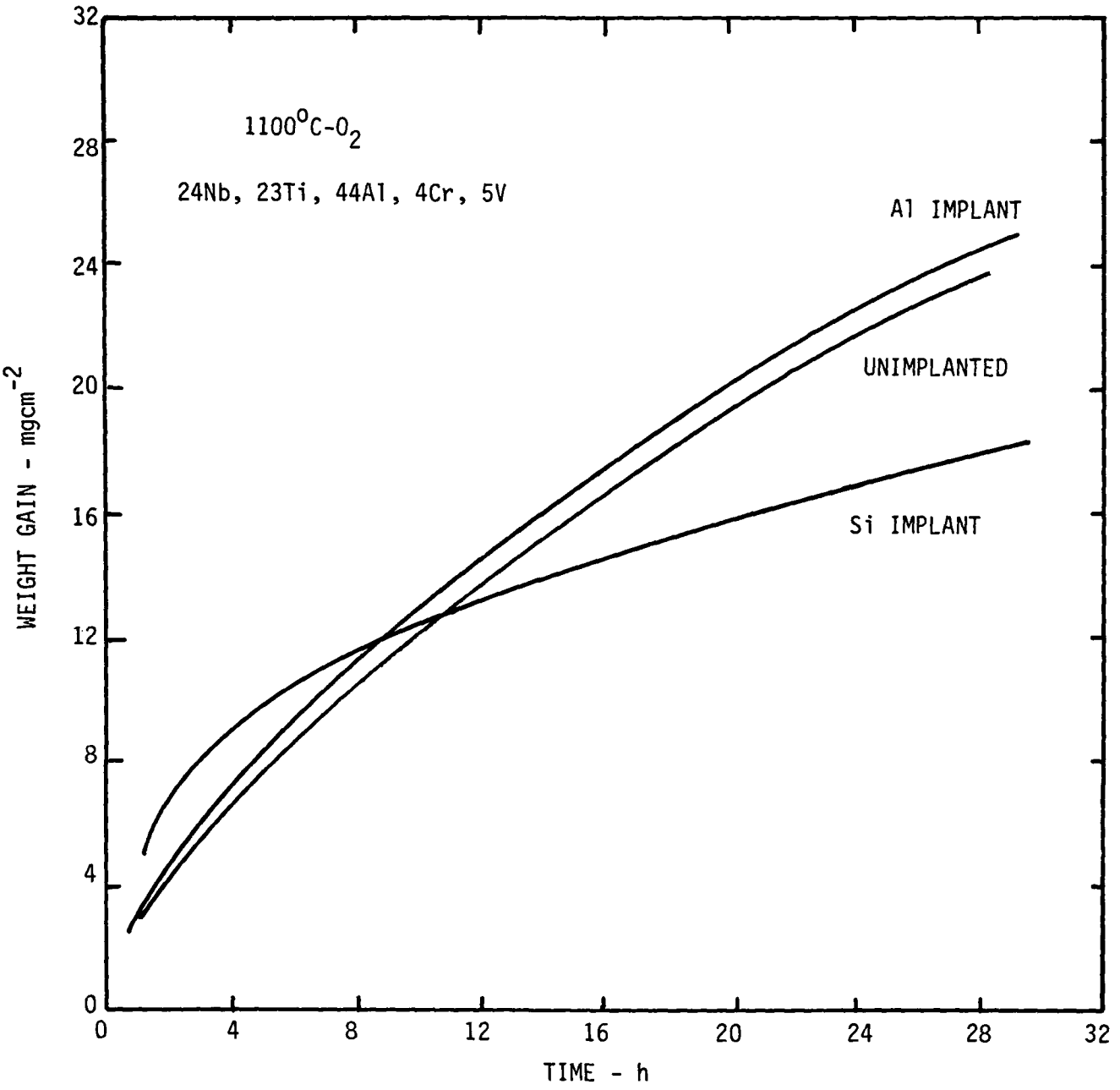

Figure 69: Effect of implanted Si and Al ions on oxidation kinetics of alloy 70-1 in oxygen at 1100°C.

effect may involve enriching the surface with an element which supports protective scale formation or producing implantation damage which accelerates diffusion of Al. The fact that Al and Si implants produce identical effects is taken as evidence for the importance of implantation damage. It should be noted that this alloy (70-3) is a marginal alumina former at 1200°C with a peak in oxidation rates at 1100°C (Fig.44). Alloy 70-1, on the other hand,

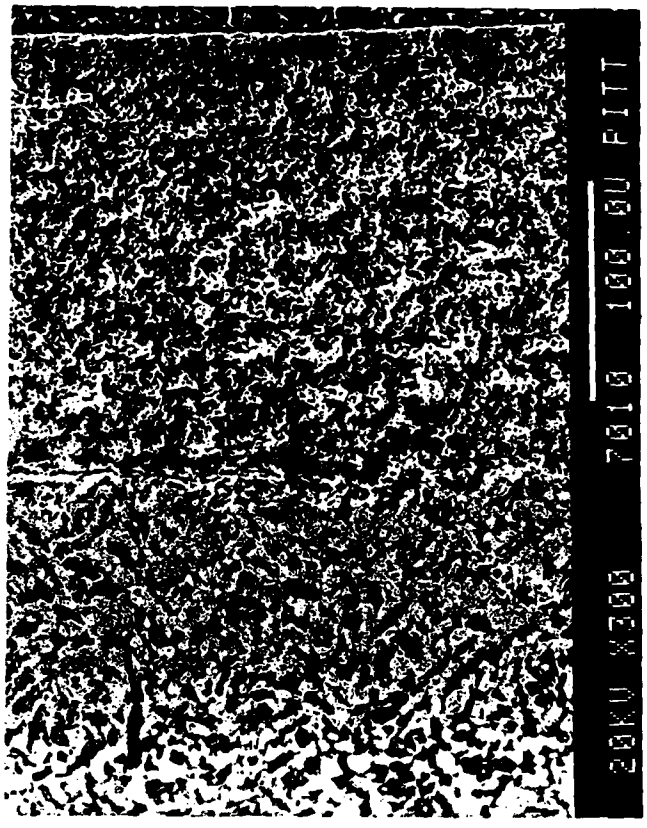

A- Oxide Scale and Internal Oxidation Zone

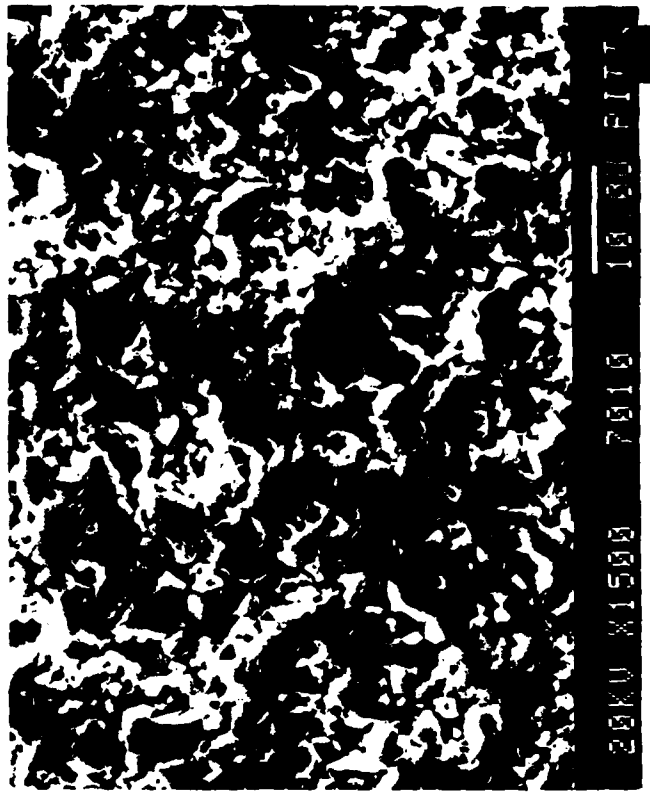

B- Oxide Scale

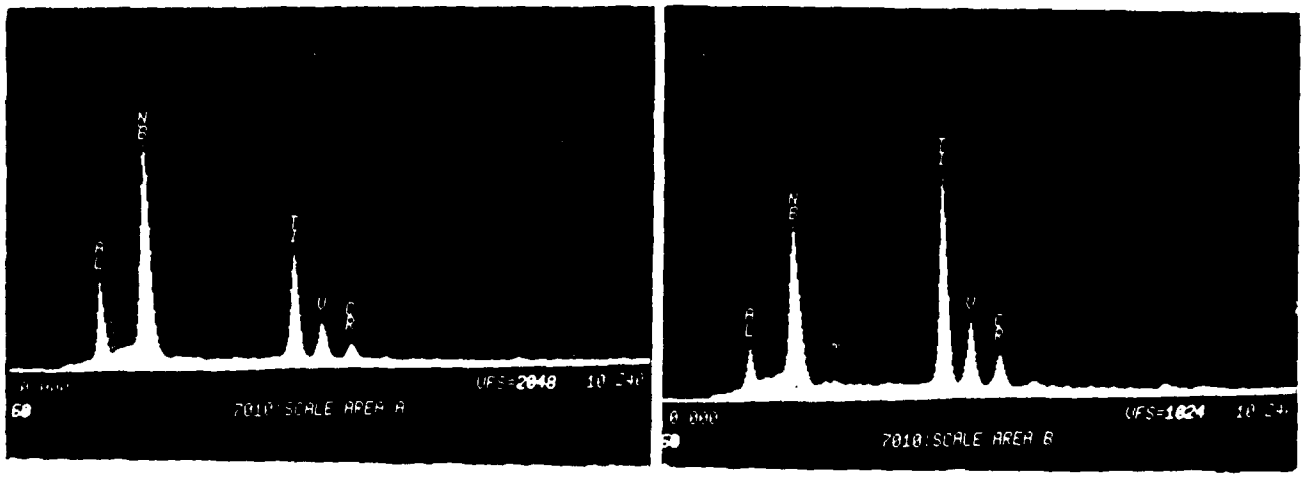

Alloy 70-1, Al Implanted
29h-1100°C, Oxygen

Figure 70: Elements in outer scale of Al implanted alloy (70-1) after oxidation at 1100°C in oxygen.

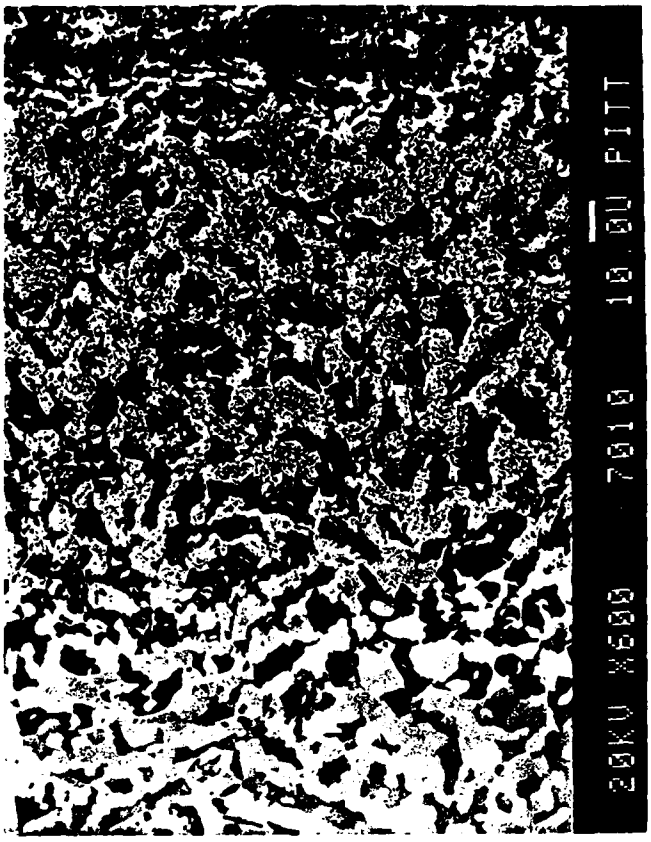

A- Internal Oxidation Zone

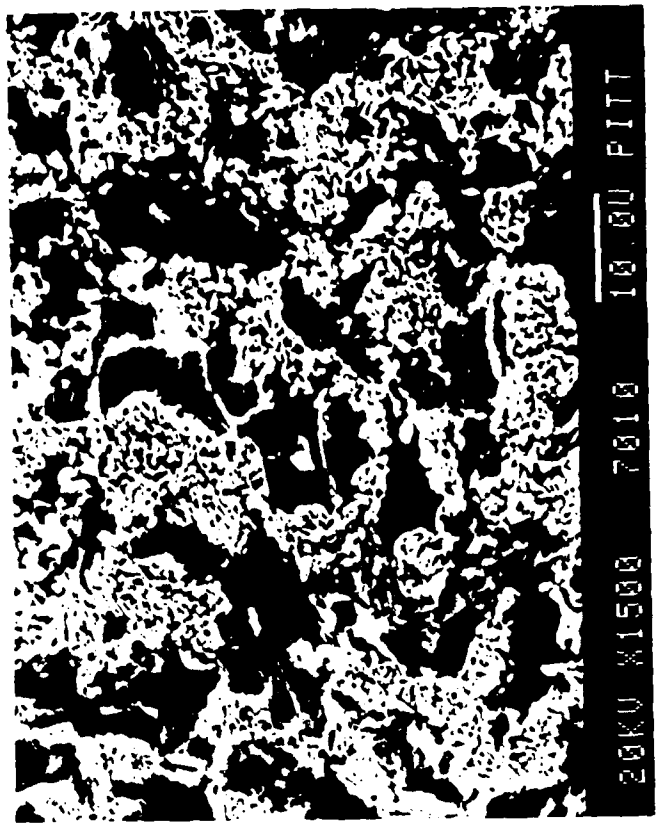

Area A- Light Grey areas
Area B- White areas
Alumina- Black areas

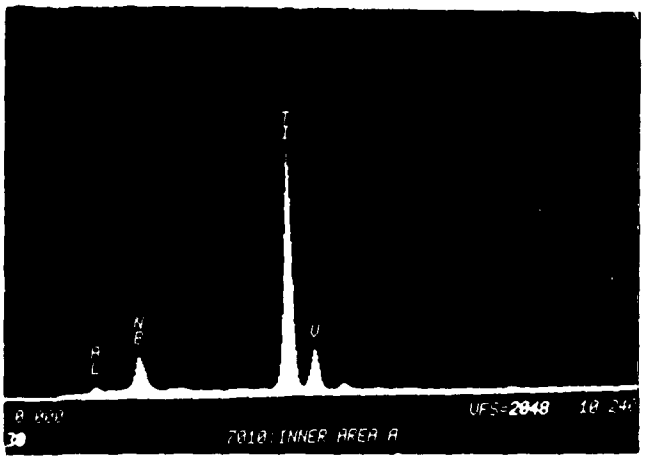

Area A

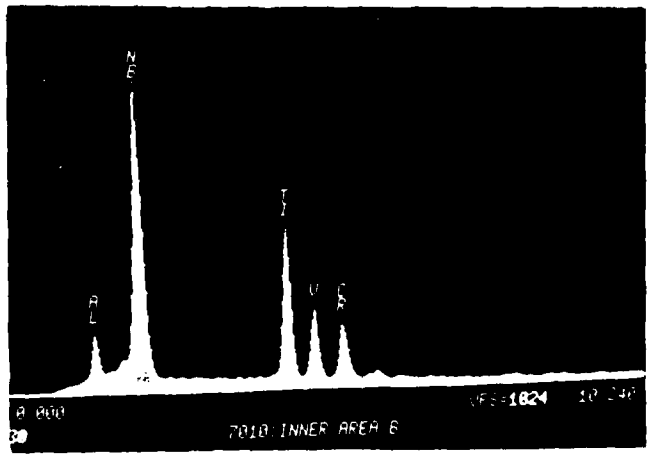

Area B

Alloy 70-1, Al Implanted
29h-1100°C, Oxygen

Figure 71: Elements in internal oxidation zone of Al implanted allov (70-1) after oxidation at 1100°C in oxygen.

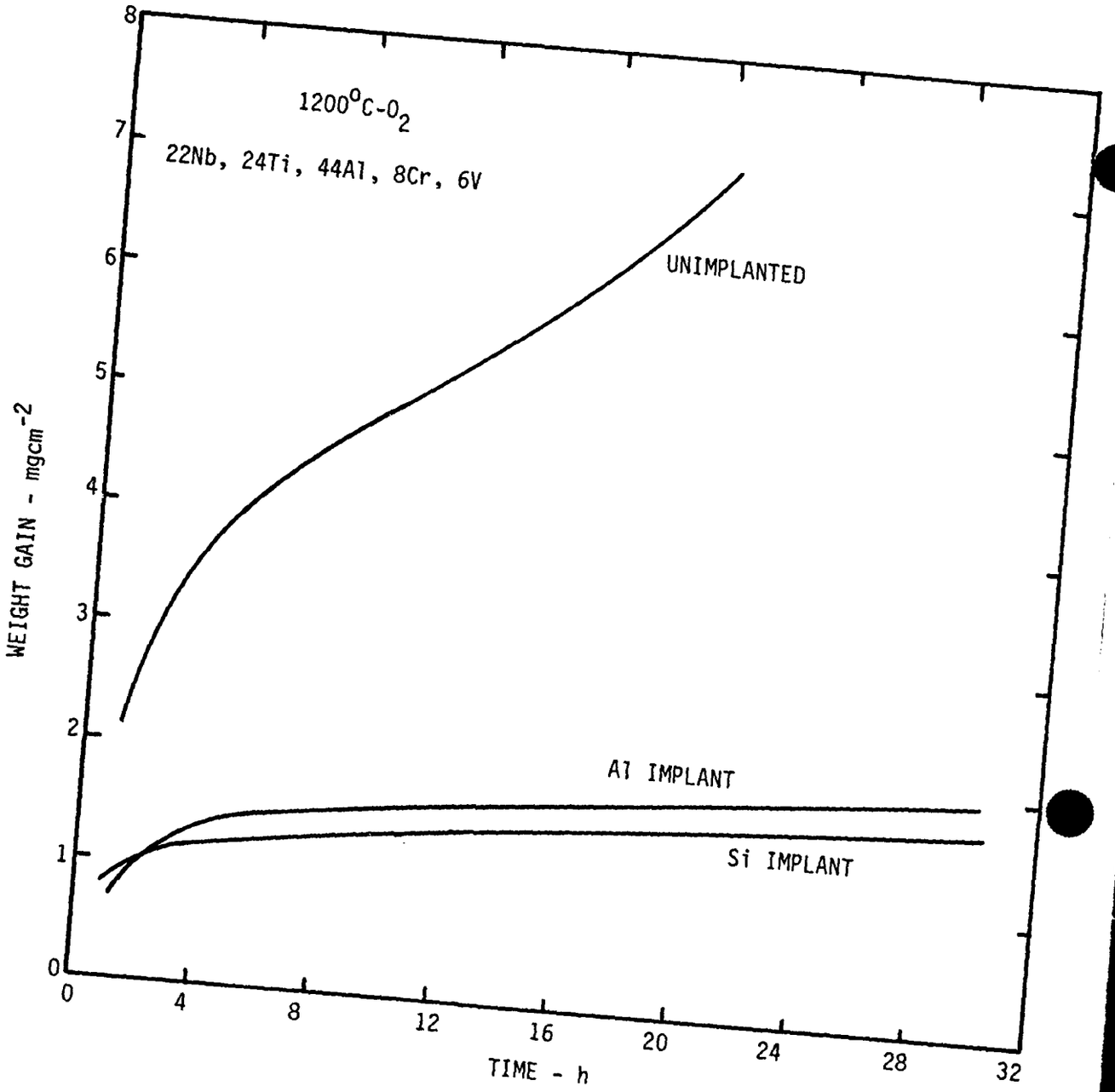

Figure 72: Effect of implanted Al and Si ions on oxidation kinetics of alloy 70-1 in oxygen at 1200°C.

has a peak in oxidation rates at 1200°C (Fig.41) and is far from being an alumina former at 1100°C, the temperature at which the implanted sample was tested. As in the the case of RS processing, the results indicate that ion implantation can be effective in forming protective alumina scales only in cases where the alloy already is borderline in this respect.

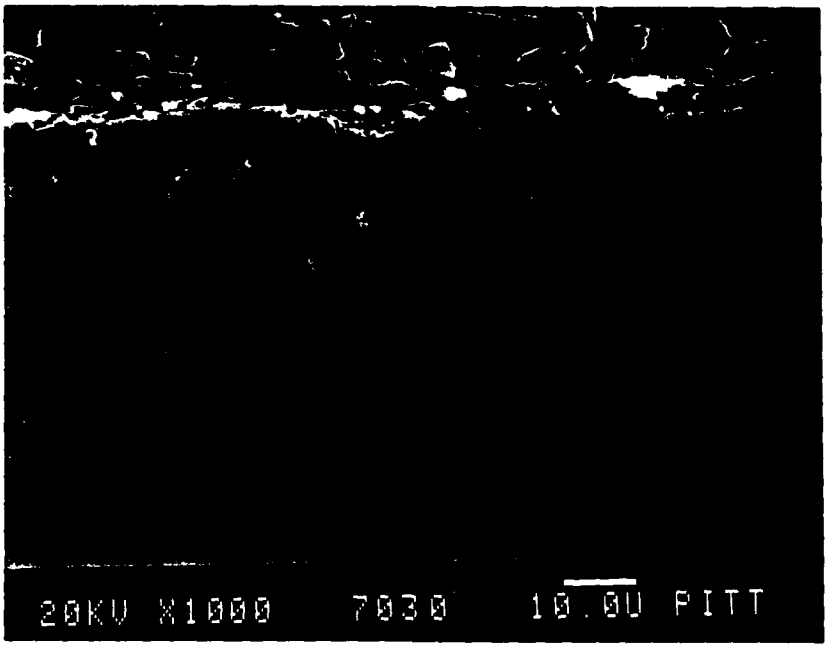

Transient Oxide

Alumina scale

A- Continuous Alumina + Transient Oxide Scale

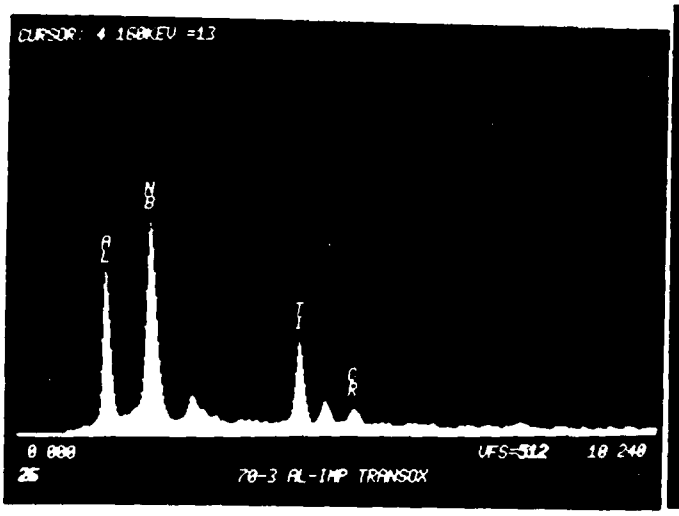

A- Transient Oxide

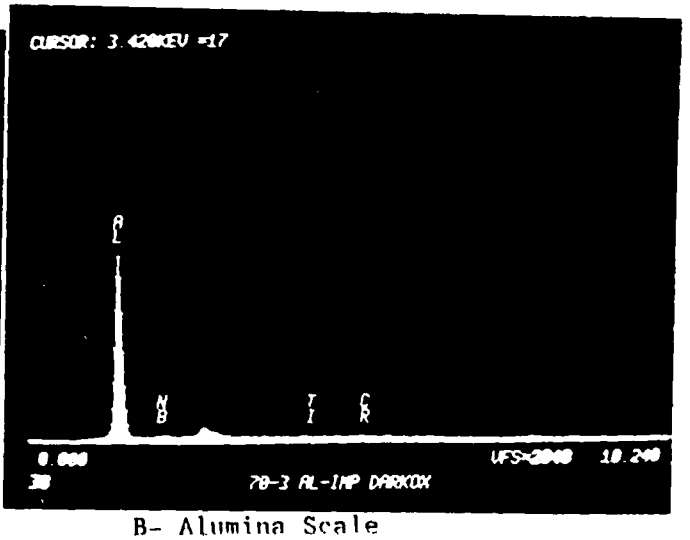

B- Alumina Scale

Alloy 70-3, Al Implant

48h-1100°C, Oxygen

Figure 73: Oxide scales formed on Al-implanted alloy (70-3) in oxygen at 1200°C.

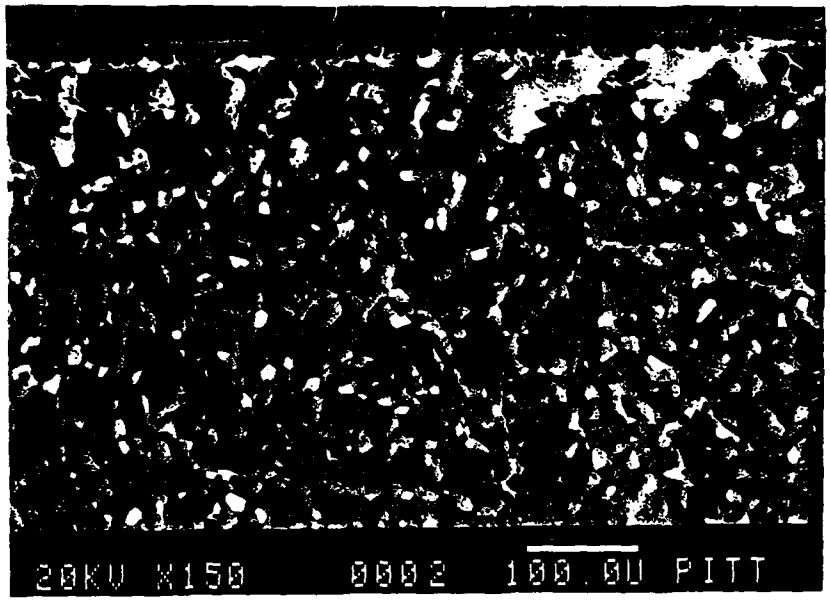

A- Alloy Depletion Zone

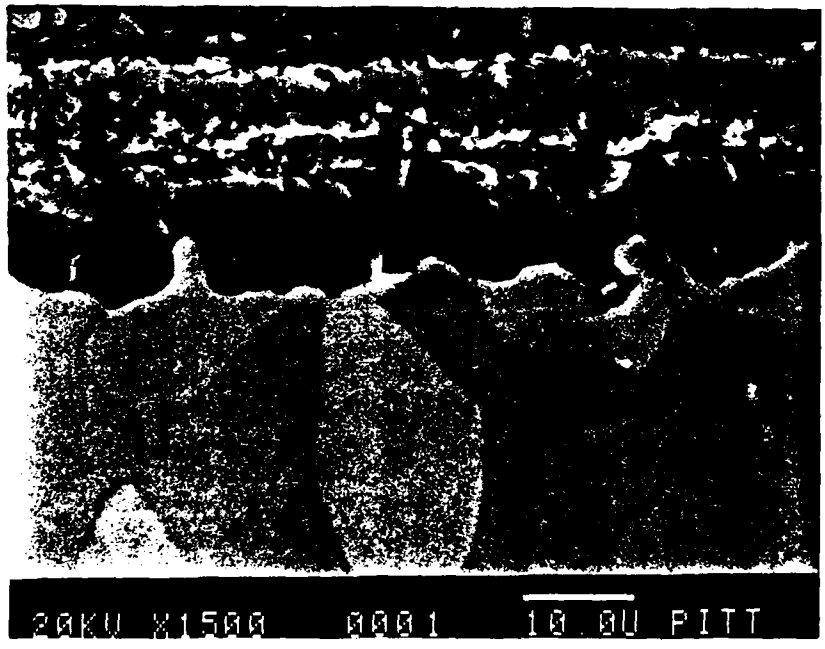

Transient Oxide

Alumina Scale

Alloy 70-3, Si Implant

48h-1200°C, Oxygen

Figure 74: Alloy depletion and oxide scales formed on Si-implanted alloy (70-3) exposed to oxygen at 1200°C.

MELTING POINT OF ALLOYS

The large additions of Ti and Al required to form continuous alumina scales significantly reduces the melting point of niobium. Wukusick (5) reported melting points as low as 1300°C for NbTiALCr alloys compared with 2468°C for unalloyed Nb. Melting points of selected alloys produced for this study were checked and results are summarized in Table 9.

Table 9

Melting Points of Nb-Ti-Al-Cr-V-Si Alloys

Alloy	Composition- at.%						Solidus	liquidus
	Nb	Ti	Al	Cr	V	Si	°C	°C
	100							2468
79-5	44.4	22.2	33.4				1805	1840
79-4	40.0	26.6	33.4				1755	1795
79-1	33.3	33.3	33.4				1610	1645
82-1	27.5	27.5	45.0				1670	1710
	25.0	25.0	50.0				1658	1730
	31.0	21.0	44.0	4.0			1690	1775
	29.9	19.2	43.4	7.6			1650	1705
70-1	24.0	23.0	33.0	4.0	5.0		1638	1700
70-3	22.0	20.0	44.0	8.0	6.0		1542	1600
82-2	28.0	27.0	45.0			1.0	1595	1630
82.3	29.0	26.0	45.0			3.0	1548	1588
82-4	30.0	25.0	45.0			5.0	1555	1600
82-5	32.5	22.5	45.0			10.0	1628	1663
P098	31.0	25.0	37.0	3.0	4.0	5.0	1590	1615
P099	36.0	25.0	32.0	3.0	4.0	10.0	1590	1630

The melting point was found to be strongly dependent on the Nb:Ti ratio in the alloys at any given Al content. At 33% Al the solidus was reduced from 1805°C to 1610°C by decreasing the Nb:Ti ratio from 2.0 to 1.0. Increasing Al content from 33% to 50% at a Nb:Ti ratio of 1.0 had a minor effect and tended to increasing melting point by 50°C. Adding Cr in the range of 4-8% had little, if any, effect on melting point. Vanadium additions tended to reduce melting point and had a significant effect at a level of 6%. As might be expected, Si depressed the melting point, having a significant effect with as little as 1 at.% addition. The nominal solidus temperature of the Nb-Ti-Al and Nb-Ti-Al-Cr-V alloys with a Nb:Ti ratio of 1.0 and 44% Al is about 1650°C. The addition of 3-10% Si depresses the melting point by 60-100°C to an average of about 1575°C.

Considering that structural alloys can be strengthened in creep at temperatures to about 80% of their absolute melting point ($0.8T_m$), oxidation resistant alloys in the Nb-Ti-Al-Cr-V system would have a maximum service temperature of about 1265°C as limited by ability to creep strengthen effectively. Melting point would have to be increased significantly to utilize the good oxidation resistance that these alloys exhibit at temperatures of 1300-1600°C. Melting point could be increased by reducing the Ti and Al content to move toward the Nb-rich corner of the ternary field (Fig.5). However, results of research on oxidation resistance of Nb-Ti-Al alloys to date have shown that alloys rich in sigma (Nb_2Al) phase have poor resistance to oxidation. Oxidation resistance in this system lies in a narrow field of compositions around a base of 25Nb-25Ti-50Al. The lowest Al content for alumina formation at 1400°C is 38% while >55% Al is required to form alumina at 1100°C. There would appear to be little hope of altering the Nb baseline composition to increase melting point significantly.

SUMMARY AND CONCLUSIONS

The factors affecting the formation of protective alumina scales on Nb-base alloys by selective oxidation have been extensively investigated. The existing theoretical knowledge of selective oxidation has been applied to oxidation of Nb-Al alloys to evaluate the effects of Al-content, temperature, atmosphere, third element additions, and microstructure on the transition from internal to external oxidation of the alumina. The results of the theoretical analysis were used to guide experiments to evaluate the effects of these variables on protective alumina formation. The investigation has established the conditions under which protective alumina scales can form on Nb alloys. The specific conclusions drawn from this work are listed as follows.

1. The feasibility of forming compact, adherent alumina scales on Nb alloys at greatly reduced Al contents has been demonstrated. Formation of protective alumina scales by selective oxidation of Al at concentrations of 32 at.% is possible.

2. Third element additions are required to allow protective alumina formation on Nb-Al alloys. The most effective additions are those which can reduce the solubility and diffusivity of oxygen, enhance diffusion of Al, and limit transient oxidation.

3. The addition of high e/a elements such as Mn and Ru, which should reduce oxygen solubility, suppressed the internal oxidation of Al and reduced the overall rate of oxidation. However, they did not promote formation of external alumina scales and formed alloys that oxidized with linear kinetics.

4. The addition of oxygen-active elements such as Zr, Hf, and Be, which should reduce the oxygen diffusivity, are less effective in reducing rates and do not inhibit internal oxidation of Al. Ternary alloys with these additions oxidize at linear rates.

5. The addition of Ti has the greatest single effect of any addition. Ternary Nb-Ti-Al alloys can form continuous external alumina scales in air at 1400°C at an Al content of 44 at.%. The Ti additions produce a favorable microstructure including a high-temperature B2 phase which readily forms

external alumina scales.

6. Although alumina scales can be formed on Nb-Ti-Al alloys in air at 1400°C, the rates are greater than those for NiAl. This is the result of slow growth rates for alumina on the alloys and the resultant formation of transient oxides rich in Nb, Ti, and Al.

7. Chromium and vanadium are effective additions to Nb-Ti-Al alloys for decreasing the solubility and diffusivity of oxygen. A synergism exists whereby the two elements together are more effective than either one alone. Additions of 3 at.% Cr and 4 at.%V resulted in protective alumina formation at 32 at.%Al which is the lowest Al content to produce alumina scales at 1400°C. Similar results were obtained by replacing V with Mo.

8. The ability to form protective alumina scales decreases as the temperature of oxidation decreases. The Nb-Ti-Al-Cr-V alloys were unable to form alumina scales when the temperature was decreased to 1100°C. Only alloys which were modified with 5-10 at.% Si formed alumina at this temperature.

9. The Nb-Ti-Al-Cr-V alloys were studied in great detail with regard to their oxidation mechanisms. The major conclusions from these studies are the following.

a. The major effect of Al content is on the transition from internal to external oxidation and the amount of transient oxidation that occurs before growth is cut off by a continuous alumina scale. When continuous alumina does not form the rate of oxidation is relatively independent of Al content at all temperatures.

b. Higher Nb:Ti ratios reduce the extent of internal oxidation when continuous alumina is not formed and allow continuous alumina to form at lower Al contents.

c. The alloys show a maximum in oxidation rate with increasing temperature. At low temperature the alloys form mixed oxide scales whose growth rates increase with increasing temperature. At a critical temperature, which is composition dependent, the alloys form continuous alumina and the rate drops

precipitously.

d. No subsantial difference in oxidation behavior was observed between specimens exposed in pure oxygen and air.

e. Preoxidation is effective only if the alloy is not cooled to room temperature prior to exposure. Thermal stresses generated in even one cooldown cycle are sufficient to crack the alumina scale. This result indicates the alloys will be susceptible to cyclic oxidation degradation.

f. Rapid solidification processing results in finer initial grain sizes which provides enhanced Al diffusion and enhanced alumina-forming capability of alloys that are borderline alumina formers. There appears to be little effect on alloys that are far from being alumina formers with the possible exception of alloys solidified with a high degree of supercooling (>100°C).

g. Ion implantation of Al or Si was shown to improve alumina-forming capability but only for alloys which were already borderline with respect to being alumina formers.

h. The type of alloying elements and the concentrations necessary to ensure alumina formation lowered the alloy solidus temperatures to around 1650°C. Additions of Si further reduced the solidus temperature to below 1600°C.

REFERENCES

1. J.F. Stringer, "High Temperature Corrosion of Aerospace Alloys", AGARD-AG 200, "Advisory Group for Aerospace Research and Development, NATO, August 1975.

2. J.A. Roberson and R.A. Rapp, TMS-AIME, 239, 1327 (1967)

3. R.A. Perkins and G.H. Meier, "Acoustic Emission Studies of High Temperature Oxidation" in High Temperature Materials, Chemistry II, Z.A. Munir and D. Cubicciotti eds., The Electrochemical Society, 1983, p. 176.

4. R.C. Svedberg, "Oxides Associated with the Improved Air Oxidation Performance of Some Niobium Intermetallics and Alloys" in Properties of High Temperature Alloys, Z.A. Foroulis and F.S. Pettit eds, Electrochem. Soc. 1976, p. 331.

5. D. Geiselman, "Identification of Oxides Formed in Columbium-Titanium and Columbium-Iron Alloys", Columbium Alloy Research Progress Rept. #2, Metals Research Lab., Union Carbide Corp., Nov. 1958.

6. C.S. Wukusick, "Oxidation Behavior of Intermetallic Compounds in the Nb-Ti-Al System", US Atomic Energy Commission Contract AT(40-1)-2847, General Electric Report GEMP-218, 31 July, 1963.

7. N.Birks and G.H.Meier, Introduction to High Temperature Oxidation of Metals, Edward Arnold, Ltd., London, (1983), p. 54.

8. C. Wagner, Z. Elektrochem., 63 772 (1959)

9. E. Fromm and E. Gebhardt, "Gase und Kohlenstoff in Metallen", Springer-Verlag, Berlin, 1976, p468.

10. R.T. Bryant, J. Less Comm. Metals, 4, 62 (1962)

11. G. Horz, "The Nitriding of Refractory Metals and Alloys", in Properties of High Temperature Alloys, Z.A. Foroulis and F.S. Pettit eds, The Electrochemical Society, (1976) p. 753.

12. G. Horz and R. Ziegeldorf, "Kinetics and Thermodynamics of the Behavior of Niobium and Tantalum-Base Alloys", in Properties of High Temperature Alloys, Z.A. Foroulis and F.S. Pettit, eds, The Electrochemical Society, (1976), p. 787.

13. E. Albert, E. Fromm, and R. Kirchheim, "Met. Trans. A", 14A, 2117 (1983)

14. R.J. Lauf and E.J. Altstetter, Acta Met., 27 1157 (1979)

15. R.J. Farraro and R.B. McClellan, Mater. Sci. and Eng., 33, 113 (1978)

16. Park and C.J. Alstetter, Acta Met, 34, 2217, (1986)

17. R.A. Perkins and R.A. Padgett, Jr., Acta Met., 25 1221 (1977)

18. G.I. Nikolaev and N.V. Bodrov, Zh. Fiz. Khim., 52, 1430 (1978)

19. K. Hirano and Y. Iijima, "Inter- and Reaction Diffusion Between Alloys of Very Different Diffusional Properties," in Diffusion in Solids: Recent Developments, M.A. Dayananda and G.E. Murch eds., AIME, 1985, p. 141.

20. J.E. Morral, M.S. Thompson, and O.J. Devereux, Scripta Met., (1986)

21. Binary Alloy Phase Diagrams, Vol.1, T.B. Massalski, ed., American Society for Metals (1986).

22. J.H. Perepezko, presented at the Materials Research Society Fall Meeting, Nov. 28 - Dec. 3, 1988, Boston, MA.

23. M.J. Bennett and A.T. Tuson, "Improved High Temperature Oxidation Behaviour of Alloys by Ion Implantation", UKAEA Harwell Report AERE R 13309, October, 1988.

24. U. Bernabai, M. Cavallini, G. Bombara, G. Dearnaley, and M.A. Wilkins, Corr. Sci., 20, 19(1980).

25. F. Gesmundo and F. Viani, Oxid. Metals, 25, 269 (1986)

26. F.S. Pettit, Trans. Met. Soc. AIME, 239, 1296, (1967).

27. R.A. Perkins, Alloying of Chromium to Resist Nitridation, NASA-CR-72892, July, 1971.

28. R.A. Perkins and S.J. Vonk, Materials Problems in Fluidized Bed Combustion Systems: Part IV- Corrosion Chemistry in Low Oxygen Activity Atmospheres, EPRI-FP-1280, Project 979-6, Interim Report, December, 1979, Electric Power Research Institute, Palo Alto, Ca.

APPENDIX A1

Experimental Nb-Ti-Al Alloys

ALLOY DENS. NO.	COMPOSITION (SEM/XES) ATOM % Nb	Ti	Al	Cr	V	Nb:Ti RATIO	Nb	Ti	Al	Cr	V	CALC. WEIGHT % gm/cc
Nb-Ti-Al												
79-1	33.3	33.3	33.4			1.00	55.4	28.5	16.1			5.33
79-4	40	23.6	33.4			1.69	66.3	18.8	15.0			5.73
79-5	44.4	22.2	33.4			2.00	67.7	17.5	14.8			5.79
29-11	32.8	32.4	34.9			1.01	54.9	28.1	17.0			5.28
59-4	40	25	35			1.60	63.5	20.4	16.1			5.58
29-14	30.4	30.1	39.5			1.01						5.07
79-3	28	28	44			1.00	50.7	26.1	23.1			4.92
82-1	27.5	27.5	45			1.00	50.2	25.9	23.9			4.89
81-0	29.4	22.6	48			1.30	53.5	21.2	25.4			4.92
79-2	25	25	50			1.00	47.7	24.6	27.7			4.69
Nb-Ti-Al-Cr												
29-12	29.1	31.6	34.1	5.2		0.92	50.0	28.0	17.0	4.99		5.26
29-13	25.6	30.9	33.3	10.2		0.82	45.0	28.0	17.0	10.0		5.18
29-15	23.9	29.4	38.6	5.0		0.81	47.6	27.0	20.0	5.00		5.05
59-8	41.4	13.8	35	9.8		3.00	64.5	11.1	15.8	8.55		5.86
29-16	23.6	28.8	37.8	9.8		0.82	43.0	27.0	20.0	9.98		5.01
26-2	30.5	31.9	34.4	3.1		0.96	52.1	28.0	17.0	2.95		5.08
Nb-Ti-Al-V												
26-3	29.8	31.7	34.2		4.3	0.94	51.0	28.0	17.0		4.03	5.11
59-7	42.9	14.4	35		7.8	2.98	66.2	11.5	15.7		6.61	5.82
Nb-Ti-Al-Cr-V												
18-14	39.8	29.0	22.3	4.0	4.8	1.37	60.3	22.6	9.78	3.38	3.97	5.92
18-15	37.4	27.2	27.1	3.8	4.5	1.38	58.5	22.0	12.3	3.33	3.86	5.45
18-16	34.9	25.5	31.8	3.5	4.4	1.37	56.5	21.4	15.0	3.18	3.92	5.33
18-17	32.3	23.7	36.7	3.3	4.0	1.36	54.5	20.6	18.0	3.12	3.70	4.76
26-4	27.7	31.3	33.7	3.1	4.2	0.88	48.0	28.0	17.0	3.00	3.99	5.02
26-6	25.6	29.1	38.3	3.0	4.0	0.88	46.0	27.0	20.0	3.02	3.94	5.01
48-1	23	29	44	3.2	3.3	0.79						
54-1	29	29	35	3	4	1.0						
54-2	26.5	26.5	40	3	4	1.0						
54-3	24	24	45	3	4	1.0						
77-2	23	23	46	3.5	4.5	1.0	43.7	22.5	25.4	3.72	4.68	4.81
54-4	21.5	21.5	50	3	4	1.0						
54-5	19	19	55	3	4	1.0						
54-17	22	24	46	3.5	4.5	0.92						
70-1[a]	24.1	22.9	44.3	3.8	4.9	1.05	45.0	22.0	24.0	3.97	5.01	4.90
70-3[a]	22	24	44	8	6	0.92	35.4	24.3	25.0	8.79	6.46	4.74
96-1	32.1	24.1	38	2.4	3.4	1.33	54.6	21.1	18.8	2.28	3.17	5.30
96-2	29	21.3	44.2	2.3	3.2	1.36	51.9	19.7	23.0	2.3	3.14	5.06
96-3	26.1	20.1	47.7	2.5	3.6	1.30	48.6	19.3	25.8	2.60	3.67	4.88
97-1	23.5	17.9	52.8	2.3	3.4	1.31	46.0	18.0	30.0	2.5	3.63	4.67
97-2	20.8	15.6	57.8	2.5	3.4	1.33	42.4	16.5	34.4	2.86	3.82	4.46
97-3	25	19.5	49.8	2.8	2.9	1.28	47.5	19.1	27.5	2.97	3.01	4.79

APPENDIX A1 (Cont.)

ALLOY NO.	COMPOSITION (SEM/XES) ATOM % Nb	Ti	Al	Cr	V	Nb:Ti RATIO	WEIGHT % Nb	Ti	Al	Cr	V	CALC. DENS. gm/cc
L4001[a]	24	25	44	3	4	0.96	44.8	24.1	23.9	3.13	4.09	4.87
L4002[a]	30	25	38	3	4	1.20	51.9	22.3	19.1	2.90	3.79	5.23
	Nb	Ti	Al	Others			Nb	Ti	Al	Others		
Oxygen Active Elements												
39-4	77.7		20.6	1.7 Zr		91.0			7.00	1.95 Zr		7.39
39-5	70.7		27.7	1.6 Zr		88.0			10.0	1.95 Zr		7.00
39.6	69.1		27.7	3.2 Zr		86.1			10.0	3.91 Zr		6.96
54-11	28	28	40	4 Hf		45.4	23.4	18.8		12.4 Hf		5.43
54-12	28	28	40	4 Zr		48.3	24.9	20.0		6.8 Zr		5.09
39-7	67.4		28.7	3.9 Hf		81.0			10.0	9.00 Hf		7.22
81-3	28.8	22.2	48	1 Hf		51.3	20.4	24.8		3.42 Hf		5.00
81-4	26.6	20.4	48	5 Hf		43.8	17.3	23.0		15.8 Hf		5.35
81-5	23.7	48	18.3	10 Hf		35.8	14.2	21.0		29.0 Hf		5.77
81-6	26.6	20.4	48	5 Be		51.6	20.4	27.0		0.94 Be		4.74
High e/a Elements												
40-9	67		17	15.0 Mn,1	Zr	81.9			6.04	1.2Zr, 10.84Mn		7.45
40-10	64		20	15.0 Mn,1	Zr	80.3			7.29	1.23Zr, 13Mn		7.27
40-11	61		23	15.0 Mn,1	Zr	78.7			8.62	1.27Zr, 11.44Mn		7.09
40-15	72		17	10.0 Ru,1	Zr	81.1			5.56	1.10Zr, 12.25Ru		7.89
40-16	69		20	10.0 Ru,1	Zr	79.6			6.70	1.13Zr, 12.55Ru		7.72
40-17	66		23	10.0 Ru,1	Zr	78.1			7.9	1.16Zr, 12.87Ru		7.55
48-2	23	28	44	3.3Cr,1.2	Mo							
48-3	20	30	37	7.7Cr,5.2	Mo							
48-4	17	27	43	7.8Cr,5.3	Mo							
54-6	25	25	40	10 Re		35.9	18.5	16.7		28.8 Re		6.30
54-7	25	15	40	10Re,10Ru		33.2	10.3	15.4		26.6Re,14.5Ru		6.99
54-8	25	15	40	10Re,10Mo		33.5	10.4	15.5		26.8Re,13.8Mo		6.85
54-9	25	15	40	10Re,10Cr		35.7	11.1	16.6		28.7Re,7.8Cr		6.56
54-10	25	15	40	10Re,10V		35.8	11.1	16.6		28.7Re,7.9V		6.48
54-14	48		20	32 Re		40.7			4.9	54.4 Re		10.92
54-15	42		30	28 Re		39.3			8.2	52.6 Re		9.89
54-16	36		40	24 Re		37.6			12.2	50.3 Re		8.87
54-13	25		40	25V,10Cr		44.7			20.8	24.5V,10.0Cr		5.46
57-1	41.6		23.9	34.6 Fe		60			10.0	30.0 Fe		10.09
57-2	38.2		30	31.7 Fe		60			13.2	28.9 Fe		6.53
57-3	35.5		35	29.5 Fe		60			16.0	28.0 Fe		6.24
57-4	54.9		25	20.0 Fe		60			9.8	16.2 Fe		6.98
57-5	51.3		30	18.7 Fe		60			12.2	15.8 Fe		6.69
57-6	47.6		35	17.4 Fe		60			14.9	15.3 Fe		6.41
59-1	57		35	8 Mo		75.6			13.5	11.0 Mo		6.72
59-2	53		35	12 Fe		75.3			14.4	10.2 Fe		6.47
59-3	50		35	15 Cr		72.9			14.8	12.2 Cr		6.36
59-5	45		35	20 Ta		47.8			10.8	41.4 Ta		8.28
59-6	44.8	15	35	5.2 Mo		65.8	11.4	14.9		7.89 Mo		6.06
59-9	39	16.3	35	9.8 Ta		50.8	11.0	13.3		24.9 Ta		6.76
76-1	80		20			93.2			6.77			7.47

APPENDIX A1 (Cont.)

	COMPOSITION (SEM/XES)								
	ATOM %				WEIGHT %				CALC.
ALLOY	Nb	Ti	Al	Others	Nb	Ti	Al	Others	DENS.
Si Modified									
81-1	26.6	20.4	48	5 Si	50.6	20.0	26.5	2.87 Si	4.67
81-2	23.7	18.3	48	10 Si	47.3	18.8	27.8	6.03 Si	4.42
82-2	27	27	45	1 Si	49.7	25.6	24.1	0.55 Si	4.84
82-3	26	26	45	3 Si	48.7	25.1	24.5	1.69 Si	4.75
82-4	25	25	45	5 Si	47.7	24.6	24.9	2.88 Si	4.65
82-5	22.5	22.5	45	10 Si	44.8	23.1	26.0	6.02 Si	4.42
82-7	26	26	45	3 Si	48.7	25.1	24.5	1.69 Si	4.75
82-12	24	24	45	3Cr,4V,3Si	41.0	24.2	25.5	3.3Cr,4.3V,1.8Si	
86-1	32.5	32.5	30	5 Si	54.6	28.2	14.7	2.54 Si	5.22
87-1	30	30	35	5 Si	52.5	27.1	17.8	2.64 Si	5.04
90-1	20	20	45	15 Si	41.7	21.5	27.8	9.46 Si	4.19
93-1	27.5	27.5	40	5 Si	50.2	25.9	21.2	2.75 Si	4.84
93-2	30	30	30	10 Si	52.4	27.0	15.2	5.28 Si	4.99
93-3	27.5	27.5	35	10 Si	50.1	25.8	18.5	5.51 Si	4.80
94-1	25	25	40	10 Si	47.6	24.5	22.1	5.75 Si	4.61
P098[b]	26	25	37	3Cr,4V,5S	47.3	23.4	19.5	3.1Cr,4.0V,2.7Si	
P099[b]	26	25	32	3Cr,4V,10Si	47.2	23.4	16.9	3.0Cr,4.0V,5.5Si	
Noble Metal Additions									
76-2	75		25	5 Pt	79.8		8.27	11.96 Pt	7.73
77-4	20.5	20.5	46	3.5Cr,4.5V,5 Pt					
81-7	26.6	20.4	48	5 Pd	46.8	18.5	24.6	10.08 Pd	5.12

a- Arc-melted by Teledyne Wah Chang, Albany, OR.
b- Arc-melted by Pratt & Whitney, W. Palm Beach, Fl.

APPENDIX A2

RESULTS OF OXIDATION SCREENING TESTS IN AIR

ALLOY NO.	ATOM % Nb	Ti	Al	Cr	V	Other	WEIGHT GAIN- $mgcm^{-2}$ 2h-1100°CC	1h-1400°C	1h-1500°C	1h-1500°C
Nb-Ti-Al										
79-4	40	27	33					17.9		
79-1	33	33	33				3.39	14.1		
29-11	33	32	35					10.2		
29-14	30	30	40					4.7		
79-3	28	28	44				1.98	2.94		
82-1	28	28	45				1.48			
79-2	25	25	50				2.14	2.92		
Nb-Ti-Al-Cr										
29-12	29	32	34	5				1.9		
								1.52		
29-13	25	31	33	10				6.7		
29-15	24	29	40	5				2.0		
29-16	24	29	38	10				1.3		
26-2	31	32	43	3				3.6		
Nb-Ti-Al-V										
26-3	30	32	34		4			4.3		
Nb-Ti-Al-Cr-V										
26-4		31	34	3	4			0.4		
								5.5		
26-6	26	29	38	3	4		1.01	2.2		
							1.78			
48-1	23	29	44	3	3		0.75			
70-1	24	23	44	4	5		2.54	1.71	1.87	2.26
70-3	22	24	44	8	6		2.93	1.51	1.86	2.44
									1h-1550°C	1h-1600°C
54-1	29	29	35	3	4		1.25	4.87		94.3[a]
18-17	32	24	37	3	4		5.3	-0.71		
							1.78			
54-2	27	27	40	3	4		0.97	2.93	4.12	114.0[a]
54-3	24	24	45	3	4		0.87	1.33	2.43	1.69
54-17	22	24	46	3	4		0.18	3.54		2.13
54-4	22	22	50	3	4		0.64	0.99	3.04	2.83
54-5	19	19	55	3	4		0.77	1.45	4.49	1.65
High e/a Elements										
48-2	23	28	44	3		1 Mo	1.23			
48-3	20	30	37	8		5 Mo	1.33			
48-4	17	27	43	8		5 Mo	0.93			
54-13	25		40	10	25			2.46		
54-14	48		20			32 Re		1.81		
54-15	42		30			28 Re		2.86		
54-16	36		40			24 Re		0.72		
54-6	25	25	40			10 Re		-3.20		
54-7	25	15	40			10Re, 10Ru		10.60		
54-8	25	15	40			10Re, 10Mo		8.15		
54-9	25	15	40	10		10 Re		8.38		
54-10	25	15	40		10	10 Re		3.78		
54-18	49		40			10Ru, 1Zr		3.14		

APPENDIX A2 (CONT.)

RESULTS OF OXIDATION SCREENING TESTS IN AIR

ALLOY	ATOM %						WEIGHT GAIN- $mgcm^{-2}$			
NO.	Nb	Ti	Al	Cr	V	Other	2h-1100°CC	1h-1400°C	1h-1500°C	1h-1500°C
Si Modified										
82-2	27	27	45			1 Si	0.76			
82-3	26	26	45			3 Si	0.75			
82-4	25	25	45			5 Si	0.65			
82-5	23	23	45			10 Si	0.55			
P098	26	26	37	3	4	5 Si	1.24			
P099	26	25	32	3	4	10 Si	0.63			
Noble Metal Additions										
76-2	75		20			5 Pt	17.1	12.4		
77-4	21	21	46	4	5	5 Pt	1.98	1.60		

a- Liquid Transient Oxide

APPENDIX A3

OXIDATION RATE LAW EXPONENTS[a]

ALLOY NO.	ATOM % Nb	Ti	Al	Cr	V	Other	ATM.	800°C	1100°C	1300°C	1400°C	1500°C
Nb-Ti-Al												
79-1	33	33	34				Air		1.6	0.4,0.7		
59-13	49	16	35				O_2	1.24				
82-1	28	28	45				Air	0.5,CU	1.0,1.5	0.5,0.8		
79-2	25	25	50				Air	1.0	1.0	0.5,0.9		
Nb-Ti-Al-Cr-V												
26-6	26	29	38	3	4		O_2	0.6	0.6			
96-1	32	24	38	2	3		Air	0.6,0.5	0.5,0.9	0.3,1.0		
96-2	29	21	44	2	3		Air	0.8,0.5	0.5,0.9	0.7,0.9		
77-2	23	23	46	4	5		Air	0.5	0.4,0.8	CU		0.3,0.5
96-3	26	20	47	3	4		Air	0.6	0.9	1.0		
97-3	25	20	50	3	3		Air	0.6	0.7,0.9	CU		
97-1	24	18	53	2	3		Air	0.7,0.9	0.8	0.6,1.0		
97-2	21	16	58	3	3		Air	0.4	0.5,0.8	0.3,1.0		
54-1	29	29	35	3	4		O_2	0.6				
54-2	27	27	40	3	4		O_2	0.7				
54-3	24	24	45	3	4		O_2	0.4,0.6				
54-17	22	24	45	3	4		O_2	0.6,0.7				
54-4	22	22	50	3	4		O_2	0.3,0.7				
54-5	19	19	55	3	4		O_2	0.4,0.8				
70-1	24	23	44	4	5		Air	0.4	0.4,CU	0.3,CU	0.4	0.4
70-3	22	24	44	8	6		Air	0.5	0.5,CU	0.2	0.4,0.6	0.3
								800°C	1000°C	1100°C	1200°C	1300°C
70-1	24	23	44	4	5		O_2	0.2	0.6	0.9	1.0	0.3
70-3	22	24	44	8	6		O_2	0.5	1.5,0.9	0.8	0.9	0.2
								800°C	1100°C	1300°C	1400°C	1500°C
L4001	24	25	44	3	4		Air		0.6	0.5,1.3	1.0	
L4002	30	25	38	3	4		Air		0.6,0.4	0.5,CU	0.4,2.16	
RS Splats												
70-1	24	23	44	4	5		O_2		0.6			
70-3	22	24	44	8	6		O_2		1.5,0.9			
L4001	24	25	44	3	4		Air		0.5	0.4,0.7	1.6	
L4002	30	25	38	3	4		Air		0.5	0.5,CU	0.7	
High e/a Elements												
54-16	36		40			24 Re	Air	1.0	1.0	0.5,0.9		
Si Modified												
86-1	33	33	30			5 Si	Air		0.5	0.5,1.2		
87-1	30	30	35			5Si	Air		0.5,0.6	0.5,1.0		
93-1	28	28	40			5Si	Air		0.6	0.5,1.2		
93-2	30	30	30			10 Si	Air		0.4	0.4,0.7		
93-3	28	28	35			10 Si	Air		0.7	0.6,1.0		
94-1	25	25	40			10 Si	Air		0.5.0.7	0.6,0.7		
82-2	27	27	45			1 Si	Air	1.0,>1	0.6,1.2	0.7,>1		
82-3	26	26	45			3 Si	Air	0.2,0.4	0.4,CU	0.5		
82-4	25	25	45			5 Si	Air	0.9	1.5	0.5,0.6		
P098	26	25	37	3	4	5Si	Air		0.5			
P099	26	25	32	3	4	10 Si	Air		0.5			

a- Most curves have two slopes, first number is the initial slope and the last number is the final slope, CU- continuous upward curved

APPENDIX A4

OXIDATION RATE CONSTANTS[a]

ALLOY NO.	ATOM % Nb	Ti	Al	Cr	V	Other	ATM.	800°C	1100°C	1300°C	1400°C	1500°C
Nb-Ti-Al												
79-1	33	33	34				Air		-5.86	-8.77	-7.18	
59-13	49	16	35				O_2	-7.20, CU				
82-1	28	28	45				Air	-10.03, -7.57	-6.36, CU	-8.30, -6.52		
79-2	25	25	50				Air	-9.20	-6.57	-8.09, CU		
Nb-Ti-Al-Cr-V												
26-6	26	29	38	3	4		O_2	-10.44	-7.93			
96-1	32	24	38	2	3		Air	-10.93	-9.02, -6.99	-8.92, -6.75		
96-2	29	21	44	2	3		Air	-11.91	-9.03, -6.92	-8.19, -6.61		
77-2	23	23	46	4	5		Air	-11.35	-9.65, -7.24	-7.43	-7.79	-9.78
96-3	26	20	47	3	4		Air	-11.05	-6.83	-6.46		
97-3	25	20	50	3	3		Air	-10.83	-6.59	-6.05		
97-1	24	18	53	2	3		Air	-10.85 -7.88	-6.66	-8.75 -6.51		
97-2	21	16	58	3	3		Air	-9.18	-8.4, -6.37	-8.95, -6.57		
54-1	29	29	35	3	4		O_2	-10.25				
54-2	27	27	40	3	4		O_2	-10.51				
54-3	24	24	45	3	4		O_2	-10.84, -10.48				
54-17	22	24	45	3	4		O_2	-10.82, -10.63				
54-4	22	22	50	3	4		O_2	-10.73, -10.37				
54-5	19	19	55	3	4		O_2	-10.58, -6.53				
70-1	24	23	44	4	5		Air	-10.94	-9.44, -7.23	-9.75, -7.28	-10.31	-9.65
70-3	22	24	44	8	6		Air	-10.77	-8.76, -6.78	-10.37	-8.08	-10.04
								800°C	1000°C	1100°C	1200°C	1300°C
70-1	24	23	44	4	5		O_2	-10.65		-8.12, -7.06	-5.45	-10.01

a- log k_p in $g^2cm^{-4}s^{-1}$, log k_1 in $gcm^{-2}s^{-1}$. Many curves have two slopes, an initial parabolic region and a final linear region. Both parabolic and linear rate constants are give in such cases. In some cases, the second region also is parabolic and two parabolic rate connstants ,one for the initial and the other for the final segments of the curve, are presented. Some plots curve continuouslt upward (CU) and no constant could be derived.

APPENDIX A4 (CONT.)

OXIDATION RATE CONSTANTS[a]

ALLOY NO.	ATOM % Nb	Ti	Al	Cr	V	Other	ATM.	800°C	1100°C	1300°C	1400°C	1500°C
70-3	22	24	44	8	6		O_2	-10.87		-6.96, -5.08	-6.01, -9.25	-10.02
								800°C	1100°C	1300°C	1400°C	1500°C
L4001	24	25	44	3	4		Air	-11.11	-8.03, -6.56	-6.79		
L4002	30	25	38	3	4		Air	-10.55	-9.75, 7.27	-8.63, CU		
RS Splats												
70-1	24	23	44	4	5		O_2					
70-3	22	24	44	8	6		O_2					
L4001	24	25	44	3	4		Air	-11.89	-9.72, -7.83	CU		
L4002	30	25	38	3	4		Air	-11.01	-9.33, -6.91	-7.25, -6.61		
High e/a Elements												
54-16	36		40			24 Re	Air					
Si Modified												
86-1	33	33	30			5 Si	Air		-9.67	-8.69, -6.46		
87-1	30	30	35			5Si	Air		-9.66, -9.95	-8.75, -6.54		
93-1	28	28	40			5Si	Air		-9.87	-9.02, -6.62		
93-2	30	30	30			10 Si	Air		-9.87	-8.51, -6.70		
93-3	28	28	35			10 Si	Air		-8.97, -6.96	-8.69, -6.65		
94-1	25	25	40			10 Si	Air		-9.15, -7.07	-9.20, -7.09		
82-2	27	27	45			1 Si	Air	-7.85	-9.75, -6.15	-8.53, -6.43		
82-3	26	26	45			3 Si	Air	-9.87	-9.56	-8.97, CU		
82-4	25	25	45			5 Si	Air	-7.90	CU	-9.09, -8.85		
P098	26	25	37	3	4	5Si	Air		-10.48			
P099	26	25	32	3	4	10 Si	Air		-10.18			

a- log k_p in $g^2cm^{-4}s^{-1}$, log k_l in $gcm^{-2}s^{-1}$. Many curves have two slopes, an initial parabolic region and a final linear region. Both parabolic and linear rate constants are give in such cases. In some cases, the second region also is parabolic and two parabolic rate connstants ,one for the initial and the other for the final segments of the curve, are presented. Some plots curve continuouslt upward (CU) and no constant could be derived.